1984

Oxidation Of Methyl Mercaptan And Hydrogen Sulphide In A Flow Reactor With Corona Discharge

Mohamed Ibrahim El-khashab

CANADIAN THESES ON MICROFICHE

I.S.B.N.

THÈSES CANADIENNES SUR MICROFICHE

National Library of Canada
Collections Development Branch

Canadian Theses on
Microfiche Service

Ottawa, Canada
K1A 0N4

Bibliothèque nationale du Canada
Direction du développement des collections

Service des thèses canadiennes
sur microfiche

NOTICE

The quality of this microfiche is heavily dependent upon the quality of the original thesis submitted for microfilming. Every effort has been made to ensure the highest quality of reproduction possible.

If pages are missing, contact the university which granted the degree.

Some pages may have indistinct print especially if the original pages were typed with a poor typewriter ribbon or if the university sent us a poor photocopy.

Previously copyrighted materials (journal articles, published tests, etc.) are not filmed.

Reproduction in full or in part of this film is governed by the Canadian Copyright Act, R.S.C. 1970, c. C-30. Please read the authorization forms which accompany this thesis.

THIS DISSERTATION
HAS BEEN MICROFILMED
EXACTLY AS RECEIVED

AVIS

La qualité de cette microfiche dépend grandement de la qualité de la thèse soumise au microfilmage. Nous avons tout fait pour assurer une qualité supérieure de reproduction.

S'il manque des pages, veuillez communiquer avec l'université qui a conféré le grade.

La qualité d'impression de certaines pages peut laisser à désirer, surtout si les pages originales ont été dactylographiées à l'aide d'un ruban usé ou si l'université nous a fait parvenir une photocopie de mauvaise qualité.

Les documents qui font déjà l'objet d'un droit d'auteur (articles de revue, examens publiés, etc.) ne sont pas microfilmés.

La reproduction, même partielle, de ce microfilm est soumise à la Loi canadienne sur le droit d'auteur, SRC 1970, c. C-30. Veuillez prendre connaissance des formules d'autorisation qui accompagnent cette thèse.

LA THÈSE A ÉTÉ
MICROFILMÉE TELLE QUE
NOUS L'AVONS REÇUE

NL-339 (r. 82/08)

Canada

OXIDATION OF METHYL MERCAPTAN AND HYDROGEN SULPHIDE IN A FLOW REACTOR WITH CORONA DISCHARGE

by

Mohamed I. El-KHASHAB

Faculty of Engineering Science

Submitted in partial fulfillment
of the requirements for the degree of
Doctor of Philosophy

Faculty of Grarduate Studies
The University of Western Ontario
London, Ontario, Canada

December, 1983.

ABSTACT

An unfortunate consequence of the operation of kraft pulp mills is the release of the malodorous methyl mercaptan and hydrogen sulphide to the atmosphere. Although the present technology is managing to greatly reduce the emissions of these compounds their extremely low odour threshold values still cause the odour problem to exist.

Motivated by the existence of this problem, a novel method to control the emissions of methyl mercaptan and hydrogen sulphide to the atmosphere was investigated. Such method would allow the removal of these compounds through oxidation by air in which a corona discharge is established.

The method investigated would moreover have the advantages inherent in the use of electrostatic precipitators among which is the removal of low concentration pollutants from large amounts of air, an inevitable circumstance in the pulp mills.

The reactions of methyl mercaptan and hydrogen sulphide with air were studied separately in a tubular flow reactor which was essentially an electrostatic precipitator of the wire-cylinder type. The operating conditions used throughout the study were within the range of industrial

interest.

The products of each reaction were first identified using spectroscopic methods such as NMR, IR, and MS as well as analytical chemical methods. The oxidation products of methyl mercaptan found were water, sulphur dioxide, and dimethyl sulphone as end products and dimethyl disulphide and dimethyl sulphide as intermediates. These intermediates were found to react further by using higher values of current and/or mean residence time of gas mixture through the reactor. On the other hand, the products of the hydrogen sulphide oxidation were always water and sulphur dioxide.

Having identified the products of the above reactions, the composition of the feed and product streams were determined by a gas chromatograph calibrated for the compounds of concern. The data collected were then used to evaluate the kinetic parameters of the reactions. The evaluation process was conducted using the integral method of analysis considering that the reactor was an integral reactor.

The main contribution found of the corona discharge is to produce several species of excited molecular oxygen which are responsible for the oxidation of the sulphur compounds. The concentration of these species was correlated to the

electrical parameters of the corona system and the flow rate of gases through the reactor.

Both of the above reactions were found to proceed totally in the gas phase. Expressions for the oxidation rate of both methyl mercaptan and hydrogen sulphide were obtained.

Variables "energy yield" and "volumetric rate" were used to present the data obtained. These two variables are of industrial interest should an economic appraisal be required. The effect of the operating conditions and of the reactor physical dimensions on these two variables was studied in detail.

To those, wherever they may be, who silently
plant a seed.
The growing tree might sustain life
for some,
provide shade for others, offer pleasure
for the eye,
or may just exist.

ACKNOWLEDEMENTS

The author wishes to express his deep indebtedness and appreciation to Professor K.A. Shelstad who suggested this project and contributed to it through his interest, valuable advice, and criticism of the manuscript. My thanks are also due to my advisory committee, Professors M. Bergougnou and G.S.P. Castle for their critical review of the text. My special appreciation is also due to Professor G.S.P. Castle for his valuable discussions on the electrical part of the project.

The author also wishes to thank his fellow graduate students for their valuable discussions. A special debt of gratitude is due to Professor J.F. King of the Faculty of Chemistry and Dr. A. Mohamed for their valuable help and discussions during the chemical analysis of the compounds and to Professor W. Bulani of the Faculty of Engineering Science for his valuable discussions on the analysis of the kinetic data. Many thanks are due to Mr. A. Ahmed for his editing a great part of the text.

A part of the financial support was made available for this project to Dr. K.A. Shelstad from the Natural Sciences and Engineering Research Council of Canada, a fact which is greatly appreciated. The other part was made possible by

the Graduate School through Dean Chess, for this the author expresses his sincere gratitude and appreciation.

The author is extending his sincere thanks to the individuals in the Faculty of Engineering Science, the Faculty of Chemistry, and at Western in general who had a helpful hand in so many ways, through Store, Shop, Libraries, Laboratories, and Computing Facilities as well as numerous friendly discussions and tolerance.

Special thanks and appreciation are due to my sister Amal and her husband Khalil for their moral and financial support and caring.

Last, but not least, the author wishes to convey his deepest gratitude to his wife Janice for her unspoken, yet obvious, kindness, patience, and understanding.

TABLE OF CONTENTS

LIST OF TABLES

LIST OF FIGURES

NOMENCLATURE

a	radius of corona wire (m)
Δa	thickness of ionized sheath (m)
b	mobility of ions ($m^2/V.s$)
b'	average mobility of a mixture of ions ($m^2/V.s$)
b_o	mobility of ions at 273 K and 101 kPa ($m^2/V.s$)
C_A	concentration of a species A ($kmol/m^3$)
C_{Ao}	initial concentration of species A in feed ($kmol/m^3$)
C's	constants
D	diameter of reactor (m)
D_A	diffusion coefficient (m^2/s)
E_e	electron energy (J)
E_{em}	mean energy of electron (J)
E_c	onset-electric field strength (V/m)
E_o	field strength at the outer boundary of the ionized sheath (V/m)
E_a	thermal activation energy of a reaction (J/kmol)
E_y	energy yield of a reaction (g/kW.h)
$F(I_c,T)$	function defined by equation (7.20)
G'	constant, see equation (7.10)
H	length of reactor (m)
I_c	corona current (A)
I_i	threshold for ionization (eV)
k	rate constant of a reaction
m	constant defined by equation (7.17)
$\dot{m}$	mass flow rate (kmol/s)

m'	mass of gas present in the sample loop (kmol)
M_w	molecular weight (kg/kmol)
n	order of a reaction
n_e	number of electrons
n_2	number of gas molecules
N_i	number of particles of kind i
p	power density (W/m^3)
p_i	rate of energy tranferred from electrons to gas molecules per unit reactor volume (W/m^3)
P	pressure (Pa)
P_u	useful power dissipated in the ionized sheath (W)
p'	probability of an electron to make a collision
q	cross-section of collision (m)
R	radius of reactor (m)
R'	gas constant (8314.3 J/mol K)
T	temperature (K)
t	time of a total experimental run (s)
$\bar{v}_z$	average velocity of gases through reactor (m/s)
v_s	volume of the sample loop (m^3)
v_e	velocity of an electron (m/s)
v_{em}	mean velocity of electrons (m/s)
V_R	volume of reactor (m^3)
V_s	applied voltage to corona wire (V)
V_c	onset-voltage for a corona
V_o	voltage at the outer boundary of ionized sheath (V)
ΔV	voltage drop across the ionized sheath (V)
V_i	coefficient of variation (equation 7.14)

of hydrogen sulphide by air in the presence of corona discharge (the principle on which an electrostatic precipitator is operated) can be very effective to control the emission of these compounds.

Therefore, it was the aim of the present project to investigate thoroughly the oxidation of these sulphur compounds in a flow reactor with corona discharge in order to provide the information required for a sound evaluation of the process.

1.4 NOTE ON UNITS

The International System (S.I.) of Units will be used throughout this thesis for all formulae. For convenience, however, the data presented may be expressed in the appropriate sub-multiples e.g., milliampere and gram or multiples e.g., kilo-Joules and kilo-Pascals.

CHAPTER 1

INTRODUCTION

1.1 INDUSTRIAL GAS CLEANING

The problem of air pollution is one which grows with modern civilization and is generally a direct result of industralization. Industrial growth has caused increasing emission of pollutants such as smoke, dust, fumes, and various gaseous compounds.

1.2 GASEOUS SULPHUR EMISSIONS FROM THE KRAFT PROCESS

A vivid example of the above is the kraft process for pulping wood. An unfortunate consequence of this process is the release of reduced sulphur compounds such as methyl mercaptan and hydrogen sulphide. These compounds are noted for their obnoxious odour at very low concentrations (less than 0.02 ppm [1-4]) and their release, therefore, causes an air pollution nuisance in the vicinity of the pulping mills.

The kraft process for making wood pulp involves cooking wood chips in an aqueous solution containing sodium sulphide and sodium hydroxide. Recovery of these chemicals from the spent liquor is conducted in several steps [4,5]. These

steps provide many points where the malodourous gaseous sulphur compounds can escape to the atmosphere. The main potential sources for the emission of these compounds are summarized in Table 1.1.

Table 1.1 also summarizes values of gas flow rates and malodourous sulphur gas concentration for the various units in a typical kraft mill [3] as well as the temperature and water content of the off-gases from every unit. As indicated, the sulphur compounds are present in concentration no higher than one tenth of one percent. However, due to the large volume of the off-gas streams from the mill, the output rate of these compounds is substantial.

1.3 PRESENT TECHNIQUES TO CONTROL GASEOUS SULPHUR EMISSIONS AT KRAFT MILLS

Widely-used techniques for the treatment of gaseous emissions in kraft mills are liquid scrubbing [6,7] and thermal oxidation [8-12] of the off-gases from different units. Employment of these techniques is reported to eliminate only a little more than 90 percent of the malodourous sulphur compounds normally discharged to the atmosphere [1].

There also are more indirect methods to control the emissions of the above compounds where the sulphur content of the cooking solution is lowered. But these methods were

TABLE 1.1: DATA FOR METHYL MERCAPTAN AND HYDROGEN SULPHIDE AT A TYPICAL KRAFT MILL (500 tonnes pulp/day) [3].

SOURCE	Flow rate m^3/s*	Concentration ppm (v/v)			T K
		CH_3SH	H_2S	H_2O	
Digester (Batch):					
Blow gases	0.02-35	0-10,000	0-1,000	2,070-6,831	338-373
Relief gases	0.02-0.6	10- 5,000	0-2,000	207-1,450	298-333
Digester (continuous)	0 -0.1	500-10,000	10 -300	2,415-4,831	348-423
Washer seal tank	2-6	10-50	0-2	1,035-2,415	328-348
Evaporator hotwell	0-0.2	300-3,000	600-9,000	3,450-6,210	353-418
Black liquor tower exhaust	3-9	0-25	0-10	2,070-2,760	343-353
Recovery furnace	35-70	0-200	0-1,500	1,725-2,415	393-453

* At 273 K and 101 kPa.

abandoned due to their bad effect on paper quality [13].

The above discussion would indicate that high reduction in the emission of methyl mercaptan and of hydrogen sulphide is required in order to achieve the society's goal of odourless industry. This concern in fact raises the question of whether or not new techniques may be implemented in the odour abatement programs in kraft mills.

The problem as it stands is that very large volumes of air at atmospheric pressure contaminated with very low concentrations of odourous sulphur gases need to be treated. A device is required which should operate at atmospheric pressure and possesess a high removal efficiency of the sulphur gases. Futhermore, because of the large volume of gases to be treated, it is desirable that these devices have a minimum pressure drop so that compressor costs are minimized.

Electrostatic pricipitators are widely employed nowadays in industry. Their task is to control emissions of particulates in large flow rates of gases e.g., 200 m /s [14,15,16]. Because there is no packing in these devices the pressure drop across them is minimal.

On the other hand, the studies done by Drossos [17] and Wiseman [18] revealed that oxidation of methyl mercaptan and

of hydrogen sulphide by air in the presence of corona discharge (the principle on which an electrostatic precipitator is operated) can be very effective to control the emission of these compounds.

Therefore, it was the aim of the present project to investigate thoroughly the oxidation of these sulphur compounds in a flow reactor with corona discharge in order to provide the information required for a sound evaluation of the process.

1.4 NOTE ON UNITS

The International System (S.I.) of Units will be used throughout this thesis for all formulae. For convenience, however, the data presented may be expressed in the appropriate sub-multiples e.g., milliampere and gram or multiples e.g., kilo-Joules and kilo-Pascals.

CHAPTER 2

LITERATURE REVIEW

AND

OBJECTIVES OF THE PRESENT INVESTIGATION

2.1 GASEOUS OXIDATION OF METHYL MERCAPTAN

Only a limited amount of work has been published on the gas-phase oxidation of methyl mercaptan and of alkane sulphides in general. The first systematic study in the field was in fact reported in 1959 by Cullis et al [19]. Previous investigations were confined to the photolysis [20,21] and pyrolysis [22,23] of these compounds in the absence of air.

2.1.1 Thermal Oxidation

Cullis et al [19] studied the oxidation of methyl mercaptan with oxygen in a batch reactor over the temperature range of 483 to 533 K. The course of the reaction was followed manometrically. Complete conversion of methyl mercaptan (0.24 initial mole fraction) was obtained at 530 K after 1200 seconds of reaction time. Sulphur dioxide was the main product of the reaction. Carbon monoxide, formaldehyde, methanol, and methane were

also formed but in smaller amounts. In oxygen-lean systems, appreciable deficits of sulphur and carbon were reported. The authors attributed this to the formation of dimethyl disulphide which was undetected (no reason was given for this). In oxygen-rich systems on the other hand, a perfect sulphur mass balance was obtained whereas a deficit of carbon was still observed.

According to the above authors, the formation of sulphur dioxide suggests that the thiol group itself suffers an initial attack and does not merely activate the adjacent methyl group. Furthermore, the authors concluded that the reaction proceeded in a series of chain reactions which involved radical formation.

Harkness et al [24] also studied the reaction between methyl mercaptan and oxygen in a batch reactor made from Pyrex. They found that the rate was very slow below 573 K. At this temperature, the residence time required for a complete conversion of methyl mercaptan was found to depend on the initial concentration ratio of the mercaptan to oxygen. When the ratio was 6:1, a complete conversion of methyl mercaptan occurred in about 7800 seconds. The authors concluded that the main effect of increasing the oxygen concentration was to decrease the induction period of the reaction.

Sulphur dioxide was the chief product of the above reaction. Other products also included carbon monoxide, carbon dioxide, hydrogen, formaldehyde, and methanol. Large deficits of sulphur, particularly at higher initial mercaptan:oxygen concentration ratios, were reported. Also, regardless of this ratio, there were large carbon deficits.

To study the effect of the reactor surface, the above reaction was carried out with Pyrex tubing. No effect was found on the results. It was subsequently concluded that the reaction was homogeneous. Finally, the authors [24] proposed that the reaction takes place in a series of reactions initiated by the formation of methyl radicals.

The oxidation of methyl mercaptan by atomic oxygen was also investigated by several authors. Slagle et al [25], for example, studied the reaction at room temperature in a flow reactor at reduced pressures (266 Pa maximum). The reactants consisted of the mercaptan and a mixture of oxygen atoms and oxygen molecules. The latter mixture was prepared by flowing oxygen through a micro-wave discharge.

No information on the reaction products was provided. However, radicals such as CH_3, CH_3SO, and CH_3SOH were detected by using a photoionization mass spectrometer. Moreover, the authors suggested that other radicals such as HSO, H, or OH were present but could not be detected due to

the low resolution power of the spectrometer used. With excess of oxygen atoms the rate of reaction was found to be first-order in methyl mercaptan with a rate constant of 1.9×10^{-15} $m^3/kmol.s$. A reaction mechanism was also proposed. It consisted of electrophilic addition of an oxygen atom to the sulphur contained in the mercaptan to form an energy-rich complex which decomposed unimolecularly by C-S bond cleavage. Decomposition by breaking the S-H bond was also reported to be possible.

Kirchner et al [26] also studied the kinetics of the above reaction. The study was carried out in a tubular flow reactor. The reactants consisted of methyl mercaptan and a mixture of atomic oxygen in nitrogen. The latter mixture was prepared as follows: a flow of nitrogen was passed through a microwave resonator where about 0.1% of N_2 was split into N atoms. These N atoms and an equivalent amount of NO reacted to produce O atoms and N_2.

With an excess of atomic oxygen the decay of methyl mercaptan was described by a first order equation. In this case, the reaction products identified with high resolution mass spectrometry were water, formaldehyde, hydrogen sulphide, carbon dioxide, and sulphur dioxide.

In mixtures with an excess of methyl mercaptan, the decay of oxygen atoms was also found to be first order. The

reaction products in this case included water, dimethyl sulphide, dimethyl disulphide, and sulphur dioxide. The results showed that the increase in sulphur dioxide was at the expense of the disulphide.

Formation of SOH, OH, and CH_3 radicals was detected by the spectrophotometer used. Accordingly, the reaction was speculated to proceed as a chain of reactions involving these radicals.

The effect of the reactor surface on the reaction also was investigated by the authors [26]. They carried out the reaction in two different reactors, one made from Teflon and the other from quartz. No significant differences were noted in the results obtained from the two reactors over the temperature range examined (303-314 K). Hence, the authors concluded that the reaction was completely a gas-phase reaction in the temperature range tested .

2.1.2 Catalytic Oxidation

Haimsohn et al [27] studied the catalytic oxidation of methyl mercaptan with air. The reaction was carried out in a vertical flow reactor where a mixture of the reactants was passed upward through finely divided fluidized catalyst [U.S. Patent 2,859,249,1958]. With Bauxite (80-200 mesh) as a catalyst (no values of temperature were given), the conversion of methyl mercaptan was high (no figures were

given). Other catalysts such as activated carbon, nickel oxide, cobalt oxide, iron oxide were also examined. In this case, lower conversions of the mercaptan were obtained.

Harkness et al [28] investigated the catalytic oxidation of methyl mercaptan with oxygen in a differential reactor [29]. The effect of temperature on the conversion of methyl mercaptan and on the concentration of the products over the selected catalysts was determined. Metal powders (nickel, iron, aluminum, and cobalt) seemed not to affect methyl mercaptan when the latter was fed by itself to the reactor at 503 K and 0.51 s^{-1} space velocity.

In the presence of smaller amounts of oxygen (no figures were given), methyl mercaptan was found to form dimethyl disulphide as a major product but still large amounts of the mercaptan remained unreacted. When oxidized steel pellets as well as high values of mole fraction of oxygen (up to 0.95) were used in the range of 573-878 K for a space velocity of 0.14 s^{-1}, the mercaptan was converted to sulphur dioxide, formaldehyde, and carbon oxides. The conversion of methyl mercaptan obtained was about 24%.

At temperatures higher than 733 K, the formaldehyde content in the products decreased which was reflected in the increase in the content of carbon dioxide. In the presence of metal (iron,cobalt, nickel, and copper) oxides on silica

sand as catalysts and for a space velocity of 0.52 s , methyl mercaptan was converted to dimethyl disulphide at temperatures below 589 K and to sulphur dioxide when the temperature was higher than 617 K. Water was also a major product while carbon monoxide was produced in small amounts.

A more detailed study was done by the authors [28] using iron oxide on silica as a catalyst. When methyl mercaptan was fed by itself to the reactor at 645 K for 0.52 s^{-1} space velocity both dimethyl sulphide and sulphur dioxide were formed. In the presence of 0.91 mole fraction of oxygen, substantially complete conversion of methyl mercaptan to sulphur dioxide was obtained. This fact, the authors claimed, shows that the excess oxygen supplied from the gas phase was necessary for complete reaction. In the temperature range 453-643 K and for -20+30 mesh catalyst, the activation energy of the reaction was found equal to 50 kJ/mol. Corresponding data for -48+65 mesh catalyst gave activation energy of 38 kJ/mol. Therefore, the authors concluded that diffusion played a role in the reaction.

Studies dealt with the gaseous oxidation of methyl mercaptan and of alkane sulphide in general using catalysts other than the above were also reported in other studies. The catalysts included, for example, carbonyl compounds of monomeric complex of iron [30], iron phthalocyanine complex [31], cobalt tetraphenylporphrintetrasulphate [32]. When

these catalysts were employed, the major product of the reactions was the respective disulphides.

Recently, the reaction between thiols (including methyl mercaptan) and air or atomic oxygen was studied under pressure [33]. The reaction was carried out in an autoclave with initial pressure of 21.6×10^5 Pa, at temperature of about 333 K, and in the presence of cobalt moybdate, aluminum oxide and sodium hydroxide as a catalyst. The conversion of the mercaptans was about 99 weight percent and the major product was the respective disulphide. No more information such as on the initial concentration of the reactants, ,the reaction time or on other products of the reaction was provided.

2.1.3 Photolytic Oxidation

The oxidation of methyl mercaptan under radiation with ultra-violet light was first reported by Raymer et al [34]. The study was carried out in a batch reactor which was a flask fabricated from an ultra-violet transmitting glass. The reaction mixture composed of methyl mercaptan and air was placed in the reactor by injection. The initial mercaptan:air mole ratio was 0.1.

Upon exposing the mixture to ultra violet radiation (2537 $^{\circ}$A) at 301 K, methyl mercaptan was completely oxidized in about 2160 seconds. One of the first products of the

oxidation ,as indicated by the gas chromatography analysis, was dimethyl disulphide. This was oxidized further but no information on the products formed was given. However, mass spectroscopy data obtained on the same reaction indicated that the sulphur in the mercaptan was converted completely to sulphur dioxide.

2.1.4 Oxidation in a Corona Discharge

Drossos [17] investigated the reaction of methyl mercaptan with air in DC corona discharge. The experiments were conducted in a flow tubular reactor made from Pyrex. The grounded electrode was a stainless steel mesh placed against the walls. The high voltage electrode was a fine stainless steel wire stretched along the tube axis. The current and temperature used ranged from 0.2 to 1.6 mA and from 298 to 568 K, respectively whereas the mean residence time of the feed through the reactor was kept constant at 44 seconds. The results reported indicated that a complete conversion of methyl mercaptan was possible for a current of 0.3 mA and at temperature of 298 K.

The main products of the reaction were found to be dimethyl disulphide, dimethyl sulphide, and dimethyl sulphone. Large deficits of sulphur were reported. These deficits were almost 100% in some cases.

An increase in temperature or current was found to

lower the concentraion of dimethyl disulphide formed. Subsequently, it was concluded that this compound was an intermediate product of the reaction.

2.2 GASEOUS OXIDATION OF HYDROGEN SULPHIDE

2.2.1 Thermal Oxidation

The oxidation of hydrogen sulphide by oxygen was first studied systematically by Thompson et al [35]. The reaction was carried out in a batch reactor which was enclosed in a heated medium. Both hydrogen sulphide and oxygen were introduced into the reactor in the range of 473 to 573 K, and 0.22×10^5 to 0.40×10^5 Pa. Moreover, initial mole fraction of hydrogen sulphide in the reacting mixture ranged from 0.32 to 0.34.

The results obtained showed that the reaction took place at temperatures higher than 473 K and according to the equation

$$2H_2S + 3O_2 \rightarrow 2H_2O + 2SO_2 \qquad (2.1)$$

The reaction was speculated to proceed through a chain of reactions involving radicals such as SO and OH. No information on the reaction kinetics was given.

Semenov [36] investigated the chemistry of the above reaction in the temperature range 523-573 K. The reaction

products, as detected by mass spectroscopy, were sulphur dioxide and water. The reaction was believed to consist of several steps in which the metastable SO, detected by ultra-violet absorption spectra, was an intermediate.

Bradly et al [37] studied the same reaction in a shock wave tube within the temperature range 1,350-2,450 K. The authors reported that the reaction proceeded via a branching chain of reactions with intermediates such as SO and OH leading to the final products sulphur dioxide and water. No results on the kinetic results were reported.

The oxidation of hydrogen sulphide by oxygen was also studied by Marsden [38]. The reaction mixture consisting of the above compounds was prepared and then introduced to the reactor, which was initially under reduced pressure, through a quick-opening valve.

The reaction products identified by mass spectroscopy were again sulphur dioxide and water. Intermediates such as H and SO were also detected. No kinetic study was reported.

Recently, a kinetic study on the reaction of hydrogen sulphide and oxygen was published [39]. The reaction was found to be first order in hydrogen sulphide and no more information was offered.

The reaction between atomic oxygen and hydrogen sulphide was investigated by several authors. For example, Singleton et al [40] found that this reaction occured in accordance with the equation

$$H_2S + O \rightarrow HS + OH \qquad (2.2)$$

with a reaction constant equal to 24.1×10^6 m^3/kmol.s at 298 K. The subsequent reactions

$$HS + O \rightarrow SO + H \qquad (2.3)$$

and

$$H + H_2S \rightarrow H_2 + HS \qquad (2.4)$$

were also reported. The hydroxyl radicals generated in the initial reaction may react as follows

$$OH + O \rightarrow O_2 + H \qquad (2.5)$$

which is fast with a rate constant of 24.1×10^9 m^3/kmol.s. No reference to the atomic state of oxygen was given.

In a recent study [41], the kinetics of the reaction of ground state oxygen O (3p1) with hydrogen sulphide was investigated. Atoms of oxygen were prepared by flowing oxygen through a micro-wave discharge. The reaction was carried out within the temperature range 297-502 K and in a flow sysytem. The longest residence time used was 1 second.

The products detected were water, hydrogen, oxygen, and sulphur dioxide. The reaction was proposed to proceed by way of hydrogen abstraction from hydrogen sulphide:

$$O + H_2S \rightarrow OH + SH \qquad (2.6)$$

and also by way of addition of oxygen atoms to hydrogen sulphide followed by decomposition of the adduct to form H and HSO:

$$O + H_2S \rightarrow (H_2SO)^+ \rightarrow HSO + H \qquad (2.7)$$

The SH formed in reaction (2.6) may, according to the authors, be converted to hydrogen sulphide and elemental sulphur. However, no sulphur could be detected.

Several investigations were done on the reaction between hydrogen sulphide and ozone Gregor et al [42] studied the reaction in a batch reactor at ambient temperature and pressure. Ozonized air was prepared in an ozonizer [43] before it was introduced together with hydrogen sulphide to the reactor.

Sulphur dioxide and water were the only products formed. When a large excess of ozone was used, sulphur dioxide was oxidized further to sulphuric acid.

Cadle et al [44] studied the kinetics of the above reaction using a laminar flow, Pyrex tubular reactor at 299, 338, and 373 K. Hydrogen sulphide and ozone were mixed at the reactor entrance, and passed through the reactor tube. Ozone was generated from compressed air with a Welsbach ozonizer and then was further diluted with nitrogen.

The reaction products found were sulphur dioxide and water. Sulphur dioxide was monitored by a calibrated infrared spectrometer. The amount of water formed by the reaction was obtained by passing the product stream through a bed of anhydrous magnesium sulphate and then determining the weight gain in the latter.

The reaction was terminated at any of several points along the reactor by injecting nitric oxide to decompose the remaining ozone by the extremely fast reaction:

$$NO + O_3 \rightarrow NO_2 + O_2 \qquad (2.8)$$

Extent of the reaction of hydrogen sulphide and ozone was measured by photometric determination of nitrogen dioxide. This, assuming the absence of any side reaction involving nitrogen oxides, gave a measure of the ozone remaining at the quench point. Based on the results obtained, the stoichiometry of the reaction corresponded almost to the equation:

$$H_2S + O_3 \rightarrow H_2O + SO_2 \qquad (2.9)$$

Thereupon, three oxygen atoms were utilized per ozone molecule reacted. But the authors were not sure whether all the three oxygen atoms were furnished by ozone. Possibly, they speculated, two of them were molecular oxygen in the feed.

Also, the average order of the ozone was found to be 1.55 and that in hydrogen sulphide was 0.19. In estimating reaction-rate parameters from their data the authors assumed that the reaction taking place was totally homogeneous. Accordingly, the reaction rate was:

$$\frac{dC_{O_3}}{dt} = -7.83 \exp(-4177/T)\, C_{O_3}^{1.5} \cdot \text{kmol/m}^3\text{.s} \qquad (2.10)$$

Suspecting that a wall reaction may have influenced their results, the authors performed additional experiments with the reactor packed with several lengths of Pyrex tubing. They also tested a reactor that had been coated with potassium chloride. Conversions within each system were about double those observed in the original apparatus, indicating the presence of a surface reaction.

Hales et al [45] also measured rates of the above

reaction using laminar flow tubular reactor at 301.5 and 321 K. Hydrogen sulphide in nitrogen and ozone were separately fed to the reactor. (ozone was generated from cylinder compressed oxygen with a OREC O3V1 ozone generator and hydrogen sulphide was introduced into the nitrogen stream with a Hamilton gas-tight syringe.)

The amounts of sulphur dioxide were monitored by a calibrated gas chromatograph while no attempts were made to monitor the amounts of water formed. The authors concluded from the mass balance calculations on sulphur that the reaction proceeded according to equation (2.9).

The reaction was studied in two reactors having different surface-to-volume ratios. (The ratios differed by a factor of 1.5.) The fact that no significant differences in the results from these two reactors obtained indicated the total homogeneity of the reaction. The discrepency between these results and those mentioned above by Cadle *et al* [44] was attributed, according to Hales *et al*, to the use of nitric oxide in quenching reaction (2.9). When a reactor tube was exposed to a dilute solution of nitric oxide and hydrogen sulphide in air, Hales *et al* [45] found that the reactor walls acquired a faint translucent colour. Within one day after exposure, most of the colour disappeared. Hence, these authors concluded that nitric oxide conditioned the reactor walls in such a way that it became

catalytically active.

Finally, the reaction rate was found to follow the equation:

$$\frac{dC_{SO_2}}{dt} = 3.8\times10^{-4}\ e^{3271/T}\ C_{H_2S}^{\frac{1}{2}}\ C_{O_3}^{\frac{1}{2}} \quad kmol/m^3.s \quad (2.11)$$

The difference between this equation and that obtained above by Cadle et al [44] was attributed by Hales et.al., to the thermal decay of ozone at elevated temperatures. These authors found that 4% of ozone decomposed at 321 K which was the highest temperature they used.

2.2.2 Catalytic Oxidation

The reaction of hydrogen sulphide with oxygen is known to readily proceed in the presence of several catalysts. The most common among these are silica gels, silicates (particularly iron silicates), activated carbon, alkali and alkaline earth metals [46]. Other catalysts include aluminum [46], bauxite and molecular sieves [47].

The oxidation reaction of hydrogen sulphide on these catalysts proceeds with an appreciable rate at high temperatures i.e., 523-673 K [46].

The nature of the products of the reaction and its mechanism and rate differ from one author to another depending upon the catalyst and on the experimental conditions employed. It is not the intention here to elaborate on this point. However, the following is only given as an illustrative example.

By using active carbon, Steijens et al [48] found that the primary reaction product was sulphur which may undergo further oxidation at temperatures above 573 K forming sulphur dioxide. In this case, sulphur was considered an intermediate. Above 673 K, the sulphur dioxide itself acted as an intermediate product where it led to the formation of sulphur and water.

Whether sulphur dioxide is an intermediate was also discussed by other workers. The opinion of Brodsky et al [49] and of Cariaso [50] was that this compound was not an intermediate.

On the other hand, elemental sulphur was subject to the same type of controversy. While authors such as Prettre et al [51] stated that this element had catalytic activity, we find others such as Sreeramamurthy [52] who reported that it had none.

The reaction order of hydrogen sulphide was found by

Stijens et al [48] to be 0.79 and 0.23 in the temperature ranges of 503-523 K and 543-563 K, respectively. Screeramamurthy [52] however reported that the reaction order is unity and one-half in hydrogen sulphide and in oxygen, respectively within the temperature range of 303-373 K. Different values of the reaction order are still reported by other authors. Cariaso [50], for instance, concluded that the reaction was first and zero order in hydrogen sulphide and oxygen, respectively.

Several mechanisms were also proposed for the reaction between hydrogen sulphide and oxygen. Accordingly, diversified values were obtained for the activation energy of the reaction, see references [48] and [52] for example.

In the presence of catalysts such as sodium faujasite-type zeolite, Dudzik et al [53] reported that the oxidation of hydrogen sulphide by oxygen could proceed at temperatures as low as 273 K. These authors found that below 293 K, sulphur is the primary product whereas above 293 K they observed substantial amounts of sulphur dioxide (no figures were mentioned). In both cases hydrogen in the sulphide was converted to water. During the course of the reaction, radicals such as S_n, HS_x, O_2^-, SO_2^-, and $H_2S_2^-$ were detected by using electron spin reasonance spectroscopy.

2.2.3 Oxidation in a Corona Discharge

Wiseman [18] examined the oxidation of hydrogen sulphide in AC corona discharge. He primarily tested three types of corona reactors: i) a barrier reactor [54], which consists of glass tube wrapped on the outside by an aluminum foil to serve as the ground electrode. The high voltage electrode is a fine wire stretched along the tube axis, ii) a rectangular duct containing several fine wires. This reactor in fact simulates a wire-to-plate electrostatic precipitator [14], and iii) a point corona reactor which consisted of two parallel flat grids in a gas tight housing. Each grid carried a number of nails (no material was mentioned) uniformly distributed in a square pitch on the supports. All points on each grid were interconnected electrically to form an electrode.

Wiseman found that the last reactor to be more appropriate for use in practice since it was i) less affected by deposits from the reacting gases (no identification of these deposits was given), ii) immune to damage resulting from sparkover between the two electrodes, and iii) inherently cheaper in construction.

The feed to the reactor was a mixture of hydrogen sulphide in air. Hydrogen sulphide in the feed and in the products streams was analysed by a coulometric method [55].

The reaction was studied exclusively at 293 K and in the range 60-1100 ppm initial concentration of hydrogen sulphide. Other experimental conditions included power density (up to $12x10^3$ W/m^3) and a mean residence time from 72 to 777 s.

The results were presented in terms of the amount of hydrogen sulphide oxidized per unit electrical power input. This variable (synonymous to energy yield [54]) ranged from 1 to 9 g/kW.hr depending on: i-the power input (an inverse relation was reported), and ii-interelectrode spacing (an inverse relation was also reported. The maximum energy yield obtained was for interelectrode spacing of 0.018 m).

The energy yield was also found independent of the initial concentration of hydrogen sulphide in the feed, of the mean residence time, and of the surface area of the reactor.

Based on his results, Wiseman found that energy requirements would cost a typical kraft mill about $4.5/ton of pulp. This cost, as reported, was more than 4 times the cost by employing the conventional methods. Therefore, the author concluded that the point corona reactor investigated would not be economically competitive in practice.

2.3 ELECTROSTATIC PRECIPITATORS IN PULP AND PAPER INDUSTRY

2.3.1 Introduction

The electrostatic precipitation process consists of three fundamental steps [16]:

i) particle charging,
ii) collecting of the charged particles, and
iii) removal of the collected particles.

Particle charging in industrial precipitators is accomplished by means of a corona which produces ions and electrons that become attached to the particles. (The fundamentals of the corona discharge process will be discussed in details in the next chapter.)

Electrostatic precipitators are unique among gas cleaning equipment in that the force separating the particulates from the gas stream is applied directly to the particles themselves and hence the energy required to affect the separation is consideribly less than for the other types of gas cleaning equipment. Since the corona discharge is controlled electrically the control system of a precipitator is simpler than those of other equipment and almost instantaneous. Due to the fact that the precipitator is not associated with packing of solid catalysts, the problems related to deactivation, fouling and mechanical handling are eliminated. The absence of packed solids also results in

lowering the gas pressure drop through the precipitator. This drop may be of the order of magnitude of 248 Pa as compared to pressure drop of 2,480 Pa to 248,000 Pa for scrubbers and filters [16]. This fundamental advantage of electrostatic precipitation has resulted in its widespread use in applications where large gas volumes are to be handled and high efficiencies are required for particle collection.

Electrostatic precipitators are commonly found in one of two basic forms. Referring to Figure 2.1a [58], the simpler precipitator comprises a grounded cylinder (the collecting electrode) and coaxial with it a high potential wire (synonymous to the corona wire). This is the wire-pipe (or cylinder) type precipitator. An alternative basic design is the duct type, shown in Figure 2.1b. It consists of two grounded parallel plates (the collecting electroded) together with an array of parallel discharge wires mounted in a plane midway between the plates. Gas to be cleaned is passed either through the pipe or between the plates through the duct.

2.3.2 Typical Data of Electrostatic Precipitators

Electrostatic precipitators are used in the pulp and paper industry primarily to control emissions of the particulate material present in the off-gas from the black liquor recovery furnace [15,59].

For a typical electrostatic precipitator used in pulp mills, the following characteristics are available:

Duct width	= 0.2-0.3	m
Collecting area	= 500-1000	$m^2/1000m^3$
Average corona current	= 0.007-0.03	$A/100\ m^2$
Average corona energy density	= 100-500	J/m^3
Gas velocity	= 1.2-1.5	m/s
Length of precipitator	= 6	m
Height of precipitator	= 3	m
Width of precipitator	= 0.25	m

2.3.3 Calculation of the mean Residence Time of gases through Electrostatic Precipitator

Incorporating the above information with those flow rate of off-gases from a typical kraft mill (see Section 1.2), the mean residence time of gases through an electrostatic precipitator may be evaluated. As illustrated in Appendix A, this variable is in the order of magnitude of 5 seconds.

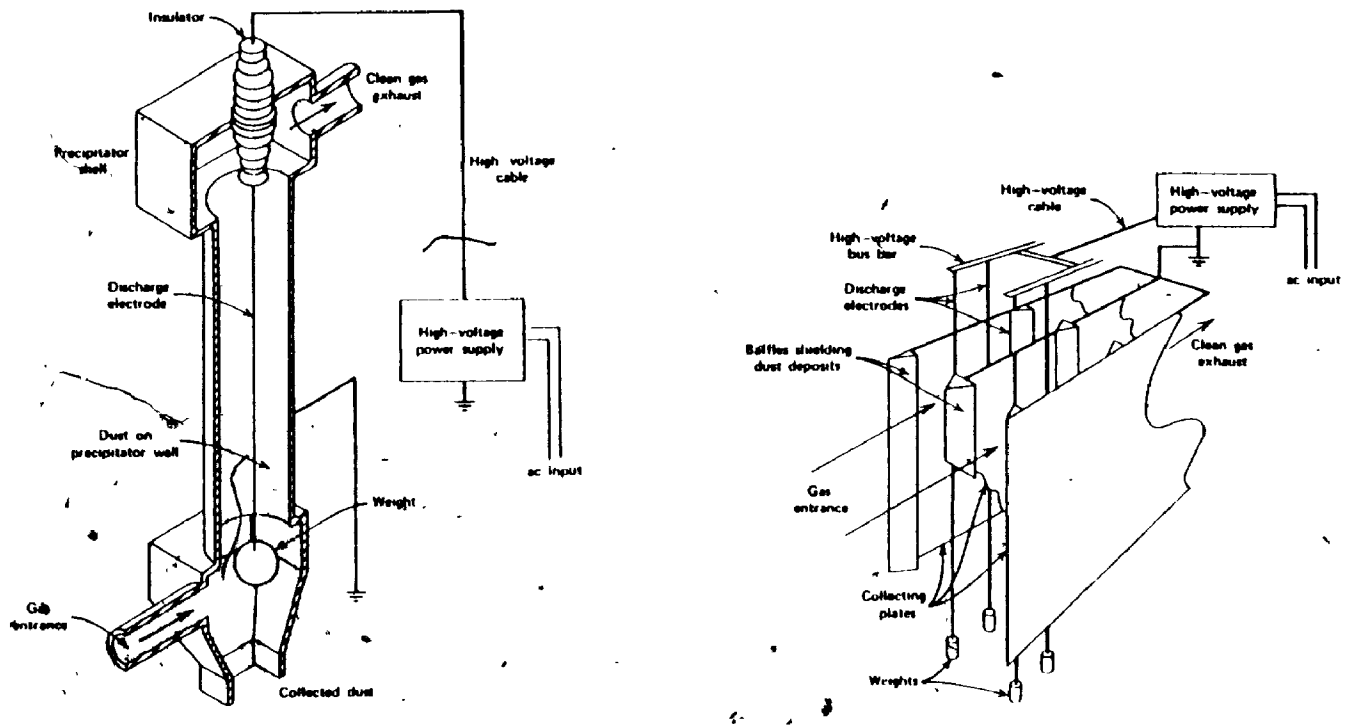

a) Wire-cylinder type.

b) Duct type.

Figure 2.1: Single-stage electrostatic precipitators [58].

The above value of the residence time can be increased by using a longer precipitator. The maximum length limit of an electrostatic precipitator is, however, about 18 m [58]. According to the above calculations, this height will allow t to reach a value as high as 15 seconds. A typical residence time will, therefore, range from 5 to 20 seconds. Longer times will be however tried to cover possibilities of future development.

It should be noted that the odourous sulphur compounds are still present in the off-gases despite their passing through an electrostatic precipitator [4]. This may seem to be in contradiction with the results mentioned above, particularly by Drossos [17], that a corona discharge completely removed methyl mercaptan from air.

An answer to this disagreement may be low values of current density used in electrostatic precipitators. (Typically, an electrostatic precipitator employs current density from 7 to 30 mA/100m^2 [58] whereas the values used by Drossos [11] were in the range of 1639 to 2459 mA/100 m^2.)

2.4 OBJECTIVES OF PRESENT STUDY

Based on the discussion given above, a research investigation was undertaken, the results of which are presented in this thesis. The primary obectives of the study can be outlined as follows:

1. A complete analysis of the reaction of methyl mercaptan and of hydrogen sulphide with air in a D.C. corona discharge. The parameters of importance are identified and reaction rates are measured.

2. Generation of data which might be used for industrial purposes. These data will be concerned with the energy and volume of equipment requirements of the process.

CHAPTER 3

CORONA DISCHARGE IN GASES

3.1 INTRODUCTION

A primary requirement for the electrostatic precipitation process is the generation of large quantities of electrons and of gas ions for charging the particulate material. In industrial precipitators, this generation process is accomplished by means of a gaseous discharge called a corona.

The physics of a corona discharge has been investigated extensively because of its importance in high-voltage transmission and plasma. The work of Loeb [60] and that of von Engel [61] provide a considerable background of information on this subject. Unless otherwise stated, these two manuscripts will furnish the basis of this chapter.

3.2 PHYSICS OF THE CORONA DISCHARGE

Gases at moderate temperatures are composed essentially of uncharged molecules. The only charge carriers present are the few electrons or ions produced by cosmic rays and radio-active decay processes.

Consider a system consisting of two electrodes immersed

in a gas such as atmospheric air, one electrode is a fine wire and the other is a coaxial cylinder. If a sufficiently high voltage is applied to the wire, the electric field near the wire surface will correspondingly be high. Electrons within this high-field region (synonymous to the ionized sheath) will be accelerated to high velocities because of their small mass and of their high electrical mobility. The energy of these electrons is sufficient to release additional electrons on impact with neutral gas molecules creating further additional positive ions and free electrons. Each of the additional electrons is accelerated to cause further impact ionization. The process is repeated over and over so that large quantities of electrons and ions are generated within the corona region. The gas at this partial break-down becomes able to conduct electricity.

If the central electrode is negative (i.e., negative corona), positive ions move toward it and electrons move toward the grounded electrode. For reversed polarity (i.e., positive corona), the opposite is true.

3.2.1 Avalanche Process and Ionization Potential

The avalanche process of producing electrons and positive ions is governed primarily by the ionization potential of the gases present in the electric field near the discharge electrode. To initiate the corona process, electrons must possess sufficient energy to release an

electron from a gaseous particles on impact. Ionization potentials of the various gases of interest in the present investigation are given in Table 3.1.

Each collision between an electron and a gas molecule does not necessarily produce ionization because of the variation of energy transfer upon every impact.

3.2.2 Electron Attachment

Beyond the corona region, the magnitude of the electric field rapidly diminishes to the point that electron velocities between the collisions are no longer sufficient for further ionizing impacts.

Collisions between electrons and molecules of electronegative gases such as oxygen result in the capture of the electrons by the molecules to produce negative ions. Table 3.2 shows (on a statistical basis) the coefficient of attachment and the average number of collisions the electron must make before attaching itself to a neutral molecule for several gases of interest.

The current that would result from the flow of a given number of ions depends upon the ion mobility in addition to the strength of the electric field. Since the ion mobility depends on the size and mass of the parent molecular species, the current would depend on the concentration and

electronegativity of the gases as well. Mobilities of gases of interest to us are given in Table 3.3

In a mixture of gases, the average ion mobility b' may be estimated from the relation [63]:

$$b' = \sum_i n_i b_i \qquad (3.1)$$

where b_i and n_i denote the mobility of ion i and its mole fraction, respectively.

Beyond the ionized sheath, there is a space charge formed from ions which are opposite in sign to that of the applied voltage to the central electrode. This space charge is necessary to stabilize the corona by bringing about an equilibrium condition between the electric field and the electrons produced by multiplication.

3.2.3 Positive and Negative Coronas

A schematic representation of the positive corona discharge in the coaxial cylindrical geometry is given in Figure 3.1a. In this case, the wire is raised to a positive DC high voltage. The high electric field present initiates a Townsend avalanche in which electrons are produced. The original and newly generated electrons are drawn to the wire and neutralized while the slower positive ions are repelled towards the ground electrode. The positive ions constitute

TABLE 3.1: IONIZATION POTENTIAL OF GASES OF INTEREST [16]

Gas	Ionization potential eV
Nitrogen	15.4
Oxygen	12.2
Water vapour	12.6
Hydrogen sulphide	10.5
Methyl mercaptan	9.4 [62]
Sulphur dioxide	13.1

TABLE 3.2: COEFFICENT OF ATTACHMENT [16]

Gas	η'
Nitrogen	infinity
Oxygen	8.7×10^3
Air	4.3×10^4
Water vapour	4.0×10^4
Sulphur dioxide	3.5×10^3

TABLE 3.3: MOBILITY OF SINGLE CHARGED GAS ION* [16]

Gas	Mobility $m^2/s.V$ β_0 (-)	β_0 (+)
Nitrogen	No attachment	1.8
Oxygen	2.60	2.20
Air	2.50	1.80
Hydrogen sulphide	0.56	0.62
Water vapour	0.95	1.10
Sulphur dioxide	0.41	0.41

* At 273 K and 101 kPa.

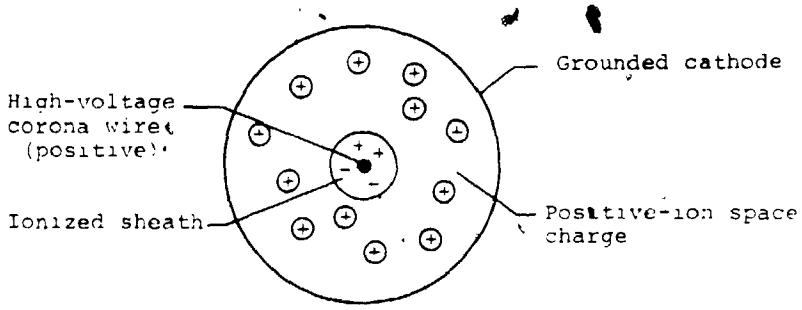

a) Positive corona

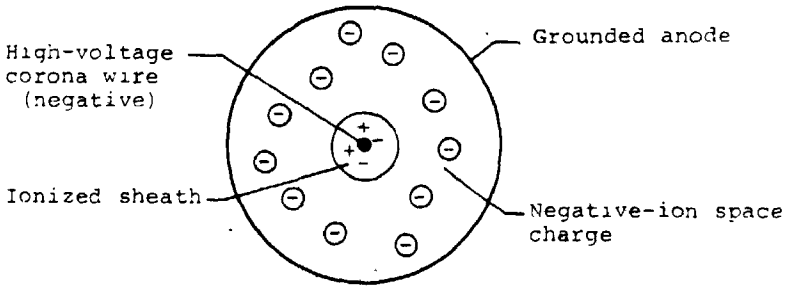

b) Negative corona

Figure 3.1: Corona discharge in coaxial cylindrical geometry

the space charge between the wire and the cylinder. The positive corona appears visually as a uniform glow surrounding the discharge wire.

In the case of negative corona discharge, schematically given in Figure 3.1b, the wire is raised to a negative DC high voltage. A Townsend avalanche is initiated as in the positive corona, but the positive ions are drawn to the wire while the electrons are repelled towards the cylinder. The negative corona appears visually as a series of localized tufts of discharge on the wire.

3.2.4 Corona Wind

This phenomenon designates the gas movement induced by the movement of ions between the two electrodes in the corona system. Little is known regarding the characteristics of the corona wind. Observed corona-wind velocities are of the order of 1 m/s [58,60,64,65] and negligible with respect to the ion velocity.

Continuity of flow was accounted [58] for by postulating a rapid, directed movement of gas molecules from the discharge electrode, balanced by a relatively slow return flow.

Under electrical and flow conditions similar to those that often prevail in practice, the electrical wind in

general appears to make an appreciable contribution to transverse gas flow. From the view-point of conducting chemical reactions, the electric wind is then highly beneficial as it provides an excellent means of mixing the reacting species.

3.3 CORONA-ONSET CONDITIONS

The field strength at which a corona begins has been studied extensively by Peek [66]. He, followed by other authors as well, showed semi-empirically that the onset of a corona in air or in gases in general occurs at an electric field strength E_c defined as:

$$\text{Eq.} \quad E_c = C_1\delta + C_2(\delta/a)^{\frac{1}{2}} \tag{3.2}$$

where a (m) is the radius of the corona wire and C_1 and C_2 are constants to be determined by experiment. Here δ, the relative density of the discharge gas, is:

$$\text{Eq.} \quad \delta = \frac{T_o P}{T P_o} \tag{3.3}$$

where T_o and P_o are conventionally equal to 273 K and 101 kPa and T (K) and P (kPa) are respectively the temperature and the pressure of the gas for which δ is calculated.

The corona-onset voltage V_c in a coaxial cylindrical system may be obtained from:

$$V_c = a\, E_c\, \ell n(R/a) \qquad (3.4)$$

in which R (m) is the inside radius of the grounded electrode.

3.3 VOLTAGE-CURRENT CHARACTERISTICS

It has been shown [16] that for the same system dimensions and gas conditions, the corona voltage-current relation is:

$$\frac{V_s - V_c}{V_c}\, \ell n(R/a) \simeq (1 + \phi)^{\frac{1}{2}} - 1 - n\frac{1 + (1 + \phi)^{\frac{1}{2}}}{2} \qquad (3.5)$$

where V_s (volt) is the applied voltage to the central electrode. The quantity ϕ is defined by:

$$\phi = \left(\frac{R}{E_c a}\right)^2 \left(\frac{I_c}{2\pi H \varepsilon b'}\right) \qquad (3.6)$$

in which I_c (A) is the current, H (m) is the height of the grounded electrode, ε (8.85×10^{-12} F/m) is the permittivity of free space, and b' ($m^2/V.s$) is the average mobility of ions in the discharge.

It is found experimentally that the mobility of ions moving in a gas is inversely proportional to the gas density over a wide temperature-pressure range [67]. Thus:

$$b' = \frac{b'_o}{\delta} \qquad (3.7)$$

where b'_o is the mobility at 273 K and 101 kPa.

The effect of adding a relatively low-mobility constituent to a high-mobility gas (e.g., water vapour to dry air) on the voltage-current characteristics of corona discharge in air is illustrated in Figure 3.2. As indicated, this effect becomes less important for values of the applied voltage near that of the onset-voltage.

3.5 THE TOWNSEND THEORY

Townsend's theory [67,68] was proposed to explain the variation of current with voltage for corona discharges from a fine wire placed coaxially in a grounded metal cylinder.

According to the theory, all ionization takes place within a cylindrical sheath (synonomous to the ionized sheath as referred to earlier). The ionized sheath has a radius a_o which does not depend on the applied voltage and depends only on the wire curvature and the density of the discharge gas. Awad and Castle [69], based on the Townsend theory, have developed and experimentally verified that the thickness Δa of the ionized sheath may be expressed as:

$$\Delta a = 0.03(\delta a)^{\frac{1}{2}} - a(1 - \delta) \quad \text{m} \qquad (3.8)$$

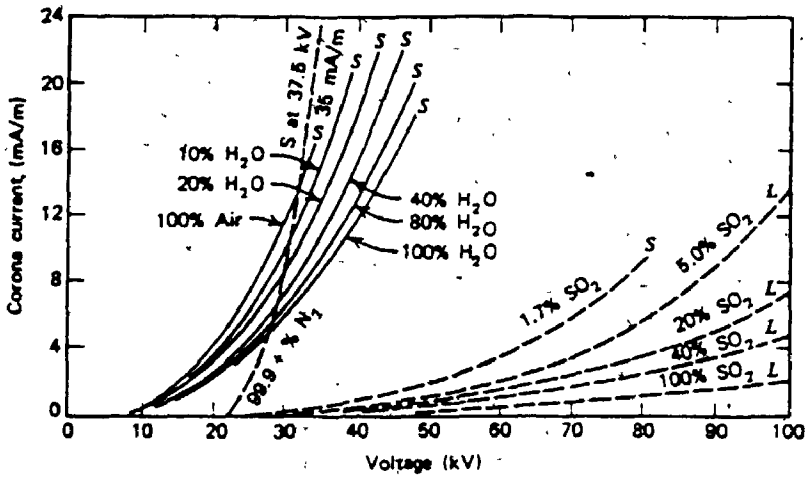

Figure 3.2: Negative corona current-voltage characteristics: the effect of adding to the gas a constituent of relatively low mobility. L designates the limiting voltage of the power supply and S sparkover [58].

It can be shown using this equation that Δa is very small. Then, it can be assumed that the average electrical field strength $\bar{E}$ in the sheath is [69]:

$$\bar{E} = (E_c + E_o)/2 \qquad (3.9)$$

where E_o is the critical field strength at which cumulative ionization results in break-down of the discharge gas. For air at atmospheric pressure E_o must approximately be equal to 3×10^6 V/m [68-70].

Moreover, the theory states that the voltage drop ΔV across the ionized sheath is constant and may evaluated from [69]:

$$\Delta V = \bar{E}\, \Delta a \qquad (3.10)$$

3.6 BASIC REACTIONS IN A CORONA DISCHARGE

Free electrons formed in a corona discharge do not possess the same energy. In fact, the distribution of electron energy may be approximated by a Maxwellian distribution [60,61,71,72]. Accordingly, there are several methods by which electrons can lose their kinetic energy upon impact with gaseous particles. The following information was extracted mainly from the work by von Engel [61].

Molecules can absorb energy from impacting electrons in four modes: translational, vibrational, rotational, and electronic. The translational mode is unimportant due to the mass disparity between an electron and a gaseous species.

The importance of the other modes depends on both the molecular structure of the gaseous species and on the electron energy. The dependency on the electron energy comes from the fact that energy transfer to these modes is quantized.

Each collision between an electron and a molecule does not necessarily result in a reaction, there exists a probability for every particular process and this probability is a function of electron energy. A convenient way to express reaction probabilities is to use the concept of the "cross-section" defined as follows: the frequency of collisions between electrons and molecules (in unit volume containing n_e electrons and n_m molecules) is $n_e.n_m.q.v_e$ [73] where q (m^2) is the cross section of a molecule and v_e (m/s) is the velocity of an electron.

According to the cross-section concept, the meaning of cross section is specialized so that q denotes a value which, upon substitution into the above expression, yields not the total frequency of collisions but the frequency of

collisions for a particular reaction. Hence, a given molecular species has several cross sections, one for each reaction. Furthermore, each cross section varies with electron energy in the same way as the probability of a reaction, since the two are directly linked. Since electrons have a continuous distribution of energy the production rate for a particular species must be calculated by carrying out the integration over the whole range of energy.

There are data published on cross sections for different processes which may be experienced by nitrogen and by oxygen. Based on these data, Dalgarno [72] concluded that, for electrons with mean energies above about 1.6x10 J (i.e., 1 eV), rates of energy transfer by electrons impacts with these gases to the vibrational and to the rotational modes may be negligible. This conclusion may also be extended to include other gases as well [74,75].

The elimination of all but the electronic mode constitutes a significant simplification which can now be made in the analysis of particle interactions in corona discharges.

Energy transfer from electrons to neutral ground state molecules through the electronic mode produces a variety of ionized and of excited species. Each of these species is

assigned a certain threshold value for electron energy below which the species cannot be formed. Experiment has shown that above this value, the probability of ionization and of excitation on collision increases rapidly to a maximum and then rather slowly falls away. Electrons in the discharge are generally more effective in producing excitation than ionization. The reason for this phenomenon lies in the fact that the maximum values of the cross-section for excitation rather than for ionization are in a lower electron energy region closer to where the maximum energy distribution of the electrons in a discharge occurs [75].

The first process which can occur at the lowest electron energy is that of electron attachment so as to form negative ions:

$$XY + e \rightarrow XY^-$$

Electron attachment occurs at energies of the order of magnitude of 5.8×10^{8} - 6.6×10^{8} J/kmol (i.e., 6-7 eV) or less [75] and is, therefore, likely to take place at reasonable efficiencies in the discharge. The probability of electron attachment is expected to increase with increasing electronegativity of gaseous species and with the decrease of the electron energy. The reason for the latter is because the electron would remain for a shorter time within the range of the molecular field.

At higher electron energies 9.7×10^8 - 13.5×10^8 J/kmol (i.e., 10-14 eV), a positive molecule can be formed:

$$XY + e \rightarrow XY^+ + 2e$$

Collisions between electrons and gas molecules may also raise the latter into electronic excited states provided that the energy of electrons is equal to or higher than the threshold of excitation:

$$XY + e \rightarrow XY^* + e$$

Molecules in these states are unstable or at best metastable. Left alone, they return to their initial configuration, the excess energy being emitted as radiation. The lifetime for emission of radiation is usually of the order of 10^{-8} to 10^{-9} s, but in many cases it may be as long as 10^{-3} s [76].

These times are fairly long when compared with collision times so that there is sufficient time for collisions with other chemical species in the mixture before excitation energy is lost. For comparison, an oxygen molecule in air at 273 K and 1.01×10^5 Pa makes about 5×10^9 collisions per second [61].

An electron in an excited molecule is raised to a state

in which it is less strongly bound to the molecule. Since the chemical behaviour of molecules depends on their most weakly bound electrons, the excited molecules are obviously more reactive than the parent ground-state molecules. An important reason for this reactivity is that [76] the excited electron, and the one left behind in the orbit from which it was excited are no longer paired (in the ground state the bound electron are paired). Upon approaching any other species, this configuration lowers the potential barrier energy of the system so that a reaction may occur more readily.

3.6.1 Reactions of the Products Formed by Electrons Impact with Neutral Molecules

The energy imparted from electrons during the processes mentioned above may be dissipated through several processes, mainly dissociation and ion-molecule and ion-ion reactions.

3.6.1.1 Dissociation

Certain of the excited and ionized states formed have enough energy to overcome the bound strength of the molecule and thus can dissociate:

$$XY^- \rightarrow X + Y^- \quad \text{or} \quad \rightarrow X^- + Y$$

$$XY^+ \rightarrow X + Y^+ \quad \text{or} \quad \rightarrow X^+ + Y$$

These reactions may occur at electron energy in the order of 5.8×10^8 to 6.8×10^8 J/kmol (or 6 to 7 eV) [72], 9.6×10^8 to 13.5×10^8 J/kmol (or 10 to 14 eV) [72], and 3.7×10^8 to 4.8×10^8 J/kmol (or 4 to 5 eV) [77], respectively. However, it is found that molecules with energies less than 7.8×10^8 J/kmol (or 8 eV) do not usually dissociate [78]. The reason for this is that dissociation is the result of accumulation of large amounts of energy in the vibrational mode [74,78], whereas this mode was found negligible compared with the electronic mode in a corona discharge. For dissociation to occur there should therefore be a transfer of energy from the electronic mode to the vibrational mode. This process is also found inefficient since dissociation must compete with radiation which is a relatively rapid process [76] and since both the two modes are quantized so that the energy transfer is usually very slow [61].

In general, then, dissociation can be eliminated as an important mechanism by which ionized and excited gaseous species can lose their energy.

3.6.1.2 Ion-Molecule Reactions

Two classes of ions are formed by electrons upon impact with neutral molecules, positive and negative ions. Reviews on reactions involving these two types of species are given by Fite [79], Ferguson [80], and Spedding [75].

Positive rather than negative ions are known to be reactive in a corona discharge. The reason for this is that negative ions have lower binding energy than the parent molecules whereas the reverse is true for positive ions [76,81]. However, due to the high values of ionization potential for molecular species (see Table 3.1 above) and to the relatively low electron energy in the discharge, the concentration of positive ions formed is so low that reactions involving them are likely to be negligible [61].

3.6.1.3 Ion-Ion Reactions

The most possible mechanism by which an ion-ion reaction may occur is the recombination of unlike-sign ions. The result is that two neutral molecules or atoms are formed. Since, in a corona discharge the two types of ions are usually segregated (each type is attracted to the opposite-sign electrode), the probability of their collision and thus of their reaction is so minute that it may be negligible. In the ionizing sheath, however these two types of ions co-exist, they move with such high velocities that they have a minute probability to react [75].

3.7 SUMMARY

The physics of a corona discharge and the reactions that occur therein were reviewed. Such a discharge comprises two regions: the ionized sheath and the space charge region. The ionized sheath is formed around the corona wire while the space charge region is present between the outer boundary of this sheath and the grounded electrode of the system. Electrons having high energy are present only in the ionized sheath. Upon impact with these electrons, gaseous molecules were found to absorb energy, mainly, in the electronic mode. As a result, a variety of ionized and excited species are produced.

The thickness of the ionized sheath and the voltage drop across it were found to depend only on the radius of the corona wire and the density of the discharge gas (equation (3.8)). The voltage-current characteristics in a corona discharge in a wire-cylinder system can be described by equation (3.5).

Furthermore, the corona wind induced by the movement of the ions in the discharge was reported to provide excellent means of mixing of the species present in the discharge.

CHAPTER 4

EXPERIMENTATION

4.1 INTRODUCTION

The chemical reaction studies discussed in the present investigation was made in a reactor which was designed to utilize DC corona discharge. The reactor was supplied with the feed mixture whose composition, temperature, and flow rate were kept constant during each experimental run. The feed and the product streams were sampled and their composition was analyzed by gas chromatography.

The first part of this chapter is devoted to a description of the apparatus. This is followed by a discussion on the experimental procedures used in conducting the reactions as well as in the identification of their products. A study on the voltage-current characteristics will also be presented.

Calibration procedure of the gas chromatograph for the reactants and for the products of the reactions will also be described. Then, samples of mass balance calculations around the reactor are presented so as to ensure the validity of the analytical procedure using the gas chromatograph.

4.2 DESCRIPTION OF THE EXPERIMENTAL APPARATUS

The experimental arrangement used in this study is schematically shown in Figure 4.1. Photograph of the overall arrangement is given in Figure 4.2. The apparatus may be divided into four main parts: the first part dealing with the preparation of the reaction mixture, the second dealing with the reactor and the corona discharge system, the third part covers the temperature control of the reactor, and finally the fourth part describing the gas chromatograph system which was the principal analytical tool in the study. Each of these parts will be described below.

4.2.1 The Reaction-Mixture System

The reaction mixture was composed of the sulphur compound (either methyl mercaptan or hydrogen sulphide) in a dilute mixture with nitrogen and air.

Methyl mercaptan and hydrogen sulphide were provided in lecture bottles from Matheson of Canada Limited with a liquid purity of more than 99.9%. Nitrogen and air, research grade (purity of 99.99 percent), were supplied in pressurized cylinders from Canadian Liquid Air Limited.

During the course of the experimental study (as shown later), the chromatographic analysis of any reaction mixture (consisting of air, nitrogen, and either methyl mercaptan or hydrogen sulphide) indicated that no other compounds were

Legends:

1- Electrostatic voltmeter.
2- Reactor.
3- Furnace.
4- Potentiometer.
5- Ammeter.
6- D.C. high-voltage supply.
7- By-pass valve (V1).
8- Sample loop (S).
9- Sampling valve (V2).
10- Gas chromatograph.
11- Mixing chamber.
12- Integrator.
13- Air rotameter (R1).
14- Sulphur compound/ nitrogen mixture rotameter (R2).
15- Lecture bottle (B).
16- Printer.
17- Recorder.
18- Pressure regulators.
19- Helium and sample.
20- Helium.

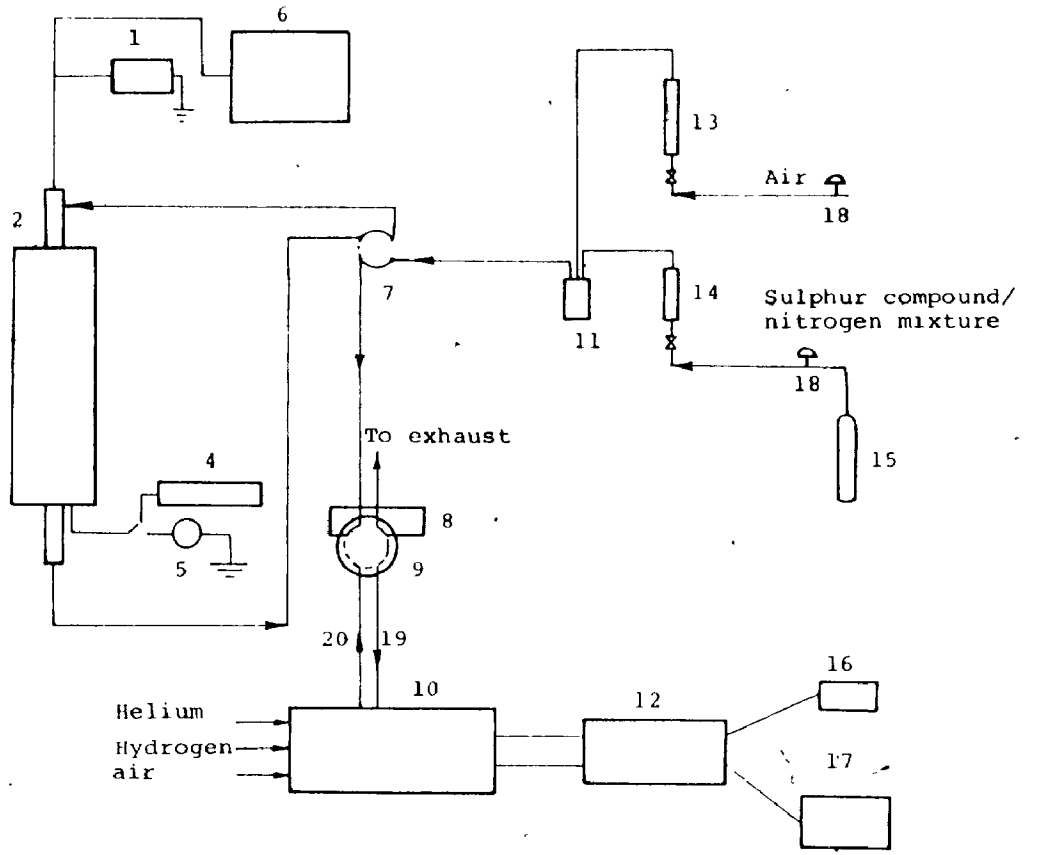

Figure 4.1: Schematic digram of the experimental arrangement.

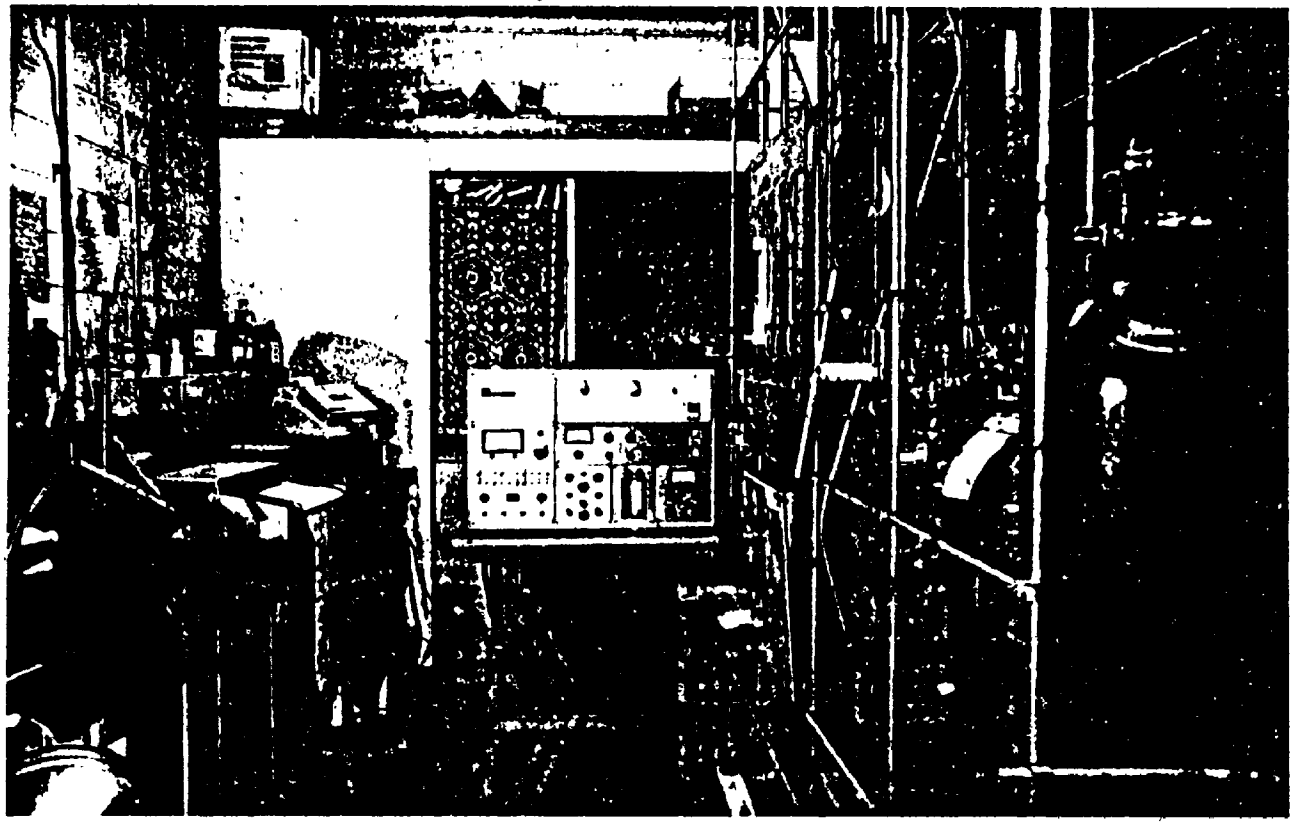

Figure 4.2: Photograph of the overall arrangement of the experimental apparatus.

present in significant quantities. Therefore, these gases were used without further purification.

A mixture of the sulphur compound (either methyl mercaptan or hydrogen sulphide) was prepared in the stainless steel bottle shown in Figure 4.1. This was done by first injecting the sulphur compound by a Hamilton gas-tight syringe (manufactured by Gas Chromatograph Company of Canada Limited) into the bottle and then by pressurizing the bottle with the nitrogen gas. Both the amount of the sulphur compound and the pressure of the nitrogen gas were adjusted so that the mixture formed was within the desired range of composition. The preparation procedure is discussed in details in Appendix B.

Referring to Figure 4.1, two streams, one of sulphur compound and nitrogen mixture and another of air, were regulated by precision rotameters and precision needles valves and directed separately into the mixing chamber. The combined stream then formed the reacting mixture.

The rotameters mentioned above were designed for low flow rates. They were supplied by Fisher and Porter Canada Limited and their specifications are given in Appendix B. The rotameters R1 and R2 were calibrated by means of a standard soap bubble flowmeter provided with the gas chromatograph instrument. The calibration procedure and

curves standarized at 101 kPa and 293 K are given in Appendix B.

The feed stream was made first to pass through the 4-port by-pass valve which was used to direct the feed mixture either to pass through or by-pass the reactor.

4.2.2 The Reactor and the Power Supply System

As schematically and photographically shown in Figures 4.3 and 4.4, respectively, the reactor vessel was a vertical Pyrex tube 0.66 m long with an inside diameter of 0.0254 m. Connecting pieces sealed to the tube by O-rings and clamps were used to bring the feed gases in at the top and to remove the product gases at the bottom.

The reactor was fitted with a co-axial stainless steel wire 0.03 mm in diameter. It was attached at the top to a stainless steel rod 4 mm in diameter which was supported at the top of the reactor by a Teflon insulator. The wire was held taut by a stainless steel weight covered with a Teflon layer for electrical insulation. This wire served as the high potential electrode for the electrical system of the reactor.

The grounded electrode of the system was made of stainless steel mesh with a 152.4 mm length and 79.8 mm width and was fitted to the inside surface of the reactor

Legend:

1- Stainless steel rod.
2- Teflon seal.
3- Reactor entrance.
4- O-rings.
5- Corona wire.
6- 50-mesh stainless steel gauze.
7- Iron/constantan thermocouple; the iron side was grounded.
8- Cylindrical weight (stainless steel).
9- Reactor exit.

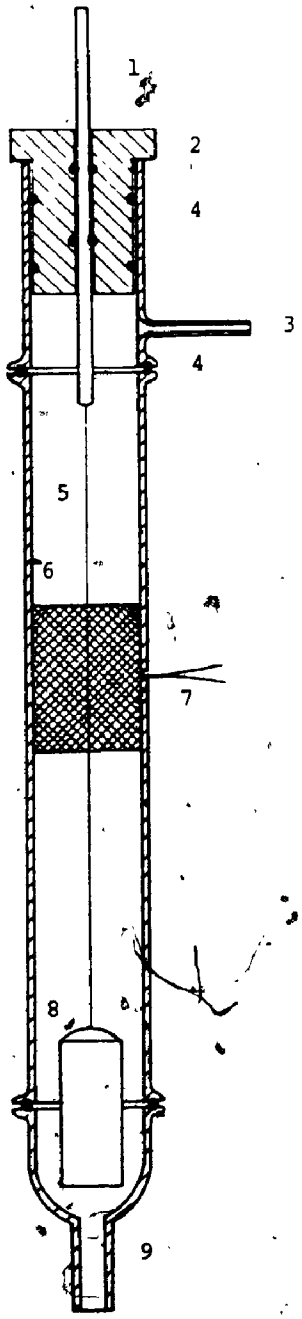

Figure 4.3: Corona flow reactor.

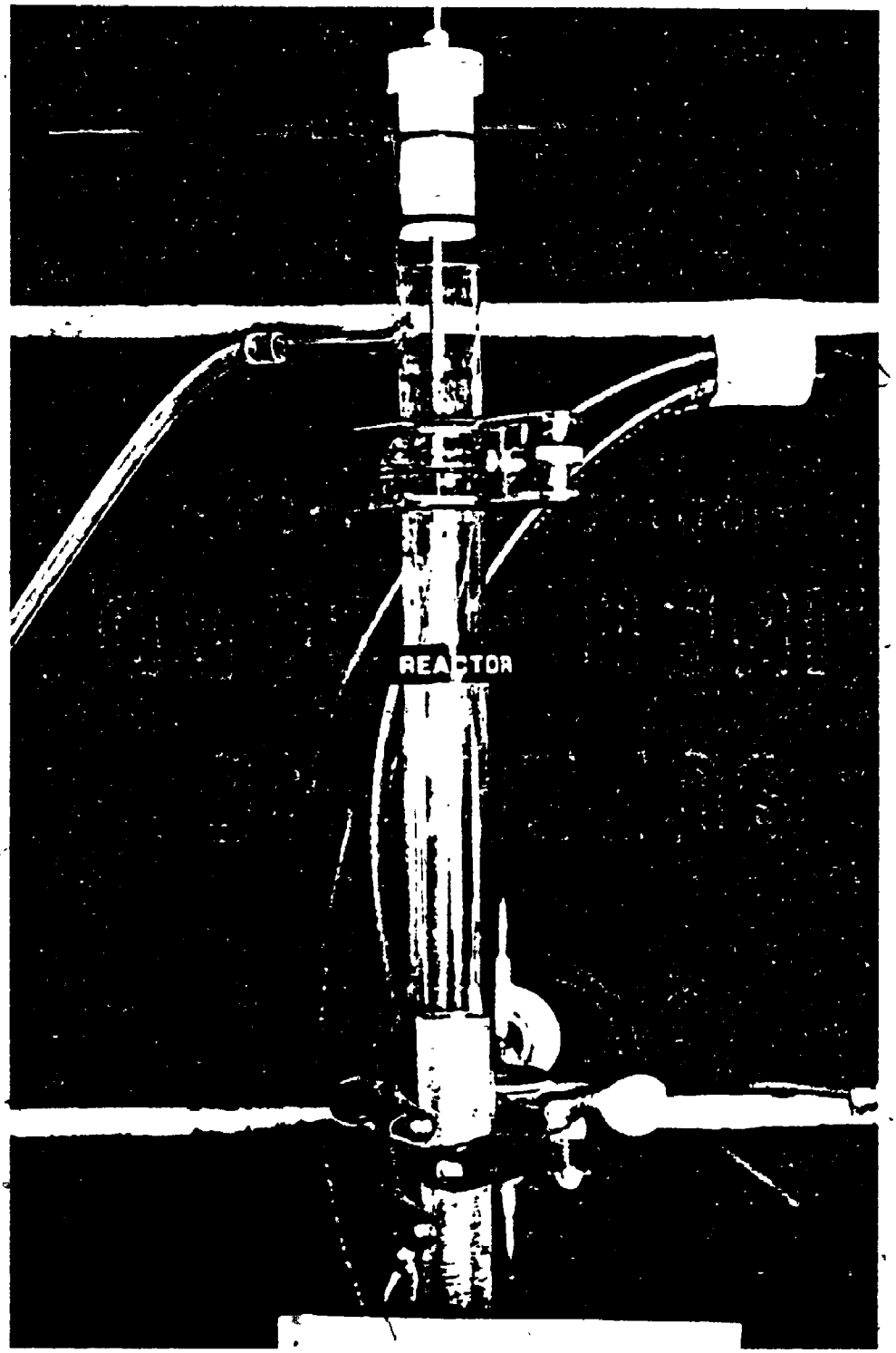

Figure 4.4: Photograph of the corona reactor.

tube. The cylindrical volume of the tube of which the mesh constituted the shell was equal to 77.22×10^{-6} m^3.

The junction of an insulated iron-constantan thermocouple was soldered to the mesh surface facing the reactor vessel walls. The thermocouple leads were allowed to pass through a tiny hole made in the reactor walls. The tiny hole was then filled with silicon seal so as to seal the reactor off from the environments. This seal also insured that the thermocouple was measuring the surface temperature of the mesh and accordingly that of the reactor (see below). The iron side of the thermocouple was grounded so as to also ground the stainless steel mesh.

The central electrode was connected from the top to a DC power supply (Model BAL 32-25, Universal Voltronics) with a capacity up to 32 kV and 25 mA.

The applied voltage V_s was manipulated so as to give the required current I_c. Both V_s and I_c were monitored using the meters provided on the control panel of the power supply. Readings of the two meters were calibrated by a sensitive research electrostatic voltmeter (manufactured by Dimond Pivoted Company, USA) and digital multimeters (Simpson Model 465), respectivly. Current and voltage measurements were accurate to 1% and 1.5% of full scale, respectively.

4.2.2.1 Preliminary Testings of the Voltage-Current Relations

The objectives of this section were to investigate the voltage-current relationship and to correlate their data which were obtained under the present operating conditions. Such a study, as will be shown in Chapters 7 and 8, was required in order to correlate the data obtained for the reaction of methyl mercaptan and of hydrogen sulphide with air.

i) Voltage-Current Characteristics

Table 4.1 summarizes a sample of the average voltage-current measurements taken during the present investigation. As indicated, the voltage-current characteristics were not influenced by the presence of the sulphur species or any other species such as water, for instance. This was due to the extremely low concentration values of these species in the mixtures so that their effect on the total mobility of the charged particles in the system and on the current values was minimal.

Moreover, Table 4.1 shows that:

a) the residence time of the gases passing through the

TABLE 4.1: VOLTAGE-CURRENT MEASUREMENTS
UNDER DIFFERENT OPERATING CONDITIONS

T	C_{A_o}	τ	I_c	V^*_{s+}	V^*_{s-}	I_c	V_{s+}	V_{s-}	I_c	V_{s+}	V_{s-}	I_c	V_{s+}	V_{s-}
K	kmol x 10^6 / m^3	s	mA	kV	kV	mA	kV	kV	mA	kV	kV	mA	kV	kV
298	26.03	3	0.1	4.63	4.61	0.3	6.68	6.66	0.6	8.33	8.38	1.2	11.11	11.08
		15		4.63	4.63		6.67	6.68		8.35	8.33		11.13	11.15
		35		4.64	4.66		6.66	6.62		8.31	8.29		11.14	11.08
	57.12	3	0.1	4.67	4.63	0.3	6.63	6.61	0.6	8.35	8.31	1.2	11.11	11.15
		15		4.66	4.63		6.61	6.59		8.29	8.32		11.13	11.10
		35		4.63	4.65		6.66	6.64		8.34	8.31		11.09	11.14
	97.42	3	0.1	4.68	4.64	0.3	6.67	6.64	0.6	8.33	8.36	1.2	11.08	11.11
		15		4.63	4.67		6.68	6.65		8.34	8.29		11.12	11.14
		35		4.66	4.62		6.69	6.66		8.32	8.30		11.12	11.10
373	18.83	3	0.1	4.18	4.16	0.3	5.96	5.94	0.6	7.37	7.39	1.2	10.24	10.25
		15		4.15	4.14		5.94	5.95		7.38	7.36		10.26	10.23
		35		4.16	4.14		5.94	5.93		7.38	7.40		10.26	10.26
	60.83	3	0.1	4.18	4.20	0.3	5.96	5.94	0.6	7.41	7.40	1.2	10.23	10.25
		15		4.20	4.18		5.90	5.92		7.42	7.40		10.26	10.24
		35		4.18	4.17		5.93	5.95		7.40	7.38		10.29	10.24
	100.32	3	0.1	4.17	4.17	0.3	5.91	5.93	0.6	7.38	7.36	1.2	10.26	10.24
		15		4.16	4.16		5.89	5.88		7.39	7.36		10.23	10.24
		35		4.18	4.16		5.89	5.87		7.39	7.36		10.24	10.21
453	27.89	3	0.1	3.65	3.68	0.3	5.33	5.34	0.6	6.93	6.96	0.9	7.98	8.01
		15		3.64	3.58		5.32	5.29		6.90	6.93		7.95	8.00
		35		3.66	3.58		5.33	5.31		6.90	6.89		7.99	7.98
	49.03	3	0.1	3.67	3.64	0.3	5.33	5.34	0.6	6.88	6.94	0.9	8.04	8.03
		15		3.63	3.61		5.34	5.31		6.94	6.90		7.98	7.97
		35		3.63	3.65		5.33	5.31		6.89	6.92		9.21	9.20
	110.26	3	0.1	3.64	3.62	0.3	5.31	5.33	0.6	6.88	6.90	0.9	7.97	7.99
		15		3.64	3.63		5.28	5.31		6.88	6.88		7.99	7.97
		35		3.64	3.67		5.33	5.35		6.93	6.90		7.99	8.02

* V_{s+} and V_{s-} are the voltages of positive and negative coronas, respectively.

reactor does not produce any effect on the voltage-current characteristics. The reason was that the gas particles were travelling longitudinally through the reactor with such low velocities that they had negligible effect on the drift velocity and hence on the mobility of the traversing charged particles moving between the two electrodes. As indicated in Appendix B, the average drift velocity of the charged particles is in the order of 2500 m/s whereas the maximum axial velocity of the gases was less than 0.06 m/s.

b) in order to acquire the same current, the applied voltage must be decreased as the temperature increases. This is primarily due to the effect of temperature on the density of gases. As temperature increases the density of gases decreases and the mean free path increases. This latter increase would in turn cause the mobility of the charged particles and thus the current to increase. To counter the increase in current, the applied voltage was lowered.

c) the above two observations hold true for both the positive and negative coronas. Regardless of the polarity, the same value of the applied voltage results in attaining the same current. The apparent differences in voltage values are within the experimental errors. These findings may only be applicable in the range of conditions presently investigated since differences between the two coronas are pronounced at higher values of voltage [58]. Accordingly,

throughout the following discussion, the term "corona" will be used indiscriminately for positive and negative coronas.

ii) Correlation of Voltage-Current Data

Based on the discussion given in Section 3.4, the relation:

$$\frac{V_s - V_c}{V_c} \ln(R/a) = (1+\Phi)^{\frac{1}{2}} - 1 - \ln\frac{1 + (1+\Phi)^{\frac{1}{2}}}{2} \quad (3.5)$$

may be used to correlate the voltage-current measurements.

Both V_c and E_c are inter-related by the expression:

$$V_c = a\, E_c \ln(R/a) \quad (3.4)$$

while on the other hand E_c may be predicted by the relation:

$$E_c = C_1\delta + C_2(\delta/a)^{\frac{1}{2}} \quad (3.2)$$

where δ is the relative gas density and given by

$$\delta = \frac{T_o P}{T P_o} \quad (3.3)$$

For a corona discharge, the constants C_1 and C_2 in equation (3.2) have been experimentally determined [58]. For both polarities, C_1 and C_2 are equal to 3×10^6 V/m and

9×10^4 V/m$^{\frac{1}{2}}$, respectively. As discussed above,, since the investigated range of concentration of the sulphur and other species seemed not to affect the voltage-current characteristics, these values of C_1 and C_2 may be used in the calculations without introducing significant errors.

The above conclusion would suggest that the mobility of ions in air [16] may be used in equation (3.5). However, the values available for this property are specific to whether the ions are positive or negative and range from about 1.8×10^{-4} m^2/s.V for positive ions to 2.5×10^{-4} m^2/s.V for negative ions [16]. Therefore, the above relations in addition to the data reported in the present study were used to obtain a value for the mobility. The mathematical procedure employed in this regard is illustrated in Appendix B. According to the results obtained, b_o was found equal to 1.961×10^{-4} m^2/s.V. Compared with the values reported in the literature and mentioned above, the value obtained here is very reasonable. These results lead to the conclusion that air can be considered as the discharge gas. They are also indicative of the high accuracy of the present data.

Figure 4.5 shows the comparison between the experimental voltage-currrent data and those predicted by equation (3.5) using the present value of mobility. The deviation between the experimental values of V and those predicted is ±8% (see Appendix B).

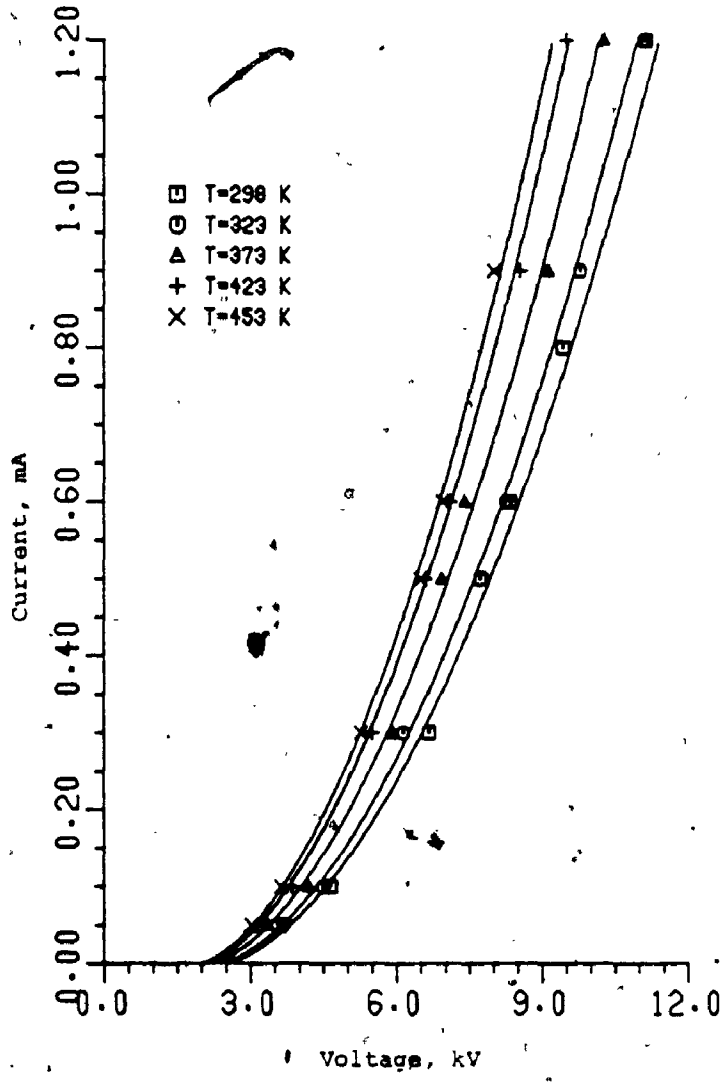

Figure 4.5: The relation between voltage and current in the corona reactor.

4.2.3 The Heating System and the Control and Measurement of the Reactor Temperature

High temperatures of the reacting mixtures were achieved by placing the reactor in a cylindrical furnace. The furnace used was manufactured by Sunnyvale Plant Products Company, USA Serial #66101052.

The furnace temperature was monitored and controlled by a precision temperature controller, a mercury relay, and a variable transformer. These devices were manufactured respectively by Gulton Industries Canada Limited Model #JP-s183, H.B. (Instrument Company Catalogue #7550), and Standard Electric Products Company Type 500b, 115-V. The sensing element of the controller was an iron/constantan thermocouple which was inserted into the thermocouple well in the furnace body.

As shown in Appendix B, excellent isothermal conditions of the reactor for the five temperatures examined (i.e., 298, 323, 373, 423, and 453 K) were possible. This was achieved by connecting shunt wires of suitable resistances to the electrical circuit of the furnace (these shunt wires were provided with the furnace).

When a temperature measurement was to be made, the thermocouple soldered to the stainless steel gauze was, as discussed earlier, connected to the Minimite potentiomenter

whose accuracy was ±1% of full scale. Temperature could be measured with a maximum fluctuation of about ±2 K at 423 and 453 K and of about ±1 K at 323 and 373 K.

Since isothermal conditions of the reactor were attainable, temperatures measured by the above arrangement were representative of the whole reactor.

Prior to use, the above thermocouple was calibrated at three temperatures: 298, 373, and 457 K by using room temperature, boiling water, and boiling aniline, respectively.

4.2.4 The Gas Chromatograph and the Sampling Systems

The gas chromatograph system is schematically shown in Figure 4.6. It consists of a gas chromatograph instrument and a supply of helium which was used as the carrier gas.

The gas chromatograph was a dual column instrument with temperature programming: Model 1520-B purchased from Varian Aerograph. The separation and the reference columns were made of 6.35 mm inside diameter stainless steel and were 2.13 and 0.60 m long, respectively. They were packed with Poropak Q (50 mesh particle size), coiled and placed in the gas chromatograph oven. These dimensions combined with the other operating conditions of the columns were (as will be shown later) adequate for an excellent resolution of the

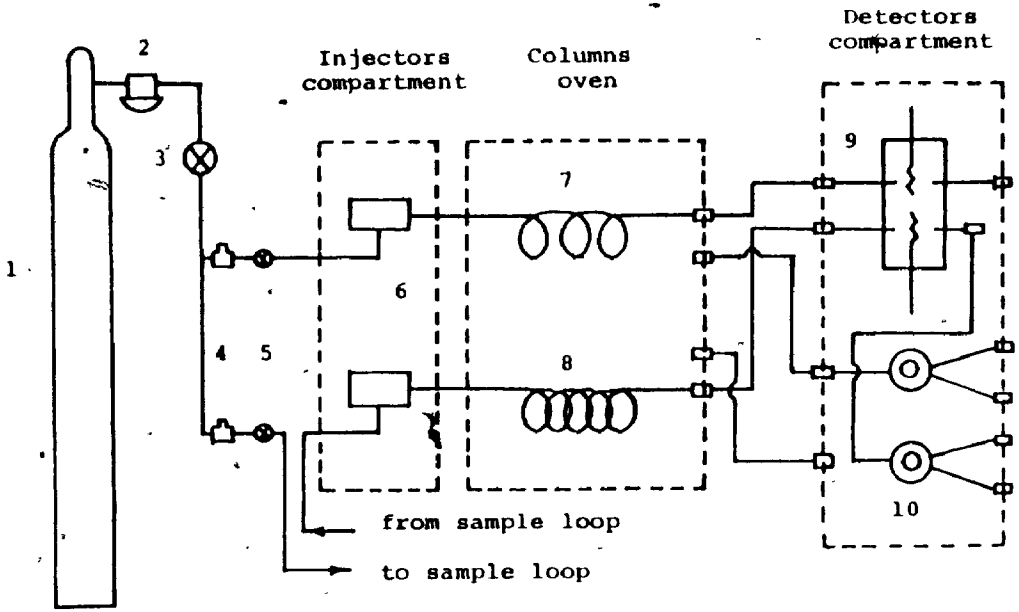

Legend:

1- Helium cylinder.
2- Pressure regulator.
3- Needle valve.
4- Precision rotameters.
5- Precision needle valves.
6- Injector tubes.
7- Reference column.
8- Separation column.
9- Thermal conductivity detector.
10- Hydrogen flame ionization detector.

Figure 4.6: Schematic diagrm of the gas chromatograph.

various compounds of interest.

The two columns were preceeded by two injector tubes provided with the instrument. The injector port which preceeded the separation column was heated so as to vapourize the sample to be analysed.

The gas chromatograph had two detectors: a thermal conductivity detector and a flame ionization detector and the two detectors were connected together in series. The thermal conductivity detector was used to respond to the present inorganic compounds such as air and hydrogen sulphide. The flame ionization detector on the other hand responded to the organic compounds such as methyl mercaptan.

Hydrogen and air required for the operation of the flame ionization detector were supplied from pressurized cylinders with C.P. grade (99.9% purity) and provided by Canadian Liquid Air Limited. The two gases, before going to the flame detector, were regulated with two-stage regulators, needle valves, and low flowrate rotameters. Specifications and calibration curves of the rotameters are given in Appendix B. The flow of helium (provided by Canadian Liquid Air Limited in a pressurized cylinder) was also regulated with a two-stage regulator, a precision needle valve, and a rotameter.

Inside the gas chromatograph instrument itself, helium from the pressurized cylinder was divided into two streams, each was monitored separately by a needle valve and a precision rotameter. These rotameters were however consulted only for relative readings. Helium flow rates to the columns were determined at their exit with a soap-bubble flowmeter.

The first of the helium streams was passed through the reference column and then through one side of the thermal conductivity detector before escaping to the atmosphere. The second stream was passed through the sample loop (described below) and then through the analytical column, the other side of the thermal conductivity detector, and then into the flame ionization detector where it was destroyed by combustion.

Samples of either the reactant or the product streams were introduced into the gas chromatograph by means of a system consisting of a sample loop and a sampling valve illustrated in Figure 4.1. The loop was 3.18 mm inside diameter stainless steel having a volume of 1.248×10^{-6} m^3 (see later for the determination of this volume). It was attached by a Swagelok to the rear of the sampling valve. By manipulating the sampling valve, gas streams could either pass through or by-pass this loop. The sampling valve was a stainless steel rotary 8-port valve, purchased from VALCO

Instruments Canada Limited. As indicated schematically in Appendix B, in one position of the sampling valve, a sample could be trapped in the sample loop. By switching the valve to its other position, helium passing through the loop would carry the trapped sample passing through the injection port to the separation column for analysis.

4.2.4.1 Temperature Control of the Gas Chromatograph

The gas chromatograph had three separate thermal regions: the injector tubes, the columns oven, and the detectors oven regions.

The heating rate to the first and to the third regions and their temperatures were adjusted and monitored by front-panel controls.

Oven temperature on the other hand was controlled by the Matrix Temperature Programmer provided with the instrument. (See Section 4.5 below.)

4.2.4.2 Column Conditioning

Prior to use, a newly packed column was pre-conditioned at about 450 K according to the manufacturer's procedure (see Appendix B). The pre-conditioning was required to avoid possible contamination of the detectors and also to avoid column bleeding during experiments.

4.2.4.3 Pressure Drop in the Sample Loop

Calculations given in Appendix B show that the pressure drop in the sample loop is equal to 130 Pa at maximum flow conditions (i.e., 25.74×10^{-6} m^3/s). The fact that this pressure drop was about 0.03% of the ambient pressure indicates that the flow rates of gases through the loop were at atmospheric pressure.

4.2.4.4 Recording the Gas Chromatograph Output

The response of the detector, either the thermal or the flame ionization detector, to each compound separated emerged as a peak on a chart recorder. The recorder was a two-channel strip chart recorder: Model 20 manufactured by Varian Aerograph Company of Canada Limited with an error of ±1% of full scale. Each of the recorder channels was used to indicate the response of each detectors of the gas chromatograph. The area of every peak produced was determined spontaneously by an electronic digital integrator (Model 480 made also by the above company) and the results were printed in numerical form by a printer obtained from Victor of Canada Limited. The integrator was calibrated to a precision of ±0.1% according to the procedure described by the manufacturer.

4.3 PRELIMINARY EXPERIMENTS

4.3.1 Procedure

In reference to Figure 4.1, the reaction of methyl mercaptan or of hydrogen sulphide with air in the presence of corona discharge was carried out as follows:

1. Conditions on the gas chromatograph were first adjusted (see Section 4.5 below).

2. The reactor was assembled in its position in the furnace tube and the stainless steel gauze was grounded by the iron side of the thermocouple soldered to the gauze.

3. The furnace was controlled so that the reactor temperature was the desired one.

4. A continuous stream of the already prepared mixture of the sulphur compound with nitrogen and another stream of air were passed into the mixing chamber. These two streams were monitored by the respective rotameters so that the mean residence time τ of the combined stream through the reactor was the required value. In this case, the following equation was used:

$$\tau = \frac{V_R}{Q_{T_R}} = \frac{V_R \, T_r}{Q_{T_r} \, T_R} \qquad (4.1)$$

where V_R (m^3) is the reactor volume, T_R and T_r are the reactor and the room temperatures in Kelvin, and Q_{T_R} and Q_{T_r} are the flow rates in m^3/s at T_R and T_r, respectively.

5. By manipulating the valve system described above, the feed was by-passed the reactor. Accordingly, samples

could be taken to the gas chromatograph for analysis.

6. The high voltage supply was adjusted so that the desired value of current was obtained.

7. Also, by using the valve system, the feed stream was led through the reactor where the reactions took place and time was recorded. The product stream was sampled and analysed by the gas chromatograph as described above.

As stated previously, despite the occurence of the reactions, the reactor temperature remained unaltered. This, as mentioned above, was attributable to the extermely low concentrations of the the sulphur compounds so that any effect of the heat of reaction was negligible. As a result, no adjustments in the flow rate of gases or in the current were needed.

8. At the end of the run, the power supply and the heating system of the furnace were turned off, time was recorded, and the reactor was left to cool.

4.3.2 Identification of the Products of the Reaction between Methyl Mercaptan and Air

The reaction of methyl mercaptan with air in a corona discharge was found to produce several products. Some of these products could be separated by the gas chromatograph while a solid material having a white colour was deposited on the reactor walls near the exit.

Typical data obtained from experiment is summarized in

Table 4.2. From this table we see that the number of the products separated by the gas chromatograph differs from two to four depending on the value of the current and the mean residence time. Identification of the maximum number of these products was then required. This was done as follows:

4.3.2.1 The Solid Material

The solid material formed in the reaction was found to readily dissolve in ethanol. It was then collected for analysis by washing the reactor walls thoroughly with ethanol and recovered as crystals by evaporation of the solvent and weighed by a precision balance (manufactured by E. Mettler, #1-910). Chemical analysis of this material was done using the techniques of nuclear magnetic resonance (NMR), infrared (IR), and mass spectroscopy (MS). A summary on each of these techniques is given in Appendix B.

i) NMR Analysis:

A test solution for NMR analysis was prepared by dissolving a sample of the solid material in deuterium chloroform $CDCl_3$. Tetramethylsilane TMS was added to the solution and used as an internal standard. The spectrometer used was model T-60, manufactured by Varian Aerograph Company. A typical NMR spectrum obtained is shown in Figure 4.7. The fact that this figure exhibits only one absorption peak indicates the symmetrical grouping of the hydrogen protons in the molecule. This, in turn, means that the

TABLE 4.2: EFFECTS OF CURRENT, MEAN RESIDENCE TIME, AND TEMPERATURE ON THE PRODUCTS OF METHYL MERCAPTAN REACTION WITH AIR *

C_{Ao} $\frac{kmol \times 10^6}{m^3}$	T K	I_c mA	t s	C_A $\frac{kmol \times 10^6}{m^3}$	X_A	Data obtained from gas chromatograph*	
						No. of products	Retention time
23.03	423	0.15	10	6.02	0.74	4	251, 613, 2267 and 3182
20.18	423	0.3	10	2.98	0.85	4	252, 613, 2266, and 3180
20.98	423	1.2	10	1.10	0.95	3	252, 615, and 2269
21.11	423	0.3	30	Traces	1.0	2	253 and 614
22.89	423	0.3	3	15.03	0.34	4	252, 614, 2261, and 3183
23.04	453	0.3	10	1.93	0.91	4	251, 615, 2265, and 3182
23.89	373	0.3	10	4.03	0.83	4	251, 615, 2260, and 3186

* The retention time data are based on the oven operating conditions discussed in Section 4.5.

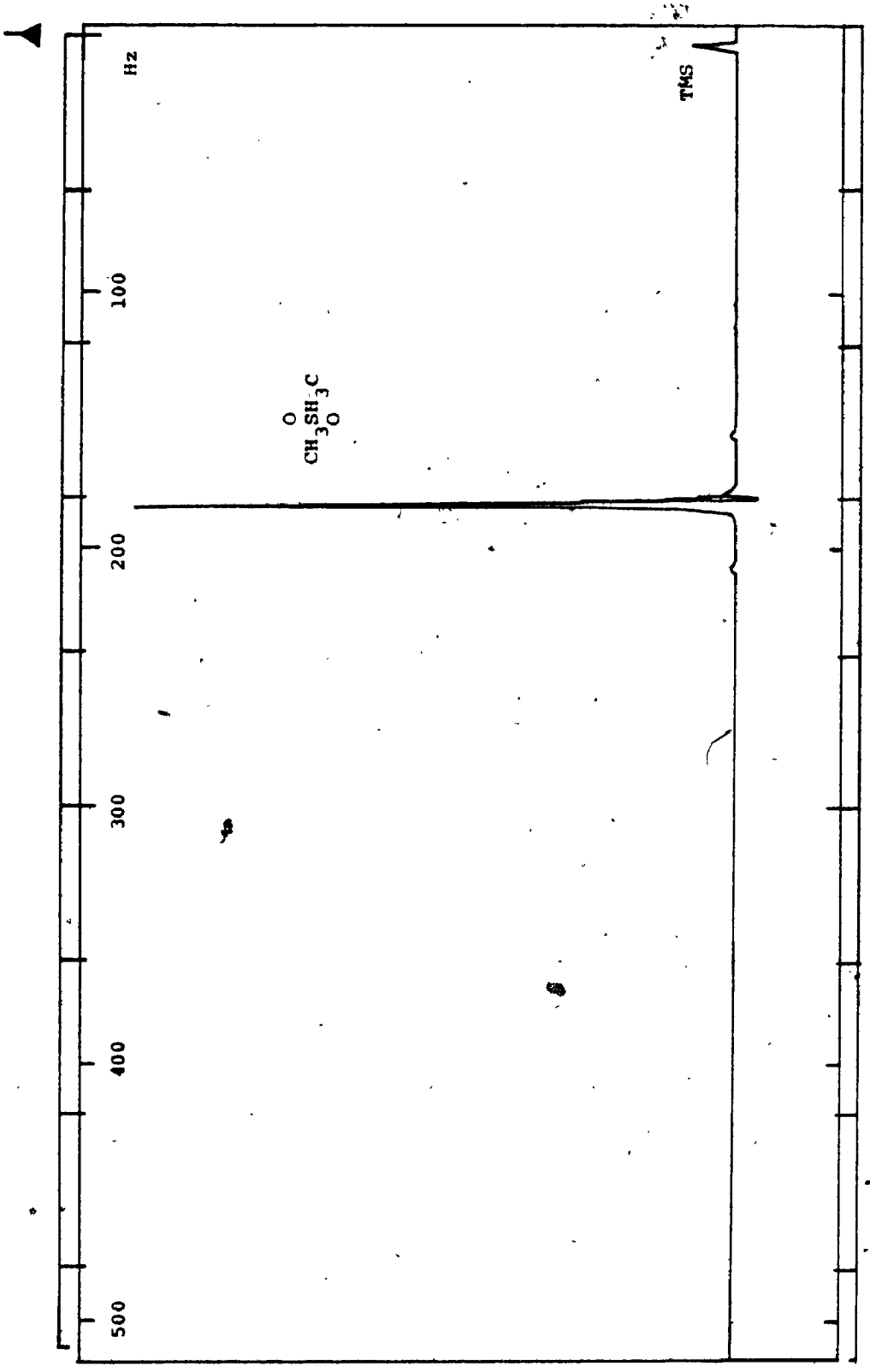

Figure 4.7: NMR spectrum of the solid product of the reaction of methyl mercaptan with air in corona discharge.

solid material was composed solely of one compound [82]. The chemical shift exhibited by the peak is about 3.0 ppm which is the same as that of dimethyl sulphone as given in the Aldrich Library of Spectra [83] under the number of NMR 10,2C (19).

ii) IR Analysis:

A test solution for IR analysis was prepared by dissolving samples of the solid compound in chloroform $CHCl_3$. The IR tests were carried out using a double-beam Beckman IR-20A spectrometer which employed sodium chloride cells.

The IR spectrum shown in Figure 4.8 exhibits strong absorption in the 1110-1150 and 1350-1290 cm^{-1} regions which correspond to the symmetrical and the asymmetrical stretching frequencies in sulphur dioxide, being 1151 and 1361 cm^{-1}, respectively [84,85]. The slight differences in values may be attributed to the adjoining methyl group [86]. Furthermore, these absorption regions are generally indicative of $-SO_2$ and more specifically in saturated sulphones [87,88].

Absorption at 1410 and 1430 cm^{-1} shown also in Figure 4.8 corresponds to the bending vibration of the $S-CH_3$ bond [89]. Absorption in the 705-570 cm^{-1} region is also characteristic of the stretching vibration of the same bond [90-92]. Absorption in the 3000-3100 cm^{-1} region is due the

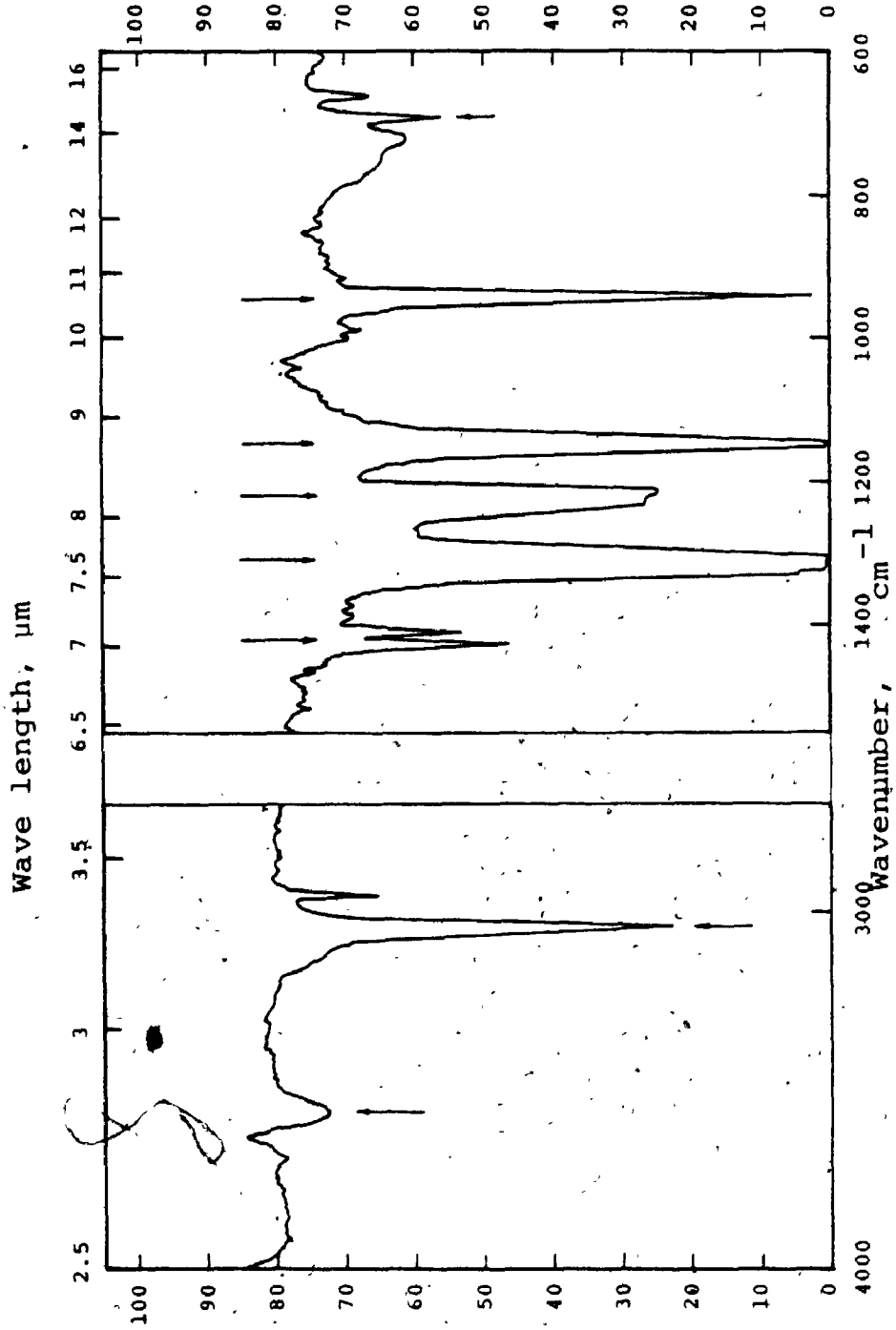

Figure 4.8: IR spectrum of the solid product of the reaction of methyl mercaptan with air in corona discharge.

stretching vibration of C-H bond [82].

This IR spectrum moreover compares with the authentic IR of dimethyl sulphone $(CH_3)_2SO_2$ as given in the Aldrich Library of Spectra [93]: # IR 1,470 (19).

iii) MS Analysis:

MS analyses were done in the Chemistry Analytical Lab, the University of Western Ontario using Varian mat-311A mass spectrometer. The results are given in Figure 4.9. The peak at mass 94 with 100% intensity indicates that the molecular weight of the parent ion is in the vicinity of 94. In fact, the exact mass found by MS analysis is 94.0095. Other important peaks are 79,62%, 64,23%, 46,46%, and 45,60% where the first number refers to the mass of an ionic fragment and the second indicates the percentage of the intensity of its peak. Furthermore, the atomic composition of the compound is summarized in Table 4.3 below.

Based on the information of Table 4.3, the peak exbibited in Figure 4.8 indicates the presence of ionic fragments such as:

$O{=}S{=}O$, $O{=}S{=}O$, $H_3C{-}S{-}$, and $HC{-}S{-}$
CH_3

The above results identify the solid product as dimethyl sulphone. Dimethyl sulphone is a white solid with a prism crystalline form and having a melting point in the range 381-383 K [94]. In fact, when the melting test [95] was

TABLE 4.3: THE CHEMICAL COMPOSITION OF THE SOLID PRODUCT OF METHYL MERCAPTAN REACTION WITH AIR

carbon	hydrogen	nitrogen	oxygen	sulphur
2	6	0	2	1

Exact mass = 94.0095

TABLE 4.4: THE CHEMICAL COMPOSITION OF THE CONDENSABLE PRODUCTS OF METHYL MERCAPTAN REACTION WITH AIR (after water was removed)

	carbon	hydrogen	nitrogen	oxygen	sulphur
#1	2	6	0	0	1
Exact mass = 62.0115					
#2	2	6	0	0	2
Exact mass = 93.9911					

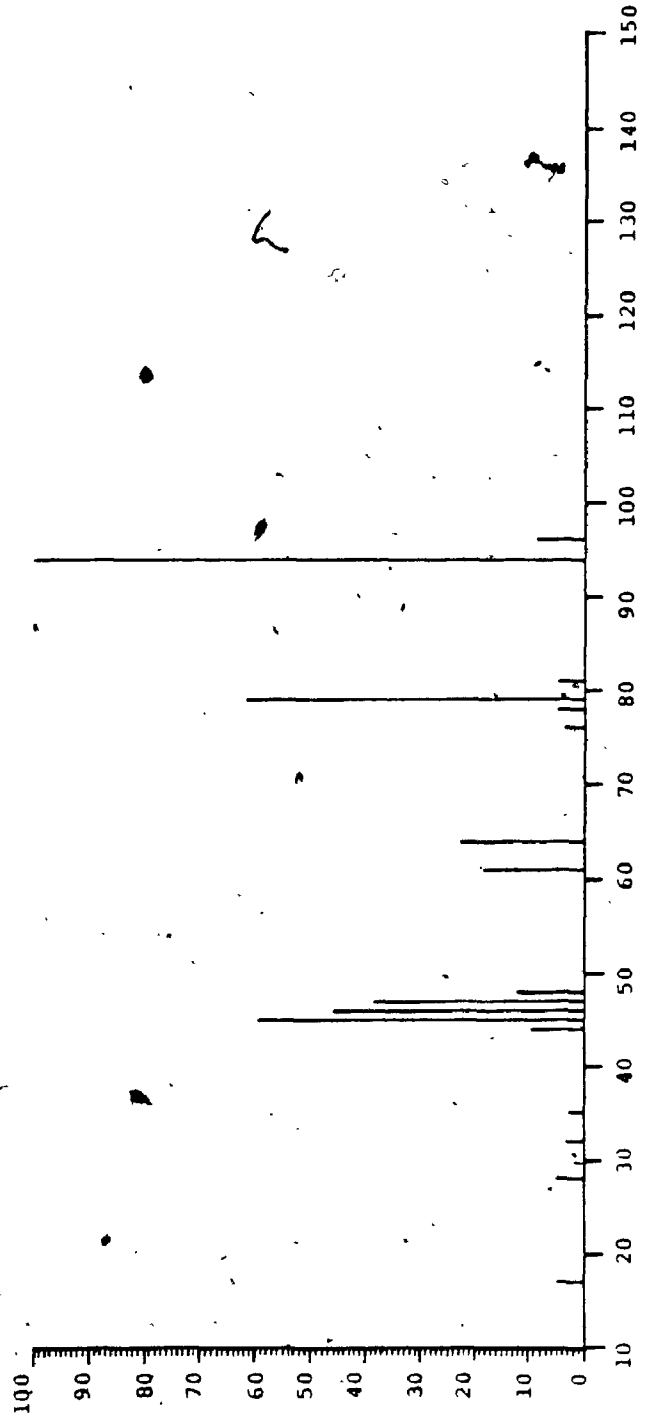

Figure 4.9: Mass spectrum of the solid product of the reaction of methyl mercaptan with air.

done on the solid product, its melting point was found in the 379-383 K range. Furthermore, when the mixed melting point test (i.e., the melting point of a mixture consisting of the solid product and dimethyl sulphone purchased from Fisher Chemical Company (99.8% purity) was carried out, no depression in the melting point range was observed.

4.3.2.2 The Products Separated by the Gas Chromatograph

In order to identify the four products which were separated by the gas chromatograph, the output stream from the reactor was directed to pass through a cold trap immersed in a salt ice bath (263-268 K).

As a result, an oily liquid having the distinct smell of the sulphur compounds was collected. This mixture was then subjected to analysis by NMR, IR, and MS techniques as described in above. The results obtained are discussed in the following sections:

i) The NMR spectrum given in Figure 4.10b indicates the presence of three peaks at chemical shifts of 2.1, 2.4, and 3.3 ppm with respect to TMS. As Figure 4.10a illustrates, when enough of deuterium oxide D_2O was added to the test solution, the peak at 3.3 ppm was completely suppressed indicating strongly that this peak was due to water [49]. Subsequently, this compound was concluded to be among the products of the present reaction.

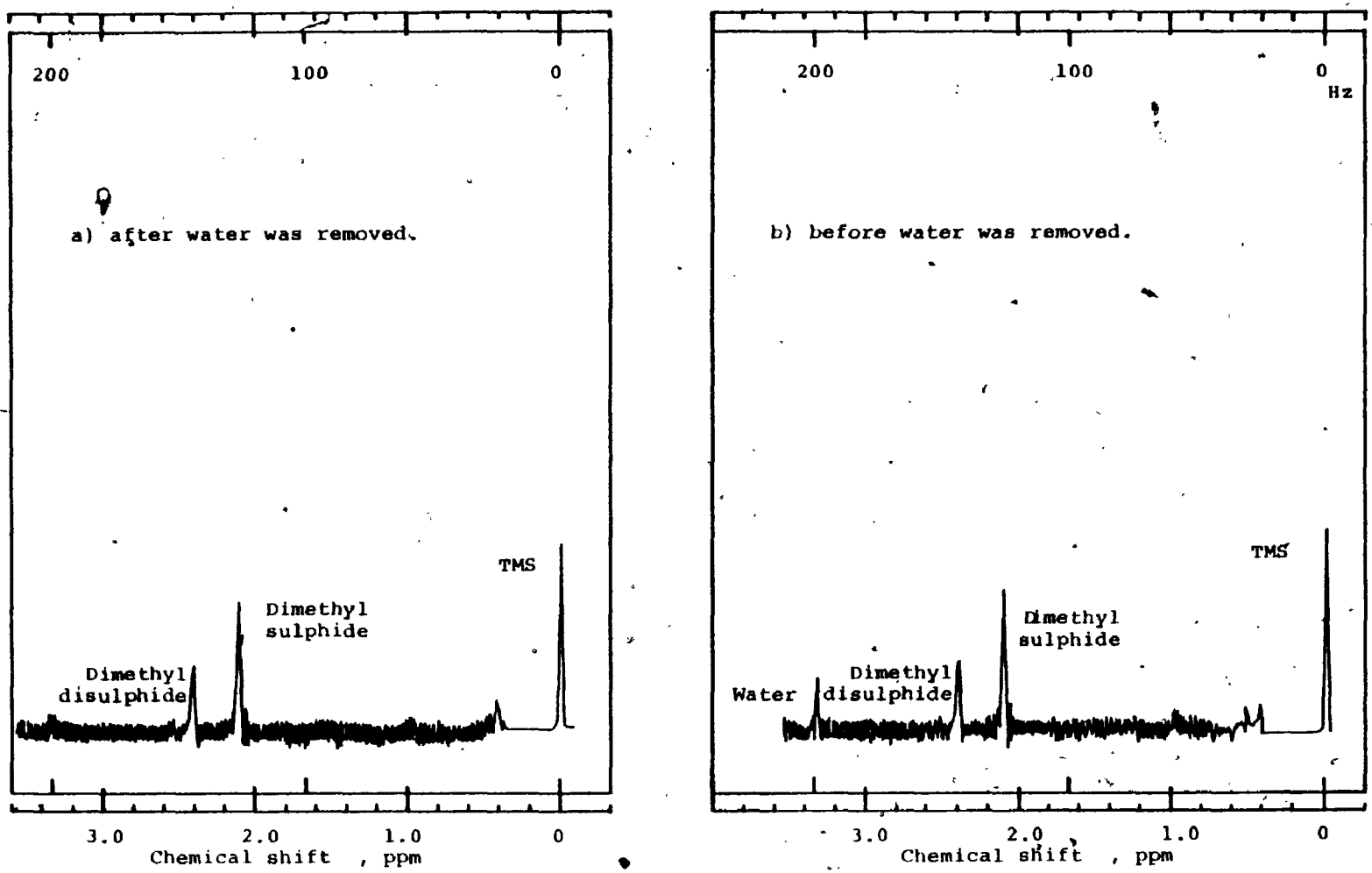

Figure 4.10: NMR spectrum of the condensable products of the reaction of methyl mercaptan with air in corona discharge.

As water was identified, it was removed from the test solution so as to simplify the process of further analysis by IR and MS techniques and more importantly to prevent the sodium chloride cells used in the IR spectrometer from dissolving.

Anhydrous magnesium sulphate was added to the test solution to absorb the water present forming hydrated magnesium sulphate. The solution was later filtrated to remove the solid material of both hydrated and anhydrous magnesium sulphate.

A sample of the filtrate was then sent for further NMR analysis in the Chemistry Analytical Lab, University of Western Ontario. The spectrum obtained is shown in Figure 4.11. The figure illustrates two absorption peaks at chemical shifts of 2.12 and 2.43 ppm with respect to TMS which compare with the authentic NMR spectra of dimethyl sulphide $(CH_3)_2S$ and dimethyl disulphide $(CH_3)_2S_2$, respectively. The authentic NMR are given in the Aldrich Library under the numbers: NMR 1,157A and NMR 1,157B [83].

ii) The IR spectrum of the oily mixture after the removal of water is given in Figure 4.12. The strong absorption bands at about 1300 and 1400 cm^{-1} are the symmetrical deformation of the two CH_3 groups adjoining to the sulphur atoms [96]. Absorption in 600-700 cm^{-1} and

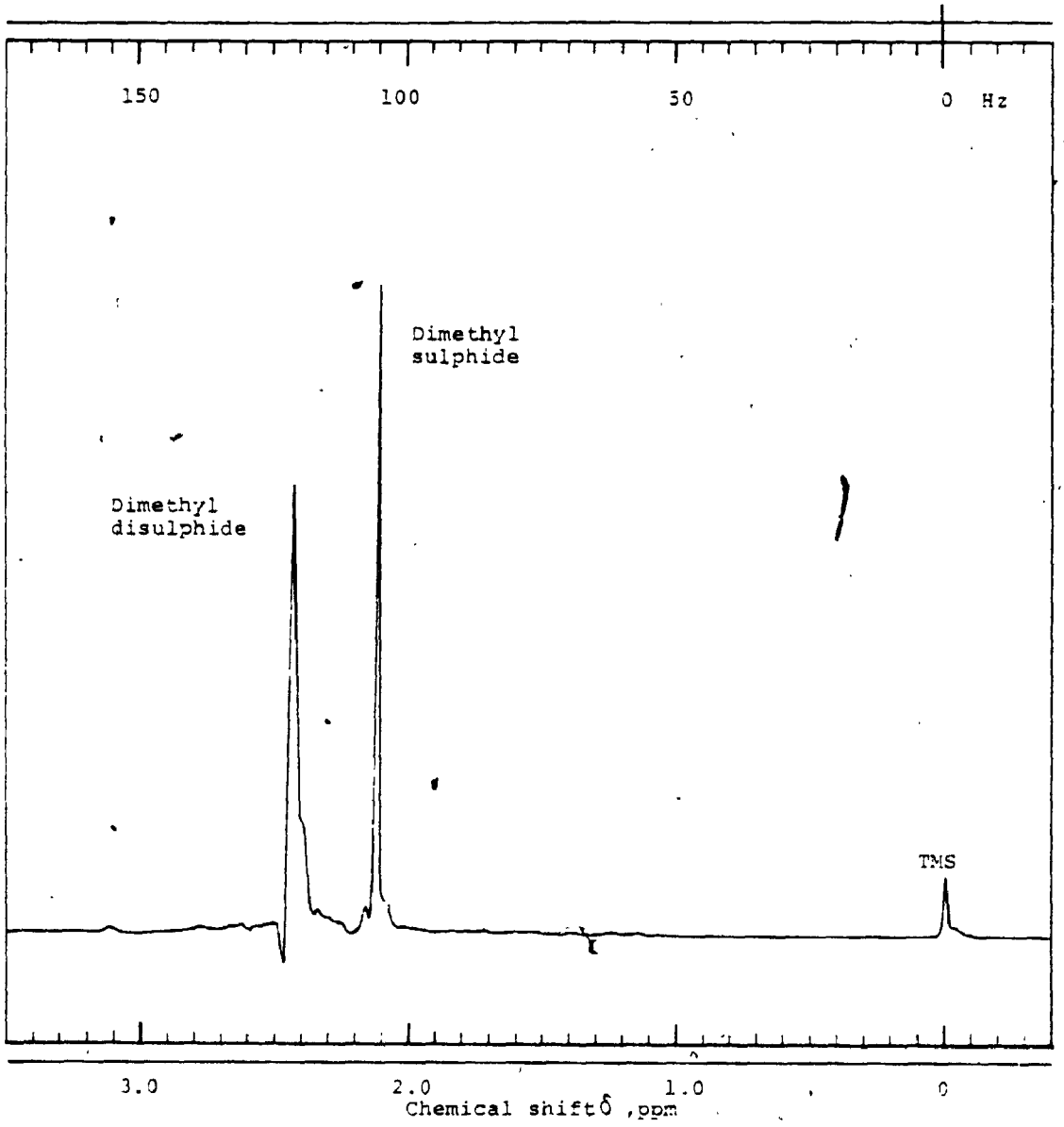

Figure 4.11: NMR spectrum of the condensable products of the reaction of methyl mercaptan with air in corona discharge (after water was removed).

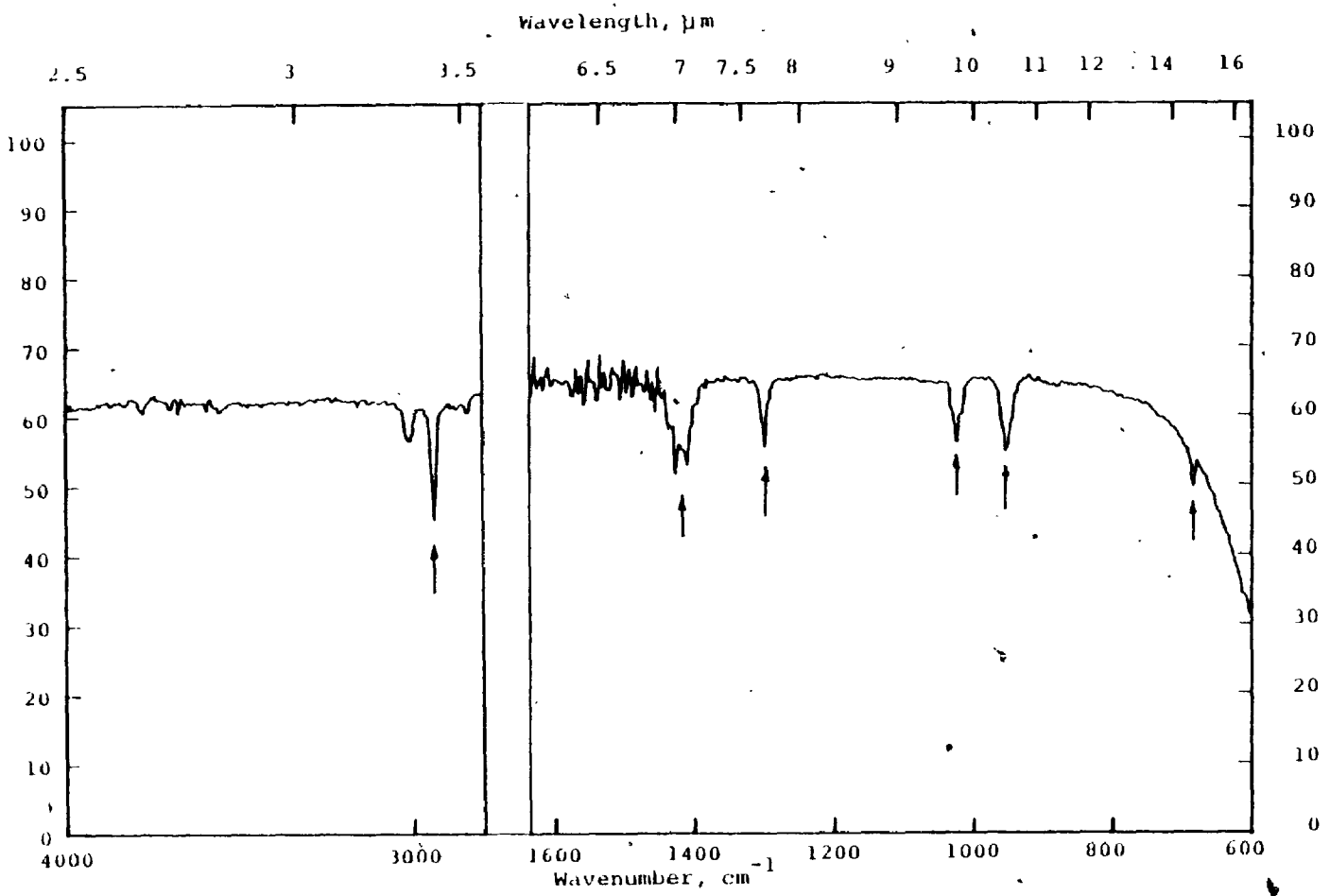

Figure 4.12: IR spectrum of the condensable products of the reaction of methyl mercaptan with air in corona discharge (after water was removed).

770-800 cm^{-1} regions is due to the stretching vibration of the C-S bond [90,96]. The fact that these two regions are adjacent strongly indicates the presence of a sulphide [88]. The absorption in 500 cm^{-1} region is due to the stretching vibration of S-S bond in disulphide [88].The absorption bands in the 2800-3000 cm^{-1} region are characteristic of the stretching vibration of the C-H bond [82].

iii) MS tests for the oily mixture after water was removed were also performed as described above. The MS spectrum is shown in Figure 4.13 while the atomic composition is summarized in Table 4.4 above.

The above data indicate that after the removal of water, two compounds were present in the mixture collected in the cold trap. One compound consists of two carbon, six hydrogen, and one sulphur atoms with an exact mass of 62.0115. The second compound present consists of two carbon, six hydrogen, and two sulphur atoms and its exact mass found equal to 93.9912. Peaks at 94,100%, 79,62%, 62,89%,, 47,44%, and 46,75% may indicate the presence of ionic fragements such as $(CH_3)_2S_2$, CH_3SS, $(CH_3)_2S$, CH_3S, and CH_2S, respectively.

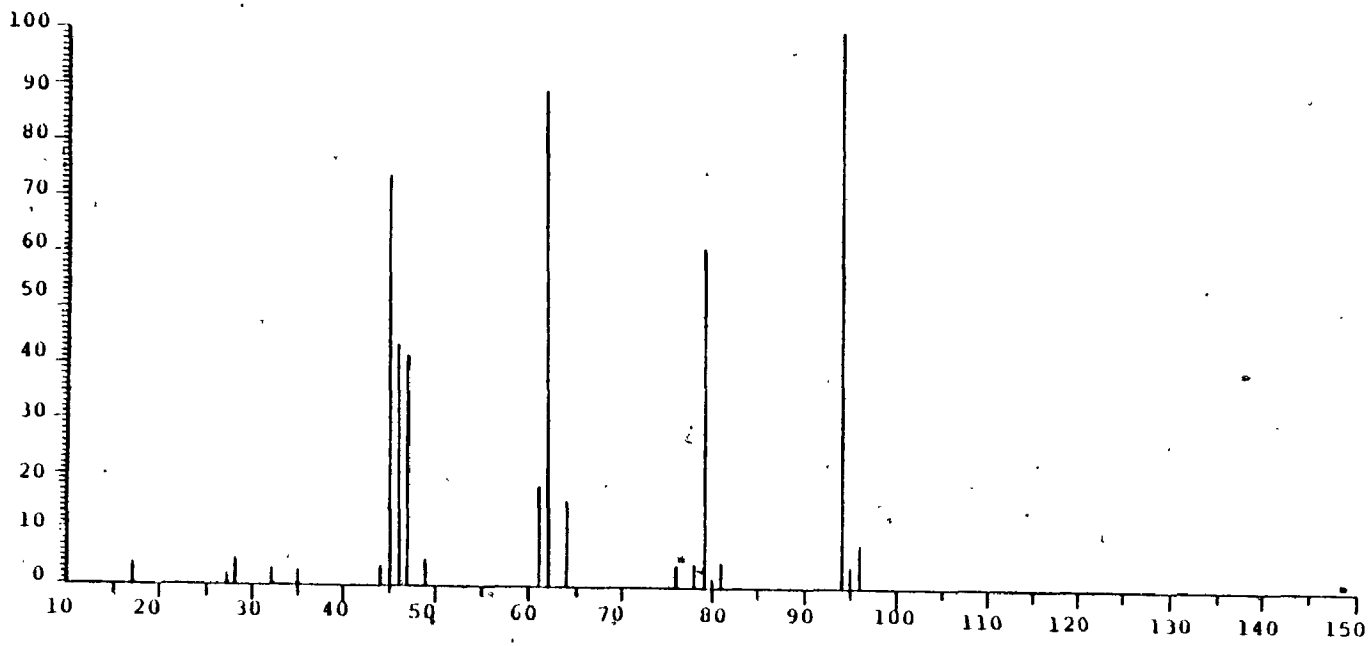

Figure 4.13: Mass spectrum of the condensable products of the reaction of methyl mercaptan with air (after water was removed)

The above results collectively indicate that these two compounds are dimethyl sulphide and dimethyl disulphide. In addition to water which was identified previously, three out of four products separated by the gas chromatograph have been identified so far. This leaves an extra product which could not be collected by condensation in the cold trap, and is still to be identified.

4.3.2.3 The Non-Condensable product

The output stream from the cold trap had the distinct odour of sulphur dioxide. Subsequently, the test which is described by Wilson et al [97] to check for the presence of sulphur dioxide was performed. A filter paper impregnated with a reagent containing starch, potassium iodate, and glycerol was exposed to the output stream from the cold trap. The fact that a purple stain was developed on the filter paper indicated the presence of sulphur dioxide in the stream.

Further tests to support these findings were also conducted. When the gas stream from the cold trap was absorbed in a dilute solution of hydrogen peroxide (5%), a colourless solution was obtained. This solution was acidic as it changed the colour of blue litmus paper to red. When a barium chloride solution (about 2%) was added to the acidic solution, a white precipitate was formed. The fact that this precipitate did not dissolve in dilute

hydrochloric acid (about 1%) indicated that the precipitate was barium sulphate [98] and the acidic solution was sulphuric acid. Moreover, when a copper chloride solution (about 2%) was added to the acidic solution obtained, the distinct blue colour of copper sulphate [99] appeared. Therefore, the gas which emerged from the cold trap was identified as sulphur dioxide.

4.3.3 Identification of the Products of the Reaction between Hydrogen Sulphide and Air

The reaction of hydrogen sulphide with air in a corona discharge was found to form only two products separated by the gas chromatograph. Unlike the reaction of methyl mercaptan, no solid products were formed.

Typical results obtained from experiment are illustrated in Table 4.5. By matching the retention time data listed in the table to those given previously in Table 4.2 at the same operating conditions of the gas chromatograph, it was concluded that these two products were water and sulphur dioxide.

4.4 CALIBRATION FOR AIR AND STANDARDIZATION OF THE SAMPLE LOOP

The Poropak Q-column employed in the gas chromatograph did not discriminate between nitrogen or oxygen. Therefore, the calibration curve discussed below may be used for

TABLE 4.5: EFFECTS OF CURRENT, MEAN RESIDENCE TIME, AND TEMPERATURE ON THE PRODUCTS OF HYDROGEN SULPHIDE REACTION WITH AIR

C_{Ao} $\frac{kmol \times 10^6}{m^3}$	T K	I_c mA	t s	C_A $\frac{kmol \times 10^6}{m^3}$	X_A	Data obtained from gas chromatograph	
						No of products	Retention time, s
33.98	423	0.15	10	13.06	0.61	2	251 and 613
35.11	423	0.90	10	Traces	1.0	2	252 and 613
21.96	423	0.30	3	19.88	0.09	2	252 and 615
17.94	423	0.30	20	Traces	1.0	2	254 and 614
29.06	298	0.30	10	19.11	0.34	2	251 and 613
30.92	543	0.30	10	2.89	0.91	2	252 and 612

nitrogen, oxygen, or any mixture thereof.

Samples of air of different volumes were measured out of the pressurized cylinder by a Hamilton gas-tight syringe at the ambient temperature and pressure. They were then introduced to the separation column by injection through the rubber septum provided on the gas chromatograph front panel. For each sample, a peak was obtained and the area under the peak was representative of the number of kmoles of air introduced. The latter quantity was determined from the ideal gas equation:

$$n = \frac{PV}{RT} \qquad (4.2)$$

Here, the pressure P is in Pa, the volume V is in m^3, and the temperature T is in degree K. The gas constant R is 8314.34 J/kmol.K.

The accuracy of monitoring the value of n due to using equation (4.2) is directly related to the accuarcy of measuring P, V, and T. Errors in the measurements of n were estimated in every case by using the normal statistical technique [102]:

$$(\Delta n)^2 = \left(\frac{\partial n}{\partial P}\right)^2 (\Delta P)^2 + \left(\frac{\partial n}{\partial V}\right)^2 (\Delta V)^2 + \left(\frac{\partial n}{\partial T}\right)^2 (\Delta T)^2 \qquad (4.3)$$

As shown in Appendix B, the accuracy of the calculated

kmoles of air was better than 0.9 percent.

By correlating the values of the peak areas obtained with the respective values of the number of kmoles of air, the calibration curve 4.14 was constructed.

Errors which may be produced from the above procedure were anticipated to be minimal since the diffusion of air into or out of the syringe was practically absent. Neverthless, this conclusion was further checked. This was accomplished by monitoring the peak area of an amount of air trapped in an auxiliary sampling loop made from Pyrex and having a volume of 1.008×10^{-6} m^3. (More details of the procedure followed here and of the determination of the volume of the auxiliary loop and its standardization are provided in Appendix B.) The results as shown in Appendix B and by ● in Figure 4.14 indicate an excellent agreement, a fact which confirms the validity of the above results.

Standardization of the sample loop was done first by attaching the loop to the sampling valve. By following the procedure mentioned above, a peak area corresponding to the amount of air trapped in the loop was measured. Figure 4.14 was then used to evaluate the corresponding moles of air. This latter value was in turn substituted into equation 4.2 to evaluate the value of the volume of the sample loop. These steps were repeated several times and the results were

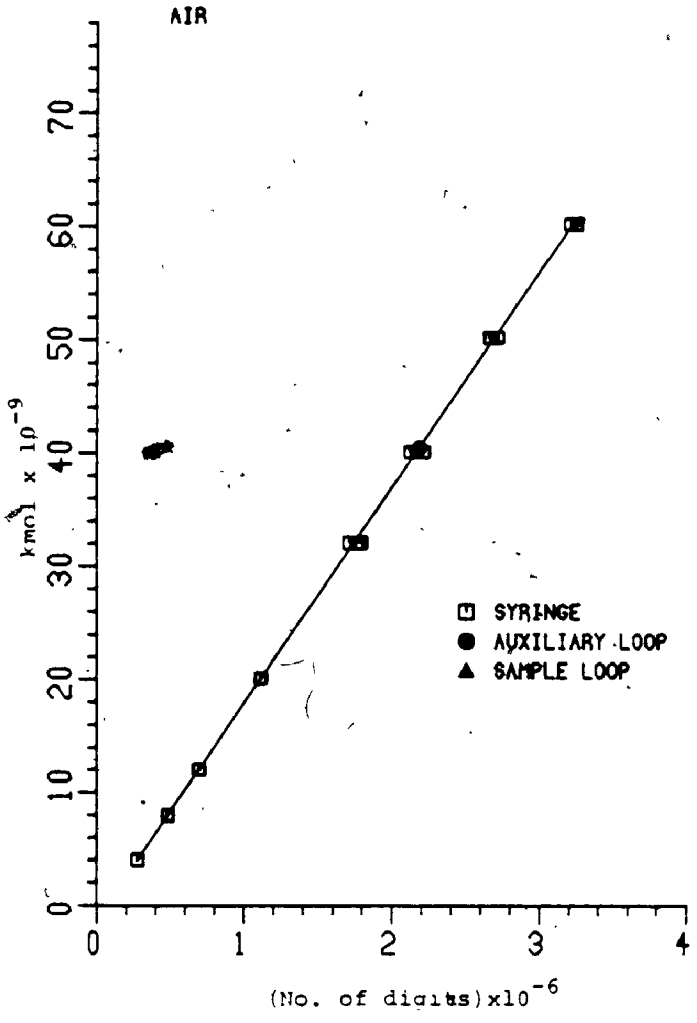

Figure 4.14: Calibration curve for air.

then averaged. From these results, illustrated by ▲ in Figure 4.14, the volume of the sample loop was found equal to $(1.248 \pm 0.003) \times 10^{-6}$ m^3. More details on the results are given in Appendix B.

4.5 CALIBRATION OF THE GAS CHROMATOGRAPH

The retention time data was obtained on a mixture composed of the compounds in concern. This mixture was prepared in the lecture bottle following the procedure described previously in Section 4.2.1. Then, several samples of this mixture were introduced into the gas chromatograph for resolution. The best resolution of the compounds present was obtained by adjusting:

i- the flow rates of helium in the reference and the operating columns, and

ii- the column-oven heating rate by means of the matrix temperature programmer.

The results obtained along with other operating conditions of the gas chromatograph are summarized in Appendix B. Under the conditions employed, the sensitivity of the thermal conductivity and the flame ionization detectors were better than 6×10^{-6} and 2×10^{-9} kg/m^3, respectively (see Appendix B).

The gas chromatograph was then calibrated separately

for every compound using the absolute method of calibration [103,104]. The methods of calibration and the results obtained are discussed in Appendix B.

4.6 MASS BALANCE AROUND THE REACTOR

4.6.1 Methyl Mercaptan Reaction with Air

In case of the reaction of methyl mercaptan with air, the mass balance around the reactor required the following:

i- the peak area of every separated compound by the gas chromatograph.

ii- the volume v_s of the sample loop.

iii- the flow rate Q of the feed through the reactor.

iv-the weight of dimethyl sulphone deposited during the reaction.

v- the total time t (s) of the experimental run.

The peak area of every separated compound was converted to number of kmoles m' existing in the sample loop via the respective calibration curve. The kmol flow rate $\dot{m}$ (kmol/s) of the compound was then obtained from:

$$\dot{m} = \frac{m'}{v_s} \times Q_R \qquad \text{kmol/s} \qquad (4.4)$$

in which v_s (m^3) is the volume of the sample loop. The use of equation (4.4) was justified since the flow through the reactor was of a constant density. This was , as will be discussed in Chapter 7, mainly due to the extremely low

concentration of the sulphur compounds employed in the experiments as well as to the isothermal conditions by which the reactor was operated.

The mass flow rate $\dot{m}$ of dimethyl sulphone on the other hand, was calculated from:

$$\dot{m} = \frac{(w/MW)}{t} \quad \text{kmol/s} \qquad (4.5)$$

where w (kg) and MW are the weight and molecular weight (kg/kmol) of the sulphone and t (s) is the total time of the experimental run.

A typical example of mass balance calculations around the reactor for methyl mercaptan reaction with air is given in Table 4.6.

The accuracy of such calculations depends generally upon the accuracy by which the parameters of equations (4.4) and (4.5) are determined. Based upon the accuracy by which each parameter present was measured, the accuracy of the results listed in Table 4.6 was better than 1.8 percent. This fact in addition to the deficits of only 2.2 %, 4.15%, and 3.2% respectively in sulphur, carbon, and hydrogen indicate that every product of the reaction has been identified.

Moreover, such a study was not necessary for the reaction involving hydrogen sulphide as both of the products formed contain oxygen.

Furthermore, since the accuracy of the gas chromatograph analysis was, as discussed earlier, extremely high, the deficits in sulphur, carbon, and hydrogen reported above were caused by the systematic errors of the collecting and weighing procedures of dimethyl sulphone.

4.6.2 Hydrogen Sulphide Reaction with Air

Mass balance calculations around the reactor in this case required the first three parametrs listed in i, ii, and iii above on page 50.

The peak area of the compounds was also converted to the number of the kmoles in the volume vs using the corresponding calibration curves. The mass flow rate M of a compound was obtained from the relation (4.4).

Table 4.7 shows an example of mass balance calculations around the reactor in this case. Deficits in sulphur and in hydrogen of 1.5% and 0.4%, respectively indicate that water and sulphur dioxide are the only products of hydrogen sulphide with air.

4.7 SIMULTANEOUS HOMOGENOUS AND HETEROGENOUS REACTIONS

4.7.1 Introduction

The occurance of simultaneous homogeneous (i.e., bulk) and heterogeneous (i.e., walls) reactions is not uncommon.

TABLE 4.7: A SAMPLE OF MASS ANALYSIS AROUND THE REACTOR FOR HYDROGEN SULPHIDE REACTION WITH AIR *

Element	Stream	Flow rate kmolx10^{11} /s			Total
		H_2S	SO_2	H_2O	
S	Feed	36.993			36.993
	Product	1.403	35.038		36.441
	Difference				0.552
	Diff.%				1.5
H	Feed	73.987			73.987
	Product	2.808		70.863	73.671
	Difference				0.316
	Diff.%				0.4

* Operating conditions:

Initial concentration of hydrogen sulphide	= 47.92*10^{6}	kmol/m^3
Temperature of reactor	= 423	K
Mean residence time	= 10	s
Current	= 0.3	mA

Therefore, the question whether or not the reaction of methyl mercaptan and of hydrogen sulphide with air in the present reactor is catalysed by the presence of the stainless steel gauze or by the presence of the Pyrex walls of the reactor vessel was investigated.

4.7.2 Effect of the Stainless Steel Gauze

Two sets of tests were conducted based upon the facts that [105,106]: i) bulk and wall reactions depend upon the volume of the reactor and its surface area, respectively, and ii) the wall reactions are very susceptible to the surface material.

In the first set, the surface and therefore the surface-to-volume ratio of the stainless steel gauze in the discharge zone were doubled by wrapping the present gauze with another layer of the same material. The double-layer gauze was then placed in the reactor vessel, held against the reactor walls, and grounded as described previously.

In the second set, the stainless steel gauze was replaced by another one made from brass (500-mesh) and having the same dimensions.

Experiments were conducted at current, temperature, and mean residence time of 0.3 mA, 423 K, and 10s,

respectively. The results are given in Tables 4.8 and 4.9 for the reaction of methyl mercaptan and of hydrogen sulphide respectively with air. For comparison, the results obtained with single-layer stainless steel gauze under similar conditions are also listed in the same tables.

Evidently, there are no substantial differences in the two sets of results. The apparent differences are within the experimental errors. Hence, it was concluded that the present reactions are not catalysed by the stainless steel gauze.

4.7.3 Effect of the Pyrex Walls

Considering the fact that wall reactions are very susceptible to the surface material, the Pyrex walls in the discharge zone were coated with a layer of the adhesive material of silicon seal (manufactured by General Electric Company of Canada). This material solidifies in a 24-hour period to form a permanent caulk. The reduction in the surface area of the Pyrex walls and therefore in the surface-to-volume ratio was 100 percent.

After the coated surface became dry, the reactor, with a single-layer stainless steel gauze, was assembled as before and experiments were carried out as usual.

The results, summarized also in Tables 4.8 and 4.9,

TABLE 4.8: EXPERIMENTAL RESULTS OF WALLS EFFECTS ON METHYL MERCAPTAN REACTION WITH AIR *

Condition of Reactor walls	Stream	Flow rate x 10^{11} kmol/s					
		CH_3SH	H_2O	SO_2	$(CH_3)_2S$	$(CH_3)_2S_2$	$(CH_3)_2SO_2$
Single-layer stainless steel gauze. Pyrex walls were uncoated.	Feed	13.645					
	Product	2.022	5.340	5.118	1.452	0.673	3.403
	Feed	16.173					
	Product	2.555	6.765	5.680	1.770	0.853	3.822
Double-layer stainless steel gauze. Pyrex walls were uncoated.	Feed	14.702					
	Product	2.013	6.205	5.005	1.580	0.738	3.627
	Feed	14.838					
	Product	2.152	6.113	5.263	1.655	0.765	3.343
Single-layer brass gauze. Pyrex walls were uncoated.	Feed	16.552					
	Product	2.323	6.385	5.205	1.342	0.732	3.349
	Feed	12.903					
	Product	1.892	5.082	4.892	1.193	0.562	3.202
Single-layer stainless steel gauze. Pyrex walls were coated with a permanent caulk material.	Feed	15.012					
	Product	1.965	6.237	5.463	1.560	0.752	3.488
	feed	17.118					
	Product	2.035	7.143	6.287	1.680	0.870	4.072

*Operating conditions:

Temperature of reactor	= 423	K
Mean residence time	= 10	s
Current	= 0.3	mA

TABLE 4.9: EXPERIMENTAL RESULTS OF WALLS EFFECTS ON HYDROGEN SULPHIDE REACTION WITH AIR *

Conditions of reactor walls	Stream	Flow rate kmolx10^{11} /s		
		H_2S	H_2O	SO_2
Single-layer stainless steel gauze. Pyrex walls were uncoated.	Feed	36.993		
	Product	1.403	35.432	35.038
	Feed	33.347		
	Product	1.003	32.404	32.178
Double-layer stainless steel gauze. Pyrex walls were uncoated.	Feed	35.015		
	Product	1.050	33.247	36.970
	Feed	31.620		
	Product	1.673	30.102	30.260
Single-layer brass gauze. Pyrex walls were uncoated.	Feed	34.093		
	Product	1.309	33.056	33.132
	Feed	30.294		
	Product	0.978	29.005	28.966
Single-layer stainless steel gauze. pyrex wals were coated with a permanent caulk material.	Feed	38.563		
	product	2.005	36.711	36.970
	Feed	40.043		
	Product	2.403	37.882	38.080

*Operting conditions:

Temperture of reactor	= 423	K
Mean residence time	= 10	s
Current	= 0.3	mA

indicate that no substantial differences were due to the coating on the surface of the Pyrex walls. The exhibited differences between the results, before and after the walls were coated, are within the experimental errors. Consequently, it was also concluded that the Pyrex material does not have any catalytic effect on the reaction.

4.8 ROLE OF OXYGEN IN THE REACTION OF METHYL MERCAPTAN WITH AIR

The fact that dimethyl sulphide $(CH_3)_2S$ and dimethyl disulphide $(CH_3)_2S_2$, which are among the products of the reaction of methyl mercaptan with air, do not contain oxygen in their chemical composition raised the possibility that these products might be formed by the reaction regardless of the presence of oxygen.

This argument was pursued by carrying out a set of experiments in which oxygen was not contained in the reacting mixture. The feed to the reactor was only composed of methyl mercaptan and nitrogen. The operating conditions otherwise were kept similar to those used earlier. These conditions together with the results obtained are listed in Table 4.10.

As indicated, no reaction occured at all. Hence, it is concluded that oxygen is essential for the reaction of the mercaptan to proceed.

TABLE 4.10: EXPERIMENTS IN WHICH FEED CONTAINED METHYL MERCAPTAN AND AIR

C_{Ao} $\frac{kmol \times 10^6}{m^3}$	T K	I_c mA	t	C_A $\frac{kmol \times 10^6}{m^3}$
27.13	423	0.30	10	27.04
22.97	453	0.90	30	23.08
27.88	453	0.90	35	27.43
22.25	323	1.20	35	22.03

Moreover, such a study was not necessary for the reaction involving hydrogen sulphide as both of the products formed contain oxygen.

CHAPTER 5

MECHANISTIC STUDIES ON THE REACTION OF METHYL MERCAPTAN WITH AIR IN THE CORONA REACTOR

5.1 INTRODUCTION

This chapter is devoted to developing a mechanism for the reaction between methyl mercaptan and air in the corona reactor. However, this mechanism will only be concerned with the path taken by the mercaptan to form the various products. Identification of the oxygen species taking part in the reaction and their role will be discussed in Chapter 6 after which the kinetic data will be correlated in Chapter 7.

In order to develop the reaction mechanism required, that part of the kinetic data which suits this purpose will only be presented here. This may be done in terms of i) the fractional conversion of methyl mercaptan (Section 5.3) and ii) the distribution of the reaction products (Section 5.4). Then, the effect of current and temperature on these two functions at various values of mean residence time will be discussed.

5.2 THE THERMAL REACTION

It was important at the begining to determine the significance of the thermal reaction in the absence of corona discharge. Therefore, experiments under controlled conditions of initial concentration of methyl mercaptan in the reacting feed, mean residence time, and temperature were carried out. Runs at different temperatures over the range from 298 to 453 K were carried out so as to cover the range of industrial interest in kraft mills. The mean residence time was fixed at 20 seconds which is probably greater than the residence time in an industrial precipitator.

Except for the high voltage power supply being turned off, the experimental procedure was similar to the one described in Section 4.3. Analysis of methyl mercaptan in the feed and in the product streams was performed using the gas chromatograph whose operating conditions were also kept similar to those described previously.

The results of the experiments along with the operating conditions are given in Table 5.1. It is evident that no substantial conversions of methyl mercaptan occurred in the temperature range tested. The differences in the concentration of the mercaptan in both the feed and the product streams shown in the table are in fact within the experimental errors as discussed earlier. Thus, we can conclude that the thermal reaction is unimportant in the

TABLE 5.1: EXPERIMENTS TO DETERMINE THE IMPORTANCE OF THE THERMAL REACTION OF METHYL MERCAPTAN WITH AIR

C_{A0} $\frac{kmol \times 10^6}{m^3}$	Temperature K	τ s	C_A $\frac{kmol \times 10^6}{m^3}$	Concentration difference $kmol \times 10^6 / m^3$	Diff.% with respect to C_{Ac}
19.88	298	20	20.04	- 0.16	- 0.80
21.38	373	20	21.29	0.09	0.42
25.82	423	20	25.77	0.05	0.19
23.09	423	20	23.06	0.03	0.13
20.31	453	20	20.34	- 0.03	0.15

TABLE 5.2: EXPERIMENTS TO DETERMINE THE IMPORTANCE OF THE THERMAL REACTION OF DIMETHYL DISULPHIDE WITH AIR

C_{A0} $\frac{kmol \times 10^6}{m^3}$	Temperature K	τ s	C_A $\frac{kmol \times 10^6}{m^3}$	Concentration difference $kmol \times 10^6 / m^3$	Diff.% with respect to C_{Ao}
24.53	298	20	24.54	- 0.01	- 0.05
25.98	373	20	24.96	0.02	0.07
30.71	423	20	30.67	0.04	0.12
27.00	453	20	27.02	0.02	0.07

present case. From this we can also conclude that neither the stainless steel gauze nor the Pyrex walls of the reactor vessel had any catalytic effect on the reaction in the range of conditions examined.

These results are in agreement with previous studies. As indicated in Section 2.3, the gas-phase reaction between methyl mercaptan and oxygen in a batch reactor does not occur at temperatures below 474 K [19]. In a tubular reactor, it was also reported [27] that the oxidation of methyl mercaptan by air starts at a temperature of about 473 K and reaches a conversion of about 45% when the temperature is 573 K for a mean residence time of 27 seconds.

5.3 EFFECT OF CURRENT, TEMPERATURE, AND MEAN RESIDENCE TIME ON THE FRACTIONAL CONVERSIONS OF METHYL MERCAPTAN

The reaction of methyl mercaptan with air was studied over a range of the following variables: current 0.05 to 1.6 mA, temperature 298 to 453 K, and mean residence time 3 to 35 seconds. The initial concentration of the mercaptan in the feed ranged from 19.8×10^{-6} to 23.3×10^{-6} kmol/m^3.

As introduced earlier, the kinetic data of the above reaction may be represented by the fractional conversion X_A of methyl mercaptan:

$$X_A = \frac{C_{Ao} - C_A}{C_{Ao}} \qquad (5.1)$$

where C_{Ao} and C_A are the concentrations of methyl mercaptan in the feed and product streams, respectively.

The results are shown in Figures from 5.1a to 5.1e. In each figure, the fractional conversion of the mercaptan is plotted against the mean residence time for several values of the current while the temperature remained constant. The solid lines shown in these figures were obtained from the data correlation as will be discussed in Chapter 7.

The most striking observation made from these results is that the reaction can proceed with appreciable rates within the temperature range investigated. As indicated by Figure 5.1a, for example, when the current is 1.2 mA complete removal of methyl mercaptan is possible at room temperature for a mean residence time of about 16 seconds.

At otherwise constant conditions, the results also show that the fractional conversion of methyl mercaptan increases as expected with increase in mean residence time. The fact that the reaction rate, given by the slope of these curves, varies with the mean residence time indicates that the reaction is concentration-dependent. The degree of this dependency will be discussed later in Chapter 7.

The dependency of the fractional conversion on the current may be discussed in reference to any of the above

a: Temperature=298 K

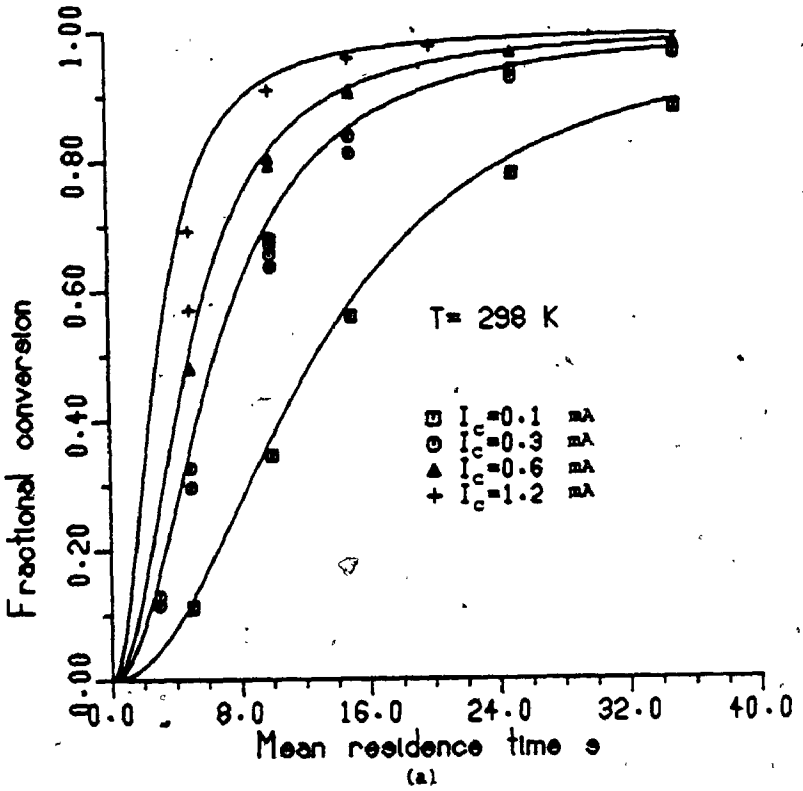

(a)

Figure 5.1 (a-e): Time-dependency of the fractional conversion of methyl mercaptan due to reaction with air.

Reactor dimensions:

$D = 2.54 \times 10^{-2}$ m

$H = 1.52 \times 10^{-1}$ m

$a = 1.52 \times 10^{-5}$ m

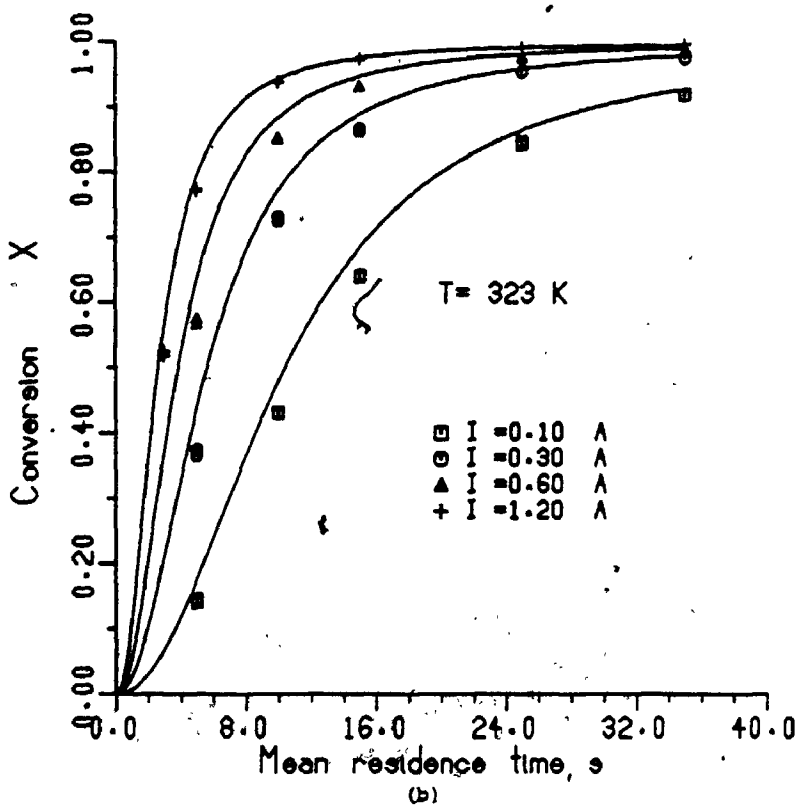

(b)

Figure 5.1 (continued)

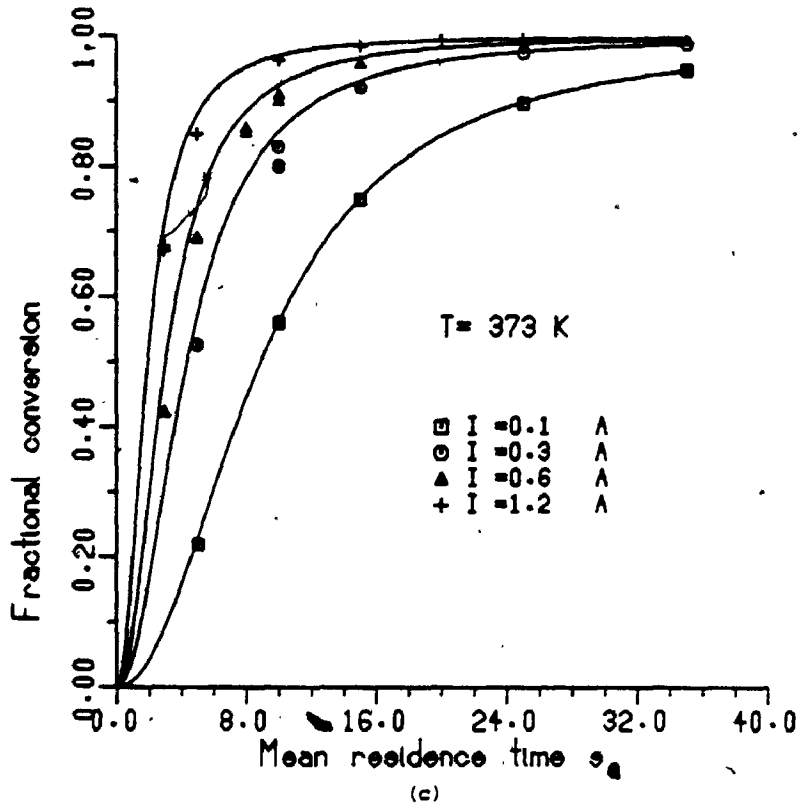

(c)

Figure 5.1 (continued).

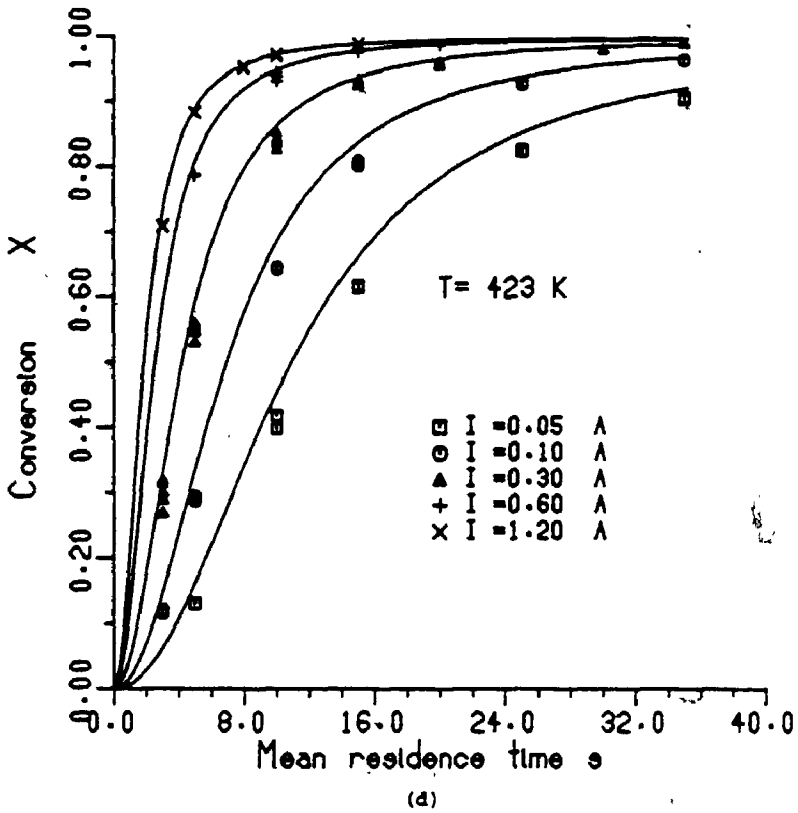

(d)

Figure 5.1 (continued).

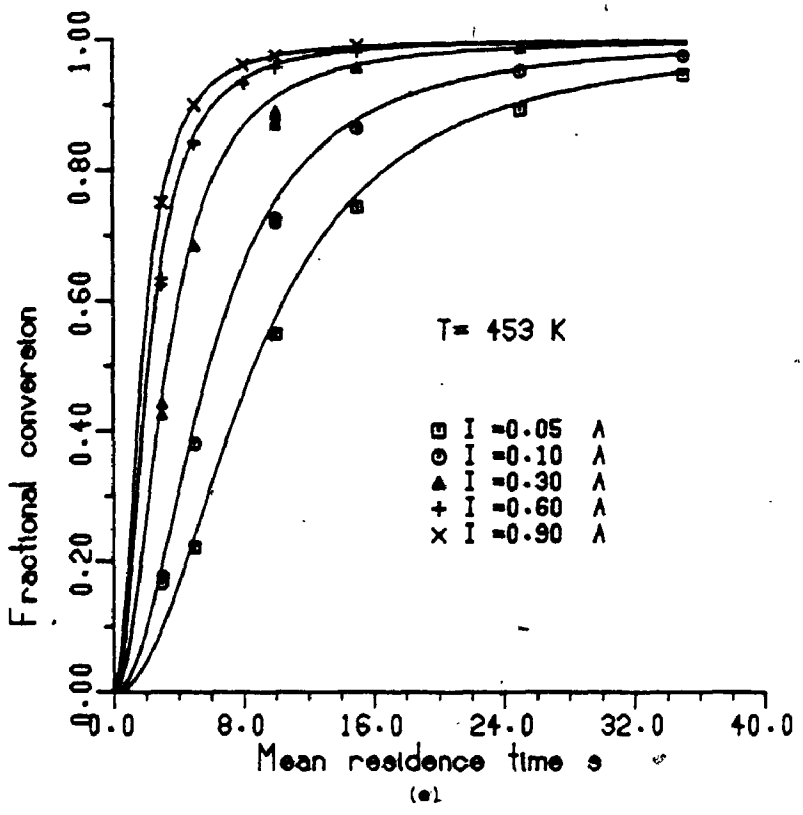

(e)

Figure 5.1 (continued).

figures at constant mean residence time. At these conditions, there is a high fractional conversion of methyl mercaptan when the current is increased. This fact combined with the findings discussed earlier that the reaction does not proceed in the temperature range examined unless the corona disharge is present emphasize the essential role of the latter in facilitating the reaction. This effect is explicity shown in Figure 5.2. The figure illustrates the fractional conversion of methyl mercaptan as a function of current at two constant temperatures (298 and 423 K) and two values of mean residence time (5 and 10 seconds). Evidently, there are values of current, depending upon temperature and upon mean residence time, at which a complete conversion of methyl mercaptan is obtained.

On the other hand, the temperature-dependency of the fractional conversion of methyl mercaptan may be discussed by referring to Figures 5.1a to 5.1e above. At constant conditions of current and mean residence time, these figures indicate that high temperatures result in high fractional conversions. For example, at 0.3 mA and 10 s, as temperature is raised from 298 to 373 to 423 to 453 K, the conversion is found to increase from about 0.65 to about 0.80 to about 0.86 to about 0.90, respectively.

This relationship shows that, in the temperature range tested, while the thermal reaction in the absence of corona

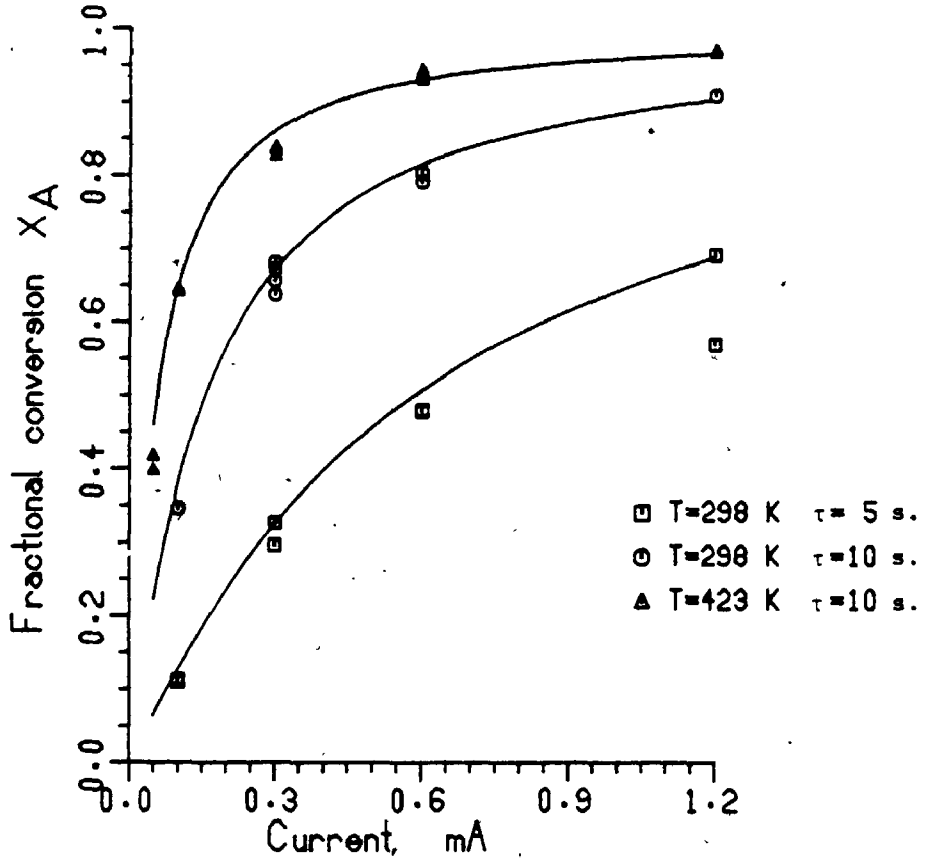

Figure 5.2: Current-dependency of the fractional conversion of methyl mercaptan due to reaction with air.

discharge is unimportant as seen earlier temperature does play a role as soon as a corona discharge is present. This effect is also emphasized in Figure 5.3 where the fractional conversion is plotted against temperature at pre-assigned constant values of current and mean residence time.

5.4 EFFECT OF CURRENT, TEMPERATURE, AND MEAN RESIDENCE TIME ON THE DISTRIBUTION OF THE REACTION PRODUCTS

The results of Section 4.3 indicated that the products of the reaction of methyl mercaptan with air in the corona reactor are water, sulphur dioxide, dimethyl sulphide, dimethyl disulphide, and dimethyl sulphone. As mentioned earlier the concentration of every product may be represented by its distribution D:

$$D_i = \frac{\text{Concentration of product i in product stream}}{\text{Concentration of methyl mercaptan in feed}} \qquad (5.2)$$

However, due to the extremely low concentrations of methyl mercaptan employed, the flow through the reactor could be considered of constant density. Therefore, the distribution of every product may also be represented by the ratio of its amount (kmol) in the gas volume trapped in the sample loop from the product stream to that of the mercaptan trapped from the feed stream, i.e.,

$$D_i = \frac{\text{kmol of product i in product stream}}{\text{kmol of methyl mercaptan in feed}} \qquad (5.3)$$

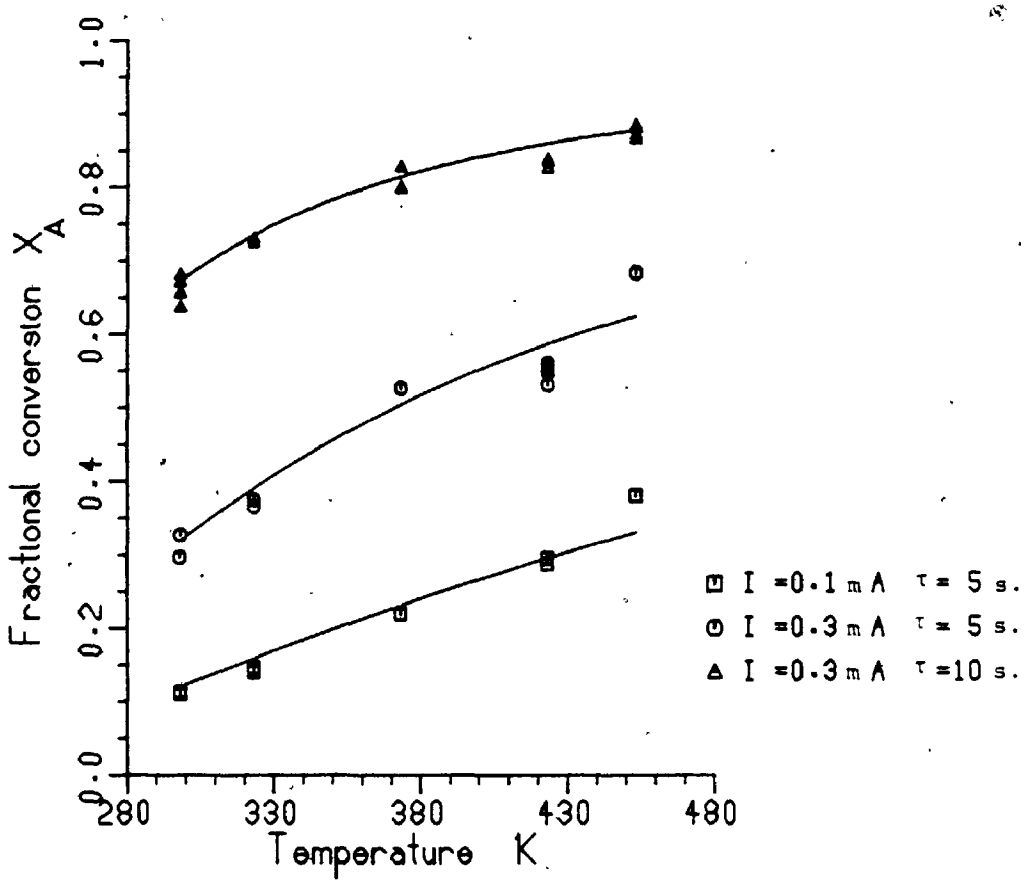

Figure 5.3: Temperature-dependency of the fractional conversion of methyl mercaptan due to reaction with air.

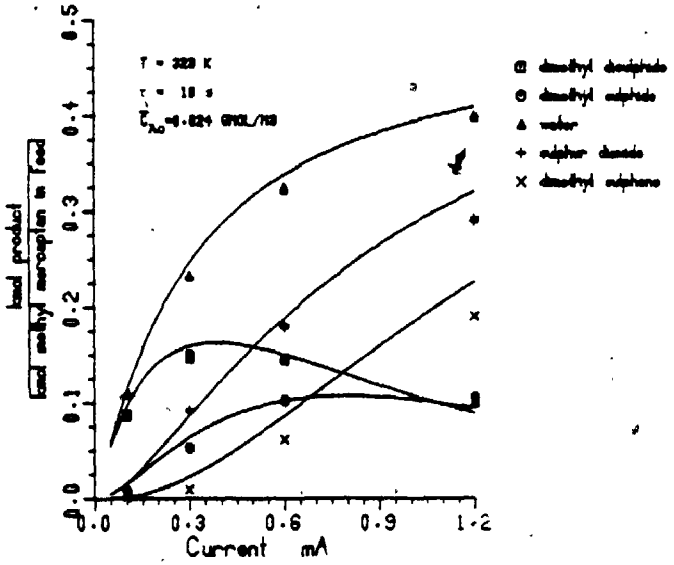

Figure 5.5: Concentration-current curves of the products of the reaction between methyl mercaptan and air.

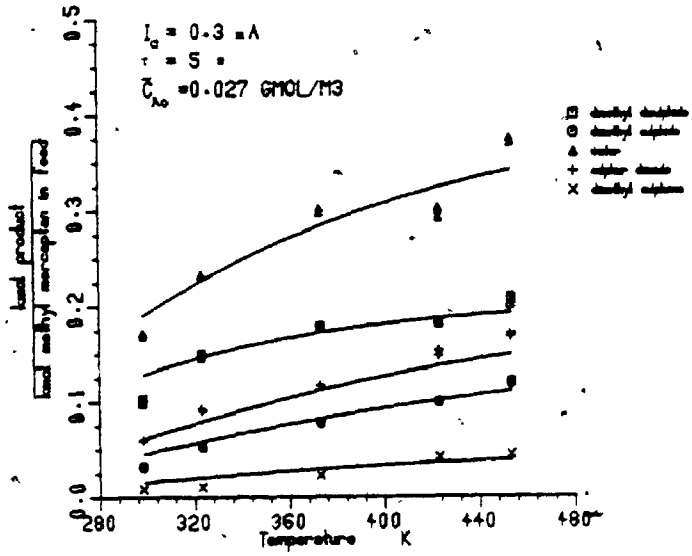

Figure 5.6: Concentration-temperature curves of the products of the reaction between methyl mercaptan and air.

Reactor dimensions for Figures 5.5 and 5.6

$D = 2.54 \times 10^{-2}$ m

$H = 1.52 \times 10^{-1}$ m

$a = 1.52 \times 10^{-5}$ m

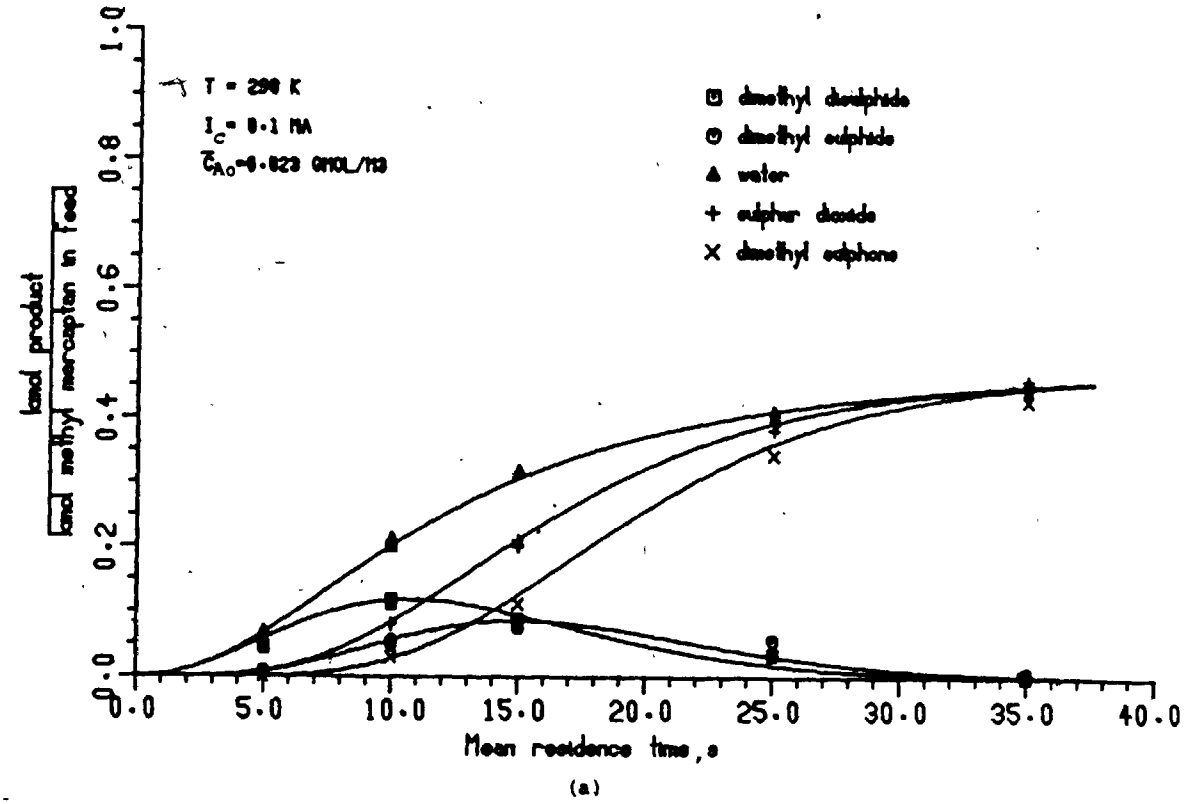

(a)

Figure 5.4 (a-e): Concentration-time curves of the reaction products between methyl mercaptan and air.

Reactor dimensions: $D = 2.54 \times 10^{-2}$ m
$H = 1.52 \times 10^{-1}$ m
$a = 1.52 \times 10^{-5}$ m

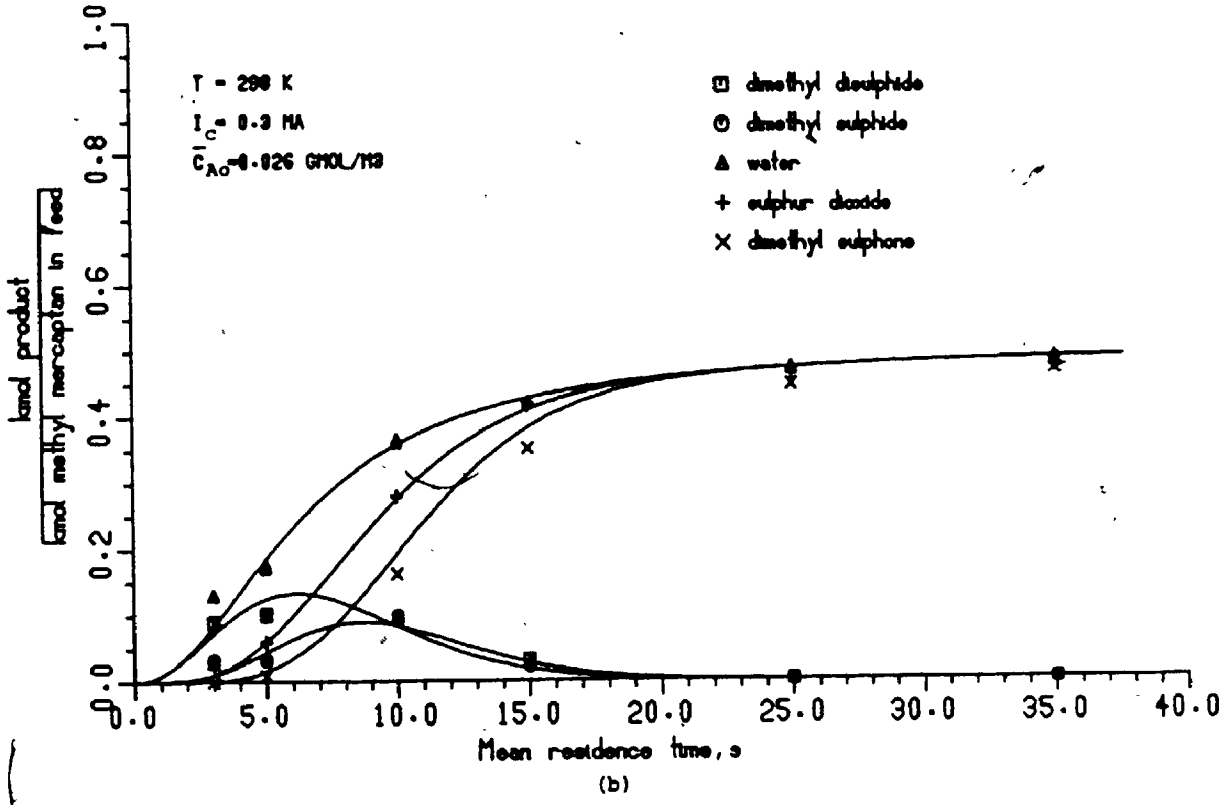

(b)

Figure 5.4 (continued).

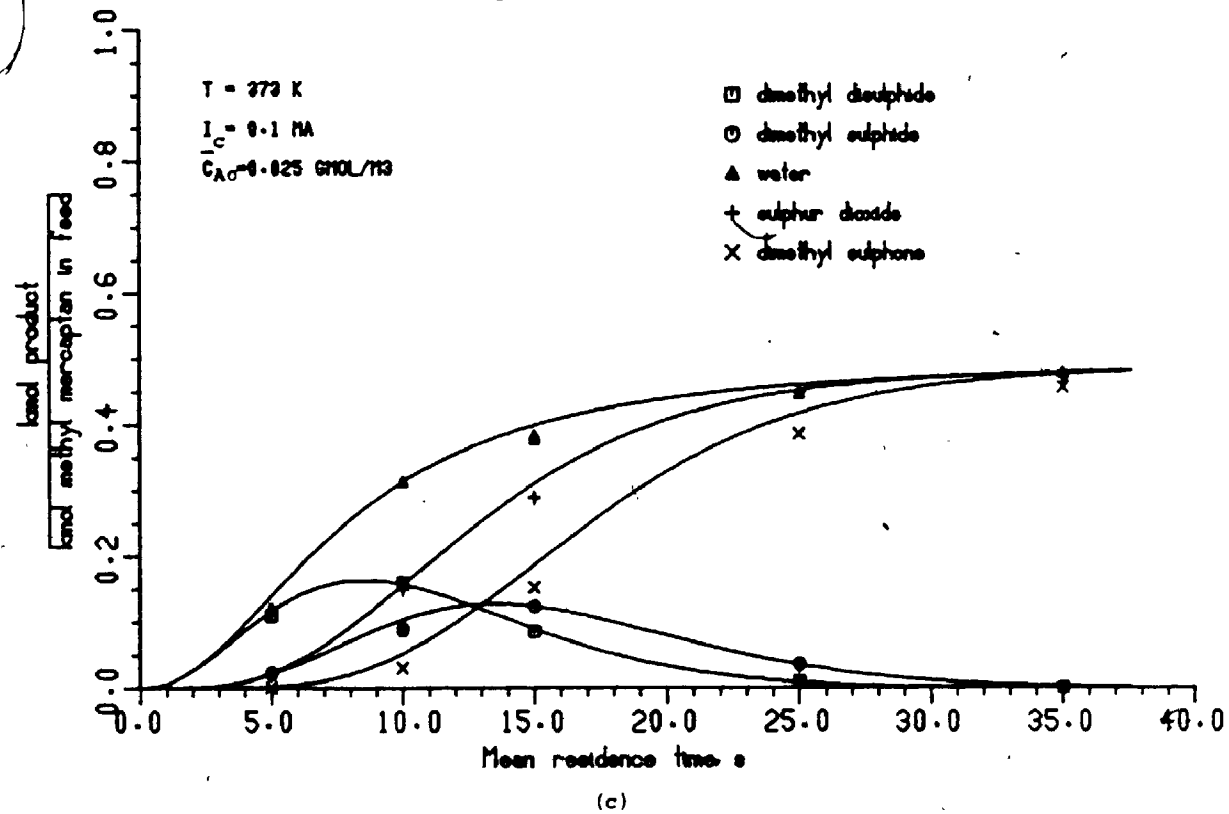

(c)

Figure 5.4 (continued)

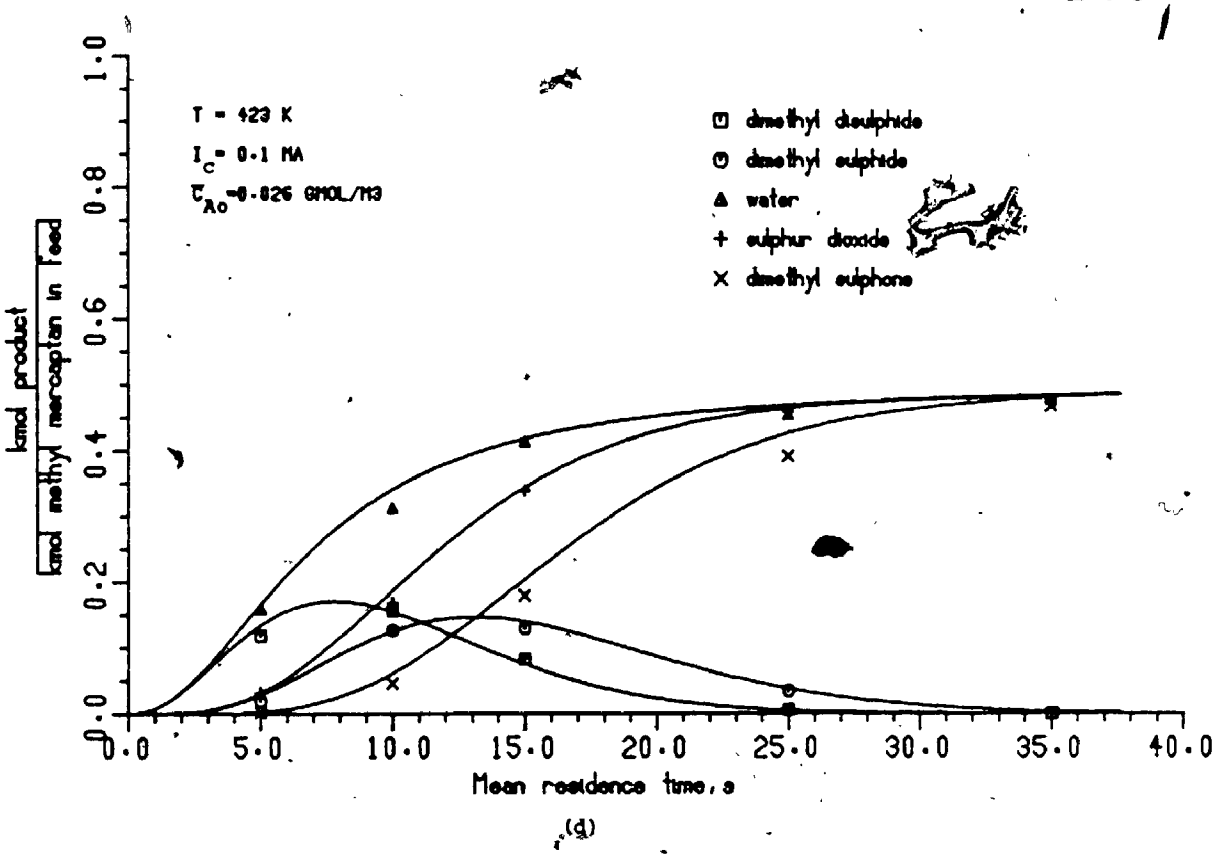

(d)

Figure 5.4 (continued)

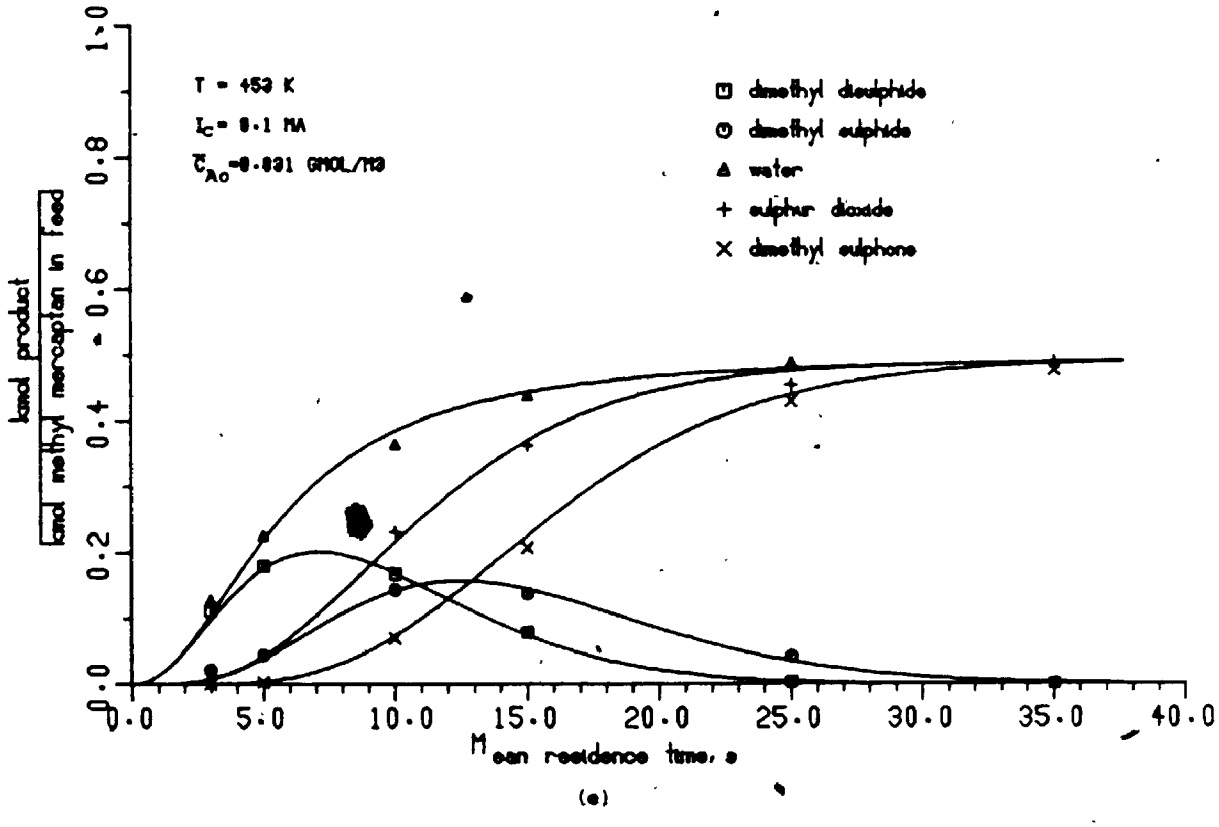

(e)

Figure 5.4 (continued)

Furthermore, a comparison between Figures 5.4(a-d) indicates, as expected, that the distribution of each product also depends on current and temperature. As observed from the figures, the distribution of the end products, namely, water, sulphur dioxide, and dimethyl sulphone and their formation rate always increases with the increase in current and/or temperature. This fact may be explicity illustrated in Figures 5.5 and 5.6.

On the other hand, the concentration-dependency of the intermediates dimethyl disulphide and dimethyl sulphide on current and temperature follow the same pattern as that of the mean residence time. The formation rate of these compounds and then that of their disappearance always increase with the increase in both variables. That is to say that higher values of current and temperature causes the maximum concentration of these sulphur compounds to shift towards shorter mean residence times. However, as shown in Figures 5.5. and 5.6, this dependency on temperature is not as significant as in the case of temperature. Then, it was concluded that the electrical energy contributes more in activating the above reactions than the thermal energy in the range of conditions attempted. The importance of each of these energies is to be determined quantitatively in Chapter 7.

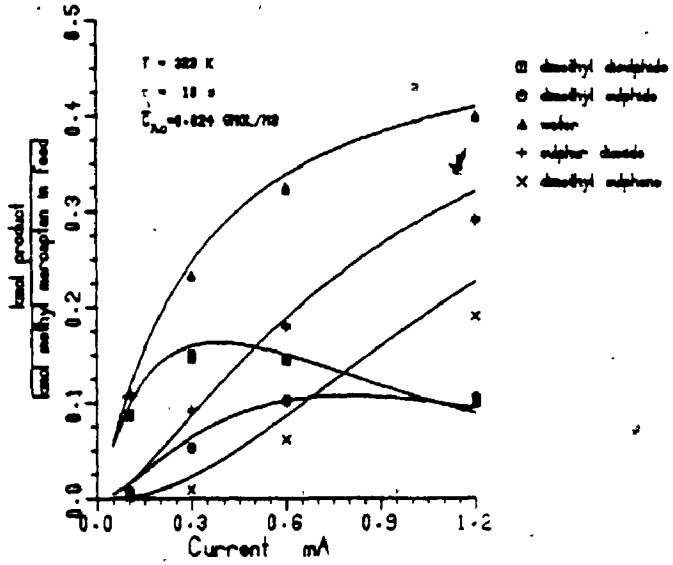

Figure 5.5: Concentration-current curves of the products of the reaction between methyl mercaptan and air.

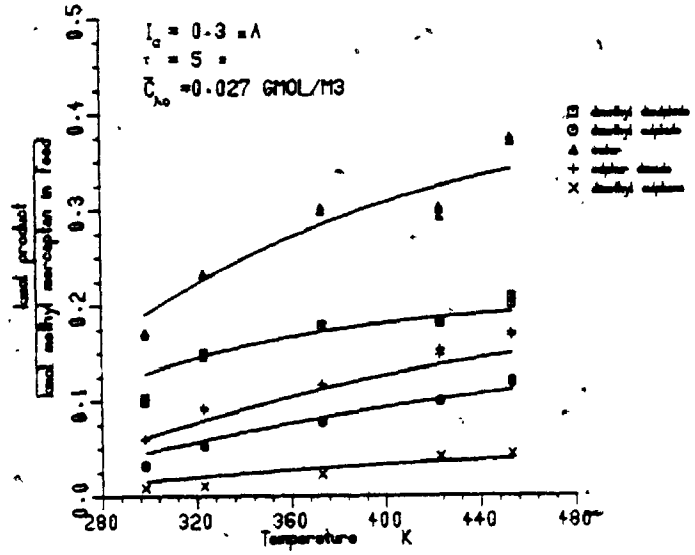

Figure 5.6: Concentration-temperature curves of the products of the reaction between methyl mercaptan and air.

Reactor dimensions for Figures 5.5 and 5.6

$D = 2.54 \times 10^{-2}$ m

$H = 1.52 \times 10^{-1}$ m

$a = 1.52 \times 10^{-5}$ m

5.5 MECHANISM OF THE REACTION OF METHYL MERCAPTAN WITH AIR IN A CORONA DISCHARGE

5.5.1 A Proposed Mechanism

In view of the above results, the reaction of methyl mercaptan with air in the corona reactor seems to proceed as a series of consecutive reactions with both dimethyl disulphide and dimethyl sulphide being intermediates and water, sulphur dioxide, and dimethyl sulphone being end products.

Now, consider a series of consecutive reactions such as:

$$A \rightarrow B \rightarrow C \rightarrow D \qquad (5.4)$$

in which A is the reactant, B and C are intermediate products and D is the end product. Figure 5.7 represents the typical concentration-time relationships for this situation [105]: as A keeps on decreasing B rises to a maximum and then falls, C also rises to a maximum and then falls, whereas D keeps on rising without falling.

A comparison between Figure 5.7 and Figure series 5.4 would suggest that the present reaction proceeds in a similar fashion. Accordingly, the reaction may be written primarily as:

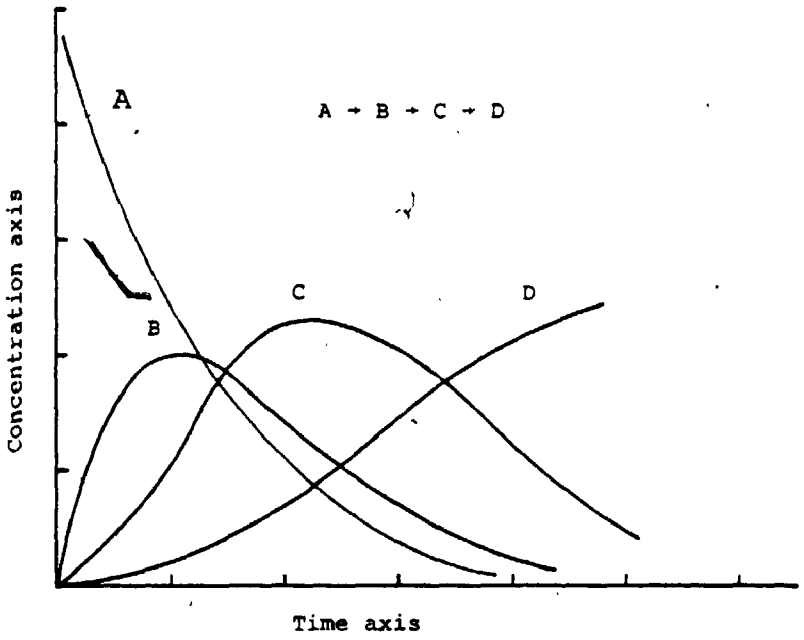

Figure 5.7: Typical concentration-time curves for three consecutive reactions.

$$CH_3SH \rightarrow (CH_3)_2S_2 \rightarrow (CH_3)_2S \rightarrow (CH_3)_2SO_2 \qquad (5.5)$$

In reference also to Figure series 5.4 we observe that water and sulphur dioxide are formed almost instantly with dimethyl disulphide and dimethyl sulphide, respectively. Therefore, reactions (5.5) may be re-written as:

$$CH_3SH \overset{O}{\rightarrow} (CH_3)_2S_2 + H_2O \overset{O}{\rightarrow} (CH_3)_2S + SO_2$$
$$\overset{O}{\rightarrow} (CH_3)_2SO_2 \qquad (5.6)$$

Based on this information together with the fact indicated previously that the reaction between methyl mercaptan and air in the corona reactor is an oxidation reaction in which oxygen is the oxidizing agent, the following mechanism was proposed:

Mechanism A

$$2CH_3SH + \tfrac{1}{2}O_2 \rightarrow (CH_3)_2S_2 + H_2O \qquad (5.7a)$$

$$(CH_3)_2S_2 + O_2 \rightarrow (CH_3)_2S + SO_2 \qquad (5.7b)$$

$$(CH_3)_2S + O_2 \rightarrow (CH_3)_2SO_2 \qquad (5.7c)$$

The occurence of these reactions has been reported by previous investigations as will be discussed next in detail.

5.5.2 Test of Mechanism A

Two sets of experiments were devised so as to verify the above mechanism. In each set, either dimethyl disulphide or dimethyl sulphide was allowed to react under controlled conditions with air in a corona discharge. Refering to Section 4.3, the experimental procedure followed consisted of preparation of dimethyl disulphide (or dimethyl sulphide) mixture with nitrogen in the lecture bottle (see Appendix B for more details). Then, two monitored streams of the prepared mixture and of air were combined together in the mixing chamber to form the feed to the reactor. For a given set of conditions such as temperature and current, reaction between the sulphur compound in concern and air was allowed to take place. Analysis of the feed and of the product streams was performed by the gas chromatograph whose operating conditions were the same as previously described. The results of the two sets of experiments and their discussion are given below.

5.6 REACTION OF DIMETHYL DISULPHIDE WITH AIR

5.6.1 The Thermal Reaction

The importance of the thermal reaction of dimethyl mercaptan with air was examined. A set of experiments under constant conditions of temperature and of mean residence time was therefore conducted. Four temperature values: 298, 373, 423, and 453 K were employed while the mean

residence time was kept constant always at 20 seconds. The initial concentration of dimethyl disulphide ranged from 24.5×10^{-6} to 30.7×10^{-6} kmol/m^3. As in the case of methyl mercaptan this range of conditions was tried since it may cover practical interests.

The results obtained are listed in Table 5.2. Evidently, no substantial conversions of dimethyl disulphide were obtained under the present conditions. The differences between the concentration of dimethyl disulphide in the feed and in the products streams indicated are in fact within the experimental errors as discussed previously. Therefore, the thermal reaction in the absence of corona discharge is concluded to be insignificant. Moreover, it could be concluded that the stainless steel gauze and the Pyrex walls of the reactor had no catalytic effect on the reaction. These results agree with previous findings. The gas-phase reaction between dimethyl disulphide and air was reported to proceed with appreciable rates only at temperatures higher than 613 K [107].

5.6.2 The Reaction in Presence of the Corona Discharge

5.6.2.1 Identification of the Reaction Products

At a temperature of 423 K and a current of 0.3 mA, the reaction between dimethyl disulphide and air resulted in two products which were separated by the gas chromatograph. In addition, a solid material deposited on the reactor walls

near the exit.

The separable compounds by the gas chromatograph had retention times of about 603 and 1609 seconds which matched those of sulphur dioxide and dimethyl sulphide, respectively. Thus, these two compounds were concluded to be among the reaction products.

The solid material formed by the reaction was found to dissolve in ethanol. It was collected by washing the reactor walls thoroughly with ethanol and recovered in a crystalline form by evaporation and then weighed. Identification of this material was done by NMR technique as well as by the melting point test (see Section 4.3.2.1).

From the NMR spectrum shown in Figure 5.8, since only one absorption peak is exhibited the solid material consists only of one compound. Furthermore, this NMR spectrum with a chemical shift of about 3.0 ppm matches that of dimethyl sulphone as given in the Aldrich Library of Spectra [83] under the number NMR 10,2C(19). The compound was therefore identified as dimethyl sulphone. The melting point test also showed that the melting point of this compound was in 380 to 384 K range which is in excellent agreement with that of dimethyl sulphone being 382 K.

Mass balance calculations around the reactor for a

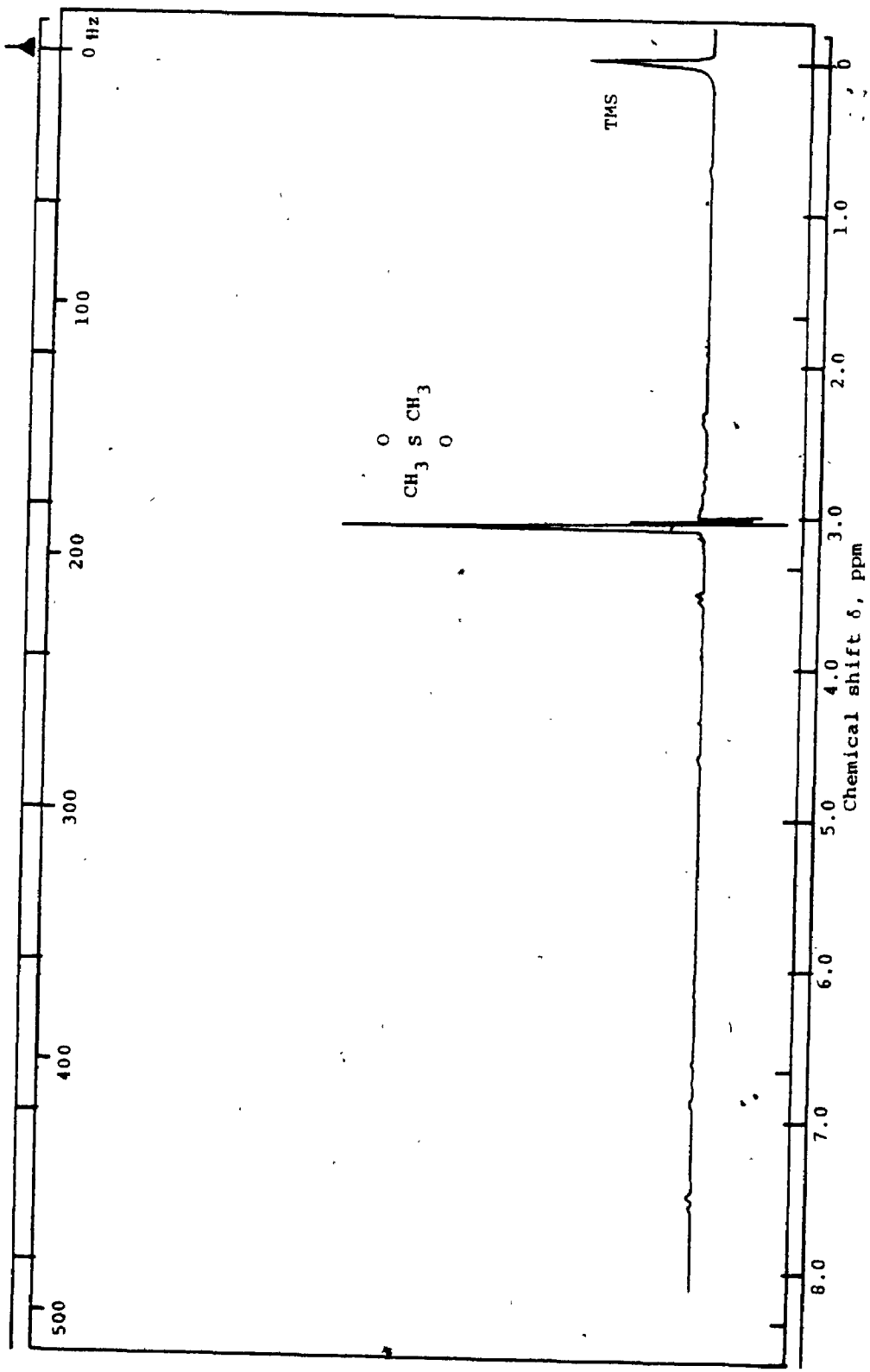

Figure 5.8: NMR spectrum of the solid product of the reaction of dimethyl disulphide with air in corona discharge

typical experimental run are summarized in Table 5.3. With a maximum sulphur deficit only of 3.7%, it could be concluded that all the reaction products were accounted for.

5.6.2.2 Kinetic Data on the Reaction

Kinetic data on the above reaction was collected i)partly for the development of a mechanism of the reaction of methyl mercaptan with air and ii)partly to evaluate the kinetic parameters required for the same reaction.

As illustrated by Figure 5.9, the concentration of every compound in the product stream with respect to the initial concentration of dimethyl disulphide is given as a function of the mean residence time at 423 K and 0.3 mA. The results show that as the concentration of dimethyl disulphide decreases the concentration of dimethyl sulphide rises, passes through maximum and then falls, the concentration of sulphur dioxide rises continuously from the beginning of the reaction, and the concentration of dimethyl sulphone rises also continuously but after what seems to be an induction period.

As indicated earlier, these of results exhibit the behaviour of a series of consecutive reactions with dimethyl sulphide is an intermediate whereas sulphur dioxide and dimethyl sulphone are end products.

TABLE 5.3: A SAMPLE CALCULATIONS OF MASS BALANCE AROUND THE REACTOR FOR THE REACTION OF DIMETHYL DISULPHIDE WITH AIR

Element	Stream	Mass flow rate x 10^{11} katom/s				Total
		$(CH_3)_2S_2$	SO_2	$(CH_3)_2S$	$(CH_3)_2SO_2$	
S	Feed	41.331				41.331
	Product	5.123	17.917	4.978	11.803	39.821
	Difference					1.510
	Diff%					3.7
C	Feed	41.331				41.331
	Product	5.123		9.956	23.606	38.685
	Difference					2.646
	Diff.%					6.4
H	Feed	123.993				123.993
	Product	15.369		29.868	70.818	116.055
	Difference					7.938
	Diff.%					6.4

* Operating conditions:

Temperature	= 423	K
Initial concentration of dimethyl disulphide	= 26.7	$x10^{-6}$ kmol/m^3
Mean residence time	= 10 s	
Corona current	= 0.3	mA

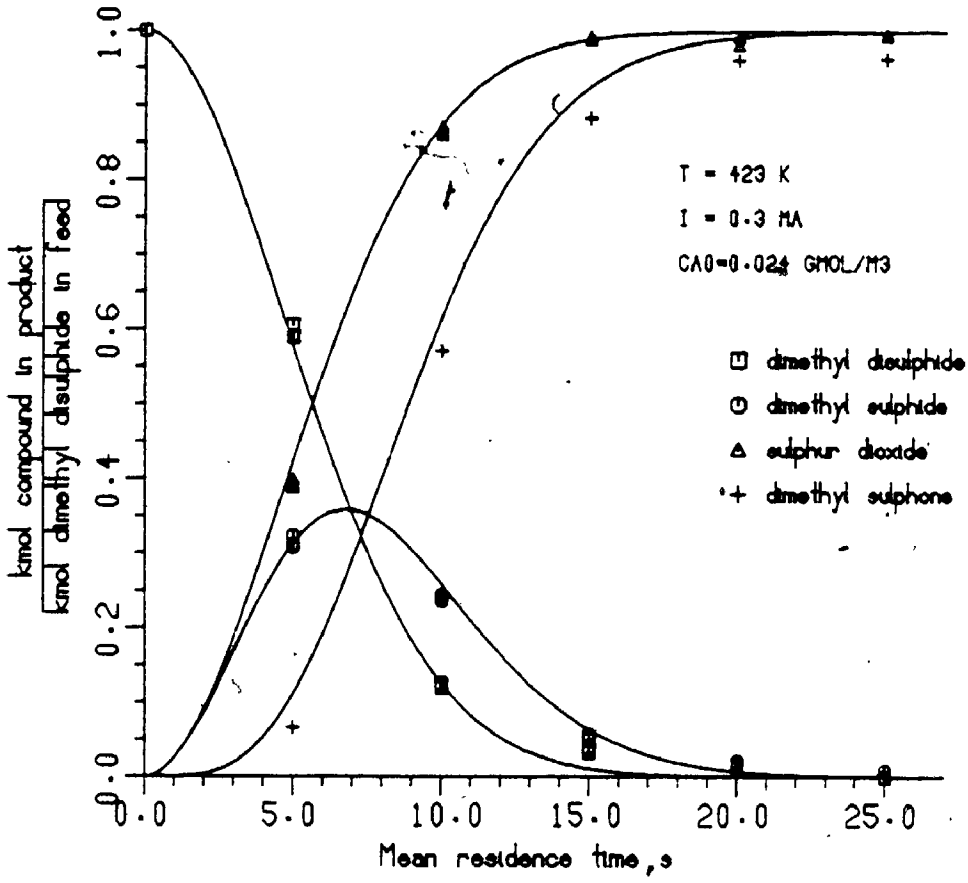

Figure 5.9: Concentration-time curves for the reaction of dimethyl disulphide with air

Reactor dimensions: $D = 2.54 \times 10^{-2}$ m
$H = 1.52 \times 10^{-1}$ m
$a = 1.52 \times 10^{-5}$ m

The fact that the concentration of dimethyl sulphide and of sulphur dioxide start to rise almost together would indicate that these compounds are formed from the common material of dimethyl disulphide. On the other hand, as the concentration of dimethyl sulphone starts to increase considerably after an induction period and more particularly when the concentration of dimethyl sulphide begins to fall it is concluded that the former compound is produced at the expense of the latter. This conclusion will further be discussed below.

As observed from these results, water was not formed by the reaction. This fact agrees with Mechanism A proposed above that the presence of methyl mercaptan is necessary for the formation of water. The formation of water as well as dimethyl disulphide from the mercaptan was reported by previous workers [108,109,110]. In accordance with the mechanisms proposed by these workers, the reactions may be explained by free radical formation:

- the reaction is initiated by the oxygen attack on the S-H bond in methyl mercaptan to form the free radicals:

$$CH_3SH + O_2 \rightarrow CH_3S^{\cdot} + HO \qquad (5.8a)$$

- a reaction of CH_3S radicals with oxygen would then result in the formation of the sulphinyl radicals:

$$CH_3S^{\cdot} + O_2 \rightarrow CH\ SO_2^{\cdot} \qquad (5.8b)$$

which would in turn react with methyl mercaptan to produce sulphinic acid in addition to more CH_3S radicals:

$$CH_3SO_2^{\cdot} + CH_3SH \rightarrow CH_3S^{\cdot} + CH_3SO_2H \qquad (5.8c)$$

- as sulphinic acid is highly unstable [110,111], it would disproportionate to dimethyl disulphide, hydrogen peroxide, and oxygen [112]:

$$2CH_3SO_2H \rightarrow (CH_3)_2S_2 + H_2O_2 + O \qquad (5.8d)$$

or it may as well react with methyl mercaptan, to form more dimethyl disulphide and hydrogen peroxide:

$$CH_3SO_2H + CH_3SH \rightarrow (CH_3)_2S_2 + H_2O_2 \qquad (5.8e)$$

- more CH_3S radicals and hydrogen peroxide may also be produced by the reaction of HO_2 radicals formed by reaction (5.5a) with methyl mercaptan [19]:

$$HO_2^{\cdot} + CH_3SH \rightarrow CH_3S^{\cdot} + H_2O_2 \qquad (5.8f)$$

- hydrogen peroxide, being a powerful oxidizing agent itself, may oxidize methyl mercaptan according to:

$$H_2O_2 + 2CH_3SH \rightarrow 2CH_3S^{\cdot} + 2H_2O \qquad (5.8g)$$

or it may disproportionate, since it is an unstable compound, to water and oxygen:

$$2H_2O_2 \rightarrow 2H_2O + O_2 \qquad (5.8h)$$

- CH_3S radicals are, on the other hand, capable of combining together to form dimethyl disulphide:

$$CH_3S^{\cdot} + CH_3S^{\cdot} \rightarrow CH_3SSCH_3 \qquad (5.8i)$$

5.7 REACTION OF DIMETHYL SULPHIDE

5.7.1 The Thermal Reaction

The thermal reaction of dimethyl sulphide with air was investigated using the same procedure and the same conditions as discussed above with dimethyl disulphide.

In reference to Table 5.4, the results obtained from the above experiments show that significant conversions of dimethyl sulphide were obtained under the present conditions. The differences exhibited between the concentration of dimethyl sulphide in the feed and in the product streams are within experimental error.

TABLE 5.4: EXPERIMENTS TO DETERMINE THE IMPORTANCE OF THE THERMAL REACTION OF DIMETHYL DISULPHIDE WITH AIR

C_{A0} $\frac{kmol \times 10^6}{m^3}$	Temperature K	τ s	C_A $\frac{kmol \times 10^6}{m^3}$	Concentration difference $kmol \times 10^6 / m^3$	Diff. % with respect to C_{A0}
21.48	298	20	21.45	0.033	0.16
25.07	373	20	24.14	- 0.07	- 0.26
24.67	423	20	24.62	0.05	0.18
24.98	453	20	24.95	0.03	0.10

These results agree with previous investigations. For example, Cullis et al [19] have reported that the gas-phase oxidation of dimethyl sulphide would only take place at temperatures higher than 473 K.

5.7.2 Reaction in the Presence of Corona Discharge

5.7.2.1 Identification of the Reaction Products

Analysis done on the product stream of the above reaction indicated that there were no products which may be separated by the gas chromatograph. However, the reaction formed a solid material which deposited on the reactor walls near the exit. It was found to dissolve in ethanol and therefore it was collected following the procedure described earlier.

Identification of this material was also done by the NMR technique and the melting point test as discussed previously. The NMR spectrum given in Figure 5.10 shows a peak at a chemical shift of about 3.0 ppm. This as before implies that the solid material consisted only of one compound which is identified as dimethyl sulphone. Moreover, the melting point of the compound also ranged from 381 to 383 K which agrees reasonbly well with that of the sulphone.

Furthermore, an example of mass balance calculations around the reactor is given in Table 5.5.

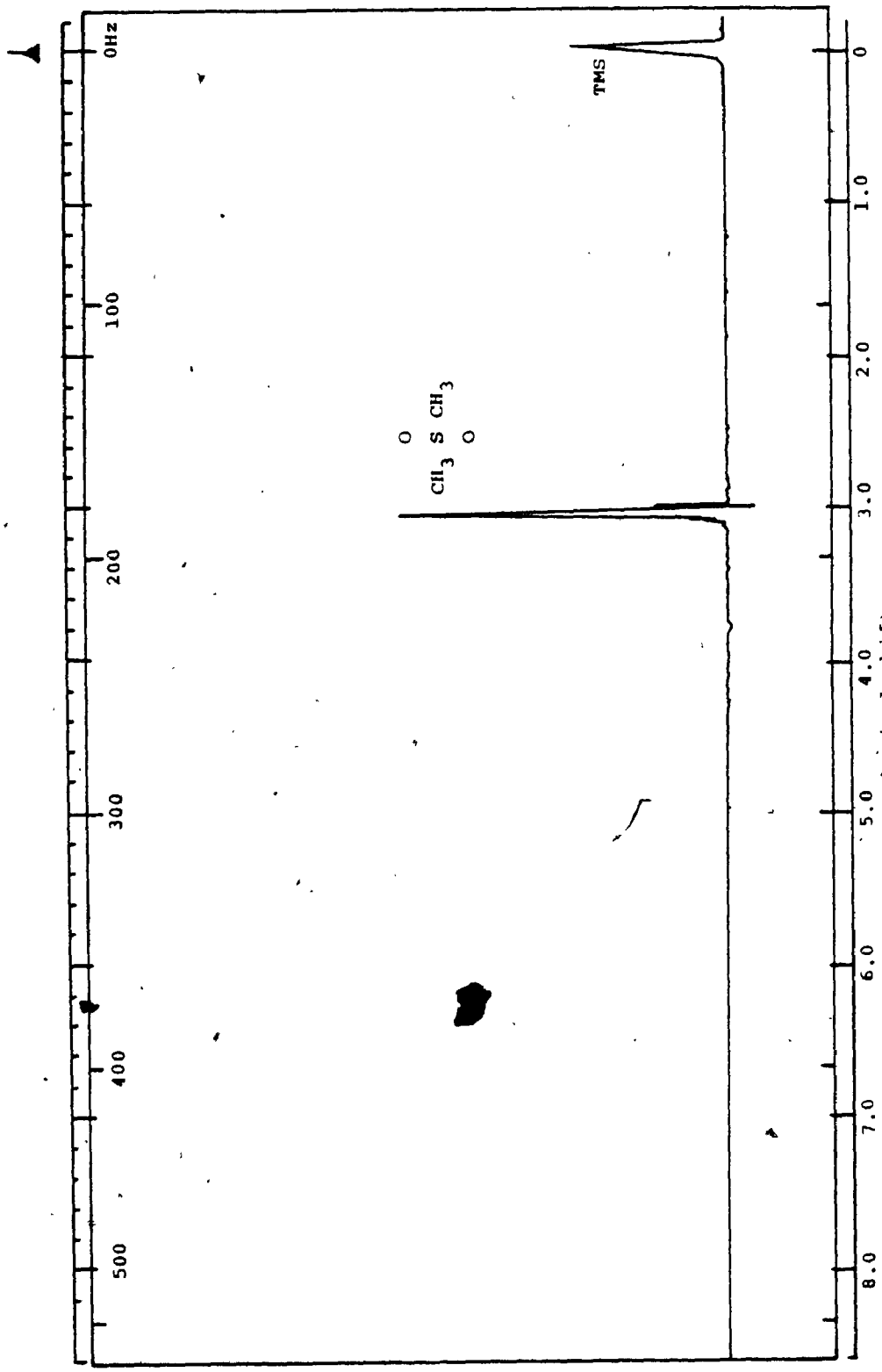

Figure 5.10: NMR spectrum of the solid product of the reaction between dimethyl sulphide and air in corona discharge.

TABLE 5.5*: A SAMPLE CALCULATIONS OF MASS BALANCE AROUND THE REACTOR FOR THE REACTION OF DIMETHYL SULPHIDE WITH AIR

Element	Stream	Mass flow rate x 10^{11} katom/s		Total
		$(CH_3)_2S$	$(CH_3)_2SO_2$	
S	Feed	18.177		18.177
	Product	5.687	11.496	17.183
	Difference			0.994
	Diff.%			5.47
C	Feed	36.354		36.354
	Product	11.374	22.992	34.366
	Difference			1.988
	Diff.%			5.47
H	Feed	109.062		109.062
	Product	34.122	68.976	103.098
	Difference			5.964
	Diff.%			5.47

* Operating conditions:

Temperature	= 423	K
Initial concentration of dimethyl sulphide	= 23.5	$x10^{-6}$ $kmol/m^3$
Mean residence time	= 10	s
Corona current	= 0.3	mA

The good balance of sulphur, carbon, and of hydrogen would indicate that dimethyl sulphone is the only product of the reaction. The relatively high deficits (about 5.5% in each) added further evidence to the previous conclusion that the large experimental errors reported above for the other reactions are inherent in the procedure used to collect dimethyl sulphone.

5.7.2.2 Kinetic Data on the Reaction

For the same reason as discussed above in Section 5.6.2.2, kinetic data on the reaction of dimethyl sulphide with air were obtained. These data are presented in Figure 5.11 in terms of the concentration of every component in the product stream to the initial concentration of dimethyl sulphide in the feed as function of mean residence time at a temperature of 423 K and a current of 0.3 mA.

The results show that as the mean residence time increases the concentration of dimethyl sulphide decreases and that of dimethyl sulphone increases. As expected, the latter compound was an end product of the reaction whereas no intermediates were detected.

The fact that sulphur dioxide was not produced by the reaction indicates that this compound is formed from a compound other than dimethyl sulphide. This conclusion together with the results of Section 5.5.2.1 will then

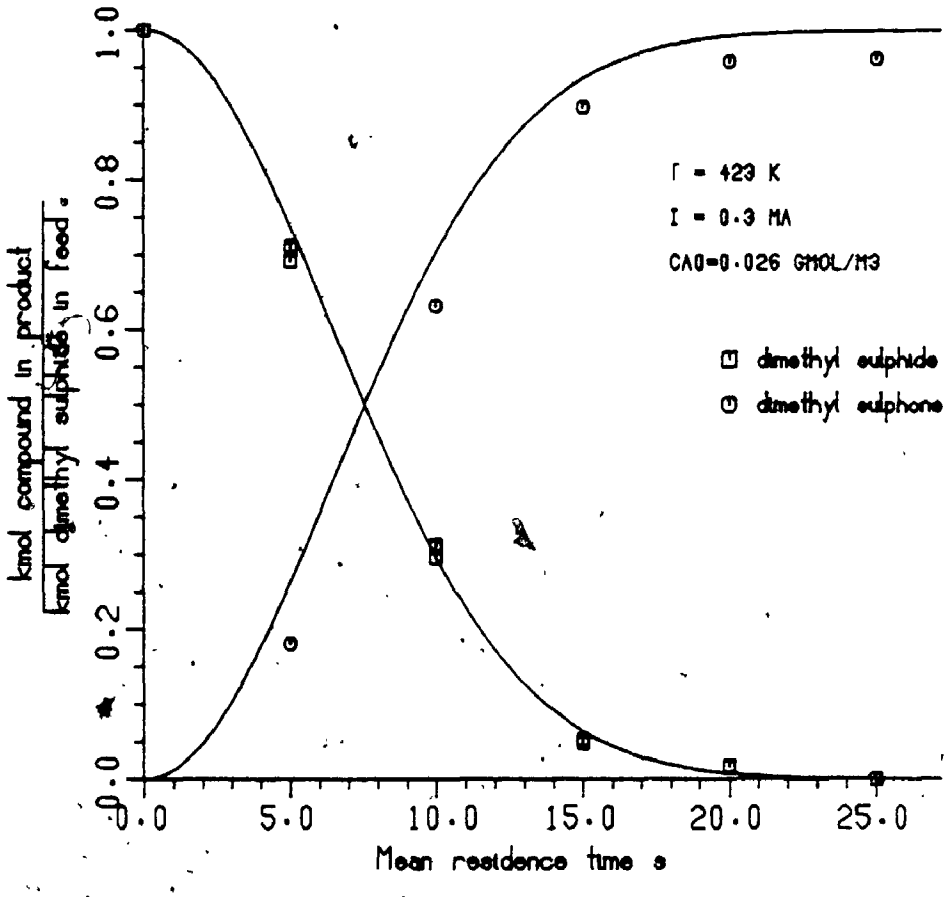

Figure 5.11: Concentration-time curves for the reaction of dimethyl sulphide with air

Reactor dimensions: $D = 2.54 \times 10^{-2}$ m
$H = 1.52 \times 10^{-1}$ m
$a = 1.52 \times 10^{-5}$ m

verify that both sulphur dioxide and dimethyl sulphide are produced from dimethyl disulphide.

The formation of monosulphides from disulphides has been reported in previous studies. Schoberg et al [112], for example, reported that bubbling air liquid in disulphide causes the latter to convert to monosulphide. They found that scission of the -S-S- bond was evident, more particularly, in the presence of oxidizing species such as oxygen. According to Bernard [114,115], it may be assumed [111] that oxygen molecules attach nucleophilically on a sulphur atom of the disulphide. Then, the reaction may be initiated as follows:

$$CH_3SSCH_3 + O_2 \rightarrow CH_3\overset{\overset{O-O^-}{\|}}{\underset{+}{S}}-SCH_3 \qquad (5.9a)$$

The formed thiosulphenate radicals may in turn react with dimethyl disulphide to form methyl methanethiosulphinate:

$$CH_3\overset{\overset{O-O^-}{\|}}{\underset{+}{S}}-SCH_3 + CH_3SSCH_3 \rightarrow 2CH_3\overset{\overset{O}{\uparrow}}{S}-SCH_3 \qquad (5.9b)$$

which then disproportionates to sulphenyl and thiol radicals:

$$CH_3\overset{\overset{O}{\uparrow}}{S}-SCH_3 \rightarrow CH_3SO^{\cdot} + CH_3S^{\cdot} \qquad (5.9c)$$

Shelton [117] presented evidence that the scission of the C-S bond in the sulphonyl may then occur and thus CH_3 and SO radicals are formed:

$$R\text{-}S^{\bullet}\rightarrow O \rightarrow R^{\bullet} + S^{\bullet}O \qquad (5.9d)$$

Then, the methyl and methiol radicals formed will combine to form dimethyl sulphide:

$$CH_3S^{\bullet} + {}^{\bullet}CH_3 \rightarrow CH_3SCH \qquad (5.9e)$$

Similarily, the SO radicals will be oxidized by the oxygen present to form sulphur dioxide:

$$2S^{\bullet}O + O_2 \rightarrow 2SO_2 \qquad (5.9f)$$

Another mechanism by which reaction (5.7a) proceeds may also be introduced based on the findings of a number of authors. In the thiosulphonate radicals formed in reaction (5.9a) above, an internal rearrangement may take place so that methyl metanethiosulphonate is formed [111]:

$$CH_3\text{-}\overset{\overset{O\text{-}O}{|}}{S}\text{-}S\text{-}CH_3 \rightarrow CH_3SO_2SCH_3 \qquad (5.9g)$$

which may then be desulphonized to dimethyl sulphide through the formation of an intermediate such as [118]:

$$CH_3-\overset{O}{\underset{O}{S}}-SCH_3 \rightarrow CH_3 \overset{SCH_3}{\cdots\cdots} SO_2 \rightarrow CH_3SCH_3 + SO_2 \qquad (5.9h)$$

In fact, reaction (5.9c) was reported to occur in the liquid phase [119]. The reaction is mainly an internal rearrangement of the molecules followed by their decomposition. Since these two processes are very insensitive to solvent ionizing power, it may as readily occur in the gas phase [120,121].

On the other hand, the conversion of dimethyl sulphide to dimethyl sulphone occurs by electrophilic attack of the oxygen on the sulphur atom of the sulphide followed by an internal rearrangement of the molecules:

$$CH_3SCH_3 + O_2 \rightarrow CH_3-S-\overset{O-O}{CH_3} \rightarrow CH_3-S-CH_3 \qquad (5.9i)$$

The extraordinary great stability of dimethyl sulphone and its very low reactivity would prevent it from going into further reactions [122].

5.8 SUMMARY AND CONCLUSIONS

The thermal reaction between methyl mercaptan and air is unimportant in the temperature range from 298 to 453 K. Within the same temperature range, the reaction is however to readily occur in the presence of corona discharge which is therefore concluded to play an essential role in facilitating the reaction.

The reaction is also found to be an oxidation reaction which proceeds in a series of consecutive reactions. During this series of reactions, both dimethyl disulphide and dimethyl sulphide are intermediate products whereas water, sulphur dioxide, and dimethyl sulphone are end products.

CHAPTER 6

THE ROLE OF OXYGEN SPECIES IN THE REACTION OF METHYL MERCAPTAN WITH AIR IN A CORONA DISCHARGE

6.1 INTRODUCTION

The results reported earlier showed that methyl mercaptan undergoes an oxidation by oxygen in the corona discharge. Oxygen in a corona discharge may however be present in one or more of the following states:

1- ground oxygen species,
2- ozone,
3- excited molecular oxygen,
4- ionized molecular oxygen (positive or negative),
5- atomic oxygen as well as ionized atomic oxygen (positive or negative).

Species numbered from 3 to 5 will be referred to as the active oxygen species in the following discussion.

The possible role of these species in the oxidation of methyl mercaptan was studied through two different schemes:

1- An experimental scheme which dealt with ozone.

2- A theoretical scheme based on information available in the literature was attempted to investigate the role of the active oxygen species.

As for the role of the ground molecules of oxygen, it may be deduced from the results presented previously in

Section 5.2. We have seen that in the absence of corona discharge and in the temperature range examined (i.e., 298-453 K), no reaction of methyl mercaptan was observed. Since under such conditions ground molecular oxygen is predominantly present we can therefore conclude that this species has no role to play in the reaction.

6.2 THE ROLE OF OZONE

6.2.1 Introduction

Ozone is known to be formed in the corona discharge of air (for example, see White [14]). Therefore, it may be expected to be present and to participate in the reactions since it is among the strongest oxidizing agents known.

The role of ozone in the oxidation of methyl mercaptan was explored by two sets of experiments:

i) the first set was devised to measure the concentration of ozone formed in the corona discharge of air under a range of conditions similar to that attempted in Section 5.2 where methyl mercaptan reacted with air. These conditions included the mean residence time of air in the ozonizer, temperature, and current. The purpose here was to check by calculations whether or not these concentrations of ozone would produce, upon reaction, fractional conversions of the mercaptan in the same order of magnitude as those reported in Section 5.2.

ii) In the second set, ozone, under controlled

conditions, was generated outside the reactor and then fed into the reactor where it was combined with another stream of methyl mercaptan where a reaction occurred. The reaction products were identified and then a comparison between these products and those obtained in Section 5.2 was made.

6.2.2 Measurement of Ozone Concentration

6.2.2.1 Experimental Apparatus and Procedure

The apparatus used here was the same as shown in Figure 4.1. In the present case however, only air was introduced to the reactor which then acted as an ozonizer.

Under known conditions of the ozonizer temperature and current, a monitored stream of air was passed through the ozonizer. Three temperatures: 298, 373, and 453 K and four mean residence times: 5, 10, 20, and 35 seconds were attempted while the current was kept constant always at 0.3 mA (both polarities were tried).

The ozone formed could be detected by its distinct odour and its yellowish colour. Moreover, when an ozone test paper[1] was exposed to the output stream from the ozonizer, purple stains were developed [97].

---

(1) An ozone test paper can be prepared by steeping a filter paper in an emulsion of starch containing a small proportion of potassium iodide.

6.2.2.2 Analysis of Ozone in the Output Stream from the Ozonizer

The present operating column of the gas chromatograph was unable to separate ozone from air. Therefore, another method had to be used to determine the ozone concentration in the ozonized air emerging from the ozonizer. The iodometry analytical method was adopted for this purpose for its accuracy and simplicity [124]. Details on the procedure used are given in Appendix C.

6.2.2.3 Results and Discussion

A summary of the results of the above experiments is shown in Figure 6.1 (more details on these results are given in Appendix C). Figure 6.1 shows that the concentration of ozone formed in the discharge is directly proportional to the mean residence time of air in the ozonizer, inversely related to the temperature of the ozonizer, and higher in the negative than in the positive corona. These results totally agree with previous investigations [56,70,125,126,127].

Ozone formation in electrical discharges occurs in accordance with the mechanism [128-131]:

$$O_2 + e^* \xrightarrow{k_5} 2O + e \qquad (6.1a)$$

$$O + O_2 + M \underset{k_7}{\overset{k_6}{\rightleftharpoons}} O_3 + M \qquad (6.1b,c)$$

$$O_3 + O \rightarrow 2O_2 \qquad (6.1d)$$

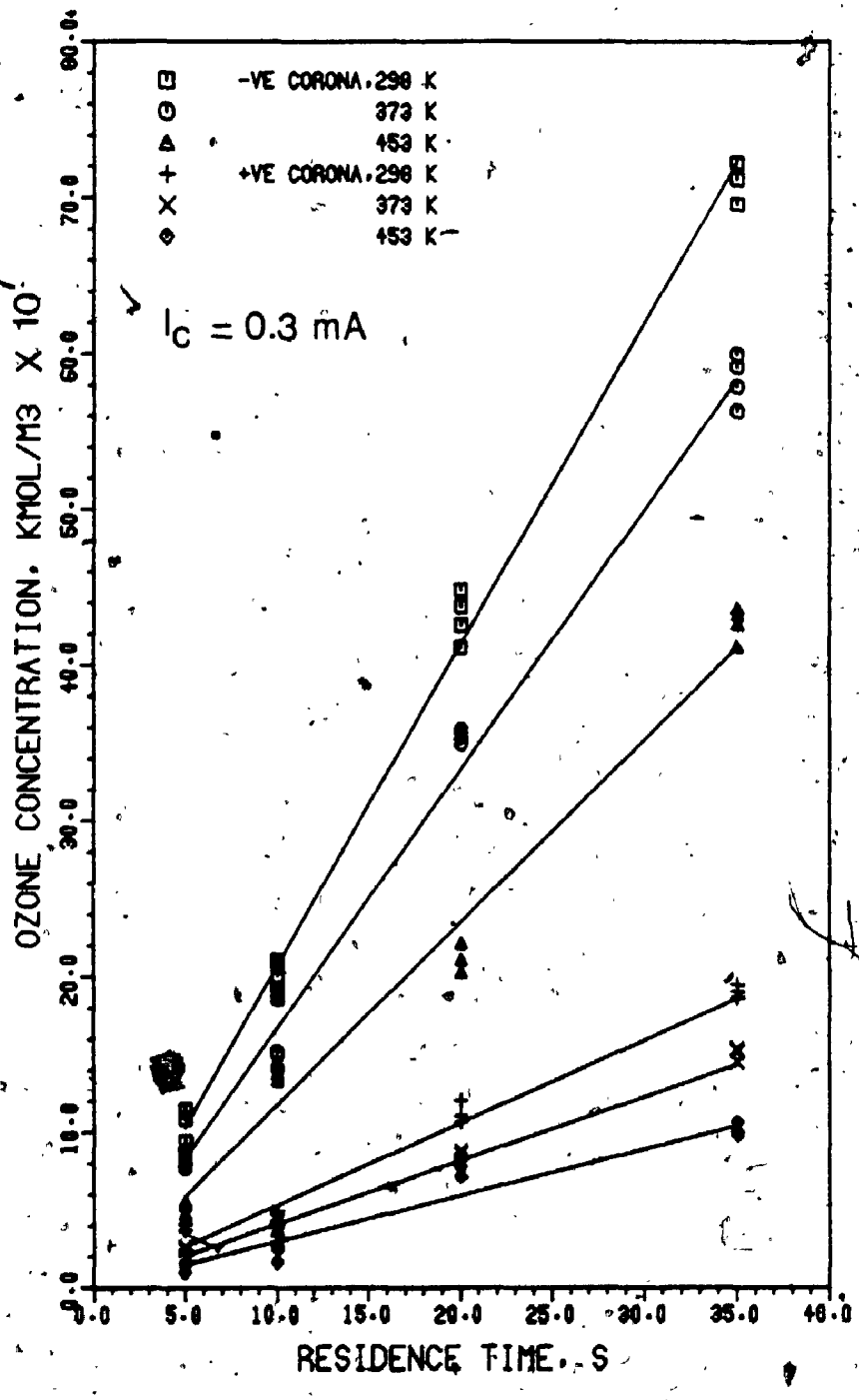

Figure 6.1: Concentration-time curves for the ozone formed in the ozonizer.

where e* denotes an energetic electron and M may be oxygen, nitrogen, ozone, or any combination thereof. (The role of the discharge is eventually the production of oxygen atoms.) Accordingly, the formation rate of ozone is:

$$\frac{dC_{O_3}}{dt} = k_5 C_O C_{O_2} C_M - k_6 C_{O_3} C_M - k_7 C_{O_3} C_O \qquad (6.2)$$

The following values of the rate constants k_5, k_6, and k_7 (for M is air) have been reported [126]:

$$k_5 = (2.5\pm0.14)\times10^{7} \exp(302/T) \quad m^6/kmol^2 s \qquad (6.3a)$$

$$k_6 = (1.5\pm0.10)\times10^{12} \exp(-12077/T) \quad m^3/kmol\ s \qquad (6.3b)$$

$$k_7 = (1.2\pm0.09)\times10^{10} \exp(-3019/T) \quad m^3/kmol\ s \qquad (6.3c)$$

where temperature T is in Kelvin.

It can be shown from the above equations that reaction (6.1c) will not compete significantly with the ozone synthesis reaction (6.1b). Thus, equation (6.2) reduces to:

$$\frac{dC_{O_3}}{dt} = k_5 C_O C_{O_2} C_M - k_7 C_{O_3} C_O \qquad (6.4)$$

Let $-r_{1b}$ and $-r_{1d}$ be the rates of reactions (6.1b) and (6.1d), respectively. Then,

$$-r_{1b} = k_5 C_O C_{O_2} C_M \qquad (6.5a)$$

$$-r_{1d} = k_7 C_O C_{O_3} \qquad (6.5b)$$

As oxygen atoms have a half life of about 1×10^{-5} s at 101 kPa [76], stationary states are quickly established in the discharge [129,130]. Then, $dC_O/dt = 0$ and C_O is therefore constant. Accordingly, the ratio $-r_{1b}/-r_{1d}$ is:

$$\frac{-r_{1b}}{-r_{1d}} = (k_5 C_{O_2} C_M) \; / \; (k_7 C_{O_3}) \qquad (6.6)$$

By substituting equations (6.3a) and (6.3c) into equation (6.6), it can be demonstrated that this ratio is inversely related to temperature, a fact which explains the lower concentrations of ozone formed at elevated temperatures as shown in Figure 6.1.

It can also be demonstrated that, within the temperature range of interest, the quantity $k_5 C_O C_{O_2} C_M$ is always greater than the quantity $k_7 C_{O_3} C_O$. By applying this fact to equation (6.6), the increase of ozone concentration with the increase in time is self-evident.

On the other hand, although it is known that negative rather than positive coronas produce ozone in greater quantities [14,56,58,70] the reason is generally still unknown. White [14], however, attributed this phenomenon to the longer ionizing paths of electrons in negative coronas so that the probability of the formation of oxygen atoms via reaction (6.4a) may increase and so may the rate of ozone formation as equation (6.6d) indicates.

As stated earlier, the purpose of the present set of experiments was to use the results, namely, the ozone concentrations shown in Figure 6.1, to calculate the fractional conversions of methyl mercaptan which would have been obtained due to reaction with ozone.

Recalling the results of Section 5.6, the reaction between ozone and the mercaptan may proceed as follows:

$$CH_3SH \overset{O_3}{\rightarrow} (CH_3)_2S_2 + H_2O \qquad (k_8) \qquad (6.7a)$$

$$(CH_3)_2S_2 \overset{O_3}{\rightarrow} (CH_3)_2S + SO_2 \qquad (k_9) \qquad (6.7b)$$

$$(CH_3)_2S \overset{O_3}{\rightarrow} (CH_3)_2SO_2 \qquad (k_{10}) \qquad (6.7c)$$

No information on the rate constants k_8, k_9, and k_{10} are available in the literature. Hence, the relative significance of these reactions to one another as well as to reactions (6.1c) and (6.1d) could not be determined.

According to Maggiolo et al [131], however, the attack of ozone on a sulphur compound occurs when a terminal oxygen of the ozone molecule executes an electrophilic attack on the sulphur forming a new bond with the sulphur. Thereupon, the second and third atoms of the ozone molecule are liberated as molecular oxygen, a process which can be compared with reaction (6.1c). Evidence for the validity of this mechanism comes from the study done by Hales et al [45] on the gas-phase reaction of ozone with hydrogen sulphide.

These authors found that annihilation of ozone by the reaction was not extremely rapid compared with the ozone thermal decay via reaction (6.1c).

Accordingly, the reactions from (6.7a) to (6.7c) may be written as:

$$2CH_3SH + O_3 \rightarrow 2(CH_3)_2S_2 + H_2O + O_2 \qquad (6.8a)$$

$$(CH_3)_2S_2 + 2O_3 \rightarrow (CH_3)_2S + SO_2 + 2O_2 \qquad (6.8b)$$

$$(CH_3)_2S + 2O_3 \rightarrow (CH_3)_2SO_2 + 2O_2 \qquad (6.8c)$$

Then, it is reasonable to assume that each of these reactions has a rate constant of the same order of magnitude as that of reaction (6.1c). Since it was concluded earlier that the latter reaction is not competitive with reaction (6.1d), the same conclusion may thus be applicable with respect to reactions (6.8a)-(6.8c). Consequently, the concentration of ozone formed in the discharge would reach its equilibrium values before it would start to react with the mercaptan, provided that no reactions other than the above take place. Stated another way, the estimated fractional conversions of methyl mercaptan based on reaction (6.8a) and the data shown in Figure 6.1 would approximate those which would have been obtained if the mercaptan had been introduced at the same time with air to the ozonizer in the above experiments.

To pursue the same argument quantitatively, consider the initial concentration of methyl mercaptan in the same order of magnitude as that tested in Section 5.3, i.e., about 25×10^{-6} kmol/m^3. Then, in accordance with equation (6.9a) and Figure 6.1, the respective fractional conversions of methyl mercaptan for complete reactions could be estimated. These results are listed in the left hand side of column 4 in Table 6.1. It is to be noted that these values of the fractional conversion of methyl mercaptan are maximum as the consumption of ozone by reactions (6.9b) and (6.9c) was negligible. This will not however affect the final conclusion as will be seen below.

For comparison, Table 6.1 also shows the average values of methyl mercaptan conversion reported in Section 5.2 at similar conditions of temperature, current, and mean residence time. It is obvious that those values are always higher than these obtained here at the same operating conditions even though the latter values are in fact less than it should be as mentioned above.

Furthermore, the values of the mercaptan fractional conversion calculated above should be even less than those if the reaction:

$$HX + O \xrightarrow{k_{11}} X + OH \qquad (6.9)$$

was considered where HX may be methyl mercaptan.

TABLE 6.1: COMPARISON BETWEEN THE FRACTIONAL CONVERSIONS OF METHYL MERCAPTAN BASED ON A) REACTION (6.4a) AND RESULTS SHOWN IN FIGURE 6.1 AND B) THOSE REPORTED IN SECTION 5.2.

Temperature K	Current mA	Polarity	τ s	Fractional conversion A*	Fractional conversion B	Difference
298	0.3	- ve	35	0.42	1.0	0.57
"	"	+ ve	"	0.11	1.0	0.80
373	0.3	- ve	35	0.35	0.81	0.44
"	"	+ ve	"	0.08	0.81	0.71
453	0.3	- ve	35	0.25	1.0	0.90
"	"	+ ve	"	0.06	1.0	0.94
298	0.3	- ve	5	0.07	0.30	0.24
"	"	+ ve	"	0.02	0.29	0.26
373	0.3	- ve	5	0.05	0.57	0.51
"	"	+ ve	"	0.01	0.57	0.55
453	0.3	- ve	5	0.03	0.76	0.72
"	"	+ ve	"	0.01	0.76	0.75

* Based on C_{Ao} of methyl mercaptan = 25.0×10^{-6} kmol/m^3.

According to Schiff [134], for most reactions involving only the transfer of a proton, the rate constant k_{11} is in the order of 10^7 m^3/kmol.s at 300 K. Obviously, reaction (6.11) is mutually competitive with reaction (6.1b):

$$O + O_2 + M \rightarrow O_3 + M \qquad (6.1b)$$

which is, as discussed above, the main reaction responsible for the ozone formation in such environments. Subsequently, the concentration of ozone and thus the conversion of methyl mercaptan due to reaction (6.7a) would suffer more reduction.

Also, as a result of the effect of corona polarity and of temperature on the concentration of ozone, we observe from Table 6.1 that the mercaptan conversions are higher for a negative than for a positive corona and decrease as the temperature increases. However, we find that the conversions of methyl mercaptan as reported in Section 5.2 acquire the same values in both types of corona and in contrary to the above, they always increase with the increase in temperature.

6.2.3 Reaction of Ozone with Methyl Mercaptan

As stated earlier, the main objective of this section was to have ozone react with methyl mercaptan and identify the products. Then, these results were compared with those obtained previously in Section 4.6 where the mercaptan

reacted with air in the corona reactor.

6.2.3.1 Experimental Apparatus and Procedure

The reaction between ozone and methyl mercaptan was studied using the main apparatus shown in Figure 4.1. However, one modification was made where another tube with similar dimensions to the reactor was placed vertically below the latter. The new tube acted as a reaction vessel for the above reaction while the original reactor itself was solely used as an ozonizer to generate the ozone required. As shown in Figure 6.2, the ozonizer and the reactor were attached together by means of a Pyrex joint. All the joints present were sealed with O-rings and kept in place by clamps. A side tube was attached to the Pyrex joint so that a stream of methyl mercaptan and nitrogen mixture could be introduced to the reactor.

As they were not required, the reactor did not contain either a central wire or a stainless steel gauze. In general, their presence was immaterial since only qualitative rather than quantitative analysis of the results was attempted. Also, gaseous reactions of ozone with hydrocarbons usually occur homogeneously [133].

The experiments were conducted as follows:

i- A monitored stream Q_1 of air was allowed to pass through the ozonizer whose temperature and current were kept

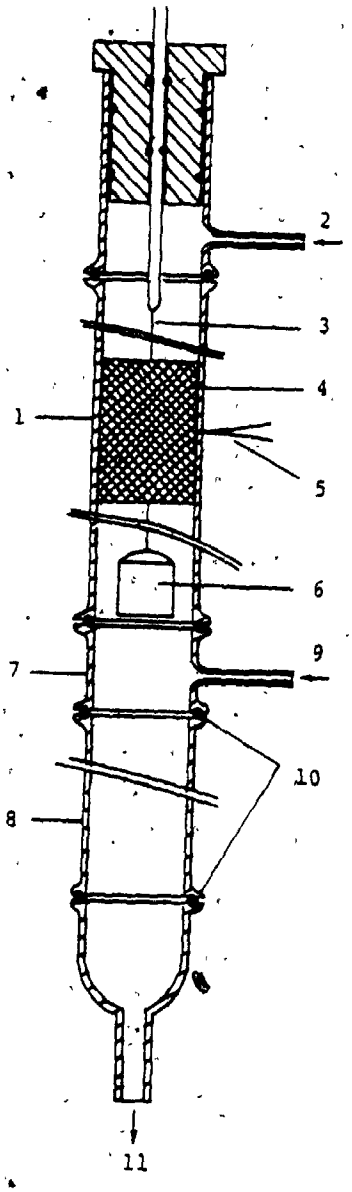

Legend:

1- Ozonizer.
2- Air stream.
3- Corona wire.
4- Stainless steel gauze.
5- Ground wire.
6- Weight.
7- Joint.
8- Reactor.
9- Methyl mercaptan/nitrogen mixture stream.
10- O-rings.
11- Reactor exit.

Figure 6.2:

Ozonizer-reactor arrangement to conduct the reaction between ozone and methyl mercaptan.

constant at 298 K and 0.3 mA. This temperature was used to minimize the thermal decomposition of ozone so as to maximize the reaction yield. Also for the same purpose, negative corona was employed exclusively in the present set of experiments.

ii- Another monitored stream Q_2 of the methyl mercaptan and nitrogen mixture was fed to the reactor.

iii- Upon combining, reactions between the constituents of the two streams took place. Analysis of the products in the exit stream from the reactor was performed by the gas chromatograph whose operating conditions were the same as in Section 4.6.

The initial concentration C_1 of ozone in the feed mixture was calculated from the equation:

$$C_1 = \frac{C_o Q_1}{Q_1 + Q_2} \quad \text{kmol/m}^3 \qquad (6.10)$$

where C_o is concentration in the exit stream from the ozonizer and was determined as described in Appendix C.

The initial concentration of methyl mercaptan in the feed was monitored as follows: no voltage was applied to the ozonizer so that no ozone was formed. Then, the combined stream between Q_1 and Q_2 was sampled and introduced to the gas chromatograph for analysis.

6.2.3.2 Identification of the Products of the Reaction and discussion of the Results

The reaction of ozone with methyl mercaptan resulted in four products which were separated by the gas chromatograph. Their retention times were about 252, 1584, 1941, and 2311 seconds. (No solid products were observed inside the reactor.) These products will be numbered from 1 to 4, respectively in the present section.

Products 1 and 3 were identified as water and dimethyl disulphide since their retention times matched the authentic values under the same operating conditions of the gas chromatograph (see Section 4.5).

Based on their retention times, products 2 and 4 were clearly never identified before in this study. For this reason, a sample of each was isolated for identification by using MS and NMR techniques:

- For every analysis cycle of the gas chromatograph, the injection time (i.e., the time at which a sample of the product stream was swept from the sample loop by helium to the operating column) was recorded.

- After about 1550 seconds, the exit stream from the thermal conductivity detector[1] was directed to pass for

(1) Throughout this set of experiments, the flame ionization detector was not used so as to keep the products intact for analysis.

almost 60 seconds through a cold trap immersed in a sodium chloride-ice bath (258 to 263 K). The stream was then directed to the atmosphere.

- after about 2280 seconds from the injection time, the above stream was directed once more to pass through another cold trap immersed in the same ice-bath for almost 60 seconds before it was allowed to escape to the atmosphere.

The above two steps were repeated several times so as to collect a large enough sample.

The two samples collected were yellow oily liquids and found to dissolve readily in water. The product whose retention time was about 1584 seconds (i.e., the second product) showed acidic characteristics as it changed the colour of litmus paper to red.

The procedure of conducting the NMR and MS analyses was described previously (see Section 4.4). The results of the MS analysis are summarized in Figures 6.3 and 6.4 as well as in Table 6.2 while those of the NMR analysis are summarized in Figures 6.5 and 6.6.

TABLE 6.2: CHEMICAL COMPOSITION OF THE PRODUCTS OF OZONE REACTION WITH METHYL MERCAPTAN

Product #	Retention time, s	Exact mass	Number of atoms			
			C	H	O	S
2	1582 - 1586	95.9881	1	4	3	1
4	2309 - 2314	125.98[illegible]	2	6	2	2

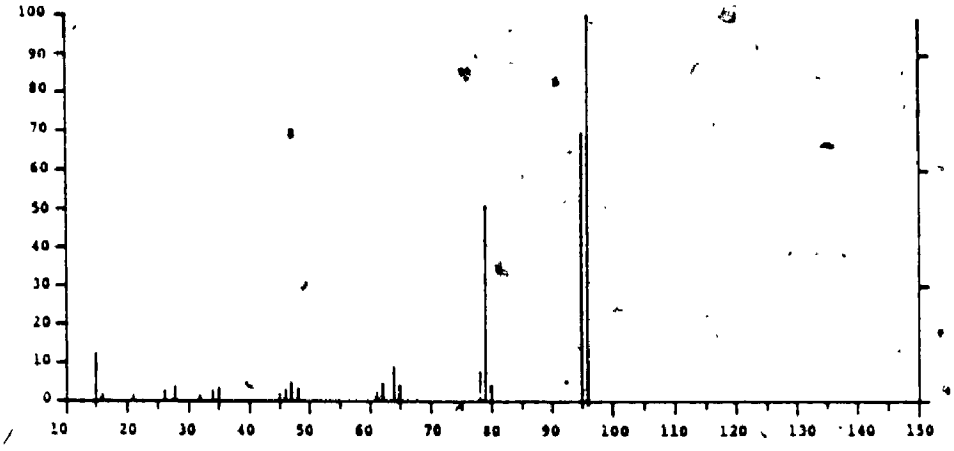

Figure 6.3: Mass spectrum of compound #2 formed by the reaction of methyl mercaptan with ozone.

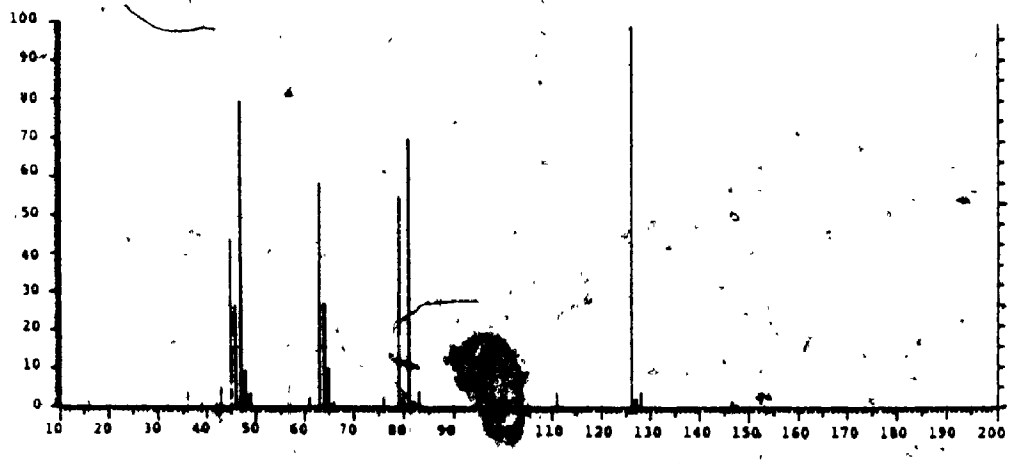

Figure 6.4: Mass spectrum of compound #4 formed by the reaction of methyl mercaptan with ozone.

3

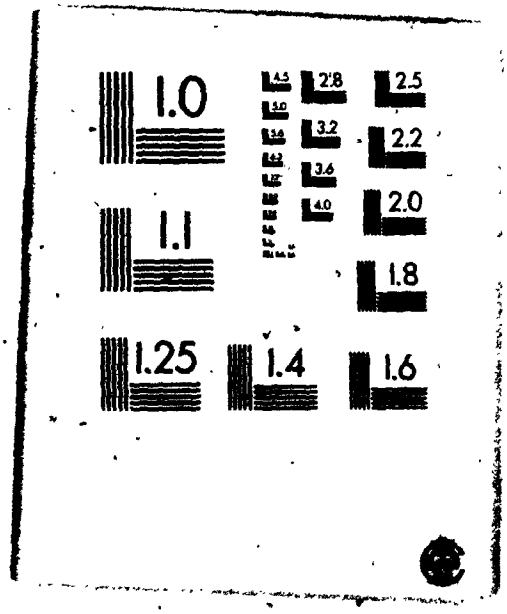

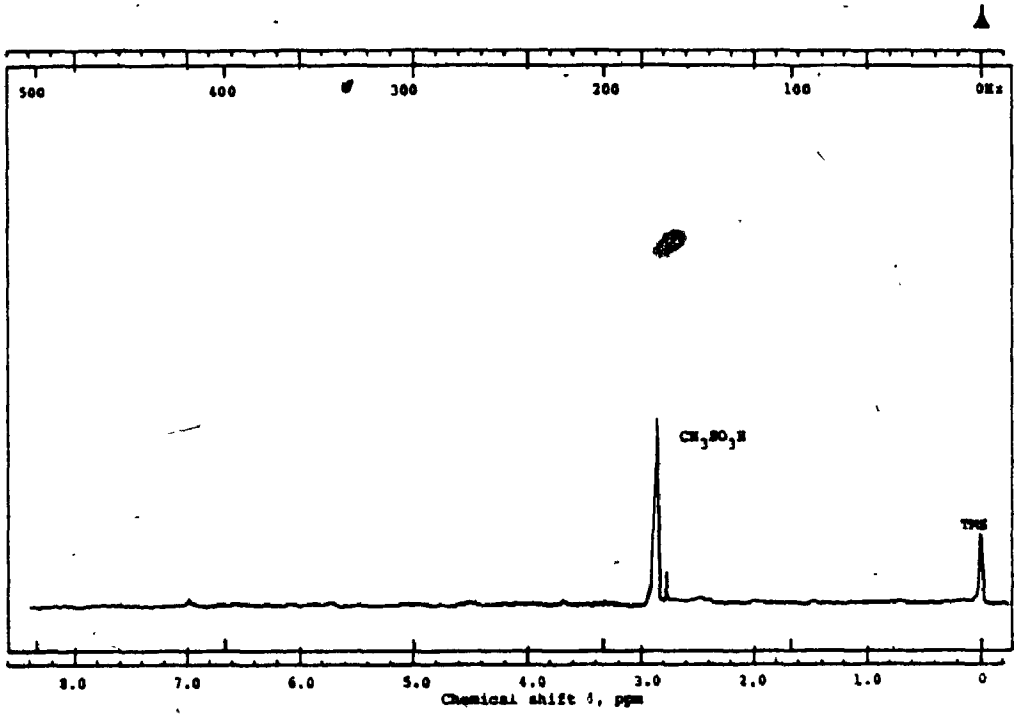

Figure 6.5: NMR spectrum of compound 82 formed by the reaction of methyl mercaptan with ozone.

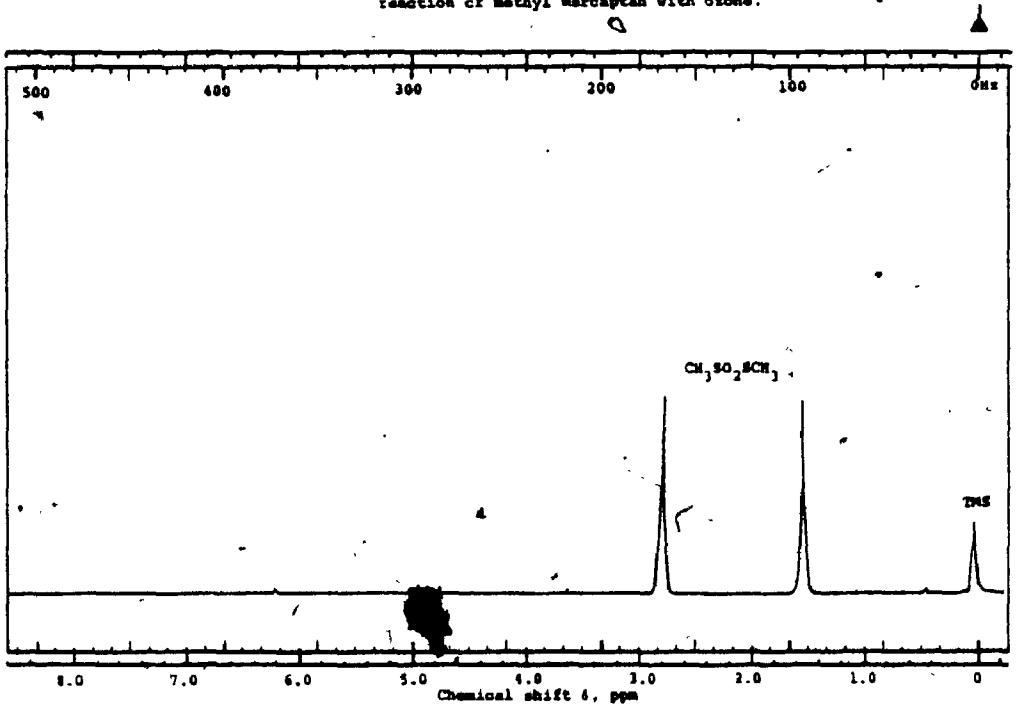

Figure 6.6: NMR spectrum of compound 84 formed by the reaction of methyl mercaptan with ozone.

Compound #2:

The mass spectrum (Figure 6.3) exhibits a molecular peak at 96 with intensity of 100% indicating that the molecular weight of the molecule is in the vicinity of 96. The exact mass is in fact 95.9881 as shown in Table 6.2. The spectrum 6.3 also shows peaks at 15,12%, 79,50%, and 95,69%. Combining these observations with the data listed in Table 6.2 (first row) strongly suggests that these fragments are CH_3, CH_3SO_2, CH_3SO_3, and CH_3SO_3H. According to the analysis, this compound was identified as sulphonic acid.

On the other hand, the NMR spectrum (Figure 6.5) shows two adjacent peaks within the chemical shift range of about 2.9 ppm with respect to TMS. This indicates first the asymmetrical grouping of hydrogen protons in the molecule [54]. Second, in reference to the Aldrich Library of Spectra # NMR 10,6c [82], this spectrum was found to match the authentic NMR spectrum of sulphonic acid CH_3SO_3H.

Compound #4:

Similarily, the MS spectrum (Figure 6.6) shows a peak at 126 with 100% intensity indicating that the molecular weight of the parent ion was in the vicinity of 126. As listed in Table 6.2 (second row), the exact mass is 125.98033. Other important peaks shown by Figure 6.4 are 45,44%, 46,27%, 47,80%, 63,59%, 79,55%, and 111,45%

suggesting that these ionic fragments are CHS, CH_2S, CH_3S, CH_3SO, CH_3S_2 (or CH_3SO_2), and $CH_3S_2O_2$. Finally, the MS analysis identified this compound as methyl methanethiosulphonate $(CH_3)_2S_2O_2$.

Also, the NMR spectrum (Figure 6.6) shows two peaks at chemical shifts of about 1.5 and 2.7 ppm with respect to the reference TMS indicating the asymmetrical grouping of hydrogen protons in the molecules which agrees with the chemical structure of methyl methanethiosulphinate. The authentic NMR spectrum of this compound was not available at the time of analysis. Therefore, no comparison could be made. Since the compound was not commercially available either, neither its NMR nor its gas chromatograph calibration curve could be obtained. As a result of the latter reason, mass balance calculations around the reactor for the above reaction were not possible to perform.

Discussion:

No similar study was reported on the reaction between methyl mercaptan and ozone. However, the above results may be discussed in light of similar investigations.

As indicated earlier, methyl mercaptan can be easily oxidized even by mild reagents to dimethyl disulphide. The disulphide under vigorous oxidation conditions can then be converted into highly oxidized products which may lead to

the formation of sulphonic acid [109]. Bernard [114] and Bernard et al [115] have studied the oxidation of organic disulphide by bubbling ozonized oxygen in their solutions. The major product reported by these authors was the corresponding sulphonic anhydride, $R.SO_2.O.SO_2.R$. Also, the corresponding thiosulphonate was detected. However, dimethyl disulphide was found in particular to form methyl methanethiosulphonate rather than the anhydride.

Now, upon oxidation by ozone as discussed above, methyl mercaptan would form dimethyl disulphide. The hydrogen in the thiol group SH would be rendered most likely as water [115,132,135]:

$$2CH_3SH + O_3 \rightarrow (CH_3)_2S_2 + H_2O + O \qquad (6.8a)$$

Even in the case that methyl sulphonic anhydride was formed during the presesnt reaction, it would immediately react with the water formed:

$$(CH_3)_2S_2O_5 + H_2O \rightarrow 2CH_3SO_3H \qquad (6.11)$$

thus adding more methyl sulphonic acid to the products.

6.2.3.3 Summary and Conclusions

In the first set of the above experiments, ozone was generated and its concentration was measured. In another set of experiments ozone was generated outside the

reactor and allowed to react with methyl mercaptan and the reaction products were identified.

Based upon the above values of concentrations, the maximum values of conversion of methyl mercaptan were found to be much less than their correspondents at the same conditions such as temperature, current, and mean residence time (see Table 6.1).

On the other hand, two of the products identified above were not produced by the reaction of methyl mercaptan with air. This would indicate that a different reaction mechanism was involved mainly due to the fact that at least one reactant (which is ozone in this case) is different.

Based upon the above discussion, it was concluded that ozone is not the oxygen species responsible for the oxidation of methyl mercaptan in the corona reactor.

6.3 THE ROLE OF THE ACTIVE SPECIES OF OXYGEN

6.3.1 Introduction

As discussed in Chapter 3, a corona discharge has at its heart an active region in which electrons are liberated and accelerated to high velocities. Upon collisions, energy is transferred from these electrons to neutral gaseous species. The most efficient mode of energy transfer found is the electronic mode by which various excited and ionized

species are formed. Moreover, some of the energy thus imparted in the excited state may be dissipated so as to result in the dissociation of oxygen molecules into atoms. Processes involving electron attachment and ion-ion interaction may also take place in such environments. Based on information available in the literature, a quantitative study on these various species will be given.

6.3.2 Mean Electron Energy in the Ionized Sheath

Estimates of the mean energy of electron swarms can be made in reference to the results of Schlumbohm [136] shown in Figure 6.7. The figure represents the mean electron energy E_e as a function of the quotient of field strength and pressure X/P for nitrogen, oxygen, and air.

It can be shown from equation (3.2) and the dimensions of the reactor that the onset value of the electric strength E_c is in the order of magnitude of 26×10^6 V/m. Using this value and that at the outer boundary of the ionized sheath (i.e., 3×10^6 V/m) in air at atmospheric pressure gives:

$$39 < X/P < 342 \qquad \text{V/Torr.cm} \qquad (6.12)$$

By applying these limits to Figure 6.7, the mean electron energy in the ionized sheath is found to range from about 2.8 to about 7.1 eV.

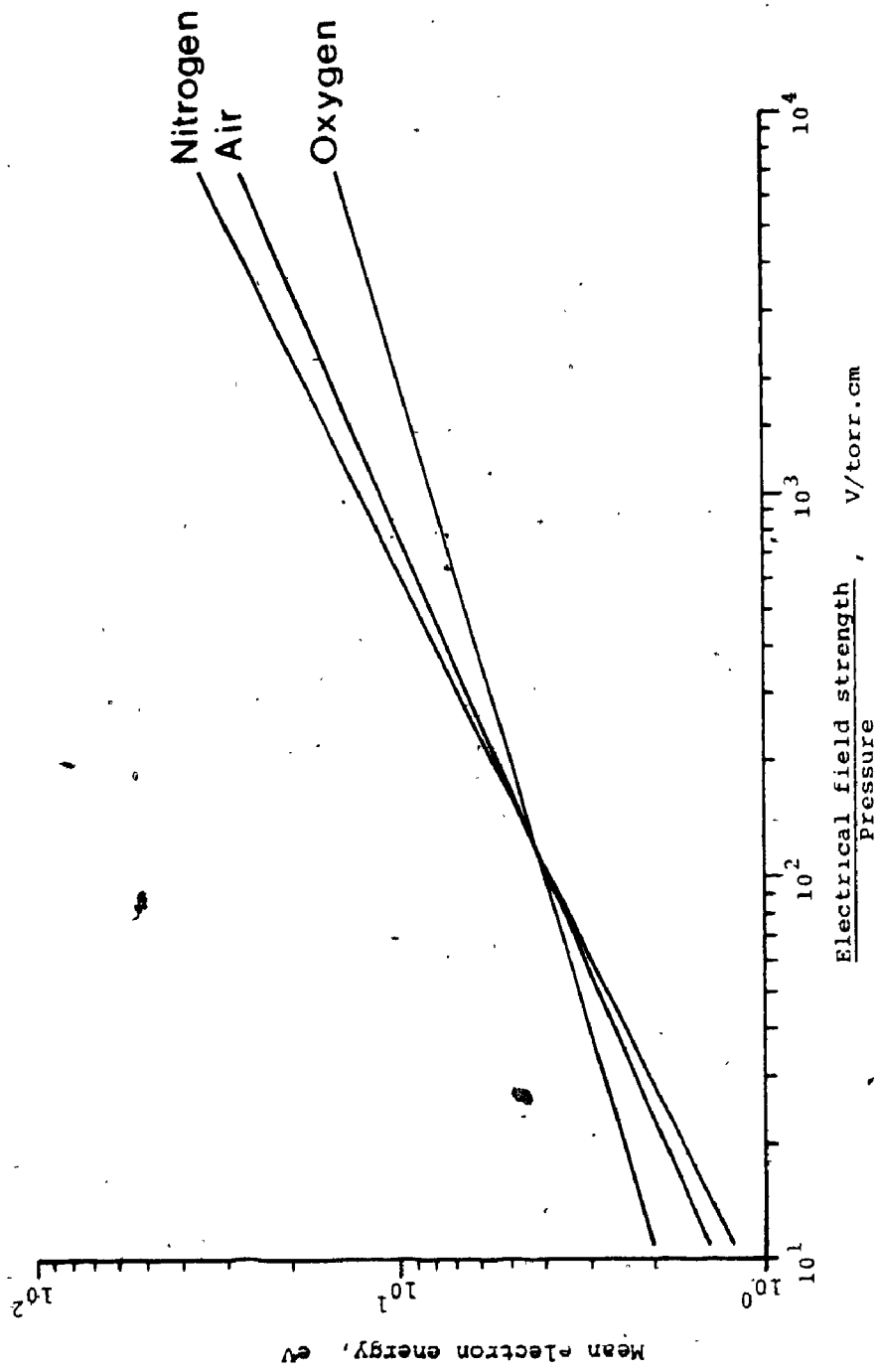

Figure 6.7: The dependency of the mean energy of electrons on the quotient, of field strength and pressure in corona discharge in nitrogen, oxygen, and air (136).

6.3.3 Production of the Active Oxygen Species

6.3.3.1 Theoretical Considerations

Let us define the following parameters:

v_e = the electron velocity in the discharge (m/s).

n_e = the number of electrons in the discharge/m^3.

n_2 = the number of oxygen molecules in the discharge/m^3.

$\sigma_i(v_e)$ = the cross-section (m^2) of a kind i of collision (it is a function of electron velocity).

The probability $p`$ of an electron to make a collision of a kind i per unit distance of its path is $p`=d(v_e)n$ and the number of collisions per unit time per electron is:

$$z = v_e \sigma_i(v_e) n_2 \qquad (6.13)$$

The concentration of electrons having velocity between v_e and v_e+dv_e is $n_e.f(v_e)dv_e$ in which $f(v_e)dv_e$ represents the velocity distribution of electrons. From equation (6.14), the number of oxygen species of kind i per unit volume per unit time in the same interval of velocity is given by:

$$dn_i = n_e f(v_e) dv_e . v_e \sigma_i(v_e) n_2 \qquad (6.14)$$

As indicated previously, the energy distribution of electrons in a gas moving in an electric field and interacting strongly with other species present is

approximately Maxwellian [60,61,137,138,140]. Accordingly:

$$f(v_e)dv_e = \frac{4}{\pi}\left(\frac{v_e}{v_{em}}\right)^2 \exp\left(-\frac{v_e}{v_{em}}\right)^2 d\left(\frac{v_e}{v_{em}}\right) \qquad (6.15)$$

where v_{em} is the mean velocity of electrons.

Substitution of equation (6.15) into equation (6.14) and then integration all over the velocity range from zero to infinity give:

$$n_i = \frac{4n_e n_2}{\pi} \int_0^\infty v_e \sigma_i(v_e) \left(\frac{v_e}{v_{em}}\right)^2 \exp\left(-\frac{v_e}{v_{em}}\right)^2 d\left(\frac{v_e}{v_{em}}\right) \qquad (6.16)$$

Now, consider the following reactions:

$$A + e^* \rightarrow A^* + e \qquad (W_j, \text{ eV}) \qquad (6.17a)$$

and

$$A + e^* \rightarrow A^+ + 2e \qquad (I_i, \text{ eV}) \qquad (6.17b)$$

which are excitation and ionization reactions, respectively. In these reactions, the excited electron e* with initial energy E_e is said to transfer enough energy W_j or I_i to produce species A* or A^+. The constants W_j or I_i are the threshold values of excitation and ionization of the neutral species A, respectively.

Let p_i be the rate of energy transfer per unit volume

of the reactor from the electron swarms to molecular oxygen to produce species of kind i. Then,

$$dp_i = W_j dn_i \quad \text{(for excitation)}$$
$$dp_i = I_i dn_i \quad \text{(for ionization)} \qquad (6.18)$$

From these relations and equation (6.16), we obtain, after substitution for v_e from the equation $E_e = \frac{1}{2} m_e v_e^2$:

$$p_i = \frac{4 n_e n_2}{\pi} \int_{W_j \text{ or } I_i}^{\infty} W_j (\text{or } I_i) \left(\frac{2E_e}{m_e}\right)^{\frac{1}{2}} \sigma(E_e) \frac{E_e}{E_{em}} \exp\left(-\frac{E_e}{E_{em}}\right) d\left(\frac{E_e}{E_{em}}\right)^{\frac{1}{2}} \qquad (6.19)$$

The lower limits of integral equation (6.17) were replaced by W_j and I_i since they define the minimun energies that electrons must posses before reactions (6.17) can occur. E_{em} is the mean energy of electrons in the discharge.

Summation of p_i's for all the species present in the discharge system gives only that part of energy per unit volume per unit time which is used in the generation of the active species of concern. Furthermore, the ratio N_i/p represents the number of particles of kind i produced per unit power density (i.e., energy per unit volume per unit time). As may be noted, this ratio is independent of the concentration of both the particles and electrons.

Work done on excitation and ionization of oxygen and of nitrogen indicates that there are five electronically excited and five ionized states of molecular oxygen and six electronically excited and fiv eionized states of molecular nitrogen. Peterson et al [141] conveniently summarized the electron-impact cross-section for all of these states in terms of semi-empirical equations as listed in Appendix C. Substitution these equations into equation (6.19) enabled us to evaluate the ratio N_i/p as a function of the mean energy of electrons.

In the present case, calculations were carried out in the range from 0 to 9 eV which covers the range of interest. The species found by these calculations to form in appreciable concentrations are shown in Figure 6.8. They include excited states of molecular oxygen and composite species of oxygen as well as other species of oxygen and nitrogen.

6.3.3.2 The Excited Species of Molecular Oxygen

The important excited species of molecular oxygen are $O_2^*(a\,^1\Delta_g)$, $O_2^*(b\,^1\Sigma_g^+)$, and $O_2^*(A\,^3\Sigma_u^+)$ (see Appendix C). Figure 6.8 shows that the concentration of each of these species increases rapidly to a maximum and then, rather slowly, falls away as E_{em} increases in the range attempted. These results may be explained as follows: every collision between an electron and a molecule does not necessarily

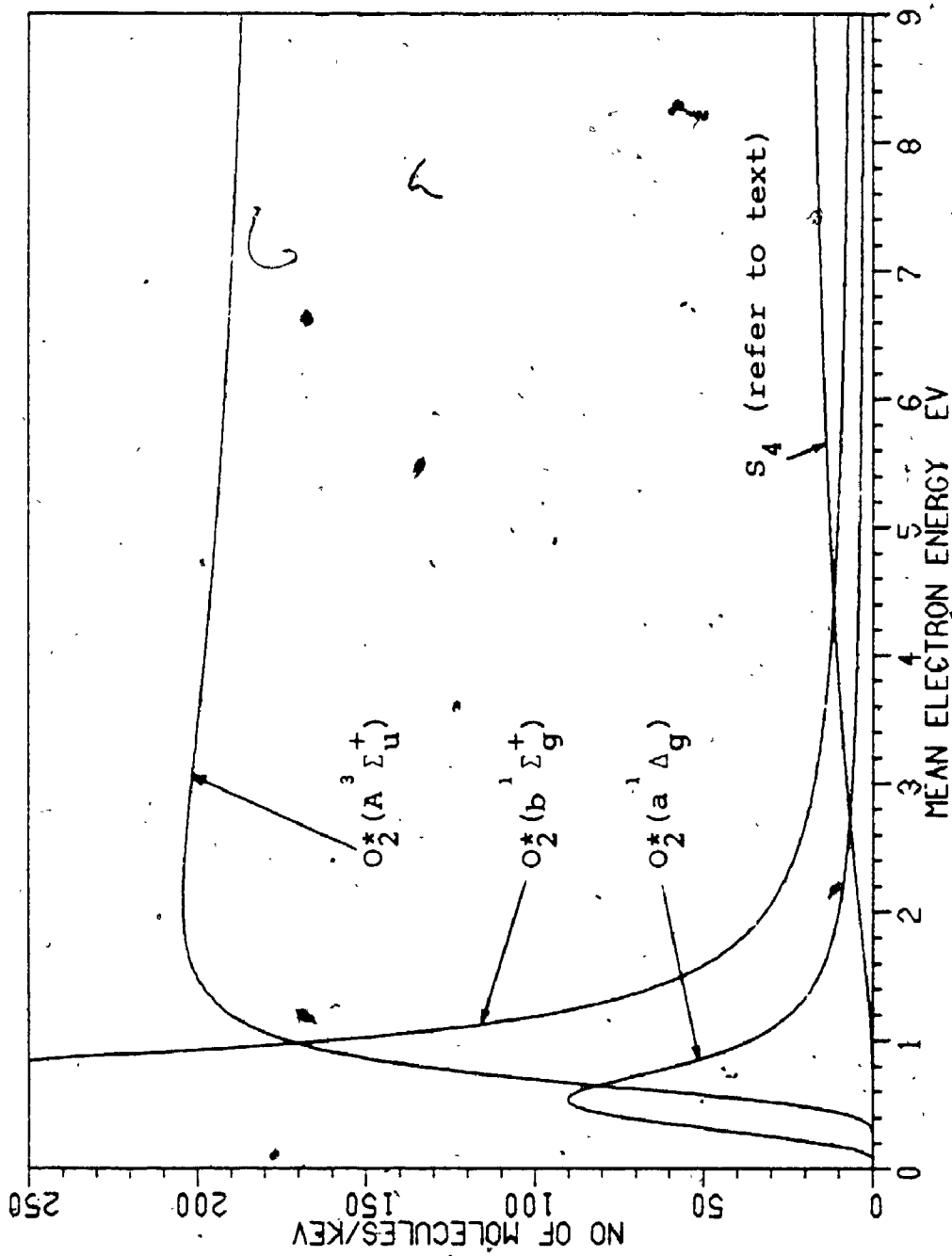

Figure 6.8: Number of excited and ionized species of air constituents due to corona discharge as a function of the mean energy of electrons.

result in a reaction even when the electron possesses a high value of energy. The probability of a reaction, which is a function of the electron energy, is zero below the threshold of the reaction. Above this value, the probability rises with electron energy to a maximum because a smaller proportion of the available energy must be transferred upon impact. At higher values of electron energy, electrons move so quickly past the molecule that they have too little time to react, and so the probability decreases.

From the results of Section 6.2, the mean electron energy in the corona discharge was found to range from about 2.8 to 7.1 eV. Figure 6.8 shows that in this range, more that 90% of the excited molecular oxygen produced in the discharge is in the triplet state $O_2^*(A\,^3\Sigma_u^+)$.

6.3.3.3 Concentration Estimation of the Excited Molecular Oxygen

An important consequence of the Townsend theory is that only part of the electrical energy is dissipated in the discharge. Most of this part goes to the electrons though. Energy gained by ions is comparatively negligible due to their much greater mass. For instance, in free space, the ratio between the velocity of an electron and that of oxygen ion is:

$$\frac{dv_e/dt}{dv_i/dt} = \frac{m_i}{m_e} = \frac{32}{1/1840} \simeq 60000 : 1$$

When collisions are taken into account, it is found that this ratio depends upon the strength of the electric field, but even at high field strength the ratio is greater than 2000:1 [61]. Hence, since power is equal to the product of force and velocity, the power expended in accelerating electrons in the ionizing sheath is much greater than that expended in accelerating ions.

Accordingly, all the energy dissipated in the ionizing sheath virtually appears as electron energy. This dissipated energy can be estimated for a given set of current, temperature, corona wire, and mean residence time of gases through the reactor. For example, for I_c of 0.3 mA, T of 423 K, a of 1.52×10^{-5} m, and τ of 10 s, equation (3.8) gives that the energy dissipated in the ionized sheath is 3.02×10^{16} keV. From Figure 6.8, for E_m of about 5.6 eV, the number of molecules of $O_2^*(A\,^3\Sigma_u^+)$ species per keV is almost 170. The total number of these molecules for the above conditions is then 5.13×10^{18} molecules or 8.5×10^{-9} kmol. By dividing this quantity by the reactor volume 7.722×10^{-6} m^3, the concentration of these oxygen species is 1.1×10^{-3} $kmol/m^3$. It should be emphasized that such a value is only a rough estimate. For more reiable data however, Section 7.2.3 is to be consulted.

6.3.3.4 The Positive and Negative Ions of Molecular Oxygen

The above computations have shown that the formation of

positive ions of molecular oxygen is minimal. This is mainly due to the high ionization energy required. For instance, the energy required to ionize an oxygen molecule is 12.1 eV [16] whereas we have seen that the maximum value of the mean electron energy available is 7.1 eV. This is not to say that positive ions of molecular oxygen are not important in the overall discharge process. On the contrary, a great number of the secondary electrons which help in maintaining the self-sustained corona discharge are produced when these ions impact on the electrode surface. However, this latter process can take place at concentrations of positive ions as low as 1 ppm [61]. The conclusion is then that the positive ions of molecular oxygen can be eliminated as a potential oxidant of the sulphur species.

On the other hand, since the molecular oxygen has a positive electron affinity, the negative ions O_2^- are readily formed and in great amounts by electron attachment[142]:

$$O_2 + e \rightarrow O_2^- \qquad (6.20)$$

These negative ions are, as discussed earlier, responsible for the stability of the corona discharge. However, it is known that these ions are more stable that their parent molecules [16]. By combining this fact with the conclusion

reported earlier (Section 6.1) that the ground molecules of oxygen have no role in the oxidation process of the sulphur compounds, we can also eliminate any role for the negative molecules of oxygen in the oxidation.

6.3.3.5 The Atomic Oxygen

Two important processes are responsible for the formation of atomic oxygen in electrical discharges. The first process is the dissociation of ground or excited oxygen [143,144]:

$$O_2 + e^* \rightarrow O + O + e \qquad (8.1 \text{ eV}) \qquad (6.1a)$$

or $$O_2^* \rightarrow O + O \qquad (6.11 \text{ eV}) \qquad (6.21)$$

However, as discussed in Section 3.7, dissociation of a molecule requires accumulation in the vibrational mode whereas we have seen that energy transferred to molecules through this mode is unimportant.

A main source of the energy requirements of the above reactions is also the excited species which radiate photons carrying enough energy to have a high probability of being absorbed. According to Peterson at al [141], Watson et al [143], and Stolarski et al [145], these species include the oxygen composite species, $N_2(^1\Pi_u^+)$, and $N_2(^1\Sigma_u^+)$ whose thresholds of excitation are 9.9, 12.85, and 14.0 eV, respectively.

Figure 6.8 shows the sum of N_i/p values of these species, designated by S_4, as a function of E_{em}. Since each photon produces two oxygen atoms when an oxygen molecule dissociates and not every photon emitted will be absorbed efficiently by molecular oxygen, there are at most $2S_4$ atoms of oxygen formed when 1 keV of energy is transferred from the electron swarms to air. Due to rather small values of the quantity S_4 as Figure 6.8 shows much less atomic oxygen than excited molecular oxygen is produced in the discharge.

The second source of atomic oxygen in a corona discharge is the ion-ion reaction [146]:

$$O_2^- + O_2^+ \rightarrow O_2 + 2O \qquad (6.22)$$

It was shown that while the O_2^- species are formed in relatively great amounts the species O_2^+ are not. Accordingly, the occurence of reaction (6.20) is rather limited and can therefore be eliminated as an important source to form oxygen atoms.

6.4 SUMMARY AND REMARKS

In review of the above discussion, it was found that the species causing the oxidation of methyl mercaptan in a corona discharge are some species of electronically excited molecular oxygen. These species include the two singlet $O_2^*(a\,^1\Delta_g)$ and $O_2^*(b\,^1\Sigma_g^+)$ and the triplet $O_2^*(A\,^3\Sigma_u^+)$ states.

These excited oxygen species are metastable and their lifetimes are measured in seconds rather than nano-seconds. For instance, the natural lifetimes for these states are in the order of magnitude of 5.1 [147],, 0.01 [147], and 0.13 [148] seconds, respectively (after correcting for atmospheric pressure [149]).

During these periods of time, many collisions will take place between the excited molecule and others. This is evident when one realizes that an oxygen molecule in air at 273 K and 101 kPa makes about 50×10^8 collisions per second [61]. Furthermore, these states are, by definition, highly reactive and can take part in chemical reactions more readily than their parent molecules. The reactivity increase in electronically excited molecules is discussed by other authors [61,76,150].

In recent years the importance of excited oxygen in atmospheric reactions has received considerable attention. Most emphasis has however been upon the singlet states since

they, due to their low excitation threshold values, are generated in relatively large amounts in the upper atmosphere [149].

On the other hand, little information is available on the reactions of the triplet-state $O_2^*(A\,^3\Sigma_u^+)$. However, there are indications that this state reacts with rates which are much greater than those of the ground oxygen molecules. Almost all reactions, certainly many of those which can be classified as oxidation reactions, involve the unpairing of a pair of electrons in one molecule [76]. As an excited triplet state where electrons are already unpaired, the reactivity of $O_2^*(A\,^3\Sigma_u^+)$ molecules is self-explanatory. This factor may then explain the fact that these species are most reactive with compounds containing hydrogen such as methyl mercaptan and hydrogen sulphide.

Moreover, this triplet state is accepted as the main oxygen species existing in a corona discharge. Benson [150] has emphasized that these species are compatible with the mechanism of the formation of ozone in corona discharge.

Finally, the reactions of the above sulphur compounds can be written as:

$$2CH_3SH + \tfrac{1}{2}O_2^* \rightarrow (CH_3)_2S_2 + H_2O \qquad (6.23a)$$

$$(CH_3)_2S_2 + O_2^* \rightarrow (CH_3)_2S + SO \qquad (6.23b)$$

$$(CH_3)_2S + O_2^* \rightarrow (CH_3)_2SO \qquad (6.23c)$$

where O_2^* denotes an excited molecule of oxygen.

CHAPTER 7

CORRELATION OF THE KINETIC DATA OF THE REACTION OF METHYL MERCAPTAN WITH AIR IN THE CORONA REACTOR

7.1 INTRODUCTION

This chapter is devoted to the correlation of the kinetic data obtained by experiment on the reaction of methyl mercaptan with air. This is to determine the order of the reaction and its rate constant.

However, the results reported earlier indicated that the above reaction proceeds in a series of three successive reactions, namely, reactions (6.23a) to (6.23c). Thus, for a complete description of the oxidation reaction of methyl mercaptan, experiment was extended to obtain kinetic data on reactions (6.23b) and (6.23c) as well. Then, each set of data was first correlated to evaluate the order of the respective reactions. This will be shown in Section 7.3.

Moreover, the corona discharge was found to play an essential role in the occurence of the reactions. As discussed in Section 6.3, this role is manifested in the production of some excited species of molecular oxygen, namely, the triplet state $O_2^*(A\,^3\Sigma_u^+)$ which are responsible for

the oxidation of the sulphur species present. Reactions leading to the formation of the excited molecules of oxygen constitute one form of discharge reactions (Section 3.5). The energy dissipating during these reactions may be related to the electrical and operating parameters of the system.

On the other hand, reactions between the excited species of oxygen and the sulphur species are thermal reactions where the activation energy is provided to the reactants by elastic collision with one another. The activation energy is usually indexed to the temperature of the reactor.

Therefore, the contribution of both the electrical and thermal energies to the reaction were taken into consideration in the correlation of the kinetic data obtained. This will be discussed in Sections 7.4 and 7.5.

Methyl mercaptan will be considered in the derivation of the following equations. However, these equations are applicable to other sulphur compounds of concern as well.

7.2 FORMULATION OF THE GOVERNING EQUATION

7.2.1 Differential Mass Balance Equation

The data presented in Section 5.3 indicated that high values of the fractional conversion of methyl mercaptan could be obtained in the corona reactor. Since these are integrated values of the conversion, the reactor was considered an integral reactor.

The figure given below shows a differential element of volume in the tubular corona reactor:

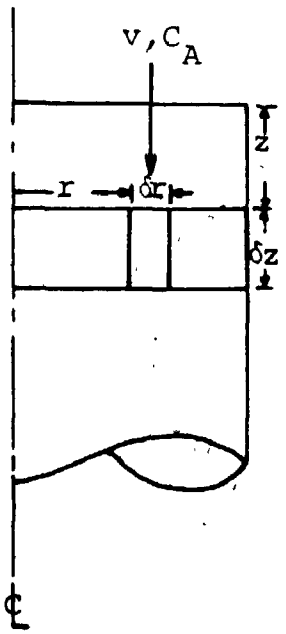

For steady-state conditions, the material balance of methyl mercaptan (denoted by A) about the volume element may be expressed by the continuity equation [151]:

$$\frac{1}{r}\frac{\partial}{\partial r}(rN_A) + \frac{\partial N_A}{\partial z} + \frac{1}{r}\frac{\partial N_A}{\partial \theta} + (-r_A) = 0 \qquad (7.1)$$

Here z and r are the cylindrical axial and radial coordinates, N_A is the mole flux ($kmol/m^2.s$) of the mercaptan and D_A is its molecular diffusion coefficient in air.

Assuming i) density and diffusivity to remain constant throughout the reactor, ii) no bulk flow in the radial direction, and iii) angular symmetry the above equation becomes:

$$-\bar{v}_z\left(\frac{\partial C_A}{\partial z}\right) + D_A\left(\frac{\partial^2 C_A}{\partial r^2} + \frac{1}{r}\frac{\partial C_A}{\partial r} + \frac{\partial^2 C_A}{\partial z^2}\right) = (-r_A) \qquad (7.2a)$$

If the diffusion effect in the axial direction is assumed to be unimportant, equation (7.2a) can be re-written as:

$$-\bar{v}_z\frac{\partial C_A}{\partial z} + D_A\left(\frac{\partial^2 C_A}{\partial z^2} + \frac{1}{r}\frac{\partial C_A}{\partial r}\right) = (-r_A) \qquad (7.2b)$$

In addition, owing to the high degree of the lateral

turbulence induced by the corona wind [175] (see also Section 3.2.4) as well as to the absence of any catalytic effect of the reactor walls on the reaction as discussed in Section 4.7 [152], radial concentration $C_A(r)$ may be assumed constant and independent of r. Whence, the concentration gradient dC_A/dr vanishes and equation (7.2b) reduces to:

$$-\bar{v}_z \frac{\partial C_A}{\partial r} = (-r_A) \qquad (7.3a)$$

(The verification of the absence of the concentration gradient dC_A/dr will further be considered in Appendix D.) Integration of equation (7.3a) leads to:

$$\frac{z}{\bar{v}_z} = - \int_{C_{Ao}}^{C_A} \frac{dC_A}{(-r_A)} \qquad (7.3b)$$

or

$$\tau = - \int_{C_{Ao}}^{C_A} \frac{dC_A}{(-r_A)} \qquad (7.3c)$$

These equation are generally referred to as the plug-flow equation. This term may be misleading since the term "plug-flow" normally pertains to situations involving a flat velocity profile. In our case however, the flow was in the laminar region since Re<2000 (where Re is the Reynold number based on the reactor diameter) and must therefore possess a non-flat velocity profile. Regardless of this fact and as far as $C_A(r)$ is constant, employment of equations (7.3) will not introduce any errors in the results [153].

Since the reactions in concern proceed totally in the gas phase and under conditions of constant flow density, the reaction rate $-r$ may be expressed by:

$$-r_A = k' \, C_{O_2^*}^{m'} \, C_A^n \qquad (7.4)$$

where m' and n are the reaction orders with respect to O_2^* and methyl mercaptan, respectively while k' is the reaction rate constant. k' is a function of temperature and can be expressed by the Arrhenius equation:

$$k' = k'_o \, e^{-E_a/RT} \qquad (7.5)$$

where k_o is the pre-exponential factor, E_a (J/kmol) is the thermal activation energy of the reaction, and T is the temperature in Kelvin.

Based on the calculations given in Section 6.3.3.3 as well as on the experimental conditions, it can be shown that the concentration of oxygen species O_2^* was about 12 to 44 times higher than that of the mercaptan. Stipulating that this was the case and therefore the concentration gradients of the oxygen species must remain zero throughout the system, equation (7.3c) may be rewritten in the pseudo form:

$$-r_A = k \, C_A^n \qquad (7.6a)$$

where $k = k' C_{O_2^*}^{m'}$ (7.6b)

The general equation was then obtained by substituting of equation (7.6a) into (7.3a):

$$\tau = - \int_{C_{Ao}}^{C_A} \frac{dC_A}{kC_A^n} \qquad (7.7)$$

7.2.2 Discussion of Assumptions Employed in Derivation of the Governing Equation

Throughout the present experimental study, the oxidation reactions were conducted on extremely dilute mixtures of the reacting sulphur compounds and under isothermal conditions. Hence, the validity of the assumptions regarding constant density and diffusion coefficient and negligible heating by reactions are self-evident.

In addition, the derivation of equation (7.2b) and its boundary conditions implies that a velocity of an average value of $\bar{v}_z$ must exist at the reactor entrance and exit while a constant concentration C_{Ao} is instantaneously formed at z=0 and the reactions are stopped precisely at z=H. The first of these conditions was provided by the experimental conditions employed. Calculations shown in Appendix D indicate that the entrance length required by a gaseous

stream of the reacting mixture to attain a fully developed flow and thus to reach a constant velocity of $\bar{v}_z$ was typically in the range from 2 to 59 mm. This range was readily accessible since the length of the reactor tube preceeding the reaction zone was greater than 300 mm.

Errors due to the second condition were also absent since the reactions could only proceed in the reactor space per se where the corona discharge was present.

For the longitudinal diffusion to be neglected, the following criterion must be met [154]:

$$\bar{v}_z \frac{\partial C_A}{\partial z} >> D_A \frac{\partial^2 C_A}{\partial z^2} \qquad (7.8)$$

In our case, the right hand side of this inequality was found to be in the order of magnitude of 3% of its left hand side (see Appendix D).

At any rate, the basis for the above assumptions will become apparent from considerations of the results. This is discussed in detail in Appendix D where solution of differential equation (7.2) was considered.

7.2.3 The Concentration of O_2^* as a Function of the Physical Parameters of the Corona Reactor

It was not possible using the present experimental set-up to monitor the concentration of O_2^*. However, as will be discussed below, another method was found to evaluate this parameter and was at the same time bound to the present constraints.

Castle [70] in his studies on the ozone generation in a corona discharge developed an equation to successfully predict the concentration of this compound. The equation obtained is based on the assumption that the concentration of ozone is directly related to the energy dissipated in the ionized sheath:

$$C_{O_3} = G \frac{\bar{E}\ \Delta a\ I_c}{Q} \qquad (7.9)$$

where G is an experimental constant and other parameters have the same significance as in above.

Experimental evidence to support this assumption was provided [155,156] where the ozone concentration was reported to be maximum near the surface of the corona wire and drops as the radial distance from the wire is increased. Indeed, this fact agrees with the results reported in Section 6.5 that electrons of enough energy to produce the excited molecular oxygen are only present in the ionized

sheath.

Furthermore, the formation of species O_2^* is an intermediate step in the process by which ozone is generated in a corona discharge (see Section 6.4). Then, it was reasonable to stipulate that the concentration of species O_2^* can be expressed as:

$$C_{O_2^*} = G' \left(\frac{\bar{E}\ \Delta a\ I_c}{Q}\right)^{m''} \qquad (7.10)$$

in which G' and m" are constants and may be determined from experiments. The exponent m" indicates the proportionality relation between $C_{O_2^*}$ and the energy dissipitated in the ionized sheath may not neccessarily be linear.

Subtitution of equation (7.10) into equation (7.8) and then the latter into equation (7.6b):

$$-r_A = k'\ G' \left(\frac{\bar{E}\ \Delta a\ I_c}{Q}\right)^{m} C_A^n \qquad (7.11)$$

in which constant m is the summmation of m' and m".

Furthermore, substitution for k' from equation (7.6) into equation (7.11) results in:

$$-r_A = \{k_o\ e^{-E_a/RT}\ \left(\frac{\bar{E}\ \Delta a\ I_c}{Q}\right)^{m}\}\ C_A^n \qquad (7.12)$$

in which constant k_o is the product of k_o' and G.

Since the species O_2^* can materialize only in the presence of corona discharge, the bracketed term in equation (7.12) may be grouped together into one constant k which will be referred to as the pseudo-rate constant of any of the above reactions. This constant is of course a function of both the electrical and the thermal parameters of the system as well as of the flow rate of gases through the reactor:

$$k = k_o \, e^{-E_a/RT} \left(\frac{\bar{E} \, \Delta a \, I_c}{Q}\right)^m \qquad (7.13)$$

7.3 DETERMINATION OF REACTIONS ORDERS

7.3.1 Procedure

In reference to Flow Chart 7.1a, the procedure used to determine the order of each of reactions (6.23) is as follows:

i- For a given set of temperature, mean residence time, and current, assume a minimum value for the reaction order e.g., n_i (a zero value may as well be used).

ii- Conduct a series of experiments over a range of initial concentration C_{Ao} of the sulphur compound in concern. For every value of the initial concentration C_{Ao}, evaluate the right hand side k_{ij} of equation (7.13).

iii- Carry out linear regression on the set k_{ij} and obtain

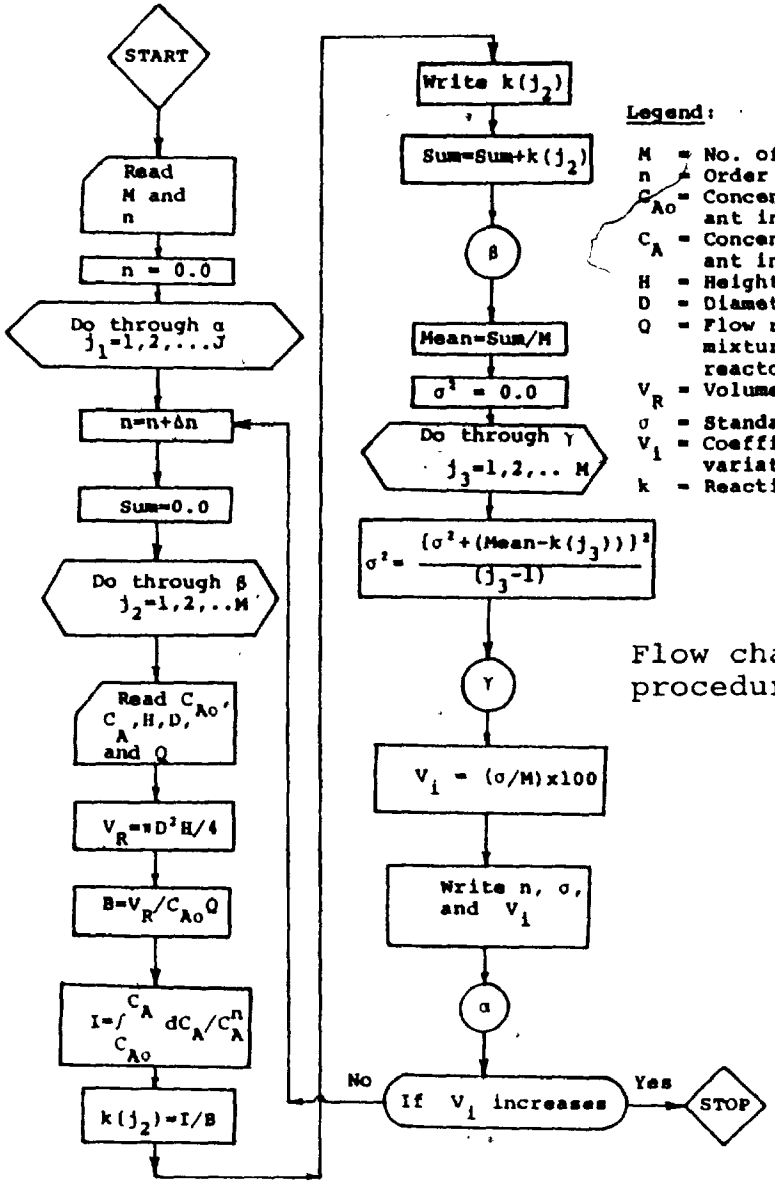

Legend:

M = No. of data points
n = Order of the reaction.
C_{Ao} = Concentration of reactant in feed stream.
C_A = Concentration of reactant in product stream.
H = Height of reactor.
D = Diameter of reactor.
Q = Flow rate of reaction mixture through the reactor.
V_R = Volume of reactor.
σ = Standard deviation.
V_i = Coefficient of variation.
k = Reaction rate constant.

(a)

Flow chart of the procedure.

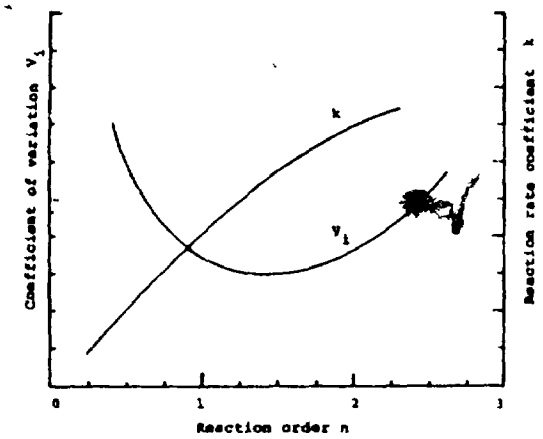

(b)

Typical results; k is the reaction constant and V_i is the coefficient of variation.

Figure 7.1: Representation of the procedure adopted to determine the orders of the chemical reactions in concern.

a value for the standard deviation S_i and another for the mean k_i'. Then, ascertain a value for the coefficient of variation V_i [157]:

$$V_i' = \left(\frac{S_i}{k_i'} \right) \times 100 \qquad (7.14)$$

The coefficient of variation V_i' simply expresses the magnitude of the variation of a set of values of a parameter relative to the size of the parameter.

iv- Assume a higher value for n_i and repeat Steps ii and iii above and obtain another value for V_i' and so on.

v- Upon comparison, the n_i value which results in the minimum value of V_i' will define the reaction order sought. Also, the corresponding value of k_i' is the rate constant at the operating conditions employed (see Figure 7.1b).

Moreover, in order to check the results due to the above procedure, current was varied and the procedure was repeated and the results were then averaged.

7.3.2 Results and Discussion

Data obtained at 423 K and 10 s for various values of current were used in the present correlation. The results are presented in Table 7.1 and in Figures 7.2a, 7.2b, and 7.2c for methyl mercaptan, dimethyl disulphide, and dimethyl sulphide, respectivly.

TABLE 7.1: ORDERS OF THE REACTIONS OF METHYL MERCAPTAN, DIMETHYL DISULPHIDE, AND OF DIMETHYL SULPHIDE WITH AIR

Sulphur reactant	T K	t s	Ic mA	Reaction order (n)
Methyl mercaptan	423	10	0.1	1.98 ± 0.02
			0.3	1.99 ± 0.03
			0.6	1.96 ± 0.08
			Average =	1.98 ± 0.04
Dimethyl disulphide	423	10	0.1	0.79 ± 0.01
			0.3	0.96 ± 0.02
			0.5	0.94 ± 0.04
			Average =	0.96 ± 0.02
Dimethyl sulphide	423	10	0.1	1.02 ± 0.01
			0.3	1.04 ± 0.04
			0.6	0.98 ± 0.06
			Average =	1.01 ± 0.04

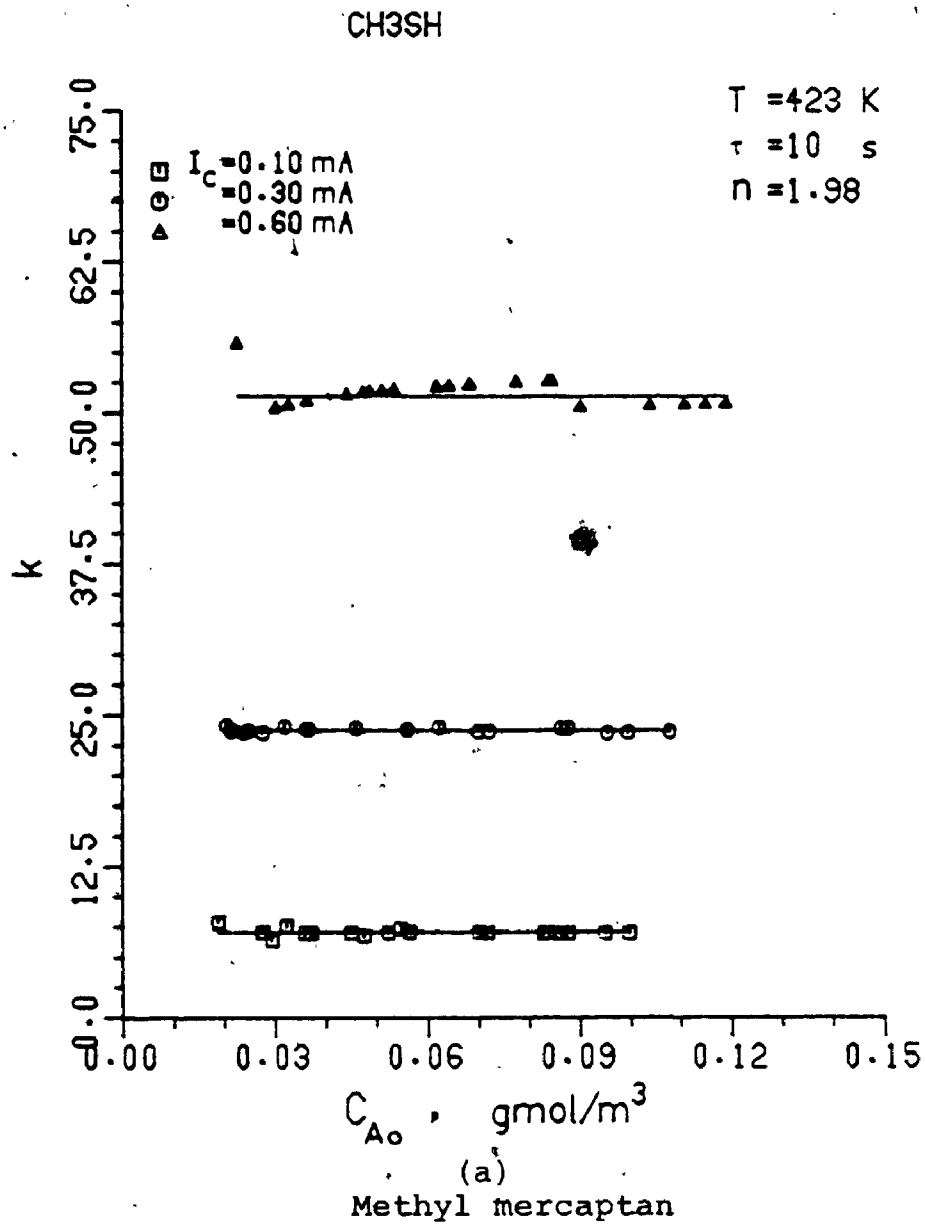

(a)
Methyl mercaptan

Figure 7.2: The dependency of the rate constant k defined by equation (7.13) on the initial concentration of the sulphur compounds:

Reactor dimensions: $D = 2.54 \times 10^{-2}$ m

$H = 1.52 \times 10^{-1}$ m

$a = 1.52 \times 10^{-5}$ m

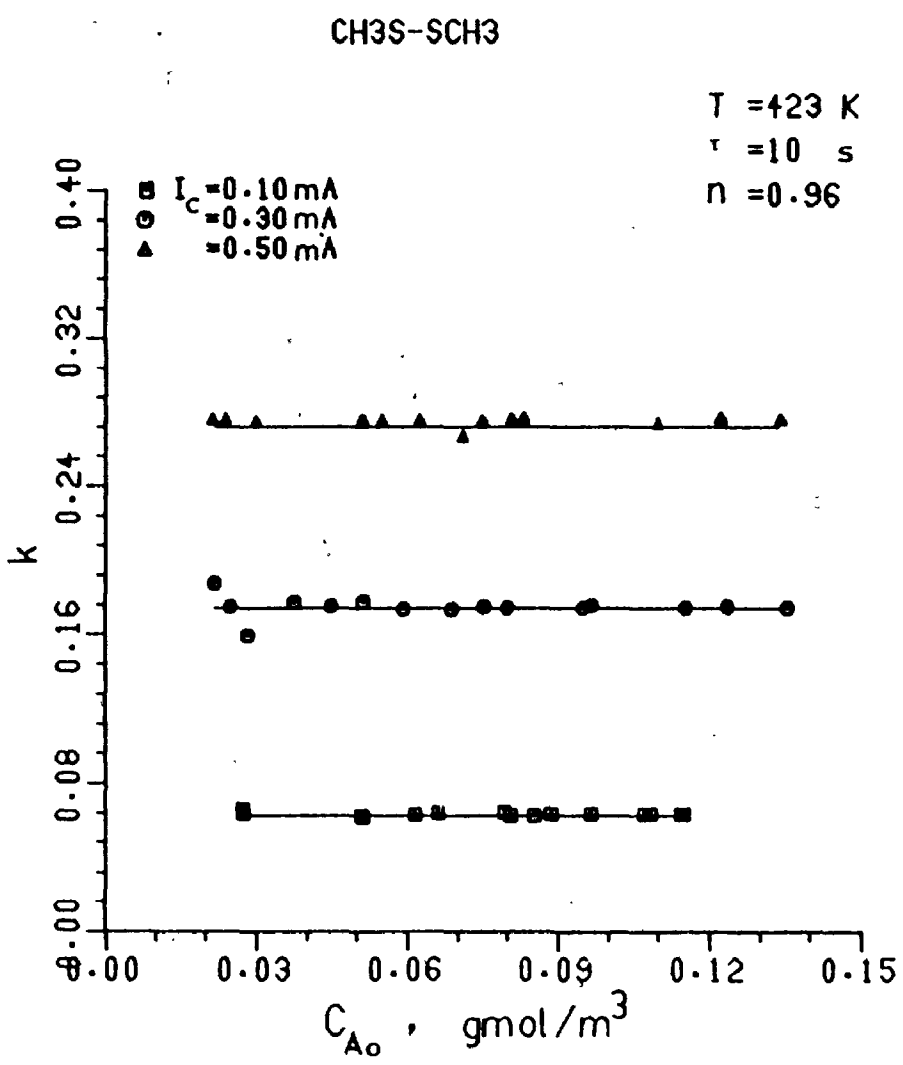

(b)

Dimethyl disulphide

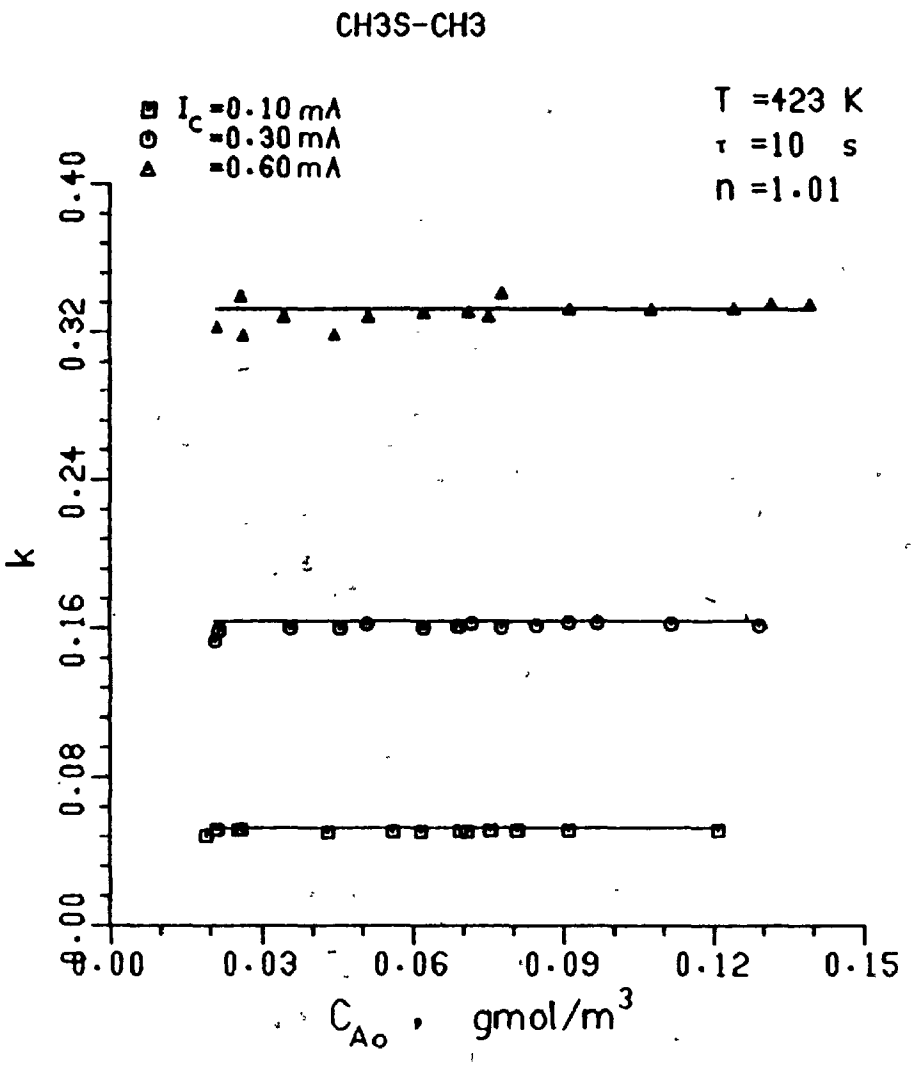

(c)

Dimethyl sulphide

Figure 7.2 (cont'd)

To date, no similar study has been published so that no comparison could be made. However, the accuracy of the reaction orders can be easily confirmed by that of the methods used in their evaluation. It was indicated earlier that the accuracy of the devices used in the experiment was in the vicinity of ±1%. It was therefore reasonable to assign the same order of magnitude of this accuracy to the orders of the reactions.

The precision of the obtained reaction orders was also determined and the results are also listed in Table 7.1 and shown by the above figures. As indicated, with such values of standard deviation, the correlation was considered excellent.

7.4 DETERMINATION OF THE PARAMETER m

7.4.1 Procedure

The constant m was defined by equation (7.13) above. Under isothermal conditions, equation (7.13) may be reduced to:

$$k = k_{o_1} \left(\frac{I_c}{Q}\right)^m \qquad (7.15)$$

where k_{o_1} here is:

$$k_{o_1} = k_o \, e^{-E_a/RT} \, (\bar{E}\,\Delta a)^m \qquad (7.16a)$$

The constant m for every reactions of concern was obtained as follows:

i- Fix the temperature at a preassigned value. Then, for every value of the ratio (I_c/Q) attempted at this temperature, obtain a value for k .

ii- By linear regression analysis, fit the two sets of values to the straight line:

$$\log k_i = \log(k_{o_1})_i + m_i \log(I_c/Q) \qquad (7.16b)$$

which was obtained from equation (7.16a) by taking the logarithm of both sides. The linear regresssion was performed by using the Statistical Package for the Social Sciences (SPSS) available at the University of Western Ontario [158].

iii- For other values of temperature tried, repeat the above procedure and evaluate the respective set of values of m_i and $(k_{o_1})_i$ in every case.

iv- Add the obtained m_i values and calculate an average $\bar{m}$. The respective value of k_{o_1} at every temperature tried was then modified by the relation:

$$(k_{o_1})_i = (k_{o_1})_{i_{old}} + (m_i - \bar{m}) \log\left(\frac{I_c}{Q}\right) \qquad (7.17)$$

7.4.2 Results and Discussion

The values of m obtained for every reaction are listed in Table 7.2 and the fitting is shown if Figures 7.3a to 7.3c.

The accuracy of these results is related to that of the used methods. Since the accuracy of the latter was about 1% we could presume the same for the values obtained for m.

7.5 DETERMINATION OF THE THERMAL ACTIVATION ENERGY E_a AND THE PRE-EXPONENTIAL CONSTANT k_o

7.5.1 Theoretical

By referring to equations (2.18), (7.4), and (7.9), the effect of temperature on the rate constant k is manifested in its effect on

i- the coefficient k',

ii- the thickness of the ionized sheath a, and on

iii- the corona onset-electrical intensity through the effect of temperature on the gas density.

To combine these effects together, we substitute the above equations into equation (7.13) so that:

TABLE 7.2: VALUES OF THE PARAMETER m DEFINED BY EQUATION (7.14)

Sulphur reactant	T K	m	$\log k_{o_1}$	m'	$(\log k_{o_1})_{new}$
Methyl mercaptan	298	1.11	-2.09	1.13±0.11	-1.82
	323	1.56	-1.95		-1.45
	373	1.13	-1.41		-1.04
	423	1.13	-1.03		-0.70
	453	1.12	-0.80		-0.51
Dimethyl disulphide	298	0.91	-5.51	0.91±0.09	-5.52
	373	0.92	-5.31		-5.28
	423	0.91	-5.17		-5.19
	453	0.91	-5.13		-5.14
Dimethyl sulphide	298	1.06	-5.75	1.06±0.06	-5.75
	373	1.07	-5.78		-5.76
	423	1.07	-5.80		-5.77
	453	1.05	-5.77		-5.81

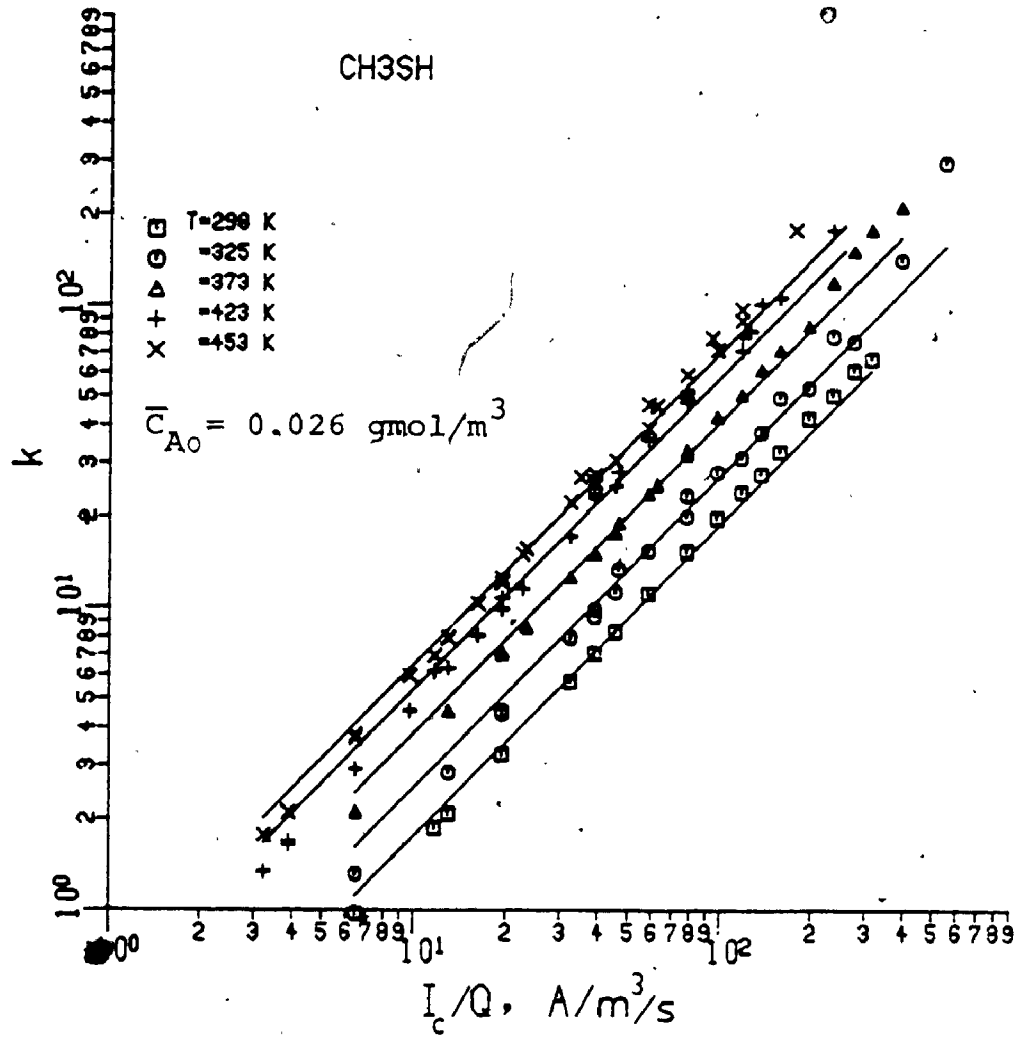

(a)
Methyl mercaptan

Figure 7.3: The relation between the rate constant k defined by equation (7.13) and the quotient I_c/Q for the reactions of the sulphur compounds with air:

Reactor dimensions: D = 2.54×10^{-2} m
H = 1.52×10^{-1} m
a = 1.52×10^{-5} m

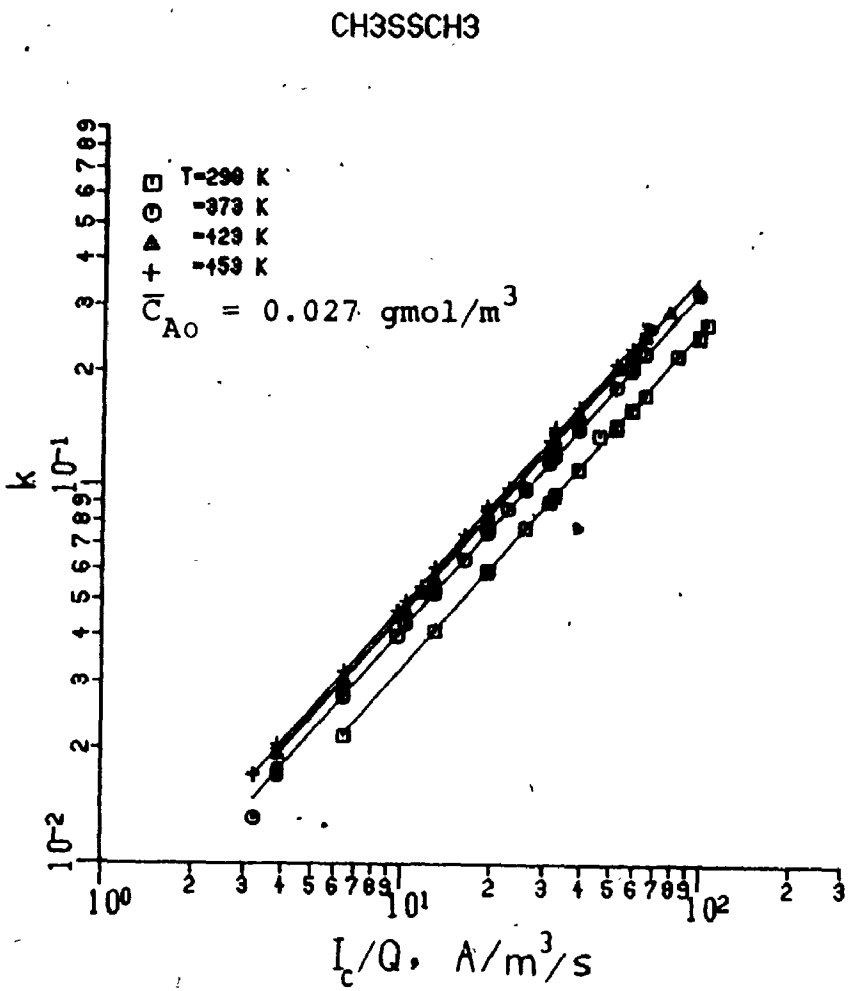

(b)

Dimethyl disulphide

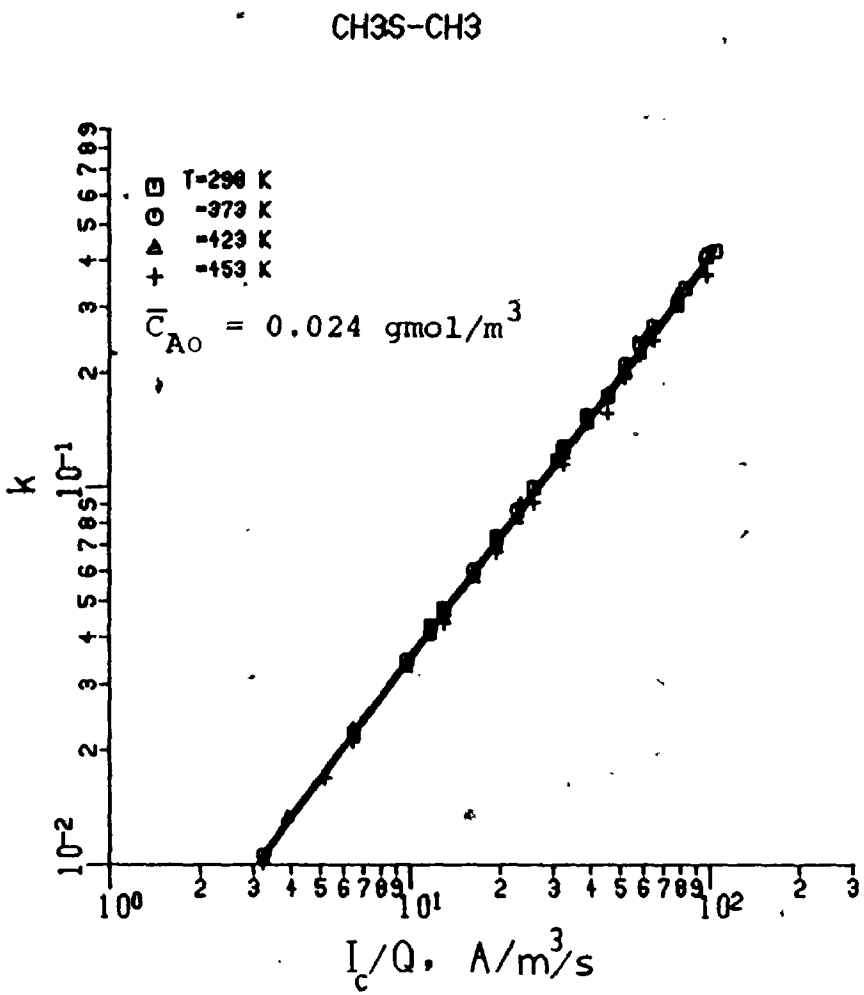

(c)

Dimethyl sulphide

Figure 7.3:(cont'd)

$$k = k_o\, e^{-E_a/RT} \left(\frac{I_c}{Q}\right)^m \left\{\left(E_o + \frac{C_3}{T} + \frac{C_4}{T^{\frac{1}{2}}}\right) \left[\left(0.03\sqrt{\frac{C_5 a}{T}} - a\left(1 - \frac{C_5}{T}\right)\right]\right\}^m \qquad (7.18)$$

where:

$$C_3 = \frac{C_1 T_o P_o}{P_o},$$

$$C_4 = C_2 \sqrt{\frac{T_o P}{aP}},$$

and $$C_5 = \frac{T_o P}{P_o}$$

P, P_o, C_1, C_2, and a were already defined earlier.

Equation (7.18) may also be expressed in the reduced form:

$$\log\left(\frac{k}{F(I_c,T)}\right) = \log k_o - \frac{2.303E_a}{R}\frac{1}{T} \qquad (7.19)$$

in which the function $F(I_c,T)$ is:

$$F(I_c,T) = \left\{\left(\frac{I_c}{Q}\right)\left(E_o + \frac{C_3}{T} + \frac{C_4}{T^{\frac{1}{2}}}\right) \left[\left(0.03\sqrt{\frac{C_5 a}{T}} - a\left(1 - \frac{C_5}{T}\right)\right]\right\}^m \qquad (7.20)$$

7.5.2 Procedure

Evaluation of E_a and k_o was done as follows:

i- fix temperature at T_1 (K). Use all the data obtained above at this temperature to calculate values for k and for the function $F(I_c,T)$. Calculate the respective values for the left hand side of equation (7.19).

ii- By linear regression, fit the latter set of values against the corresponding values of the reciprocal of T.

The slope of the straight line obtained defines the quantity E_a/R' while the interception defines k_o.

The results obtained are summarized in Table 7.3 while the fitting is shown by Figures 7.4a to 7.4c.

Following the method given above, the accuracy of these results is about ±1%.

TABLE 7.3: THE THERMAL ACTIVATION ENERGY FOR THE REACTIONS OF METHYL MERCAPTAN, DIMETHYL DISULPHIDE, AND OF DIMETHYL SULPHIDE WITH AIR

Sulphur reactant	Activation energy (J/kmol)x10^{-7}	Pre-exponential constant
Methyl mercaptan	13,606 ± 58	78±13 x 10^{-4}
Dimethyl sulphide	6,064 ± 67	72±23 x 10^{-6}
Dimethyl sulphide	3,431 ± 46	72±13 x 10^{-7}

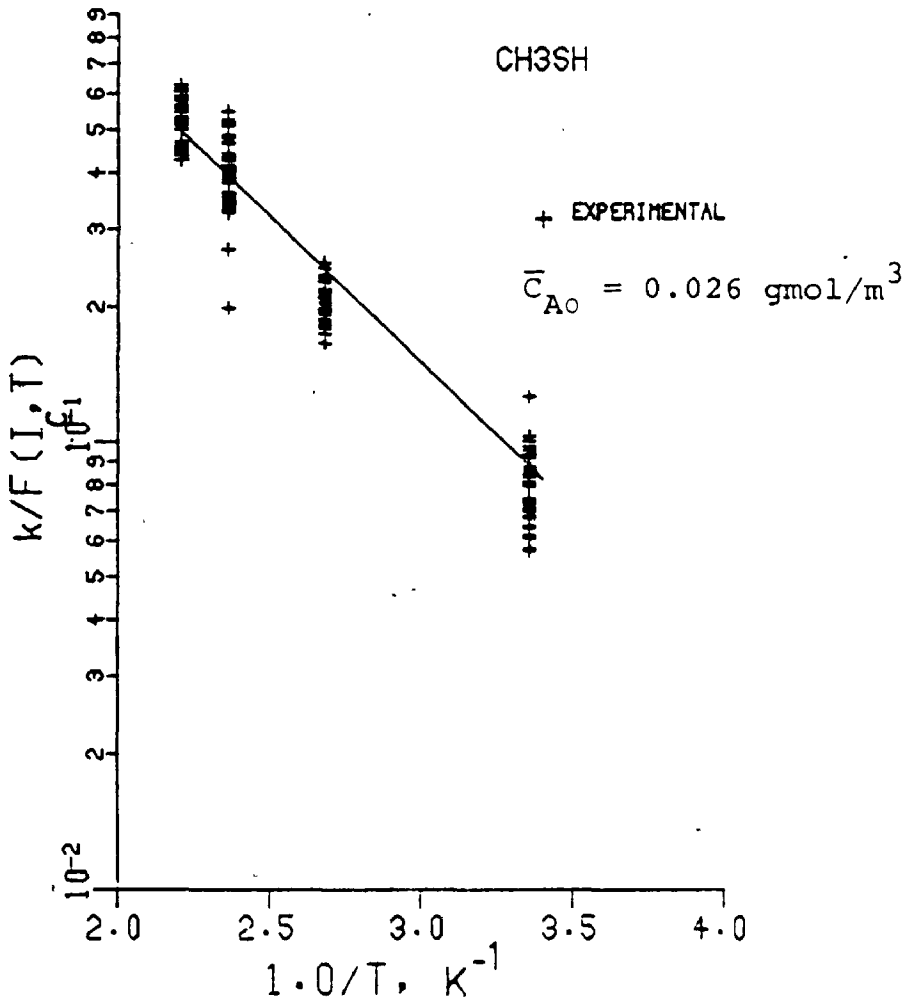

(a)

Methyl mercaptan

Figure 7.4: The temperature dependency of the rate constant k (see equation (7.19)) of the reactions between the sulphur compounds and air:

Reactor dimensions: D = 2.54×10^{-2} m
H = 1.52×10^{-1} m
a = 1.52×10^{-5} m

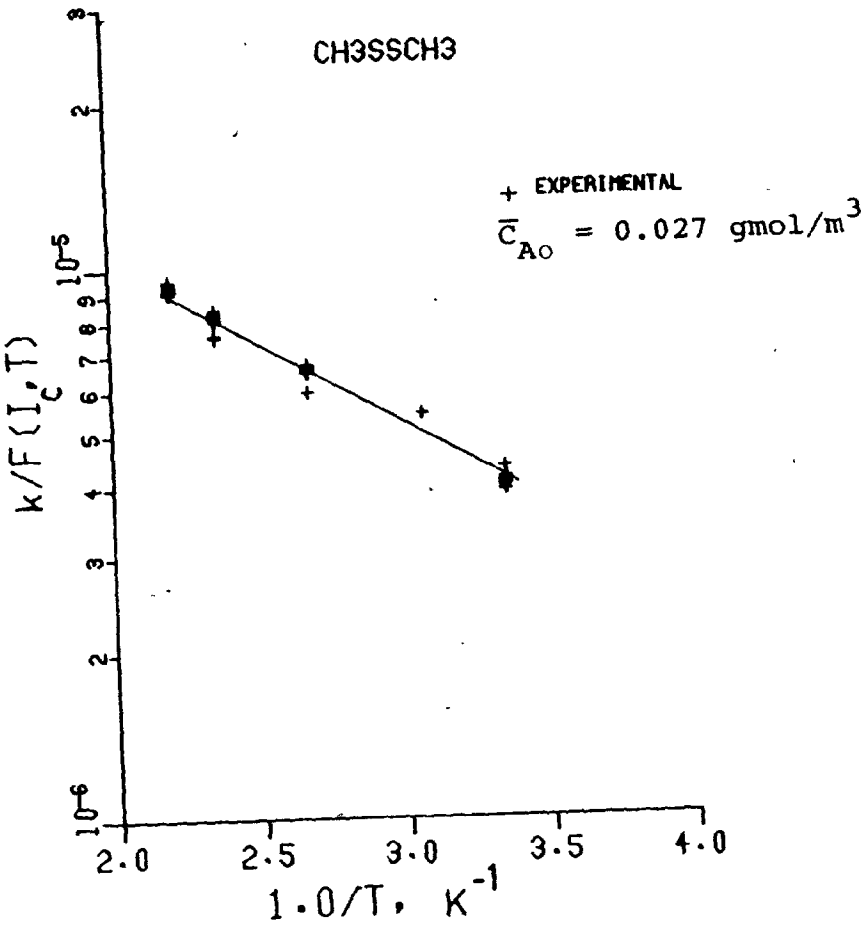

(b)

Dimethyl disulphide

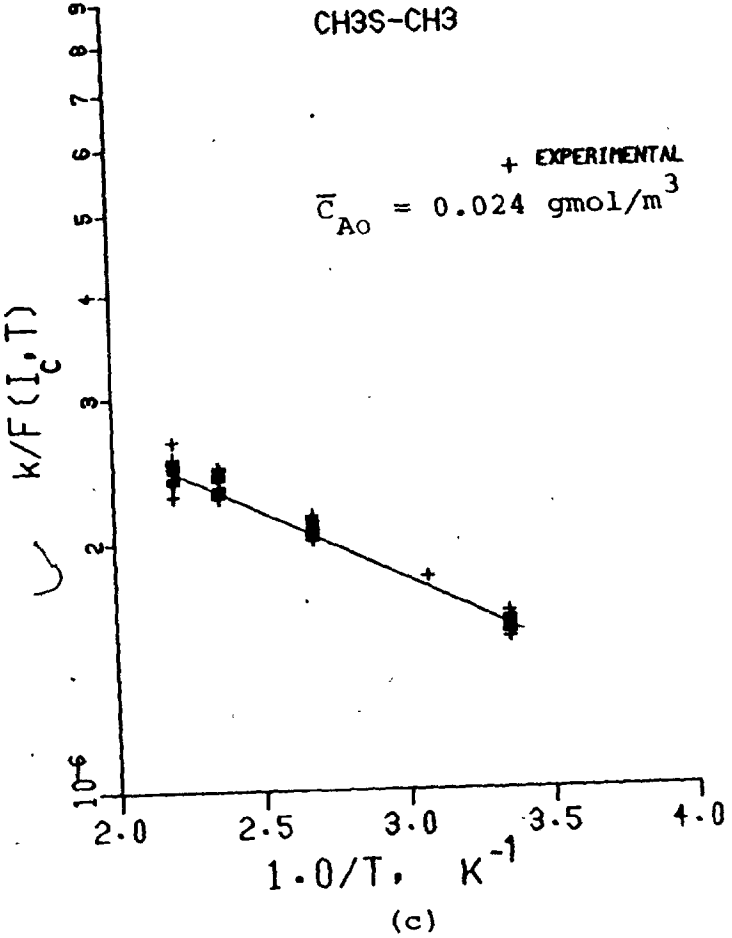

(c)

Dimethyl sulphide

Figure 7.4: (cont'd)

7.6 SUMMARY

The kinetic parameters defined in equation (7.20) were determined for the three reactions:

$$2CH_3SH + \tfrac{1}{2}O^* \rightarrow (CH_3)_2S_2 + H_2O \qquad (6.23a)$$

$$(CH_3)_2S_2 + \tfrac{1}{2}O_2^* \rightarrow (CH_3)_2S + SO_2 \qquad (6.23b)$$

$$(CH_3)_2S + \tfrac{1}{2}O_2^* \rightarrow (CH_3)_2SO_2 \qquad (6.23c)$$

which describe the reaction of methyl mercaptan in a corona discharge.

The rate equations of these reactions are:

$$-r_{CH_3SH} = 78\times10^{-4} e^{-1638/T} \left(\frac{\bar{E}\Delta a I_c}{Q}\right)^{1.13} C_{CH_3SH}^{1.98} \qquad (7.21a)$$

$$-r_{(CH_3)_2S_2} = 72\times10^{-6} e^{-730/T} \left(\frac{\bar{E}\Delta a I_c}{Q}\right)^{0.91} C_{(CH_3)_2S_2}^{0.96} \qquad (7.21b)$$

$$-r_{(CH_3)_2S} = 72\times10^{-7} e^{-413/T} \left(\frac{\bar{E}\Delta a I_c}{Q}\right)^{1.06} C_{(CH_3)_2S}^{1.01} \qquad (7.21c)$$

The values of the fractional conversion of the sulphur compounds are plotted against those obtained by using equations (7.21a) - (7.21c) and the results are shown in Figures (7.5a) to (7.5c). Comparison indicates an excellent agreement between the two sets in each case with standard deviations of ±0.024, ±0.022, and ±0.031, respectively.

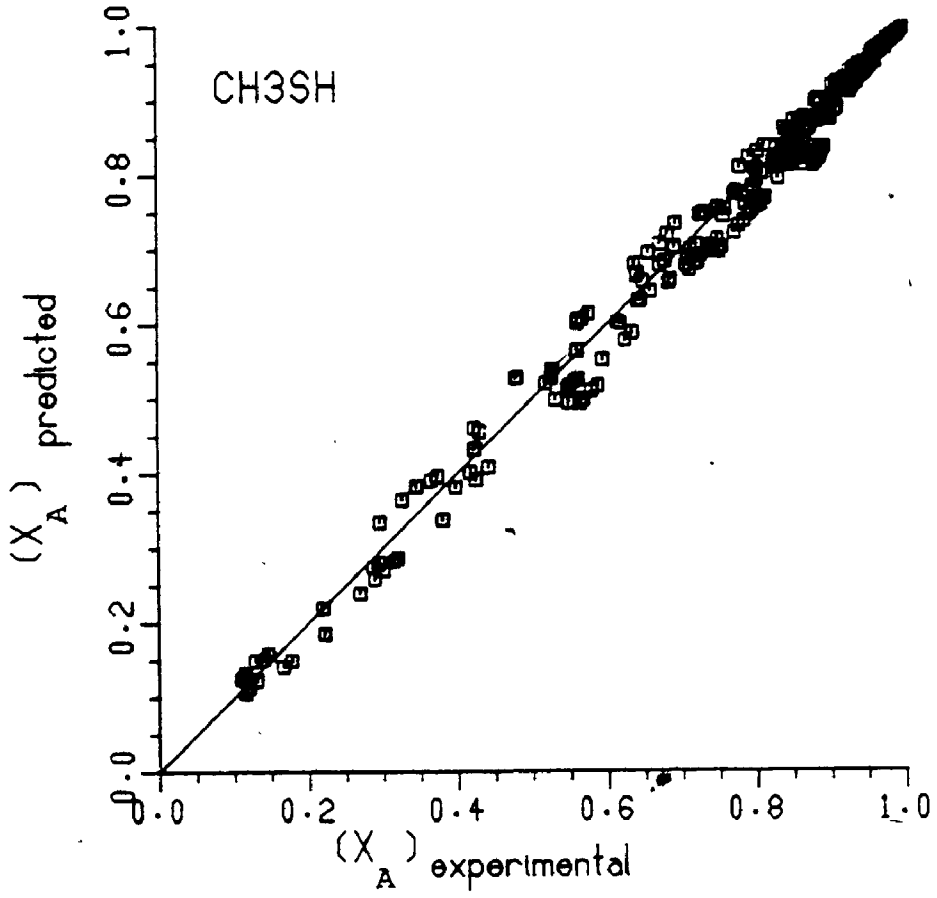

(a)
Methyl mercaptan

Figure 7.5: Experimental versus predicted values of the fractional conversion of the sulphur compounds due to reactions with air.

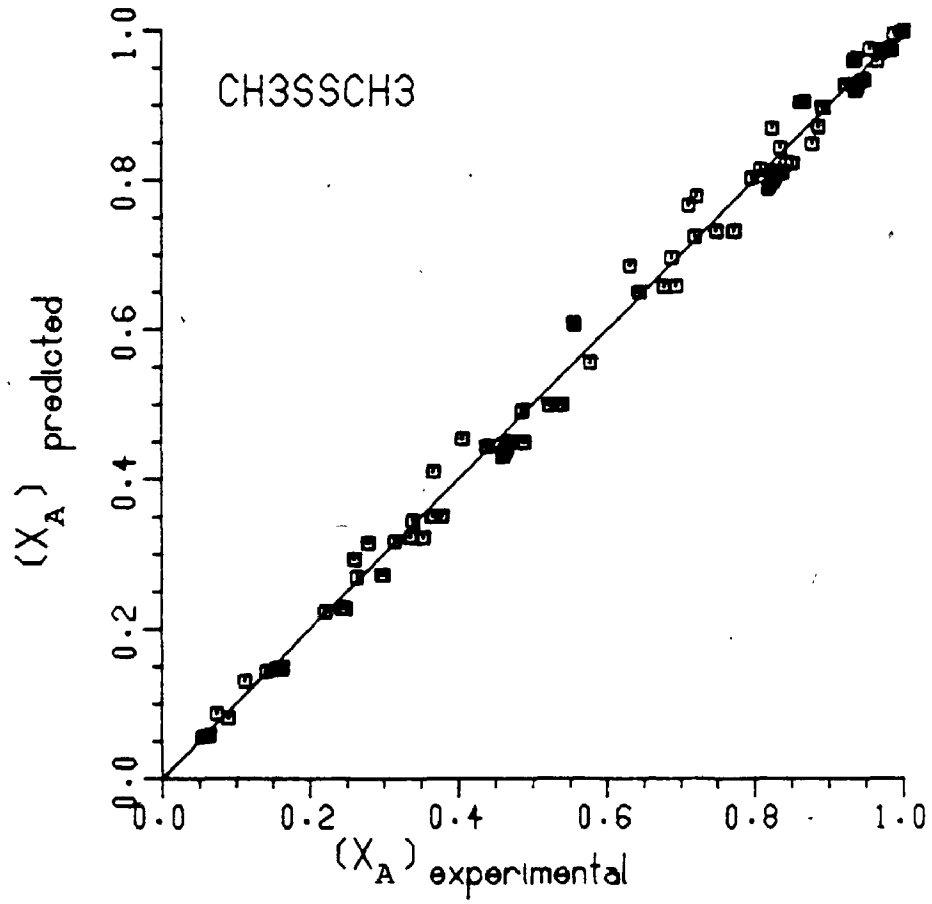

(b)
Dimethyl disulphide

Figure 7.5: cont'd

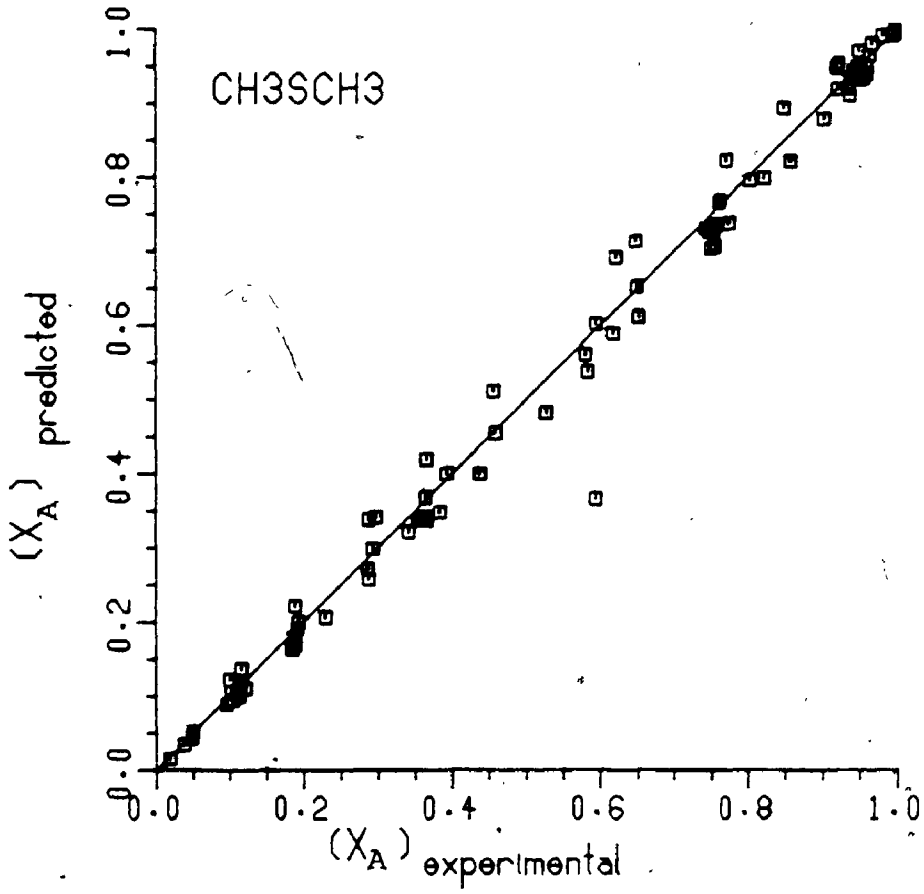

(c)
Dimethyl sulphide

Figure 7.5: cont'd.

Furthermore, in presenting the experimental kinetic data obtained as shown by, for example, Figures (5.1) and (5.9), equations (7.21) were used to draw the solid lines between the points. As may be noticed, these solid lines exhibit almost zero slope at zero time. This can be attributed to the dependency of the rate constant of the reactions between sulphur compounds and air on the mean residence time via the flow rate term.

CHAPTER 8

THE REACTION OF HYDROGEN SULPHIDE WITH AIR IN A CORONA DISCHARGE

8.1 INTRODUCTION

This chapter is devoted to presentation and correlation of the kinetic data obtained on the reaction between hydrogen sulphide and air.

The kinetic data will be presented in terms of the fractional conversion of hydrogen sulphide defined by:

$$X_A = \frac{C_{Ao} - C_A}{C_{Ao}} \qquad (5.1)$$

The effect of current, temperature, and of mean residence time on this variable will be discussed.

It was concluded earlier that excited oxygen molecules, namely, the triplet state $O_2^*(A\,^3\Sigma_u^+)$ is the species responsible for the oxidation of methyl mercaptan in the corona reactor. Subject to the same environments, hydrogen sulphide was considered to also be oxidized by this species. Thereupon, the same kind of treatment used previously to correlate the data obtained on the oxidation of methyl mercaptan will be followed with that of hydrogen sulphide.

8.2 THE THERMAL REACTION

The thermal reaction of hydrogen sulphide with air was investigated by conducting a set of experiments in the absence of corona discharge. Runs at different temperatures from 298 to 453 K (a range which may cover industrial applications) were carried out. The residence time during these experiments was fixed at 20 seconds which is probably greater than the residence time in an industrial precipitator.

The procedure followed in conducting the above experiments was described in Section 4.3.1, except for the high voltage supply being turned off. The composition of the feed and of the product streams was determined using the gas chromatograph which had the same operating conditions as mentioned previously.

Table 8.1 summarizes the results along with the operating conditions used. The table indicates that there are no substantial differences in the concentration of hydrogen sulphide in the feed and in the product streams, the apparent differences are within the experimental errors. From this fact we conclude that the thermal reaction is unimportant in the temperature range examined. In conjuction with this, it can also be concluded that neither the stainless steel nor the Pyrex walls of the reactor vessel has catalytic effects on the reaction at the

TABLE 8.1: EXPERIMENTS TO DETERMINE THE IMPORTANCE OF THE THERMAL REACTION OF HYDROGEN SULPHIDE WITH AIR

C_{Ao} $\frac{kmol \times 10^6}{m^3}$	Temperature K	τ s	C_A $\frac{kmol \times 10^6}{m^3}$	Difference in concentration, $kmol \times 10^6 / m^3$	Diff.% with respect to C_{Ao}
29.91	298	20	30.04	- 0.13	- 0.80
23.39	373	"	23.27	0.12	0.42
33.24	423	"	33.17	0.07	0.21
23.13	423	"	23.04	0.09	0.39
29.35	453	"	29.51	- 0.16	0.55

equations have already been given earlier.

From the plug-flow equation (7.8), k at a given set of current, temperature, and mean residence time may be expressed as:

$$k = -\frac{1}{\tau}\int_{C_{A0}}^{C_A}\frac{dC_A}{C_A^n} \qquad (8.2)$$

The reaction order n followed by the constant m, the thermal activation energy E_a, and the pre-exponential constant k_o, were determined as will be seen below.

8.4.2 The Reaction Order n

Following the procedure outlined in Section 7.4, the order of reaction (8.1) was determined at four values of current 0.05, 0.10, 0.30, and 0.50 mA while the temperature and the mean residence time were fixed at 423 K and 10 s, respectively.

As Table 8.2 indicates, an average value of 0.98±0.04 was obtained for the reaction order. By using these results, Figure 8.2 could be constructed.

No information on a similar study was available and no comparison could therefore be made. Yet, as discussed in Section 2.3, the reaction between hydrogen sulphide and oxygen was studied by several workers. Based on the authors

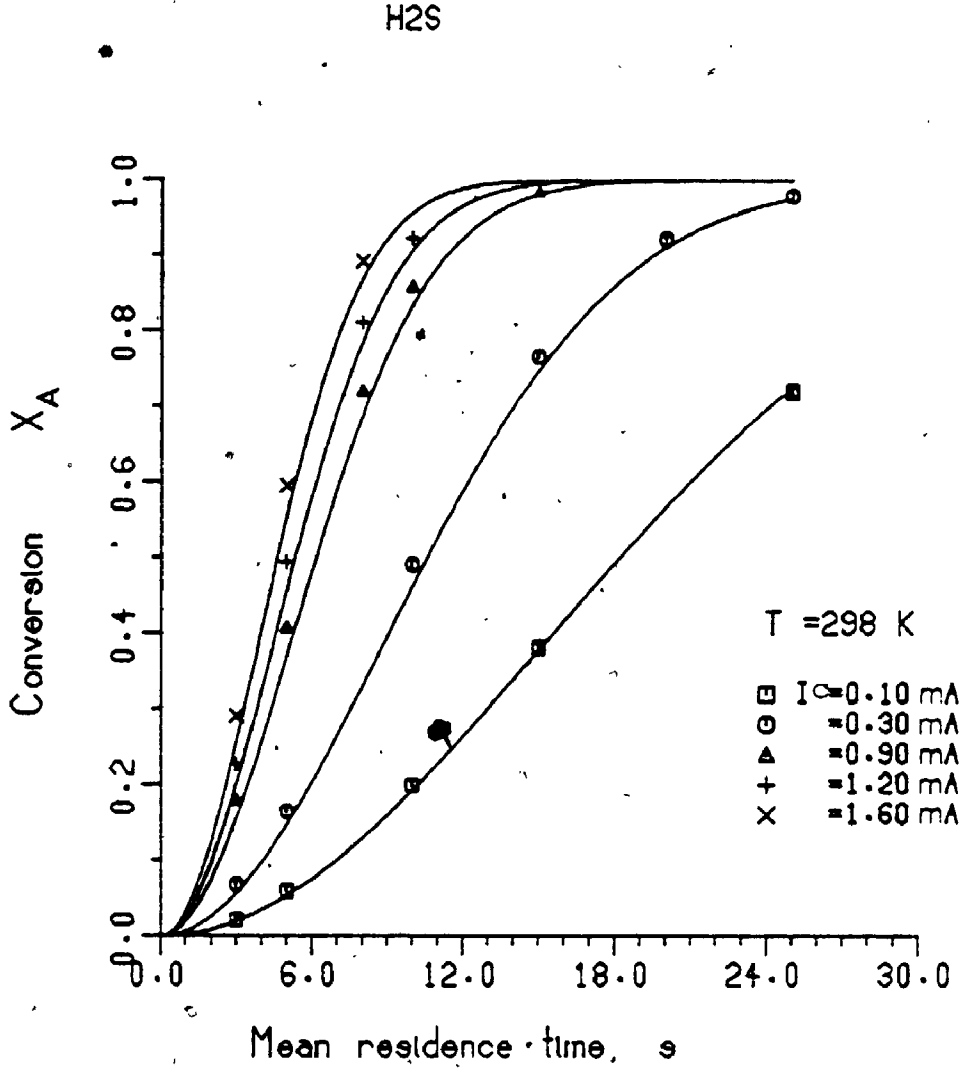

(a): Temperature=298 K

Figure 8.1 (a-e): Time-dependency of the fractional conversion of hydrogen sulphide due to reaction with air.

Reactor dimensions:

$D = 2.54 \times 10^{-2}$ m

$H = 1.52 \times 10^{-1}$ m

$a = 1.52 \times 10^{-5}$ m

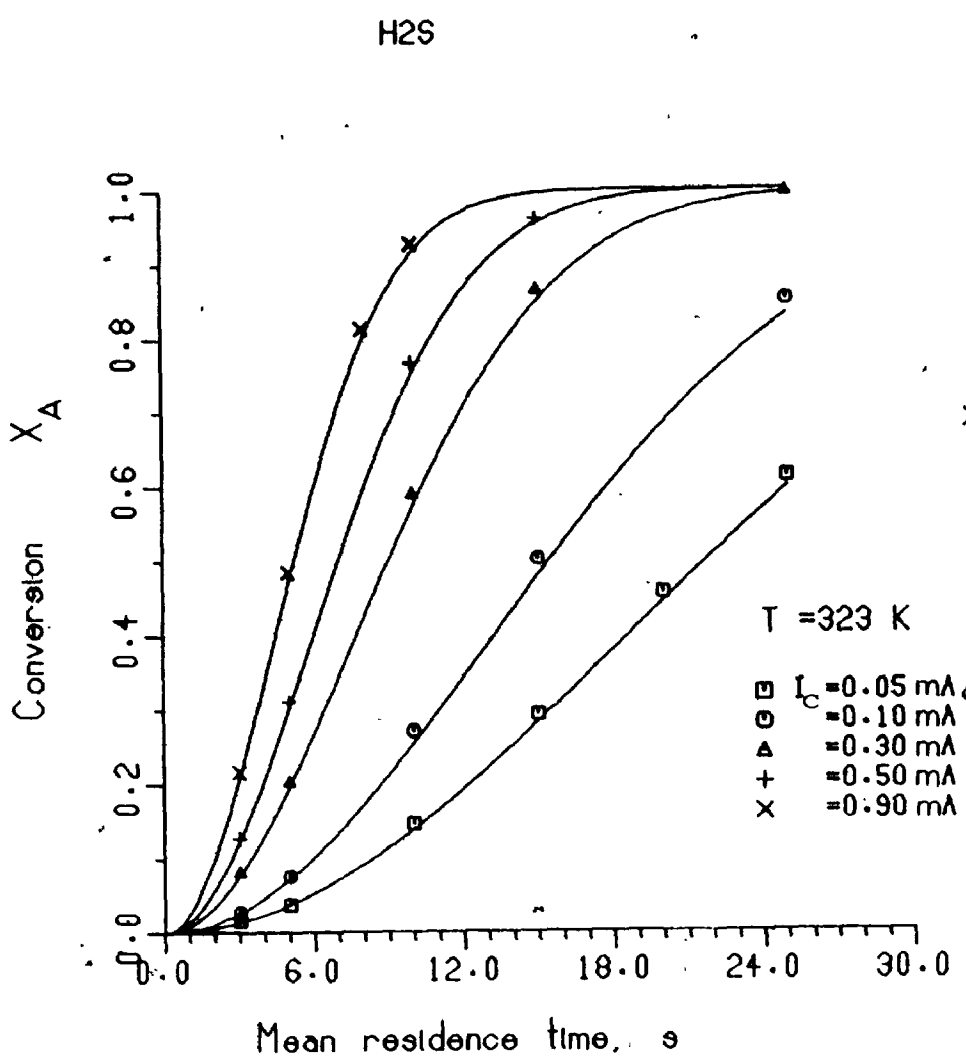

(b) : Temperature=323 K

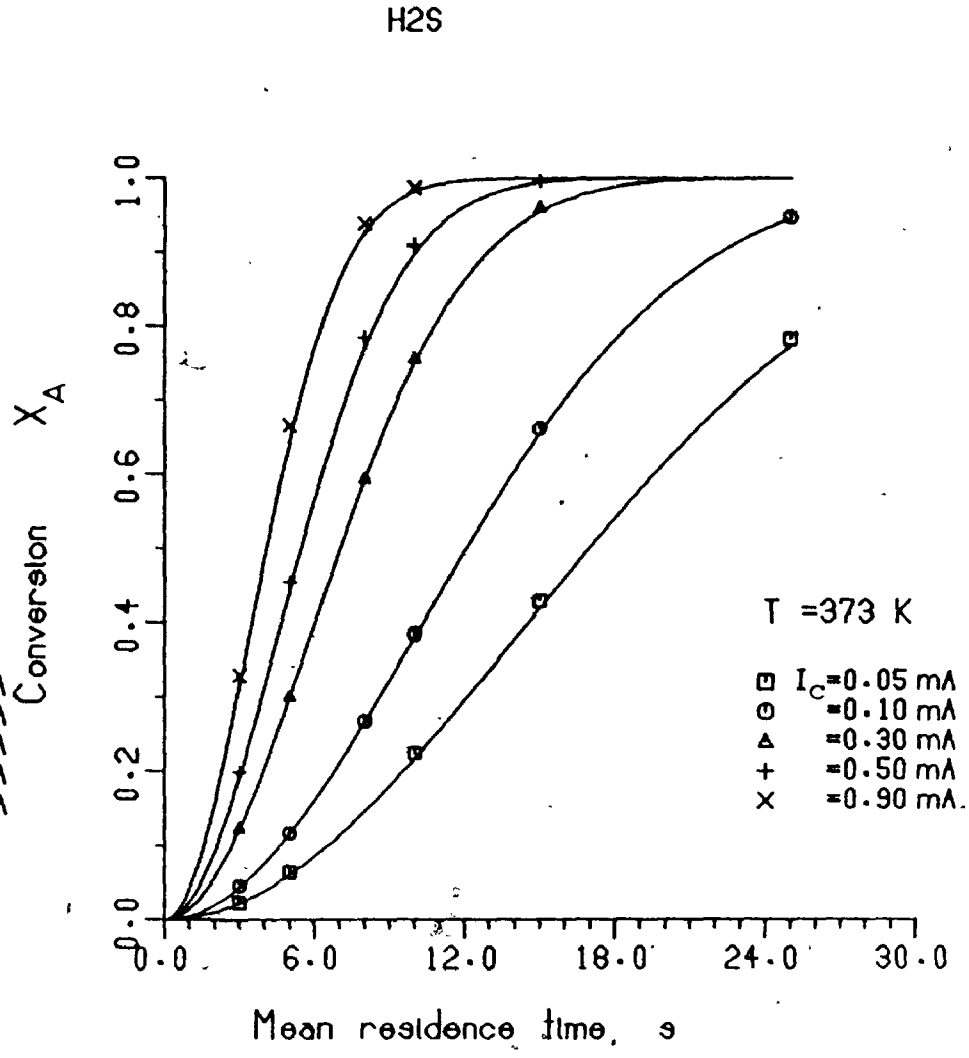

(c) : Temperature=373 K

Figure 8.1: cont'd

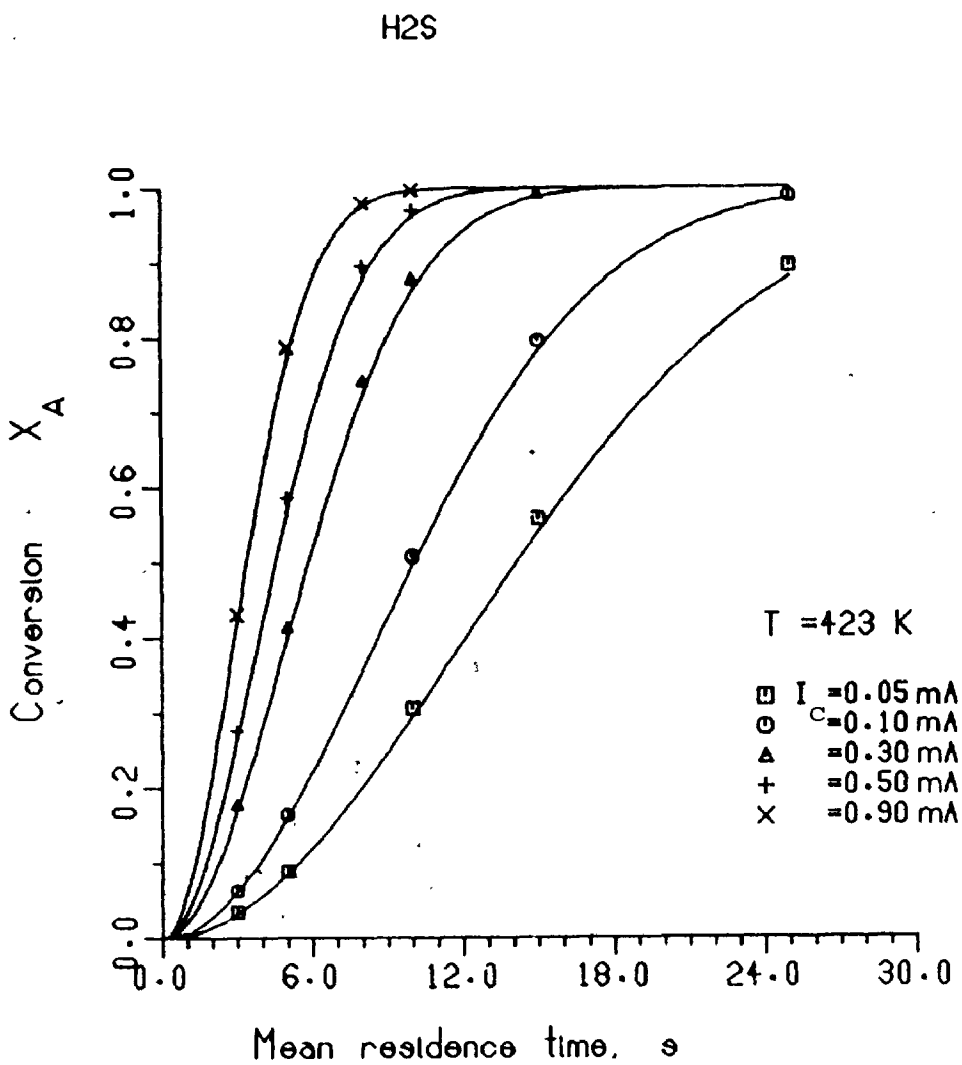

(d): Temperature=423 K

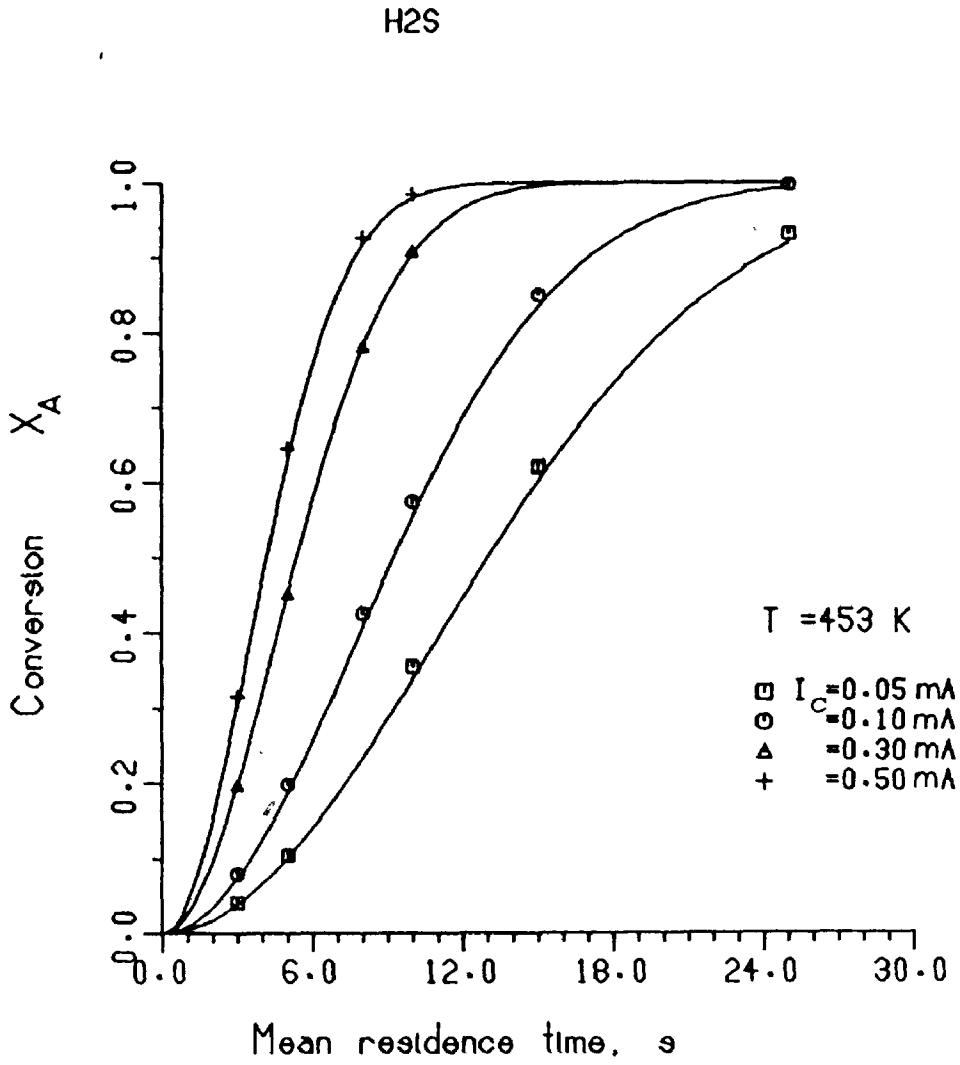

(e): Temperature=453 K

Figure 8.1: cont'd

shows that, at 298 K, a complete reaction of hydrogen sulphide is possible at 1.2 mA and about 12 s.

The above results also indicate, as expected, that the fractional conversion of hydrogen sulphide increases with the increase in mean residence time. Moreover, as the reaction progresses, its rate, given by the slope of the curves, varies. This fact indicates that the reaction is concentration-dependent. (The degree of this dependency will be discussed in Section 8.4.1.)

The effect of current on the fractional conversion of hydrogen sulphide may be discussed in reference to any of the above figures at a constant value of mean residence time. As current increases, the conversion of the sulphur compound also increases. These findings, bearing in mind the insignificance of the thermal reaction, emphasize the essential role of the corona discharge in facilitating the reaction. The effect of current at lower values is more pronounced on the conversion of hydrogen sulphide. For example, Figure 8.1a shows that at 10 s, an increase in current from 0.3 to 0.9 mA causes the fractional conversion to increase from about 0.49 to about 0.85 i.e., about 600 unit of fractional conversion per unit current. An increase in current on the other hand from 0.9 to 1.2 mA allows the fractional conversion to increase from about 0.85 to about 0.92 i.e., only about 233 unit of fractional conversion per

unit current.

The effect of temperature on the fractional conversion of hydrogen sulphide can be discussed by referring to the above figures collectively. In contrast to the results of Section 8.2 which show the insignificance of the thermal reaction in the absence of corona discharge, temperature here has indeed an effect on hydrogen sulphide reaction with air, where higher temperatures produce higher fraction conversions. As an example, at o.3 mA and 10 s, an increase in temperature from 298 to 323 to 373 to 423 to 453 K causes the fractional conversion of hydrogen sulphide to increase from 0.49 to 0.60 to 0.76 to 0.87 to 0.92, respectively.

Pursuing the above example further, we find that, as in the case of current, the temperature effect at its lower values is more noticeable on the fractional conversion. For instance, an increase of 50 K in temperature from 298 to 323 K increases the fraction conversion by about 0.005 units whereas an increase of 50 degrees K from 423 to 453 K causes an increase of only about 0.001 fractional conversion units.

8.4 CORRELATION OF THE KINETIC DATA

8.4.1 Introduction

In accordance with the high fractional conversions of hydrogen sulphide reported above, the reactor may be treated as an integral reactor. AS discussed in Chapter 7, a mass

balance of species i around such a reactor must consider terms representing the rates due to flow, reaction, and diffusion.

However, calculations given in Appendix D show that the change in the radial and axial concentrations of hydrogen sulphide are insignificant and hence the rate due to diffusion may be neglected. Mass balance of hydrogen sulphide around the reactor can be performed in this case using the plug-flow equation [105,152].

Following the discussuin given in Section 6.2, the rate equation for reaction:

$$H_2S + O_2^* \rightarrow H_2O + SO_2 \qquad (8.1)$$

is:

$$-r_A = k' C_{O_2^*}^m C_A^n \qquad (7.5)$$

or

$$-r_A = k C_A^n \qquad (7.7a)$$

in which k is given by:

$$k = k_o \cdot e^{-E_a/RT} \left(\frac{\bar{E} \Delta a I_c}{Q}\right)^m \qquad (7.13)$$

The significance of the parameters included in the above

equations have already been given earlier.

From the plug-flow equation (7.8), k at a given set of current, temperature, and mean residence time may be expressed as:

$$k = -\frac{1}{\tau}\int_{C_{A0}}^{C_A}\frac{dC_A}{C_A^n} \qquad (8.2)$$

The reaction order n followed by the constant m, the thermal activation energy E_a, and the pre-exponential constant k_o, were determined as will be seen below.

8.4.2 The Reaction Order n

Following the procedure outlined in Section 7.4, the order of reaction (8.1) was determined at four values of current 0.05, 0.10, 0.30, and 0.50 mA while the temperature and the mean residence time were fixed at 423 K and 10 s, respectively.

As Table 8.2 indicates, an average value of 0.98±0.04 was obtained for the reaction order. By using these results, Figure 8.2 could be constructed.

No information on a similar study was available and no comparison could therefore be made. Yet, as discussed in Section 2.3, the reaction between hydrogen sulphide and oxygen was studied by several workers. Based on the authors

TABLE 8.2: ORDER OF THE REACTION OF HYDROGEN SULPHIDE WITH AIR

T K	t s	Ic mA	Reaction order (n)
423	10	0.05	0.98 ± 0.01
		0.10	0.97 ± 0.02
		0.30	0.99 ± 0.03
		0.50	0.97 ± 0.08
		Average =	0.98± 0.04

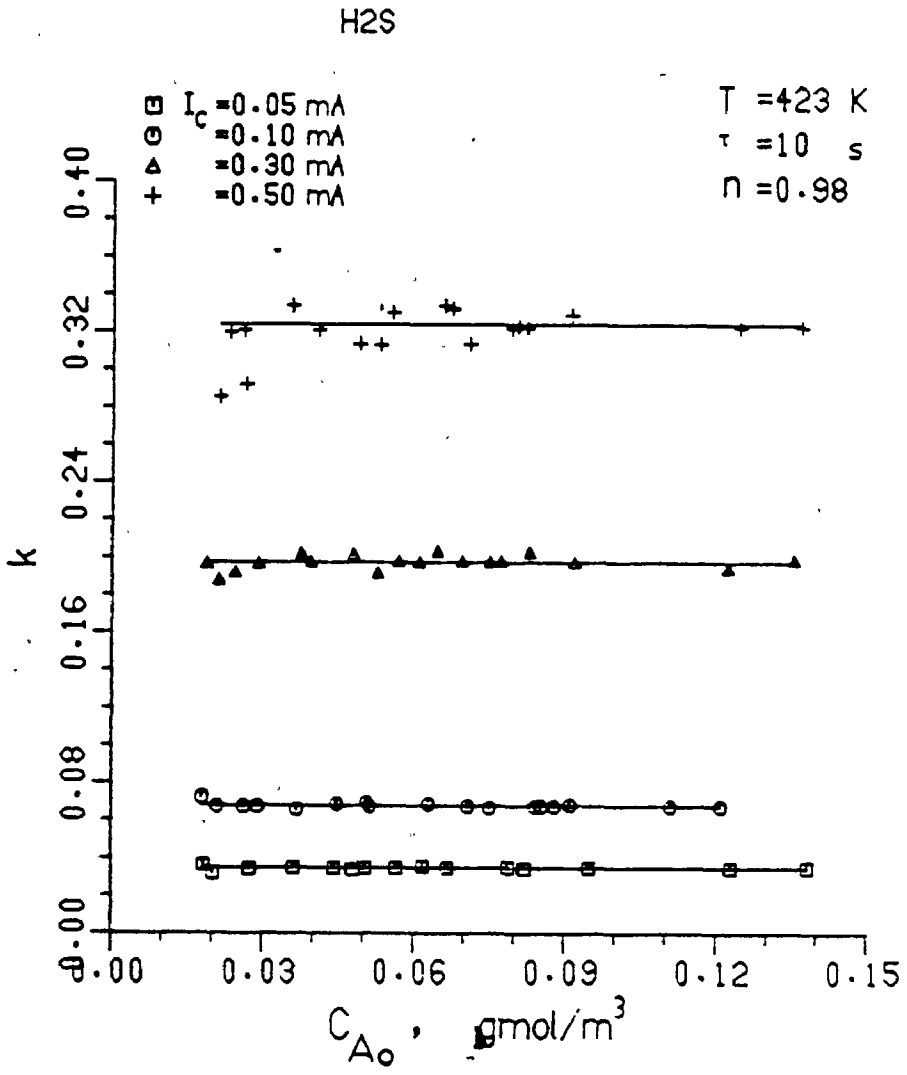

Figure 8.2: The dependency of the rate constant k defined by equation (7.13) on the initial concentration of hydrogen sulphide.

Reactor dimensions: $D = 2.54 \times 10^{-2}$ m

$H = 1.52 \times 10^{-1}$ m

$a = 1.52 \times 10^{-5}$ m

and their experimental procedure, the reaction order was found within 0.5-1.0 range. Accordingly, the reaction order of 0.98 reported here seems reasonable.

In any event, the accuracy of the results, being related to that of the procedure used in obtaining them, should be, as shown previously, in the vicinity of ±1%.

8.4.3 The Constant m

The constant m is defined as:

$$k = k_{o_1} \left(\frac{I_c}{Q}\right)^m \qquad (7.15)$$

or

$$\log k = \log (k_{o_1}) + m \log(I_c/Q) \qquad (7.16b)$$

The procedure followed to obtain a value of m for reaction (8.1) was similar to that described in Section 7.4.1. At every temperature examined, a value of m and k_{o_1} were obtained by linear regression of the respective data in accordance with equation (7.15b). As summarized in Table 8.3, the desired value of m is the average of all the values obtained. Based on this value ie., m', a new value of k_{o_1} at every temperature tested was obtained using the relation:

$$k_{o_1} = (k_{o_1})_{old} + (m - \bar{m}) \log(I_c/Q) \qquad (7.17)$$

By sustituting these values into equation (7.15b), Figure

TABLE 8.3: VALUE OF THE PARAMETER m
DEFINED BY EQUATION (7.14)
FOR REACTION (8.2)

T / K	m	$\log k_{o_1}$	$\bar{m}$	$(\log k_{o_1})_{new}$
298	0.961	-6.280	0.964±0.03	-6.28
323	0.962	-5.996		-6.00
373	0.973	-5.564		-5.56
423	0.966	-5.171		-5.16
453	0.959	-4.980		-4.99

8.3 was obtained.

The accuracy of these results is, as discussed earlier, about ±1%.

8.4.4 The Thermal Activation Energy E_a and the Pre-exponential Constant k_o

The thermal activation energy and the pre-exponential constant were already defined by equation (7.19):

$$\log \left(\frac{k}{F(I_c,T)}\right) = \log k_o - \frac{2.303\ E_a}{R}\ \frac{1}{T}$$

where the function $F(I_c,T)$ is defined as:

$$F(I_c,T) = \left\{\left(\frac{I_c}{Q}\right)\ \left(E_o + \frac{C_3}{T} + \frac{C_4}{T^{\frac{1}{2}}}\right)\right.$$

$$\left.\left[\left(0.03\sqrt{\frac{C_5 a}{T}} - a\left(1 - \frac{C_5}{T}\right)\right]\right\}^m \qquad (7.20)$$

The different prameters of these equations have the same significance as previously stated in Section 7.5.

By following the procedure outlined in Section 7.5, a linear regression was performed on the data reported according to equation (7.19). The results indicate that the thermal activation energy and the pre-exponential constant are equal to (12.743±6.830) x 10 J/kmol and (2.35±1.98) x 10^{-4} (units can be determined by considering equation (8.3)

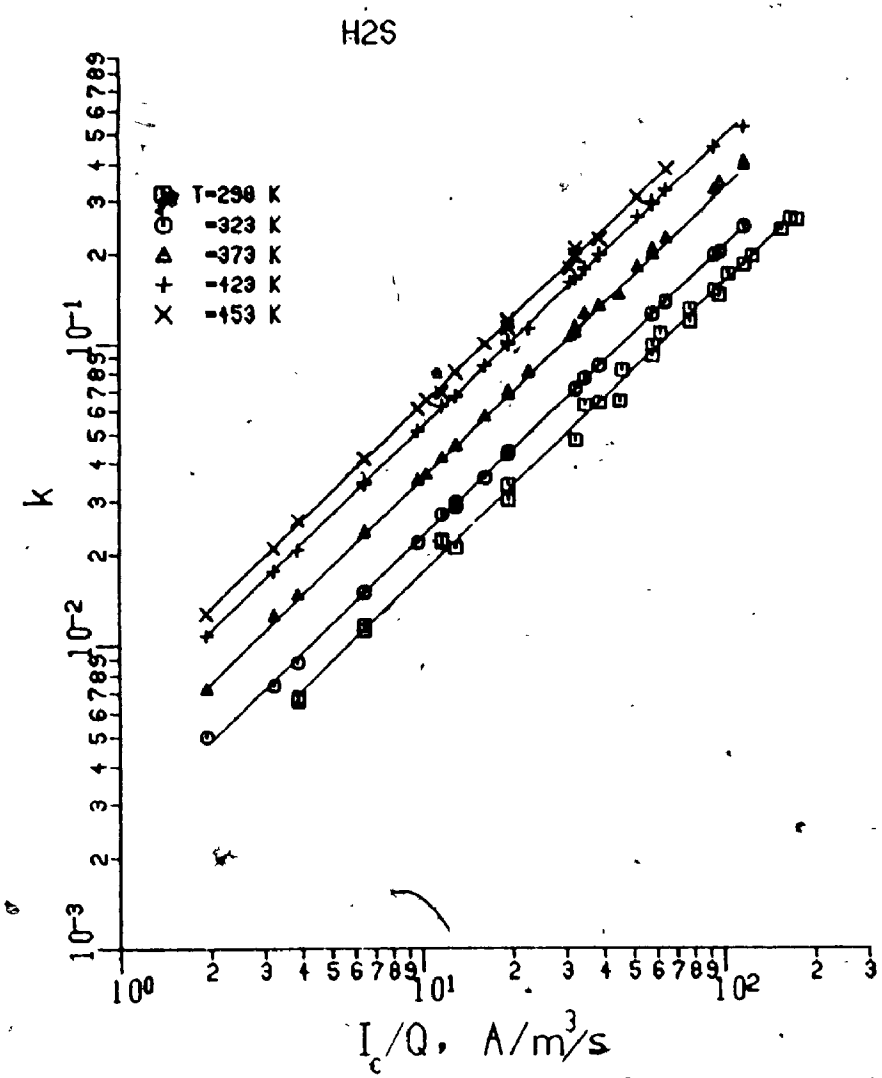

Figure 8.3: The relation between the rate constant k (equation (7.13)) and the quotient I_c/Q for the reaction of hydrogen sulphide with air.

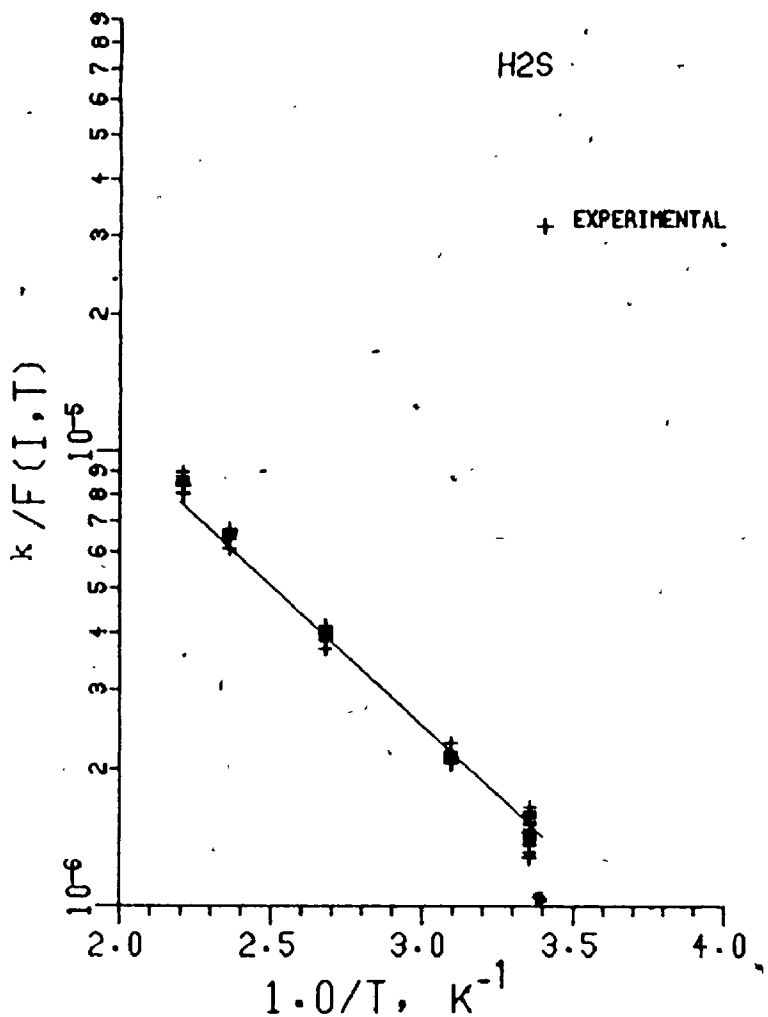

Figure 8.4: The temperature dependency of the rate constant k (equation (7.19)) of the reaction of hydrogen sulphide with air.

Reactor dimensions for both figures:

$D=2.54\times10^{-2}$ m, $H=1.52\times10^{-1}$ m, $a=1.52\times10^{-5}$ m

below), respectively. These values were then substituted in the above equation so that Figure 8.4 was constructed. As indicated, the figure exhibits an excellent correlation. The accuracy of the results as shown earlier should be within the vicinity of ±1%.

8.5 CONCLUSIONS

In conclusion then to the above results, the rate equation of the reaction between hydrogen sulphide and air in a corona discharge is given by:

$$-r_{H_2S} = 3.35 \times 10^{-4}\ e^{-1535/T}\ \left(\frac{\bar{E}\Delta a I_c}{Q}\right)^{0.96}\ C_{H_2S}^{0.98} \qquad (8.3)$$

The values of the fractional conversion of hydrogen sulphide are plotted against those obtained by using equation (8.3) and the results are shown in Figure 8.5. Comparison shows excellent agreement between the two sets with a standard deviation of ±0.06.

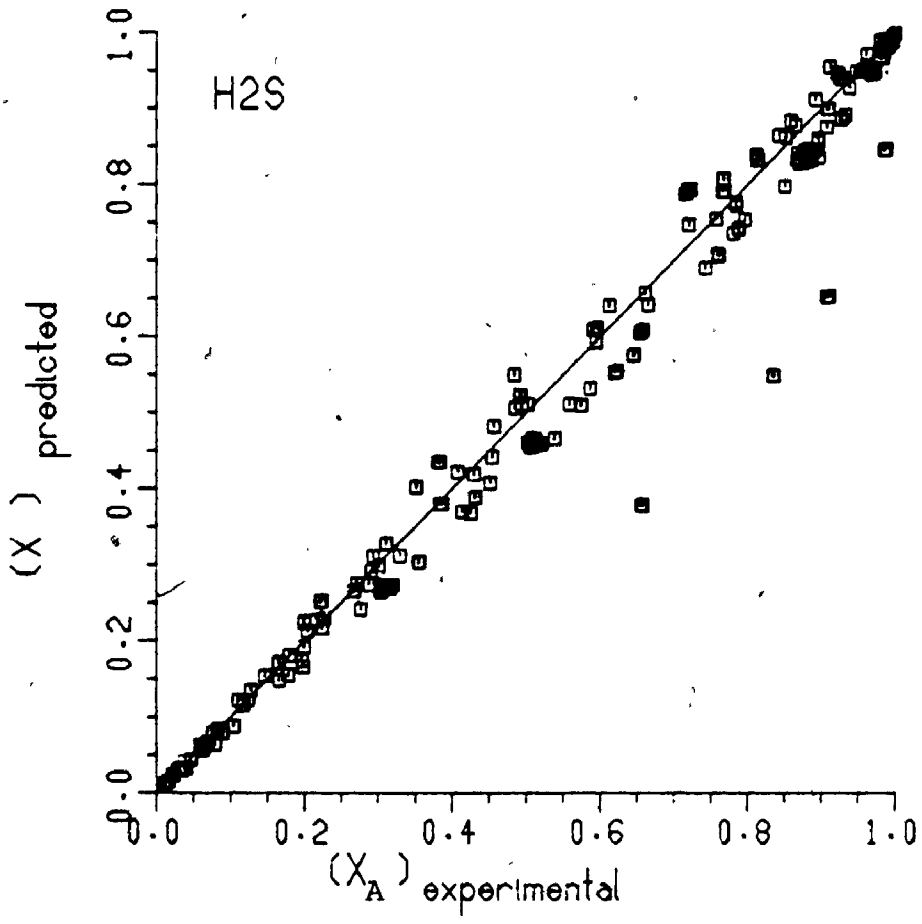

Figure 8.5: Experimental versus predicted values of the fractional conversion of hydrogen sulphide due to reaction with air.

CHAPTER 9

ENERGY YIELD AND VOLUMETRIC RATE OF THE REACTION OF METHYL MERCAPTAN AND OF HYDROGEN SULPHIDE WITH AIR IN CORONA DISCHARGE

9.1 INTRODUCTION

One basic objective of the present study was to determine the effect of the various parameters of concern on the performance of the corona reactor to oxidize low concentration methyl mercaptan and hydrogen sulphide in air. Extensive series of quantitative experiments were carried out to fulfill this objective.

For the purpose of presentation and analysis of the results, the data obtained will be expressed in terms of the variables "energy yield" and "volumetric rate".

Throughout the following discussion, the reaction of methyl mercaptan and of hydrogen sulphide with air will be referred to as reactions R1 and R2.

9.2 DEFINITIONS OF ENERGY YIELD AND VOLUMETRIC RATE

The term energy yield E_y is defined as grams of the sulphur compound (i.e., methyl mercaptan or hydrogen sulphide) oxidized per kW-hr of electrical energy dissipated

in the reactor. Accordingly,

$$E_y = \frac{Q\ C_{Ao}\ X_A\ M_w}{V_s\ I_c} \qquad (9.1)$$

This term was adopted by previous authors to describe chemical reactions in electrical discharge [159].

As may be noted, the unit kW-hr is not the S.I. unit for energy. Nevertheless, it was adopted in this chapter due to its common use in industry.

The reciprocal of the energy yield may be regarded as the consumption of energy which acts essentially as a reactant or consumable catalyst per gram of the sulphur compound oxidized.

The volumetric rate R_v, on the other hand, is defined as grams of the sulphur compound oxidized per second per cubic metre of the reactor volume [159]:

$$R_v = \frac{Q\ C_{Ao}\ X_A\ M_w}{V_R} \qquad (9.2)$$

This equation indicates that for a given set of Q, C_{Ao}, and V_R any discussion given on R_y is applicable to X_A and the opposite is also true.

In addition to being of theoretical significance [159],

energy yield and volumetric process of the operating and fixed costs in industrial applications, respectively. Values of energy yield are employed in evaluating power costs whereas volumetric rate determines the reactor size.

Both energy yield and volumetric rate are related by the relationship:

$$E_y = \frac{R_v}{p} \qquad (9.3)$$

in which p (kW/m^3) is the power density i.e., the power dissipated per unit volume of the reactor. Equation (9.3) shows that the energy yield is the slope of the line on a graph representing the relation between the volumetric rate as the ordinate and the power density as the abscissa.

A further consequence of relationship (9.3) is that variables having negligible effect on the power density will have the same effect on both the energy yield and the volumetric rate.

9.3 PARAMETERS AFFECTING THE ENERGY YIELD AND THE VOLUMETRIC RATE OF REACTIONS R1 AND R2

The parameters whose effect on E_y and R_v of reactions R1 and R2 were studied may be grouped into:

A) Parameters related to reactor electrical power:

1- Current.
2- Corona polarity: This parameter was however omitted from study following discussion based on the reason given in Section 4.5. In the present range of conditions, the corona polarity did not produce any differences in the results.

B) Parameters related to the physical dimensions of the reactor:

1- Diameter of the corona wire.
2- Height of the reactor.
3- Diameter of the reactor.

C) Parameters related to the gas conditions:

1- Initial concentration of the reactants.
2- Temperature of the reactor.
3- Mean residence time of the feed through the reactor.
4- Water vapour concentration in the feed to the reactor.

A discussion on the effect of each on the E_y and R_v of the reaction of methyl mercaptan and of hydrogen sulphide with air will now follow. Unless otherwise stated, the reactor dimensions are:

Reactor dimeter	$= 2.54 \times 10^{-2}$ m
Reactor height	$= 1.524 \times 10^{-1}$ m
Wire diameter	$= 3.05 \times 10^{-5}$ m

and the operating conditions are:

Temperature	= 423 K
Current	= 0.3 mA

Mean residence time = 10 s

Initial concentration of the sulphur reactant = 0.025 gmol/m^3

The above values of temperature, mean residence time, and the initial concentration of the sulphur reactant and of water vapour in the feed represent the average values of these parameters in a typical kraft mill (see Section 1.5).

A) PARAMETERS RELATED TO THE REACTOR ELECTRICAL POWER

9.4 THE EFFECT OF CURRENT ON E_y AND R_v OF REACTION R1 AND R2

As discussed in Section (6.3), only a part of the total power (i.e., the useful power) is utilized in the production of the excited oxygen species responsible for the oxidation of the sulphur compounds.

In accordance with the Townsend theory, we have seen that the useful power P_u is given by:

$$P_u = \bar{E}\ \Delta a\ I_c \qquad (9.4)$$

As $\bar{E}$ and Δa are both constants for the same corona system, the useful power may be directly expressed in terms of current, any discussion concerning one is accordingly applicable to the other. It should be noted that current in

the following discussion is only important for theoretical considerations. For practical purposes however, the total power dissipated in the reactor is more important.

The effect of current on the volumetric rate of reactions R1 and R2 is shown in Figures 9.1a and 9.2a, respectively. As indicated, an increase in current always results in an increase in the volumetric rate of methyl mercaptan and hydrogen sulphide. Referring to equation (9.2), these results are obtained since the increase of current causes the conversion of the sulphur reactants to increase as shown previously.

The effect of current on the energy yield of reactions R1 and R2 is illustrated in Figures 9.1b and 9.2b, respectively. They indicate that an inverse relationship between energy yield and current exists. These results appear in general agreement with those obtained by Thornton in his study on the decomposition of ammonia in a corona discharge which produced hydrazin [160]. Thornton speculated that hydrazin was produced following the discharge through a complex reaction and subsequently decomposed by electron bombardment whose rate increased with increase in current. However, a different explanation may be given to explain the present results. It is apparent from equation (9.1) that the increase in fractional conversion caused by the increase in current is less than

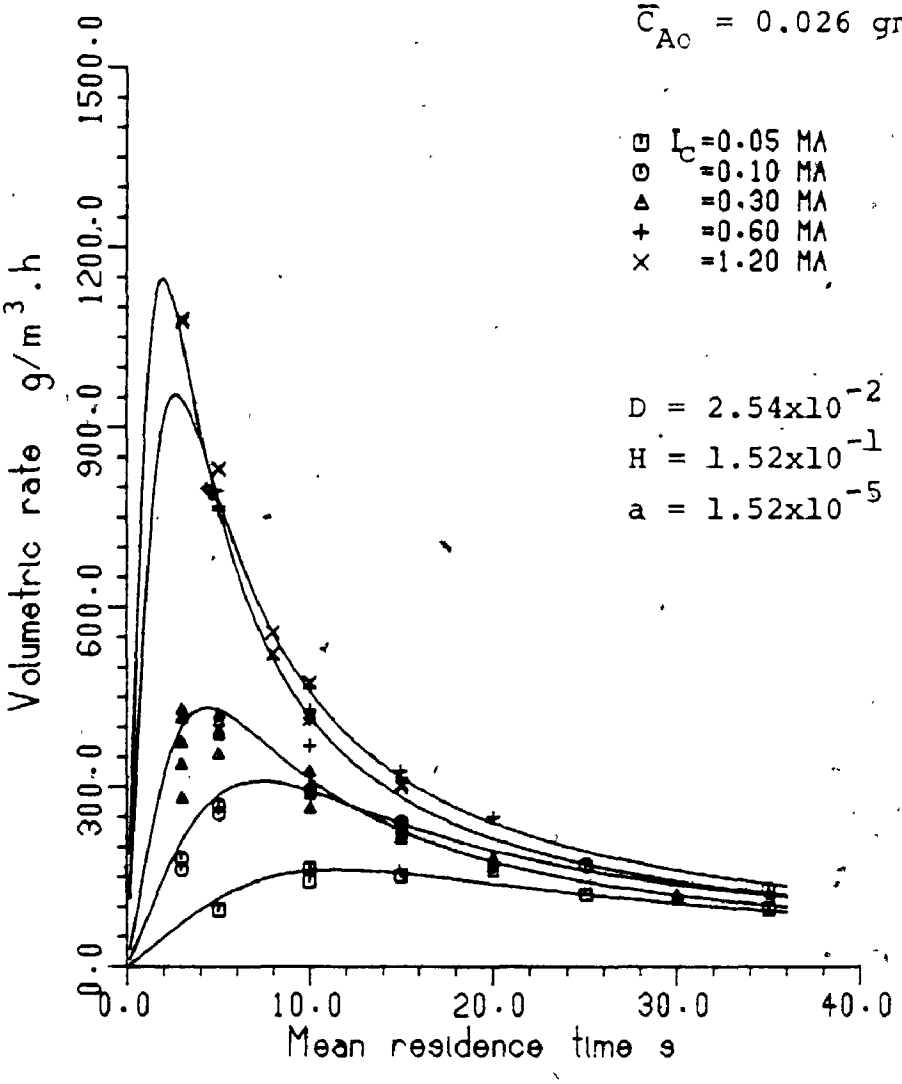

Figure 9.1a: Time-dependency of the volumetric rate of the reaction of methyl mercaptan with air

Reactor dimensions: D = 2.54x10^{-2} m
H = 1.52x10^{-1} m
a = 1.52x10^{-5} m

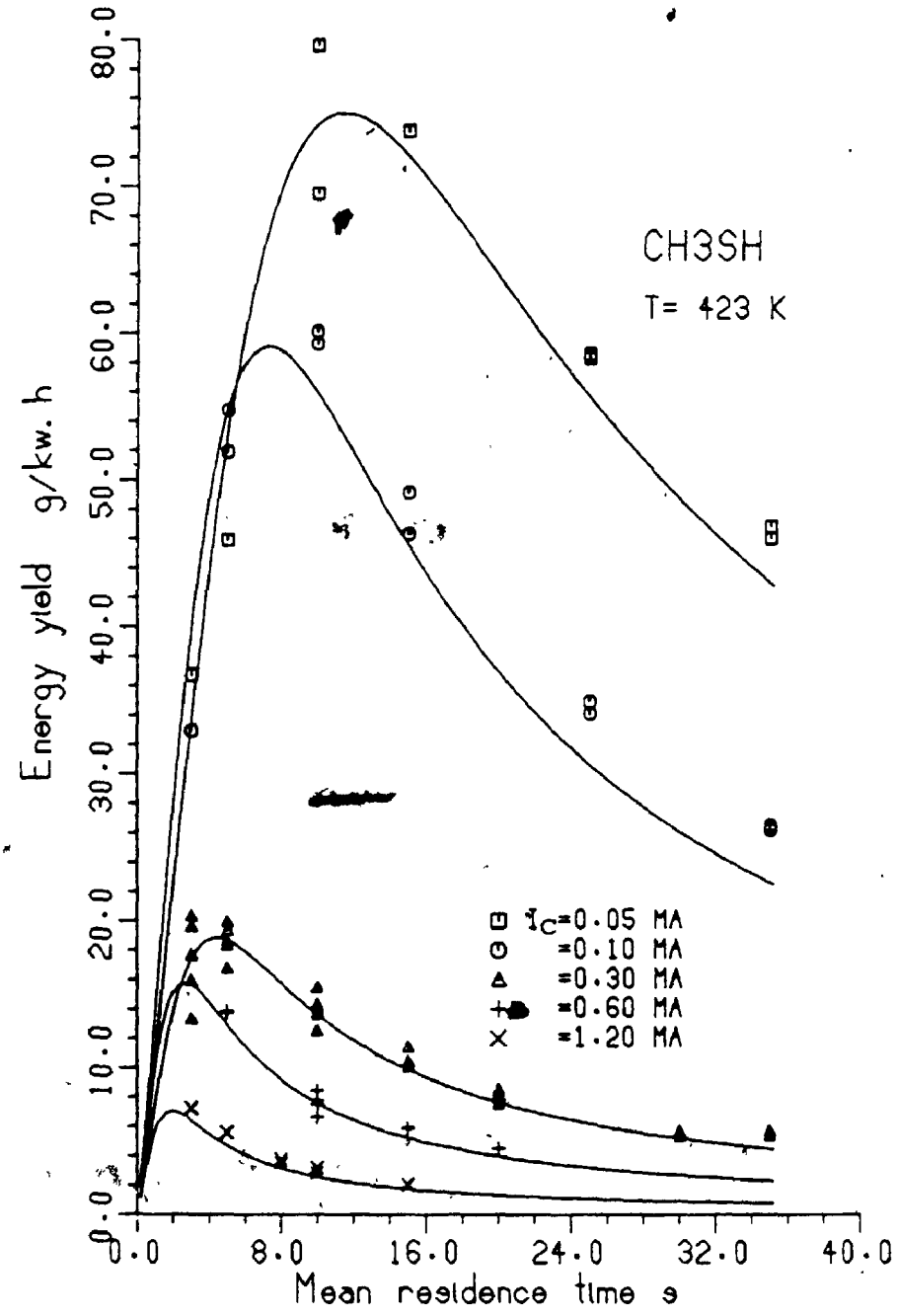

Figure 9.1b: Time-dependency of the energy yield of the reaction of methyl mercaptan with air,

Reactor dimensions: D = 2.54×10^{-2} m
H = 1.52×10^{-1} m
a = 1.52×10^{-5} m

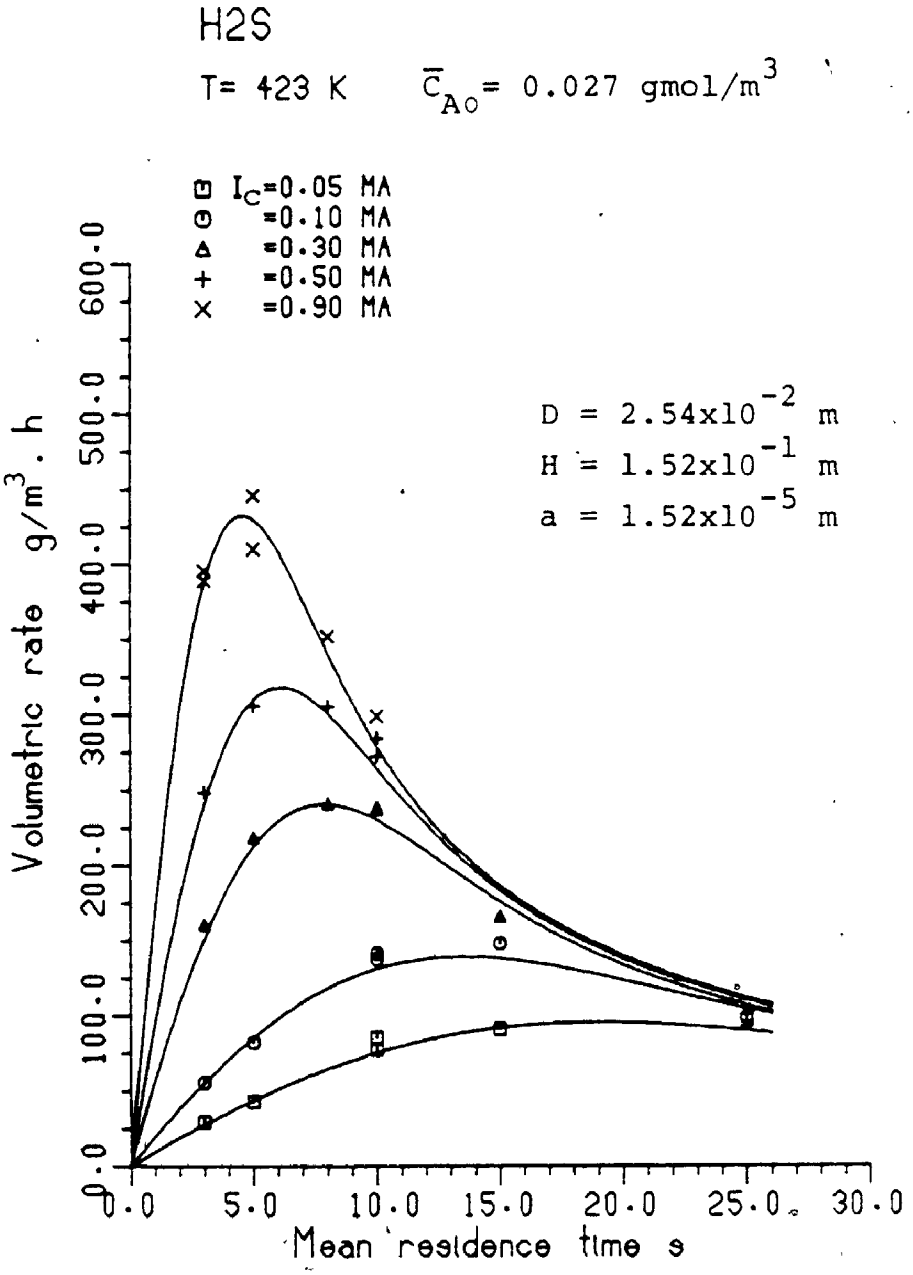

Figure 9.2a: Time-dependency of the volumetric rate of the reaction of hydrogen sulphide with air.

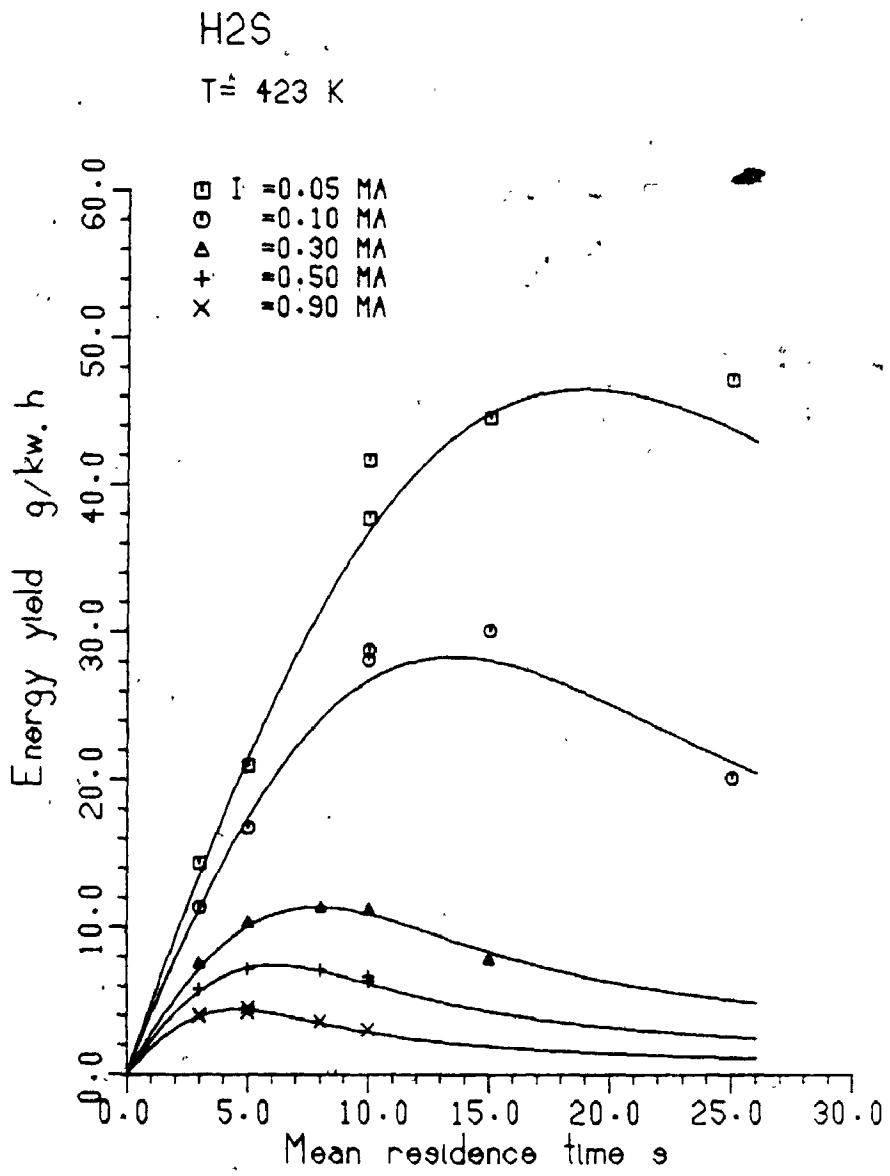

Figure 9.2b: Time-dependency of the energy yield of the reaction of hydrogen sulphide with air.

the increase in power dissipitated in the reactor (given by the product of I_c and V_s). This may be further discussed by considering the efficiency of the discharge which may be defined according to the present author by:

$$\eta = \frac{\text{Power dissipated in the discharge zone}}{\text{Total power dissipated in the reactor}}$$

$$= \frac{\bar{E}\ \Delta a\ I_c}{V_s\ I_c} \qquad (9.5)$$

$$= \frac{\bar{E}\ \Delta a}{V_s} \qquad (9.6)$$

Even though the efficiency as defined above seems not to depend on the current I_c, these two parameters are inversely related. This is due to the direct relationship between the latter and the applied voltage V_s at otherwise constant wire diameter. Therefore, as the above results show, the efficiency of the discharge decreases with increase in the current.

Finally, the results suggest that there exists an optimum value of current at which both energy yield and volumetric rate are maxima. These findings exemplified in Figures 9.3 and 9.4 should be considered in any cost evaluation of the corona reactor.

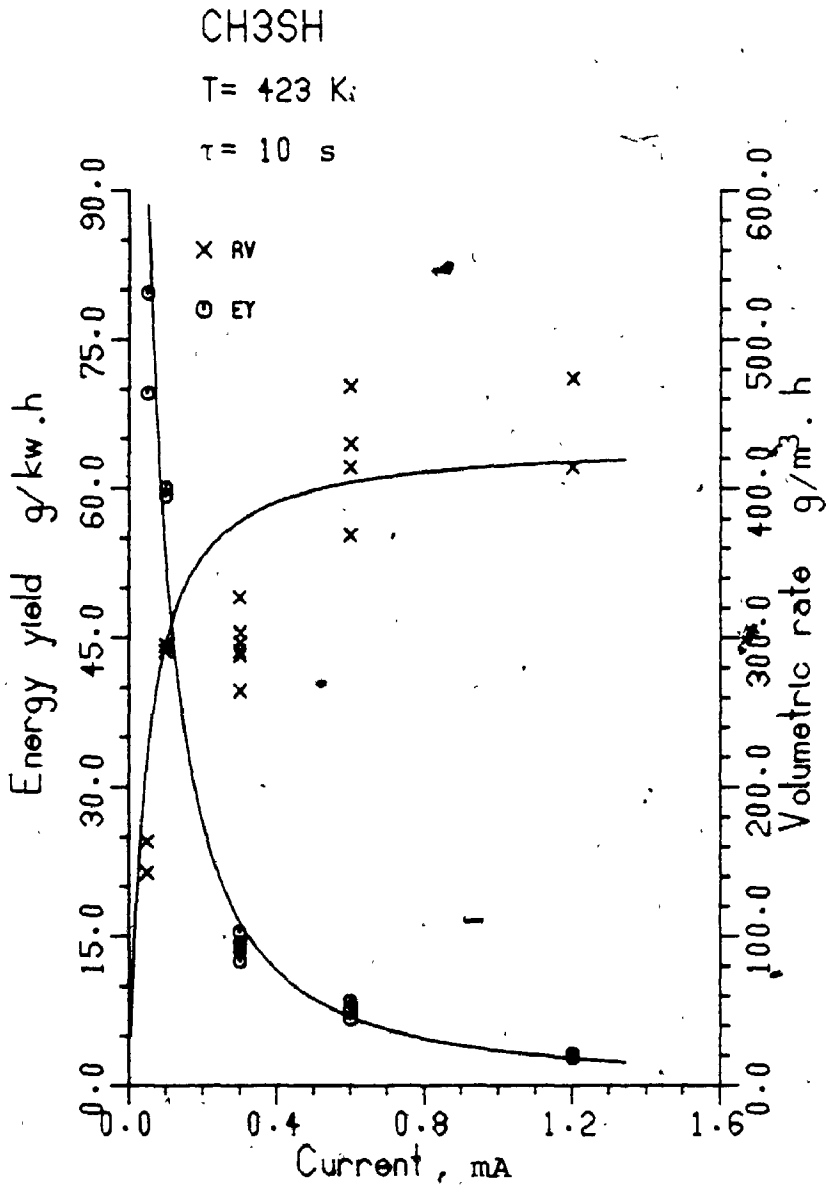

Figure 9.3: The effect of current on E_v and R_v of the reaction of methyl mercaptan with air.

Reactor dimensions: $D = 2.54 \times 10^{-2}$ m
$H = 1.52 \times 10^{-1}$ m
$a = 1.52 \times 10^{-5}$ m

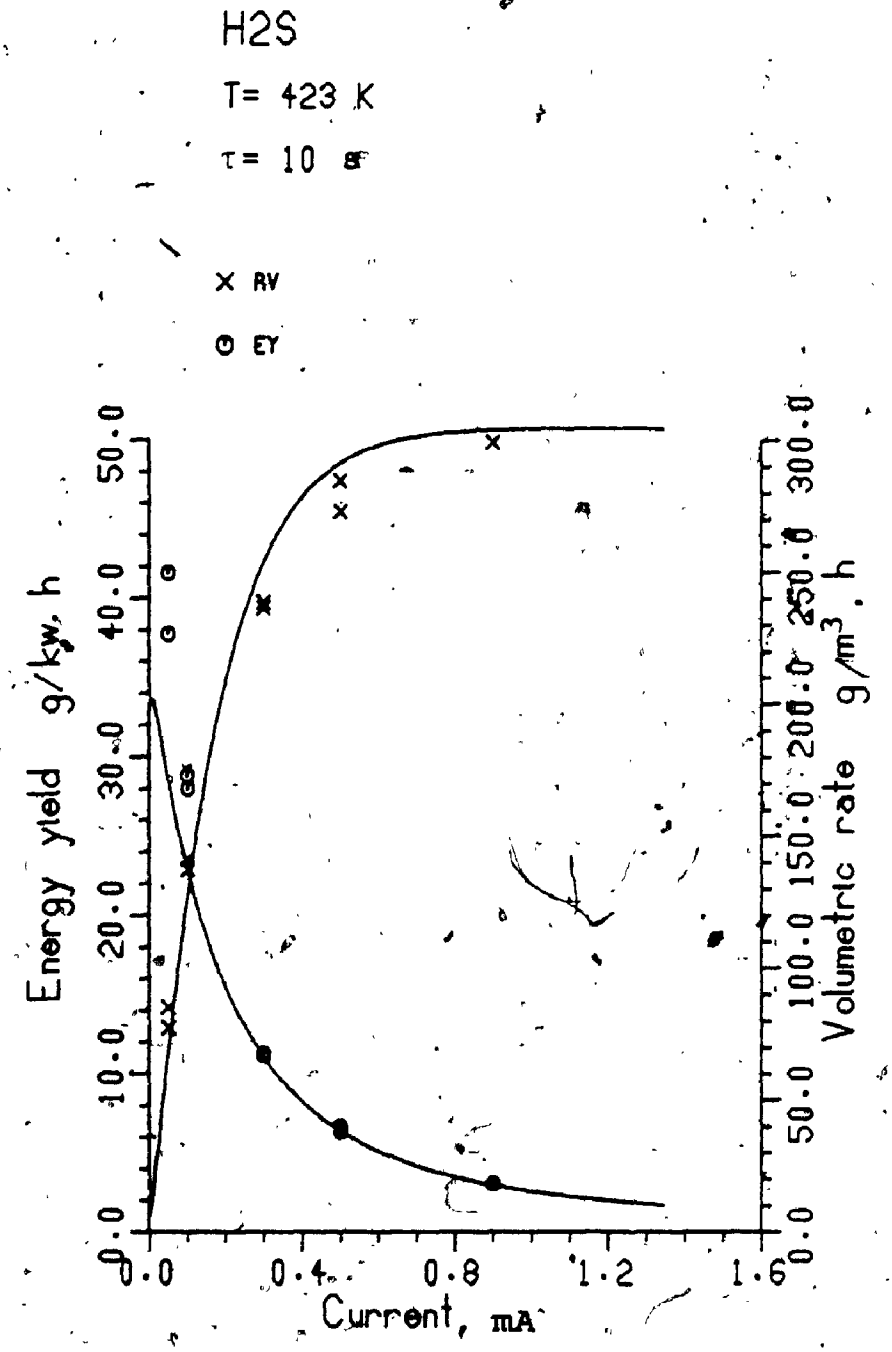

Figure 9.4: The effect of current on E_y and R_v of the reaction of hydrogen sulphide with air

Reactor dimensions: D = 2.54×10^{-2} m
H = 1.52×10^{-1} m
a = 1.52×10^{-5} m

B) PARAMETRS RELATED TO THE REACTOR DIMENSIONS

9.5 THE EFFECT OF WIRE DIAMETER ON E_y AND R_v OF REACTIONS R1 AND R2

The study of this section was initiated because both the corona onset-voltage and the diameter of the ionized sheath are direct functions of the diameter of the corona wire.

In addition to the above wire diameter of 3.054×10^{-5} m three other wire diameters were also tried: 2.45×10^{-5}, 2.79×10^{-5}, and 3.57×10^{-5} m. The experimental procedure used was explained in Section 4.6 and the results obtained are given next.

The effect of the corona wire diameter on the voltage-current characteristics is summarized in Table 9.1. As indicated, the change in the wire diameter did not produce any substantial differences in the applied voltage to obtain the same values of current. Such results may be attributed to the limited range within which the wire diameter was varied since the applied voltage for the same values of current is directly related to the wire diameter (see Section 3.4).

The effect of the wire diameter on the volumetric rate of reactions R1 and R2 is summarized in Figures 9.5 and

TABLE 9.1: THE EFFECT OF WIRE DIAMETER ON THE CURRENT-VOLTAGE CHARACTERISTICS*

Wire diameter $mx10^5$	Current mA	Voltage kV
2.45	0.3	5.33±0.02
2.79	"	5.35±0.01
3.05	"	5.50±0.02
3.57	"	5.58±0.01

* OTHER EXPERIMENTL CONDITIONS ARE:

Temperature	=423	K
Mean residense time	= 10	s
Reactor diameter	= $2.54x10^{-2}$	m
Reactor height	=$15.24x10^{-1}$	m
Average initial concentration of the sulphur reactant	=$25.0x10^{-6}$	$kmol/m^3$

9.6 , respectively. The results indicate that a change in the wire diameter does not produce any significant change in the volumetric rate of reactions R1 and R2. The differences shown are in fact within the experimental errors. In addition to the limited range of the wire dimameter variation as mentioned above, a reason for these results may be as follows: an increase in the wire diameter would reduce the corona-onset field intensity but increase the outer diameter of the ionized sheath. In reference to equation (9.4), it appears that these two effects would cancel one another so that the power dissipated in the ionized sheath remains constant. As a result, the concentration of the excited oxygen molecules, which affects the conversion of the sulphur compounds and their volumetric rates, would also remain constant. This explanation may become clear by referring to Figure 6.7 from which we see that as the corona-onset field intensity is reduced the mean energy of electrons would increase but in very small amounts. For instance, a change in wire diameter from 2.54×10^{-5} to 3.57×10^{-5} m (which were the two extreme values of the wire diameter used in the present case) would increase the electron mean energy only by about 5%. Figure 6.8 indicates that this increase practically has no effect on the concentration of the excited oxygen species and on the conversion of the sulphur reactants. As indicated above, these results may however be only valid to the range of the experimental conditions used.

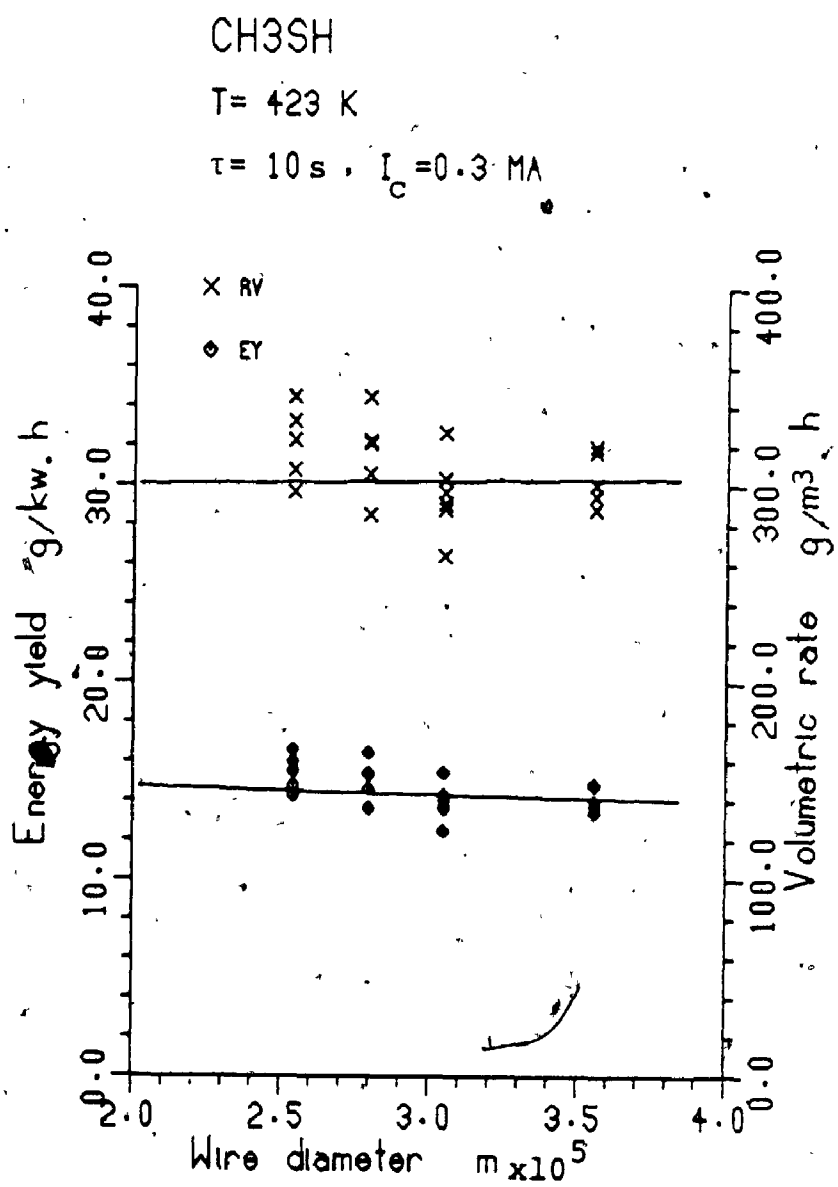

Figure 9.5: The effect of wire diameter on E_V and R_V of the reaction of methyl mercaptan with air;

Reactor dimensions: $D = 2.54 \times 10^{-2}$ m
$H = 1.52 \times 10^{-1}$ m

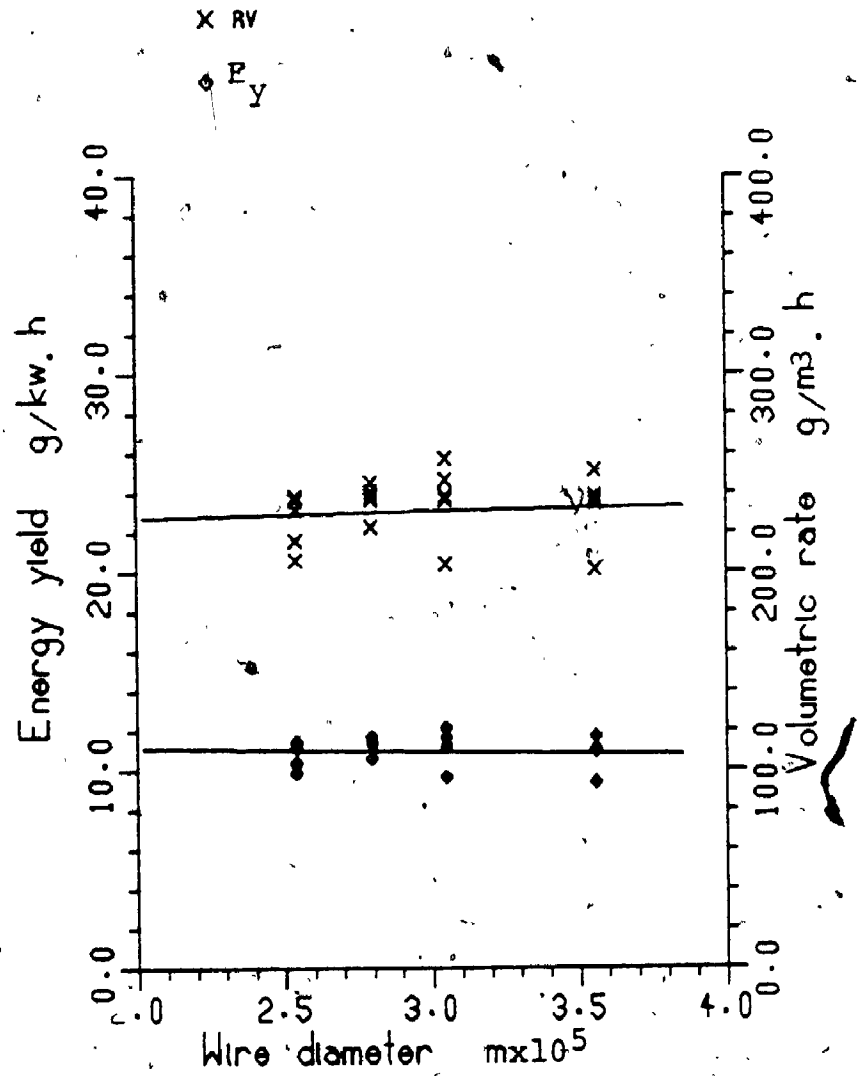

Figure 9.6: The effect of wire diameter on E_y and R_v of the reaction of hydrogen sulphide with air;

Reactor dimensions: D = 2.54×10^{-2} m
H = 1.52×10^{-5} m

The energy yield of reactions R1 and R2 as a function of the wire diameter is given in Figures 9.5 and 9.6 , respectively. Similarily to the volumetric rate, the energy yield is not affected by the change in the wire diameter. However, theoretical calculations based on the results obtained (shown by the solid lines in the figures) indicate a slight decrease in the energy yield as the wire diameter increases. This can be explained by the fact that an increase in the wire diameter results in a corresponding increase in the applied voltage. From equation (9.1) this increase would reduce the energy yield.

9.6 THE EFFECT OF REACTOR LENGTH ON E_y AND R_v OF REACTIONS R1 AND R2

The effect of the reactor length on the results was investigated due to its direct effect on the voltage-current characteristics as indicated by equations (3.5) and (3.6).

In addition to the reactor height of 152.4 mm employed in the above experiments, three other height values: 76.2, 228.6, and 304.8 mm were used. This was done by replacing the above stainless steel gauze each time by another having the respective length. During this set of experiments, the mean residence time of feed was kept constant at 10 s by adjusting the feed flow rate into the reactor. The experimental procedure is otherwise the same as described previously and the results obtained are given in Figures 9.7

and 9.8 for reactions R1 and R2, respectively. Moreover, the values of the applied voltage obtained for the same current value of 0.3mA but for the various reactor lengths are listed in Table 9.2.

Table 9.2 indicates that, within experimental error, a longer reactor always requires a lower applied voltage for the same value of current. These results are expected due to the direct relationship between the reactor height and the applied voltage (see Section 3.4).

Figures 9.7 and 9.8 indicate that the volumetric rate of reactions R1 and R2 decreases with increase in reactor length. An explanation for these results may be offered in reference to equation (9.2) which may be re-written as:

$$R_V = \frac{C_{AO} M_w X_A}{\tau} \qquad (9.7)$$

The fractional conversion X_A is directly related to the concentration of the excited moecules of oxygen (equation (6.9)) which is in turn inversely related to the flow rate of air through the reactor (equation (7.7)). Since for a given value of mean residence time a longer reactor always requires a higher flow rate X_A and R_V will have to decrease.

This explanation was further put to test by manipulating the current so that the ratio I_c/Q, which

TABLE 9.2 THE EFFECT OF REACTOR length on THE CURRENT-VOLTAGE CHARACTERISTICS*

Reactor neignt $mx10^2$	Current mA	Voltage kV
7.62	0.3	7.09±0.01
15.24	"	5.50±0.02
22.86	"	4.76±0.02
30.48	"	4.24±0.01

* OTHER EXPERIMENTL CONDITIONS ARE:

Temperature	=423	K
Mean residense time	= 10^{-2}	s
Reactor diameter	= $2.54x10^{-5}$	m
Wire diameter	= $3.05x10^{-}$	m
Average initial concentration of the sulpnur reactant	=$25.0x10^{-6}$	$kmol/m^3$

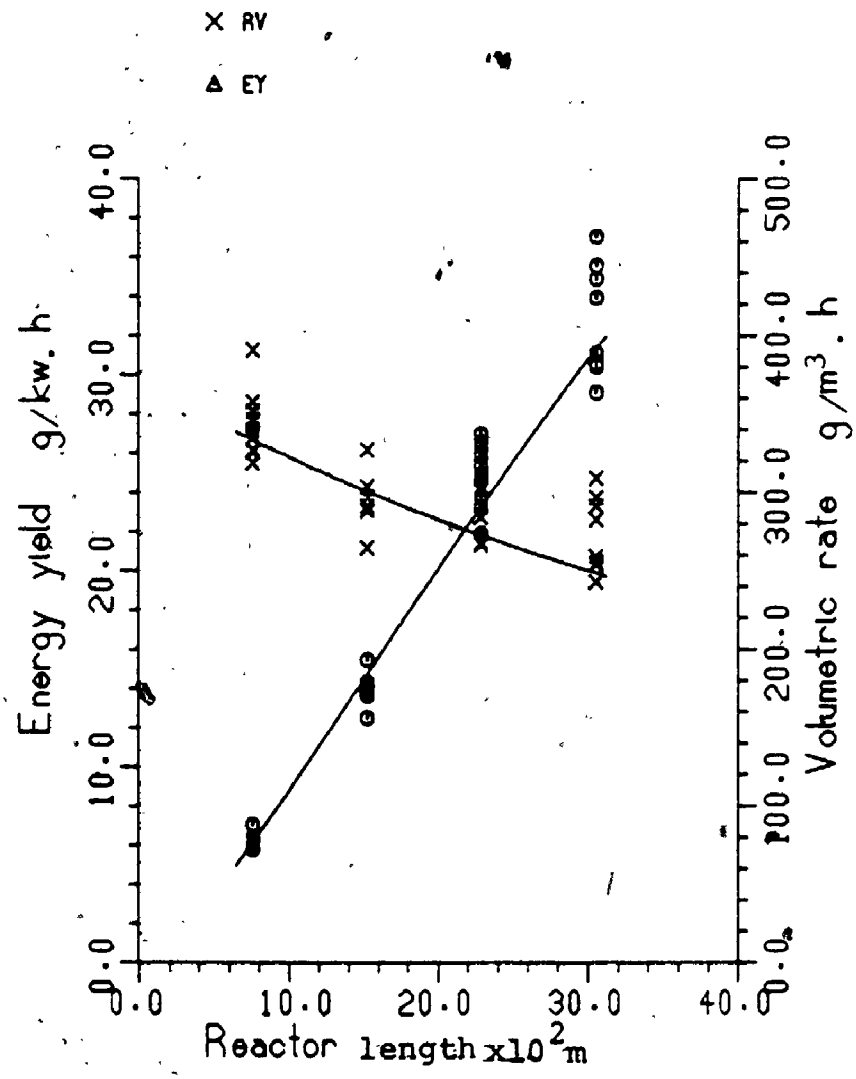

Figure 9.7: The effect of reactor length on E_y and R_v of the reaction of methyl mercaptan with air

Reactor diameter = 2.54×10^{-2} m
Wire diameter = 3.05×10^{-5} m

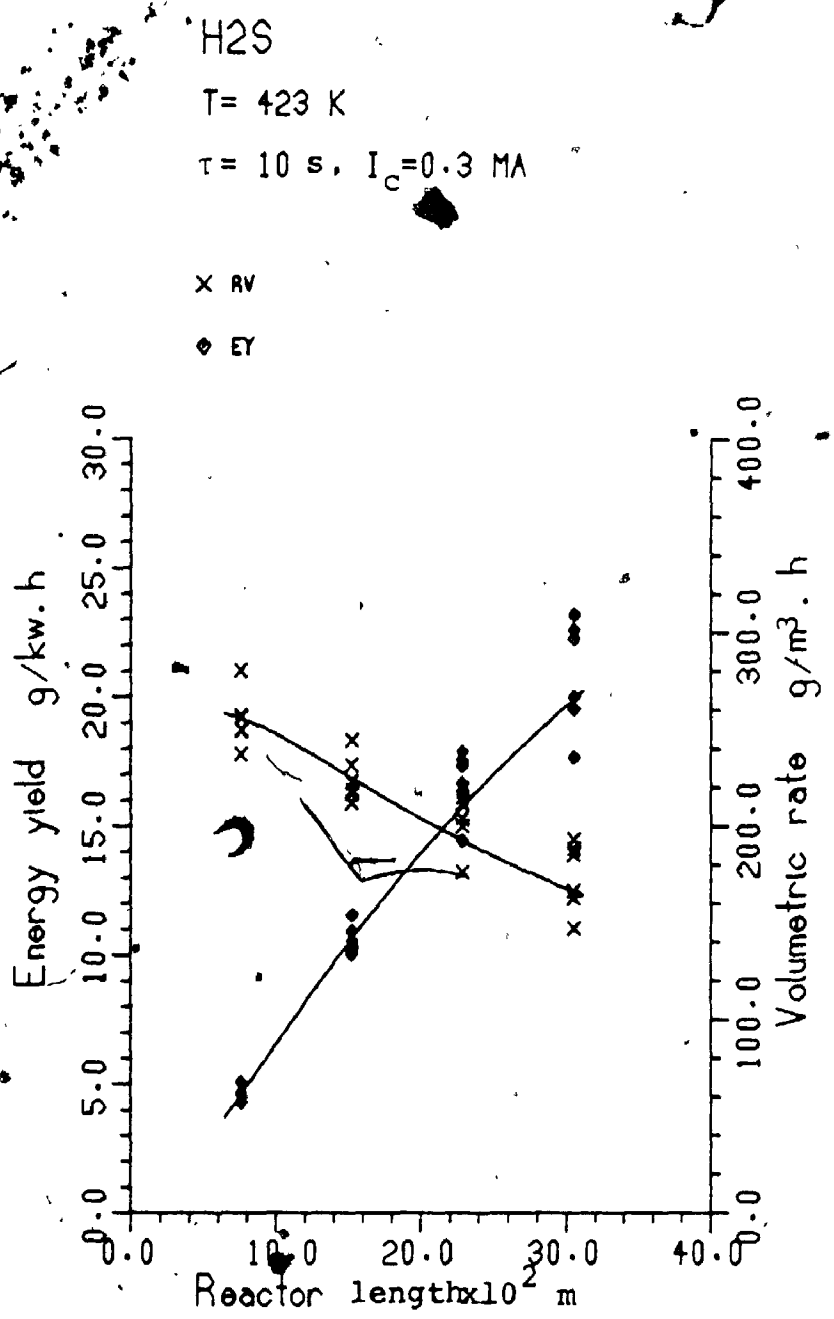

Figure 9.8: The effect of reactor length on E_y and R_v the reaction of hydrogen sulphide with air

Reactor diameter = 2.54×10^{-2} m
Wire diameter = 3.05×10^{-5} m

influences the concentration of the excited oxygen species, remained constant (equation (6.9)). This was done by increasing the current by the same ratio as that of the reactor length. The results shown in Figures 9.9 and 9.10 illustrate as expected that varying the reactor length does not produce any difference in the volumetric rate of the reaction.

Figures 9.7 and 9.8 also indicate on the other hand a proportional relationship between reactor length and the energy yield of reactions R1 and R2. As seen from equation (9.1), an increase in reactor length affects the energy yield of the reaction in three ways: i) decreasing the fractional conversion of the respective reactant, ii) increasing the applied voltage so that the current was kept constant, and finallly iii) increasing the flow rate of the feed so that the mean residence time remained unchanged. Apparently, the combined effect of these three variables is such that the increase in reactor length causes the energy yield of the reactions to increase as described above.

Furthermore, for constant value of the quotient I_c/Q of 38.86 $A/m^3/s$, for instance, Figures 9.9 and 9.10 show that, within experimental error, the energy yield of reactions R1 and R2 is independent of the reactor length. The reason for these results is that all the quantities included in equation (9.1) remain eventually constant as discussed

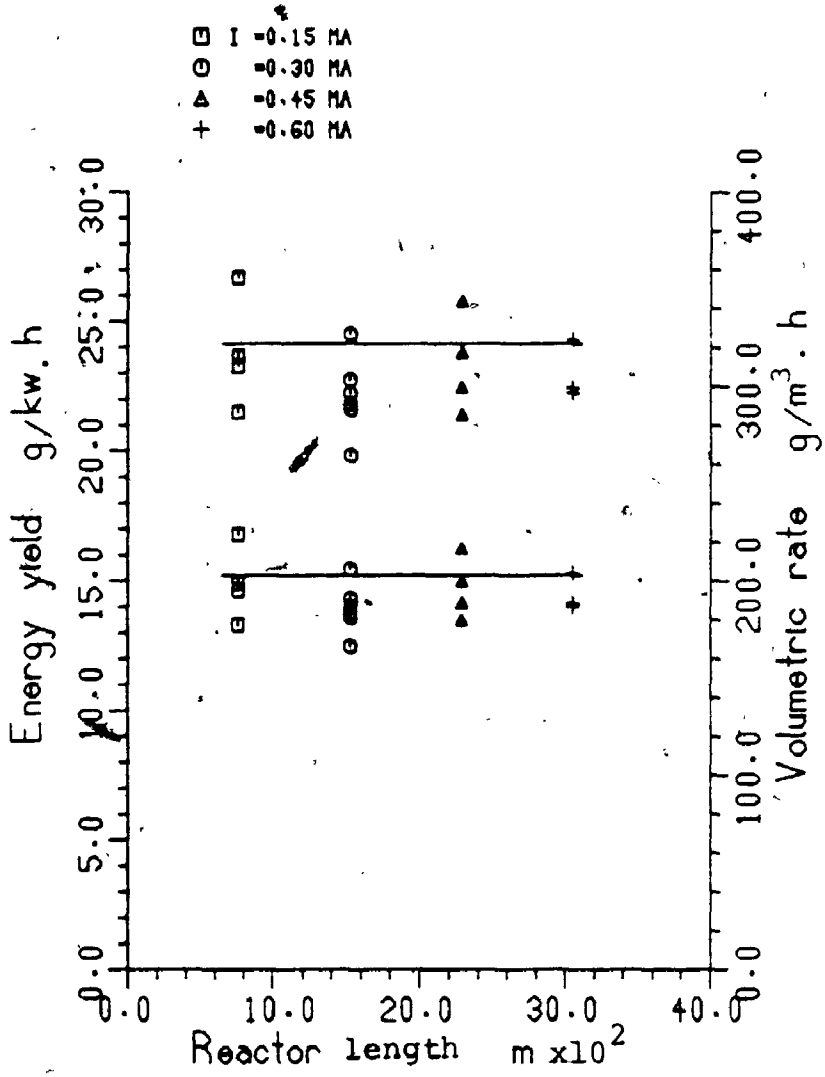

Figure 9.9: The relation between the reactor length and the energy yield of the reaction of methyl mercaptan with air at I_c/Q of 38.86 $A/m^3/s$

Reactor diameter = 2.54×10^{-2} m
Wire diameter = 3.05×10^{-5} m

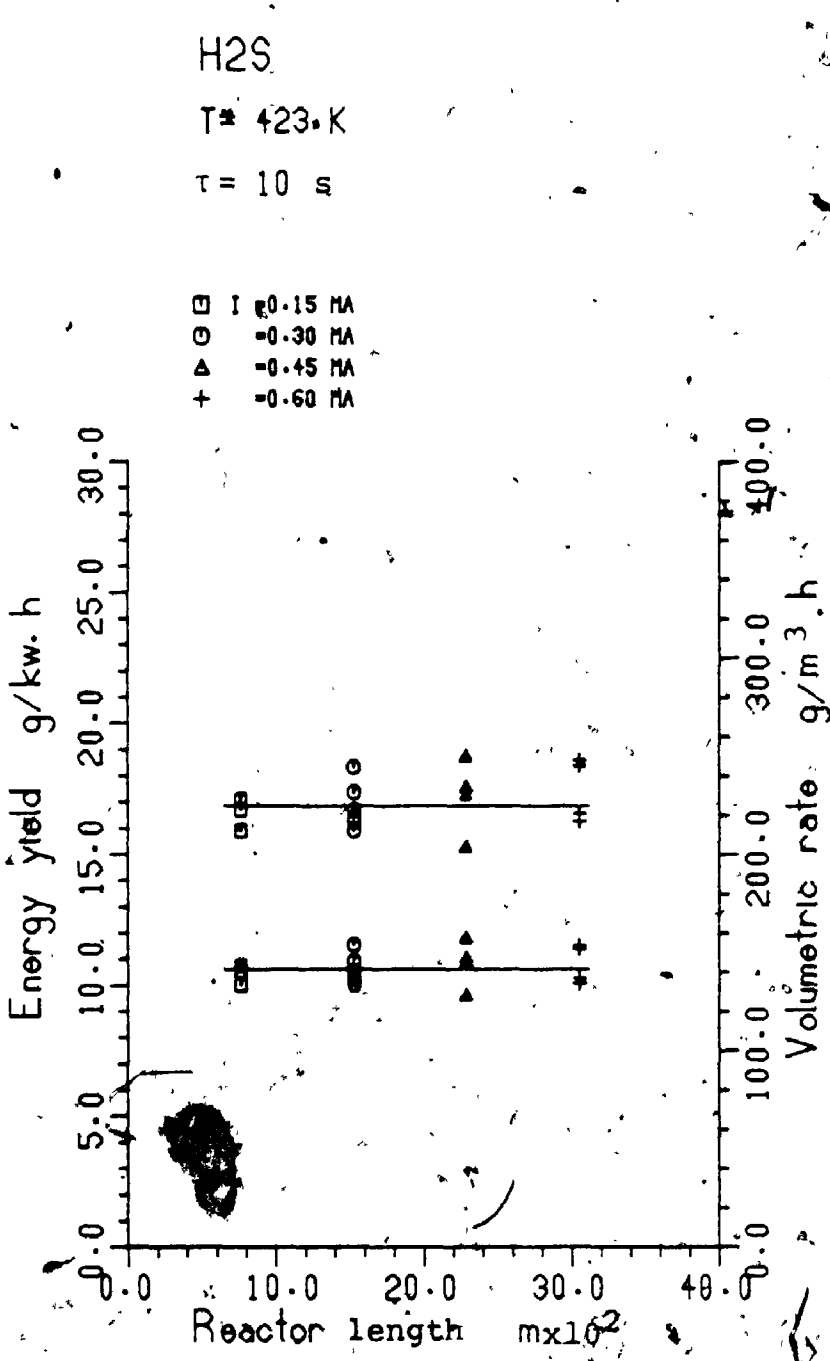

Figure 9.10: The relation between the reactor length and the energy yield of the reaction of hydrogen sulphide with air at I_c/Q of 38.86 $A/m^3/s$

Reactor diameter = 2.54×10^{-2} m
Wire diameter = 3.05×10^{-5} m

4

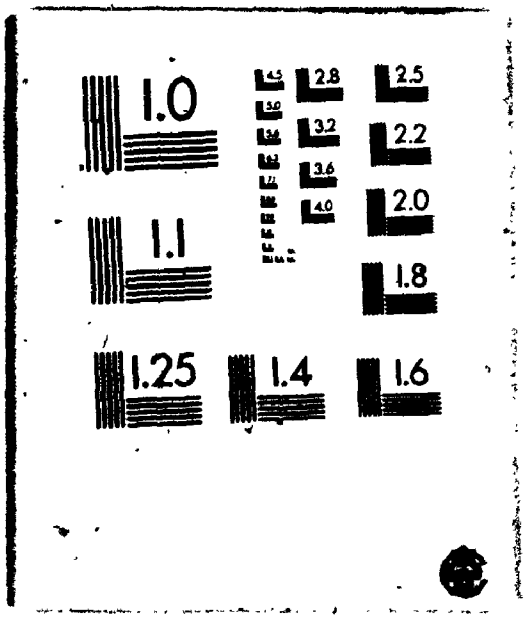

above.

9.7 THE EFFECT OF REACTOR DIAMETER ON E_y AND R_v OF REACTIONS R1 AND R2

The effect of the reactor diameter on E_y and R_v of reactions R1 and R2 was studied due it's direct effect on the voltage-current characteristics as demonstrated by equation (3.3). Furthermore, such a study would allow us to examine the effects of the scale-up factor on the results in general, an essential factor in the decision-making process to put a lab-scale study into a full-scale operation.

Experiments were attempted to carry out reactions R1 and R2 using a larger reactor having an inside diameter of 5.08×10^{-5} m i.e., double the diameter of the above reactor which will be referred to as the small reactor in the following discussion.

In order to keep the mean residence time constant, the flow rate of the feed through the larger reactor was four times that through the small reactor. The experimental procedure otherwise was the same as previously described in Section 4.3.1. The results obtained along with those previously reported using the small reactor at similar operating conditions are summarized in Figures 9.11a to 9.12b. Moreover, the values of the applied voltage and current used in this section are given in Table 9.3.

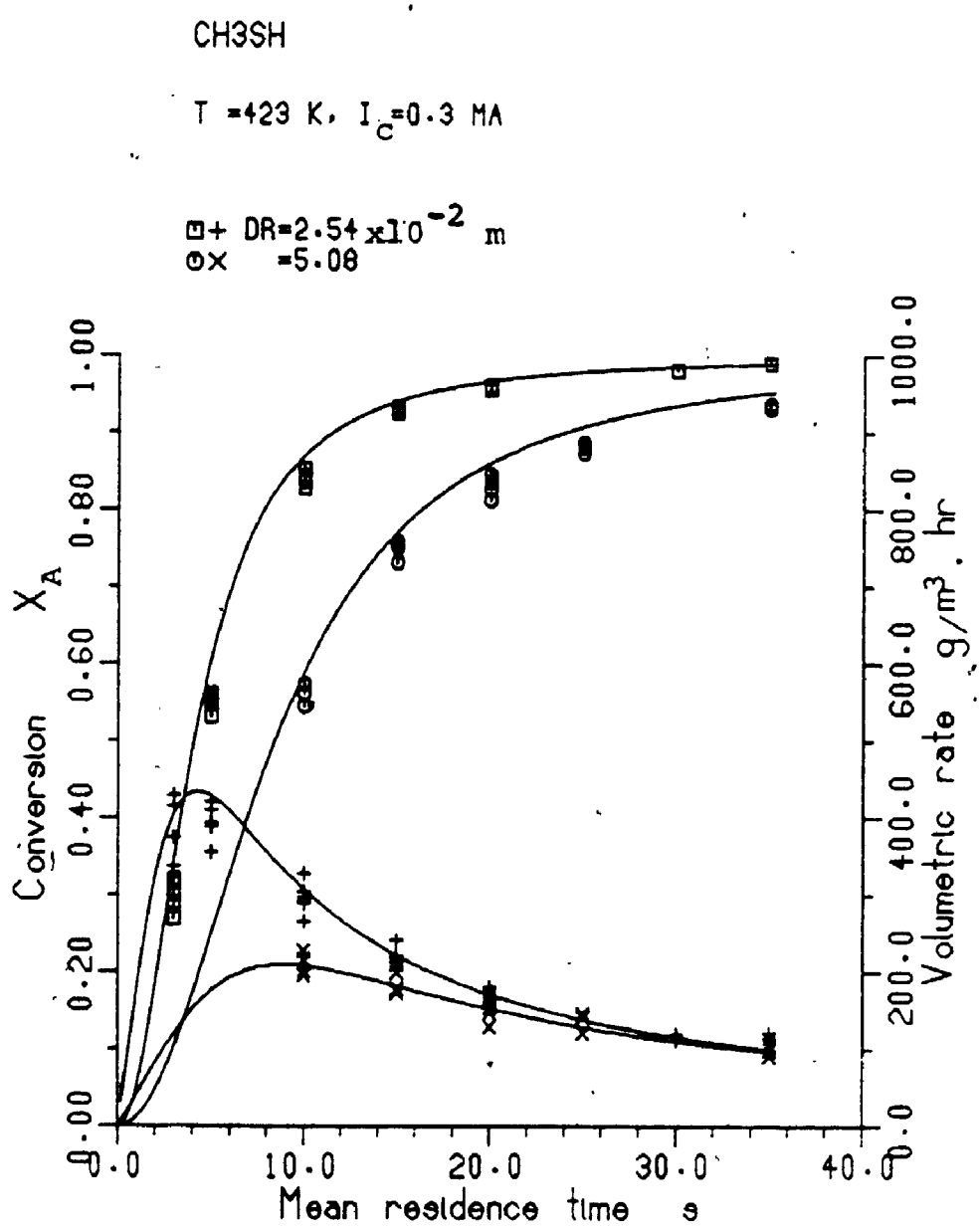

Figure 9.11a: The dependency of X_A and R_v of the reaction of methyl mercaptan with air on the reactor diameter

Reactor height = 1.52x10^{-1} m
Wire diameter = 3.05x10^{-5} m

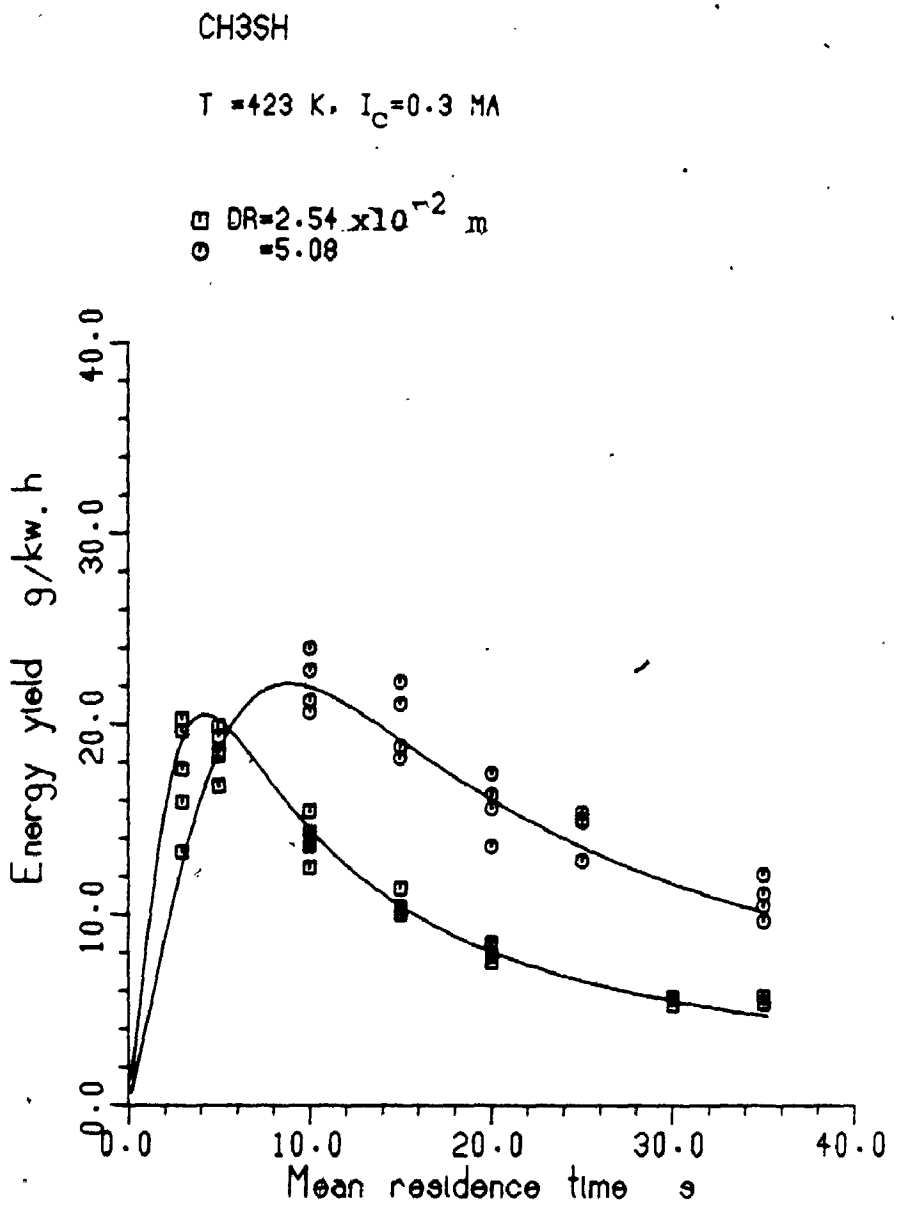

Figure 9.11b: The dependency of E_y of the reaction of methyl mercaptan with air on the reactor diameter.

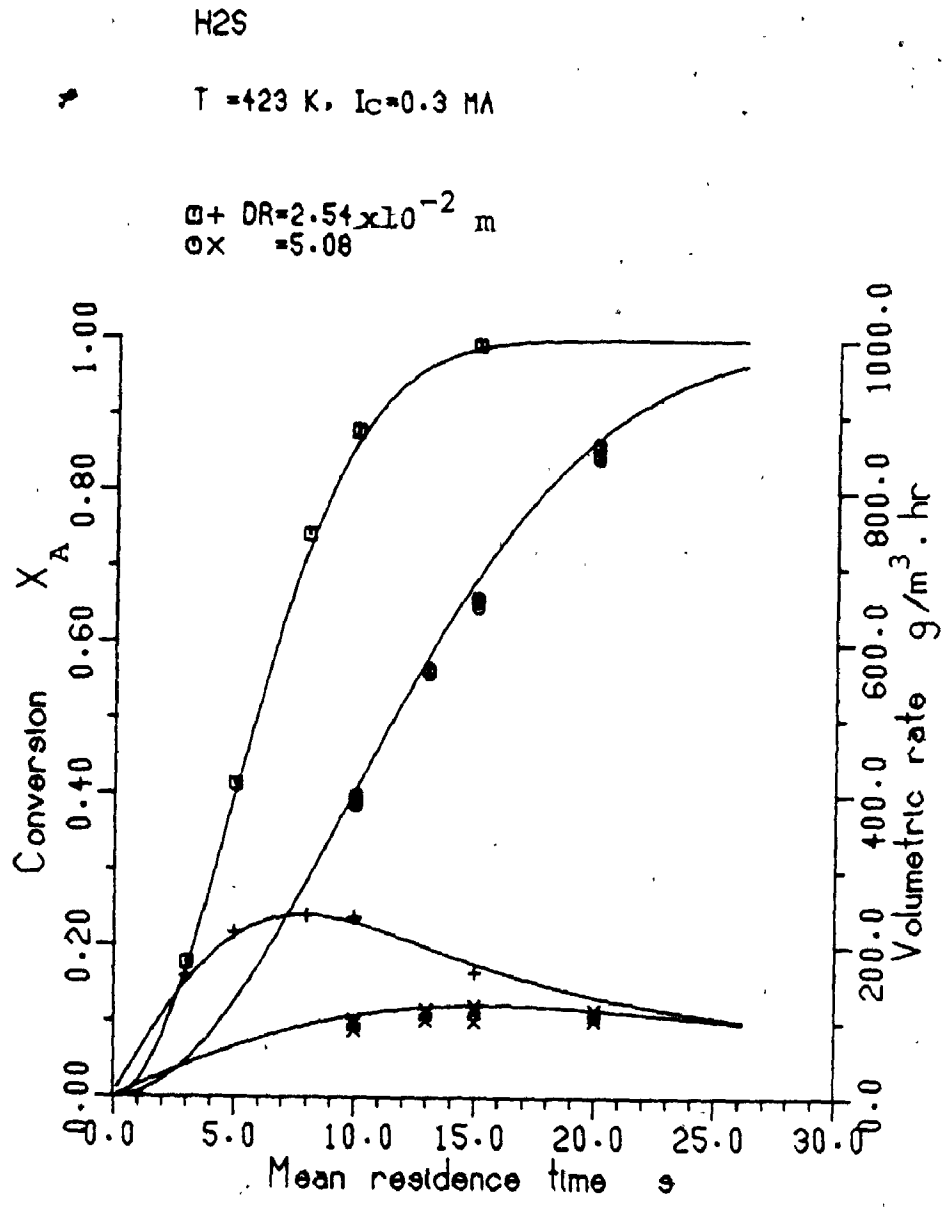

Figure 9.12a: The dependency of X_A and R_V of the reaction of hydrogen sulphide with air on the reactor diameter

Reactor height = 1.52×10^{-1} m
Wire diameter = 3.05×10^{-5} m

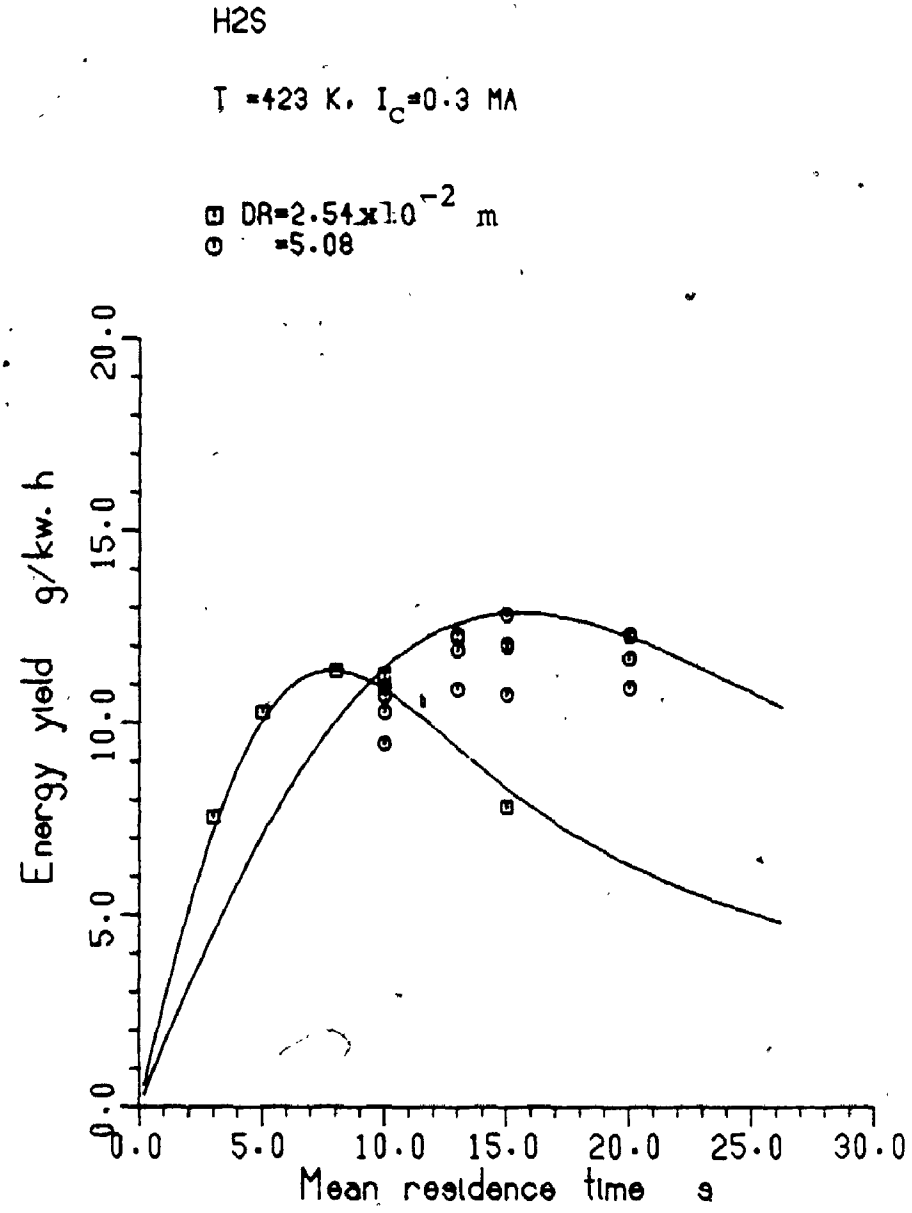

Figure 9.12b: The dependency of E_y of the reaction of hydrogen sulphide with air on the reactor diameter.

TABLE 9.3 THE EFFECT OF REACTOR DIAMETER ON THE CURRENT-VOLTAGE CHARACTERISTICS*

Reactor diameter $mx10^2$	Current mA	Voltage kV
2.54	0.05	3.12±0.03
5.08	"	5.34±0.02
2.54	0.30	5.50±0.02
5.08	"	9.69±0.04

* OTHER EXPERIMENTL CONDITIONS ARE:

Temperature	=423	K
Mean residense time	= 10	s
Reactor height	$=15.24x10^{-2}$	m
Wire diameter	$= 3.05x10^{-5}$	m
Average initial concentration of the sulphur reactant	$=25.0x10^{-6}$	$kmol/m^3$

Table 9.3 shows that, for the same value of current, the applied voltage to the large reactor is higher than that to the small reactor. These results are mainly attributed to i) the increase in the quantity Φ of equation (3.6) with the increase in the reactor diameter and to ii) the increase in the onset-corona voltage V_c (see equation (3.4)). In accordance with equation (3.5), the increase in these two quantities would increase the applied voltage.

As shown by Figures 9.11a and 9.12a, there is an inverse relationship between the fractional conversion and the reactor diameter. The existence of this relation inspite of the increase in the power dissipated with increase in the reactor diameter (see Table 9.3) can be explained in terms of the concentration of the excited oxygen molecules. As in the discussion of Section 9.6 above, the concentration of these species decreases with the increase in flow rate. This is followed by the decrease in the fractional conversion of the sulphur reactants and the volumetric rate of the respective reaction. Thus, for a given mean residence time, the large reactor produces excited oxygen at lower concentrations. This argument was further verified by carrying a set of experiments during which the ratio I_c/Q was kept constant at, for example, 38.86 $A/m^3/s$. (In this case, the current had to be raised to 1.2 mA by increasing the applied voltage to about 12.6 kV.) The results shown in Figures 9.13 and 9.14 illustrate that under

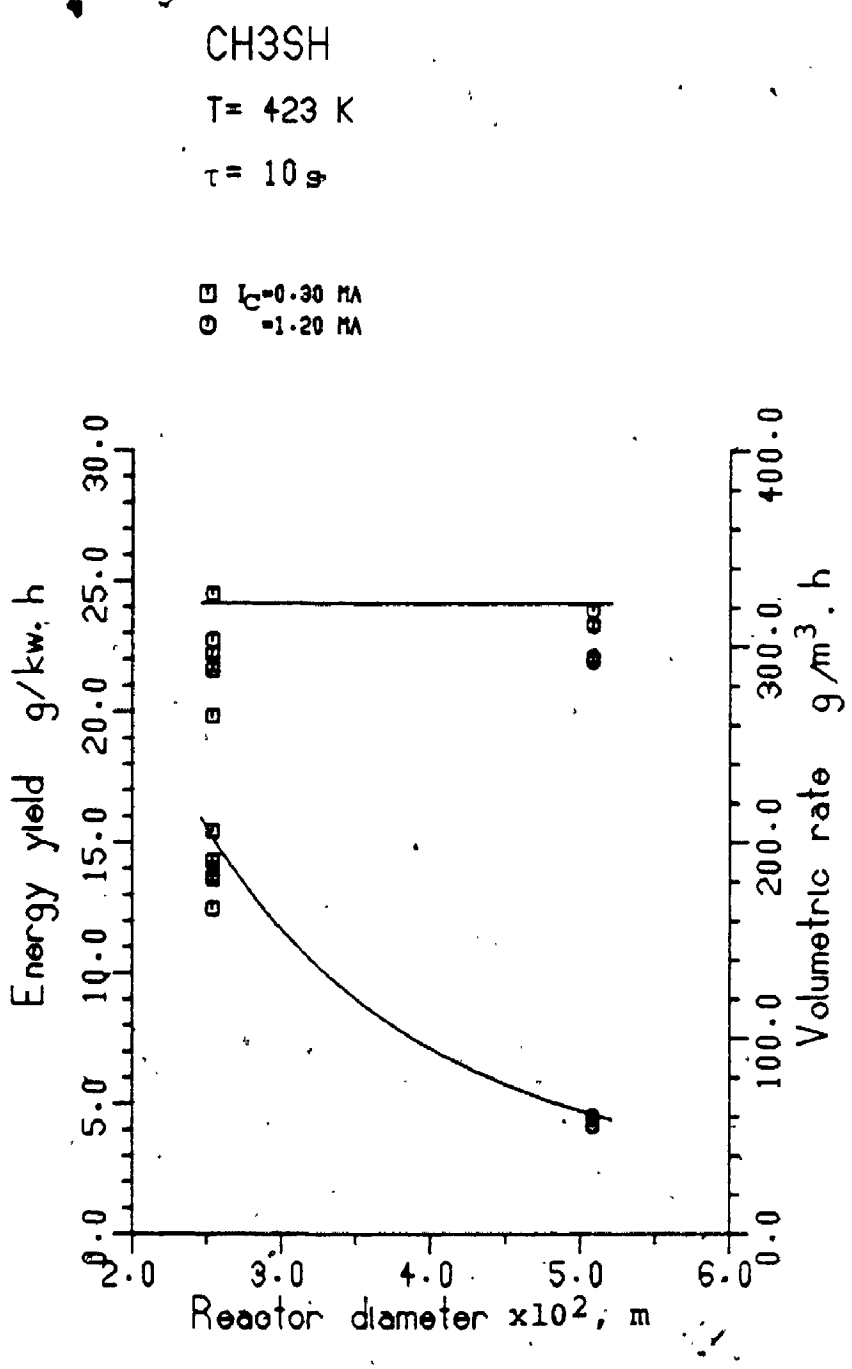

Figure 9.13: The relation between the reactor diameter and of the reaction of methyl mercaptan with air at I_c/Q of 38.86 A/m^3.s

Reactor height = 1.52×10^{-1} m
Wire diameter = 3.05×10^{-5} m

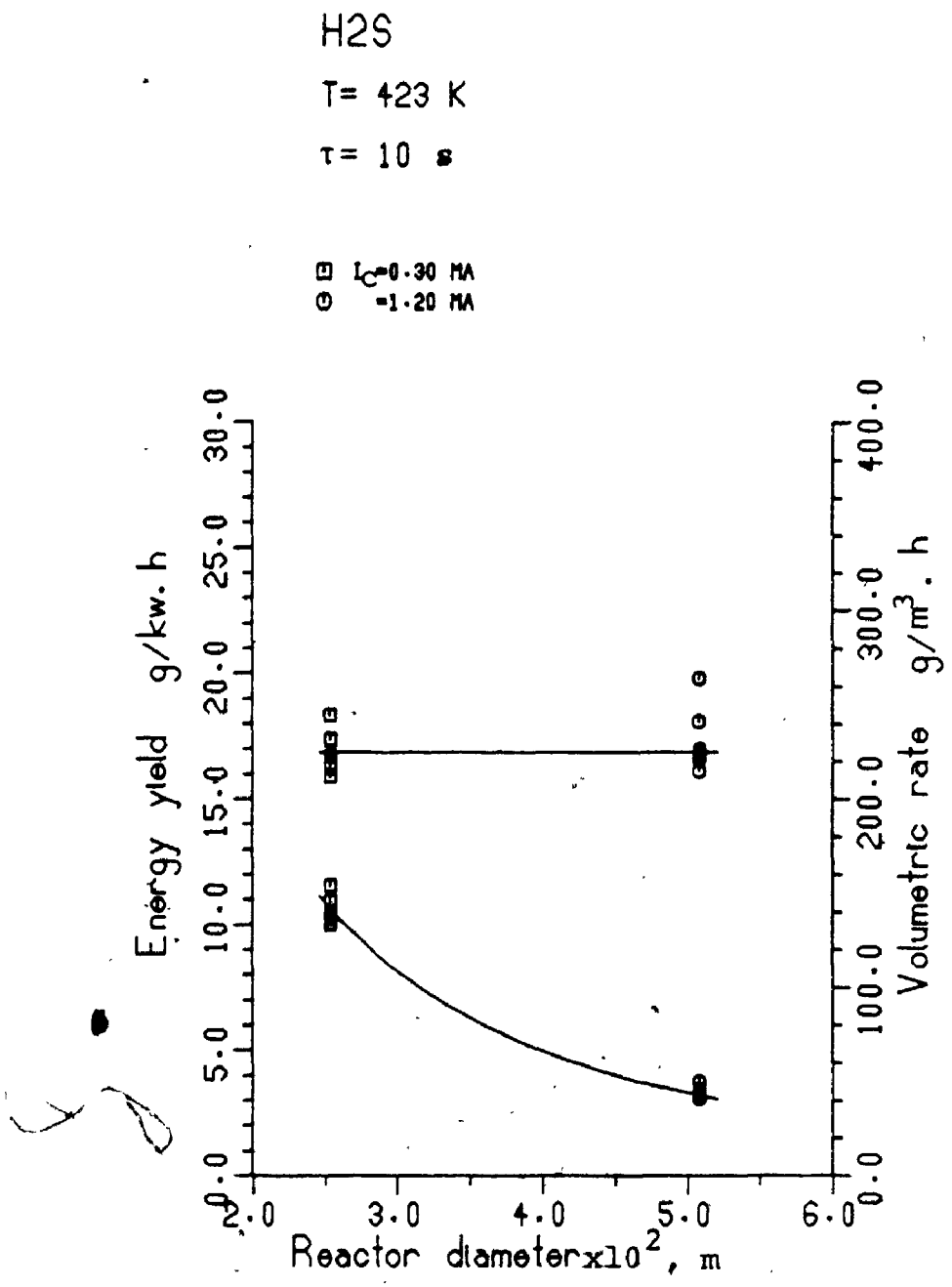

Figure 9.14: The relation between the reactor diameter and of the reaction of hydrogen sulphide with air at I_c/Q of 38.86 A/m^3 s

Reactor height = 1.52×10^{-1} m
Wire diameter = 3.05×10^{-5} m

such conditions, within the range of experimental errors, there are no differences in the results obtained in the two reactors. These results along with those of Section 6.5, indicate that the power to be considered in a corona reactor is the power dissipipated in the ionized sheath. The reason is as follows: as long as the wire size remains constant, both the ionized sheath thickness and the voltage drop across it remain constant. Consequently, the useful power dissipitated in the ionized sheath and the generation rate of the oxygen species are kept unchanged. Since the concentration of these species is inversely related to the reactor diameter (see equation (7.2)), the reaction rate defined by equation (7.3) will become smaller as the reactor diameter increases resulting eventually in lower conversion and in volumetric rate values.

Figures 9.11b and 9.12b above illustrate the dependency of the energy yield on the reactor diameter. In view of equation (9.1) and of the above discussion, an increase in the reactor diameter requires i) an increase in the flow rate of the feed through the reactor (to keep τ constant), ii) an increase in the applied voltage (to keep I_c unchanged), and, as a result, iii) a decrease in the fractional conversion of the sulphur compound. Depending on the relationship between these parameters the energy yield of reaction R1 and R2 will change with the reactor diameter. For the present range of conditions, Figures 9.11b and 9.12b

show that, based on , lower or higher values of E_y are obtained by the small or large reactor. However, as the theoretical calculations exhibited by the solid lines in the figures indicate, the energy yield has to start from zero for zero reactor diameter. In other words, reactors having diameters less than those tested above would indeed favour high values of the energy yield at shorter residence times.

Furthermore, when the quotient I_c/Q was kept constant at 38.86 $A/m^3/s$ for example, the results of Figures 9.13 and 9.14 show that the energy yield decreases as the diameter increases. This was attributed, as seen above, to the increase in the applied voltage.

Figures 9.15 and 9.16 show the fractional conversion of methyl mercaptan and hydrogen sulphide, respectively obtained from experiments carried out in the large reactor while the current was kept constant at 0.05 mA. These figures emphasize that there is an induction period in the early stages of the reaction. During this period, the rate (given by the slope) of the respective reaction is slow. Such results which were significantly observed in the reactions carried out in the smaller reactor diameter may be explained as follows: since reactions R1 and R2 proceed completely in the gas phase, as shown previously, no processes due to surface adsorption or desorption are present. Furthermore, the discussion given in Section 7.2

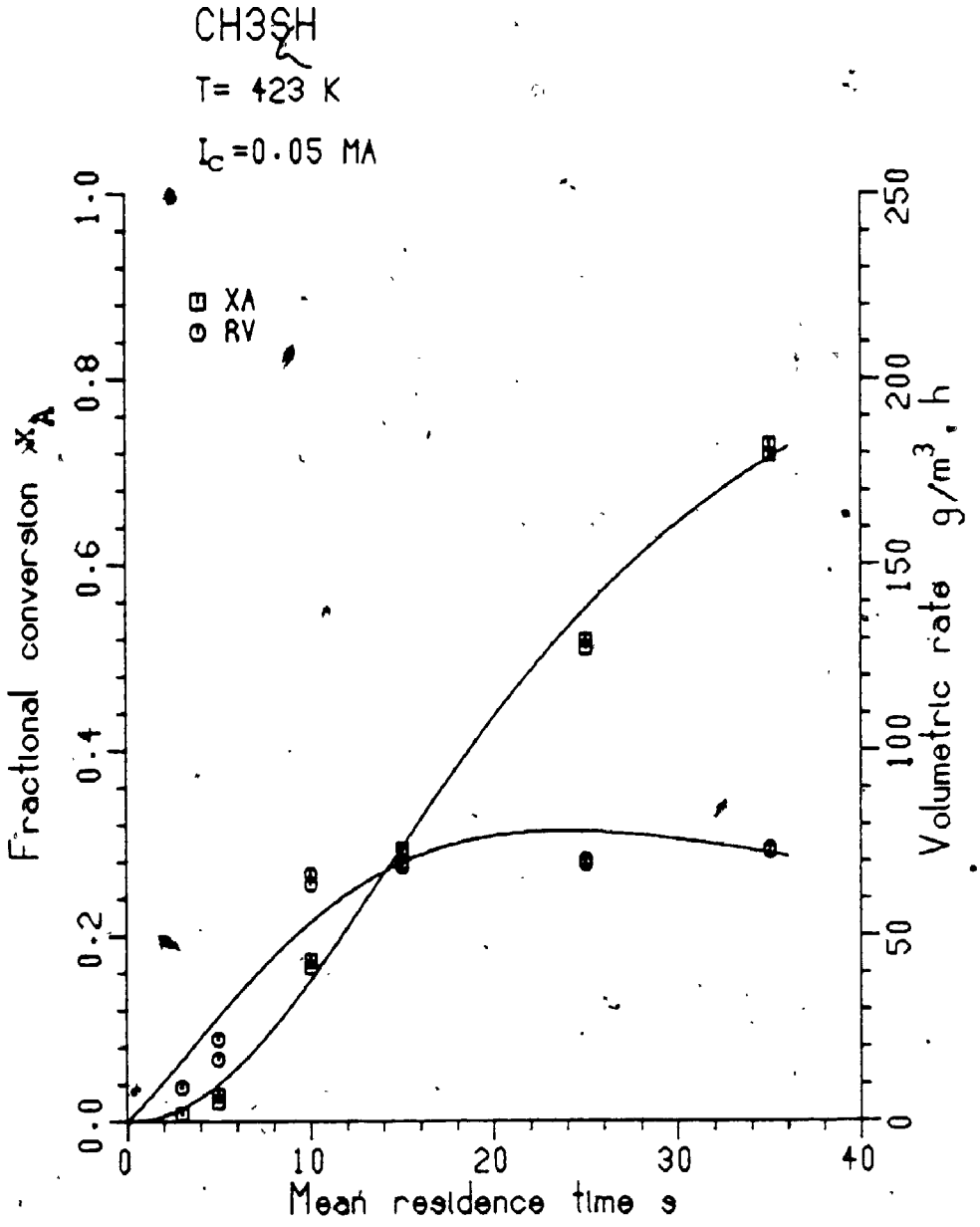

Figure 9.15: The presence of an induction period during the reaction between methyl mercaptan and air.

Reactor dimensions: D = 5.08×10^{-2} m
H = 1.52×10^{-1} m
a = 1.52×10^{-5} m

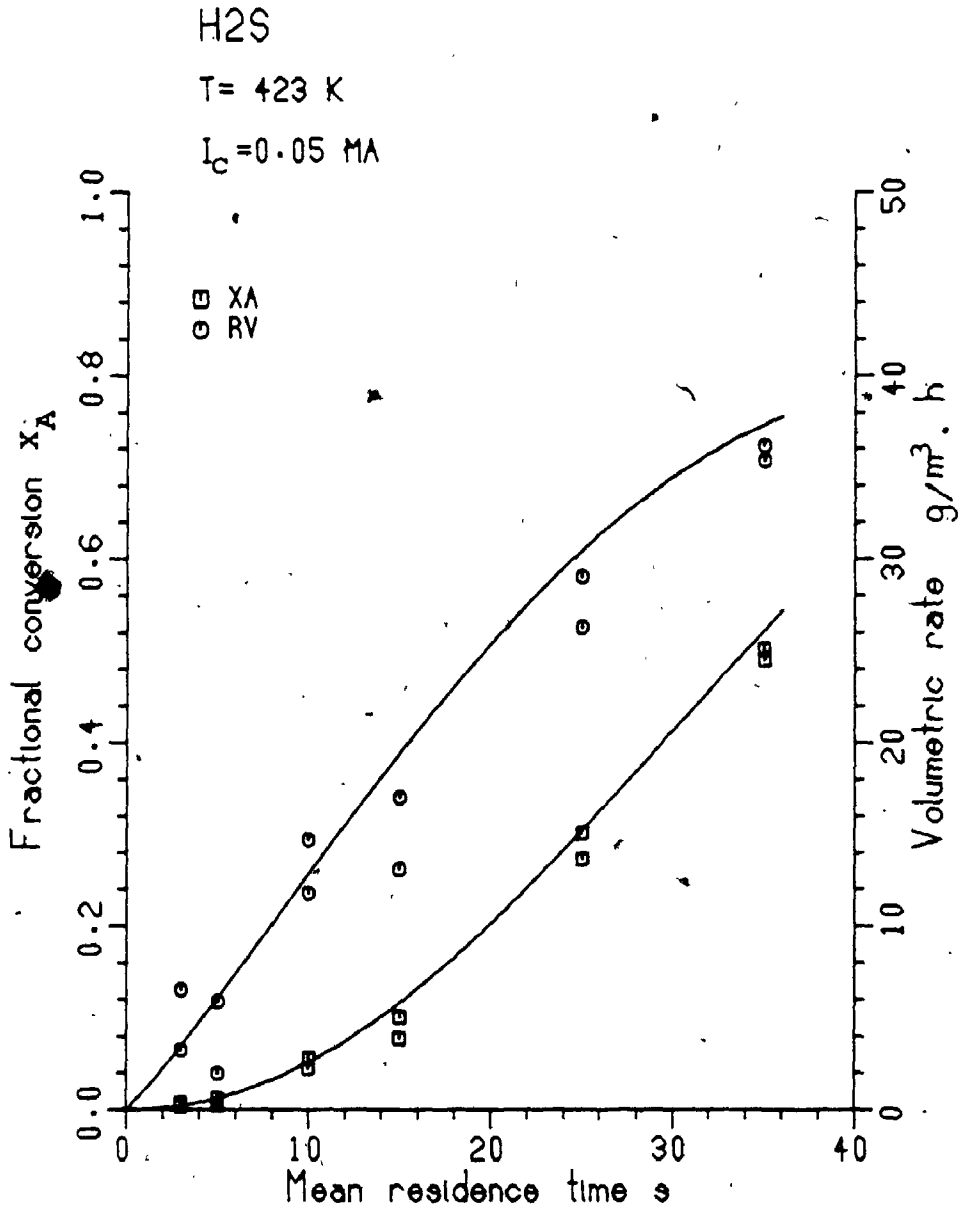

Figure 9.16: The presence of an induction period in the early stages of the reaction of hydrogen sulphide with air.

Reactor dimensions: D = 5.08×10^{-2} m
H = 1.52×10^{-1} m
a = 1.52×10^{-5} m

indicated the absence of any diffusional process. As a result, the presence of what seems to be an induction period may be attributed to the complex mechanisms of the reactions. These reactions, as discussed earlier, are initiated by radical formation. The concentration of these radicals rises first as time increases by propagation reactions, pass through a maximum before it falls due to the termination processes. Thereupon, a parabolic relationhip between the reactions rate and the radical concentration exists [96] leading eventually to the induction periods exhibited in the above figures.

C) PARAMETERS RELATED TO FEED GAS CONDITIONS

The parameters whose effect on E_y and R_v of reactions R1 and R2 was studied in this section are the mean residence time of the feed through the reactor, the initial concentration of the sulphur reactants, the temperature of the reactor, and the initial concentration of water in the feed. The results which will be presented here will largely depend upon the data reported previously describing the effect of the first three parameters on the conversion of the reactants.

9.8 THE EFFECT OF MEAN RESIDENCE TIME ON E_y AND R_v OF REACTIONS R1 AND R2

As an example of the effect of the mean residence time on E_y and R_v of reactions R1 and R2 is already illustrated above in Figures 9.1 and 9.2, respectively. It is indicated that both the energy yield and the volumetric rate of the reactions increase with the increase in the early stages of the reactions, pass through maxima, and then fall with a decreasing rate for longer mean residence times. This skewed bell-shaped relations may be explained in terms of equations (9.1) and (9.2). From these equations, by replacing Q by V_R/τ, we obtain:

$$E_y = \{\frac{V_R C_{Ao} M_w}{V_s I_c}\} (\frac{X_A}{\tau}) \qquad (9.8a)$$

and

$$R_v = C_{Ao} M_w (\frac{X_A}{\tau}) \qquad (9.9a)$$

It was demonstrated previously that the voltage-current characteristics are independent of the mean residence time. At constant conditions of initial concentration of the sulphur reactants, the above equations are reduced to:

$$E_y = K_1 (\frac{X_A}{\tau}) \qquad (9.8b)$$

and

$$R_v = K_2 (\frac{X_A}{\tau}) \qquad (9.9b)$$

where K_1 and K_2 are constants given by $(V_R\ C_{Ao}\ M_w/V_s\ I_c)$ and $(C_{Ao}\ M_w)$, respectively. Then, for otherwise constant conditions, the slope of a relation between the conversion x_A and the mean residence time τ at any value of the latter uniquely defines both the energy yield and the volumetric rate of reactions R1 and R2.

At the beginning of the reaction,, the increase in X seems greater than that in τ. As the reactions progress, the difference between these two increases gets less and less until it becomes constant, that is where the values of E_y and R_v of the reactions are maximum. For longer residence times, the opposite is true and the energy yield and the volumetric rate of reactions R1 and R2 decrease.

Figures 9.1a to 9.2b also show the change rate of the energy yield and the volumetric rate of the reactions at several values of current. It seems from these figures that the loci of the maxima of these properties are shifted towards lower values of mean residence time as the current increases. These results may be explained as follows: high currents favour higher concentrations of the excited oxygen molecules which in turn enhance the rate of the reactions as discussed previously.

9.9 THE EFFECT OF INITIAL CONCENTRATION OF SULPHUR COMPOUNDS ON E_y AND R_v OF REACTIONS R1 AND R2

The effect of the initial concentration of the sulphur reactants on E_y and R_v of the respective reaction was investigated over a wide range of the former. The initial concentration of methyl mercaptan ranged from 8.1×10^{-6} to 413.9×10^{-6} kmol/m^3 and from 6.67×10^{-6} to 411.3×10^{-6} kmol/m^3 of hydrogen sulphide.

Recalling the discussion of Section 4.6, this range of concentration had but an insignificant effect on the voltage-current characteristics. For example, to obtain a cuurent of 0.3 mA, the maximum difference in the applied voltage at 423 K was 0.13 kV, from 5.61 to 5.74 kV. That is 2.3% difference, a part of which is due to experimental errors. Such results may moreover suggest that the coefficient of attachment of electrons to the sulphur species present are small (no data is available) even though the mobility of these species when charged may be lower than that of air as in the case of hydrogen sulphide (see Table 3.3).

The effect of C_{A0} on E_y and R_v of reactions R1 and R2 is illustrated in Figures 9.17a and 9.18a, respectively.

Figure 9.17a and 9.18a show that as the initial concentration of the respective sulphur compound increases

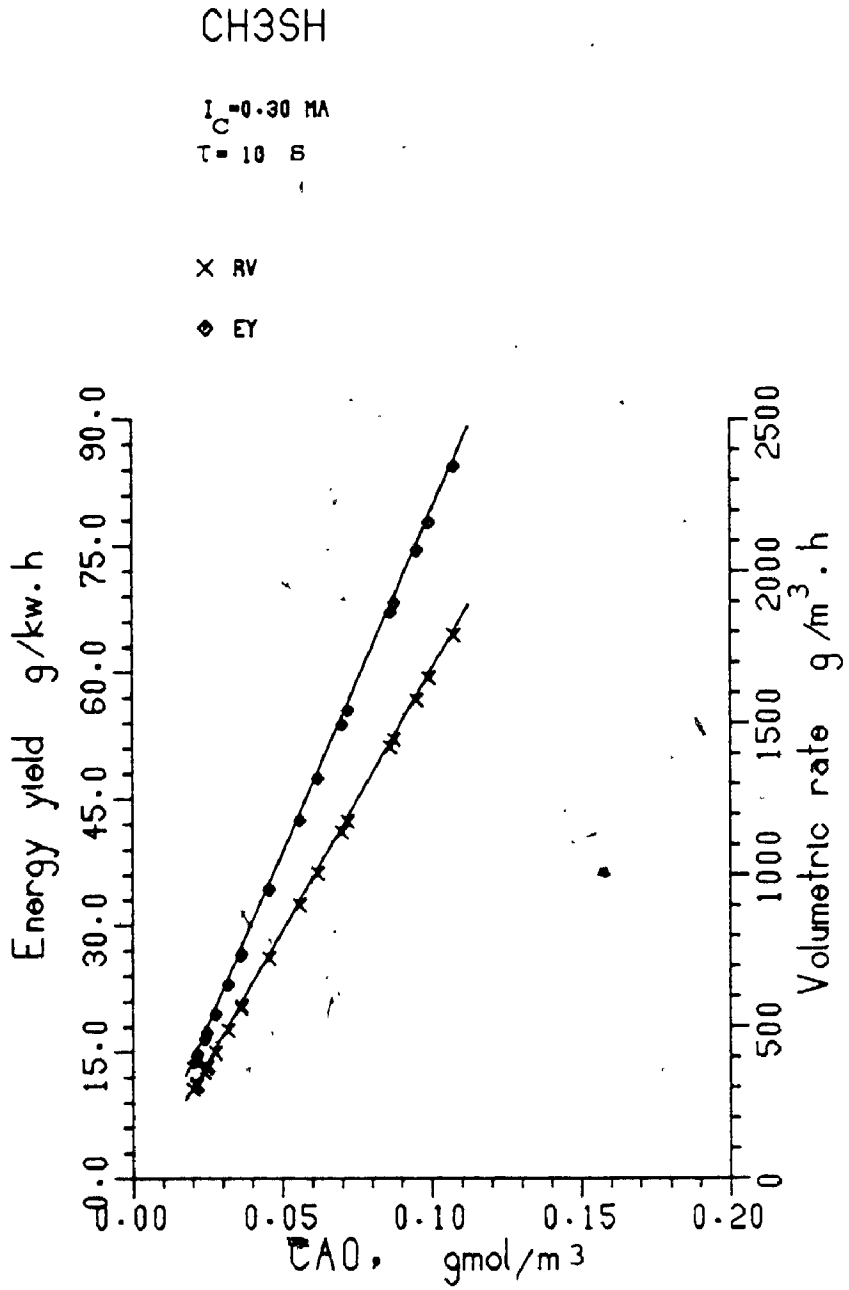

Figure 9.17a: The effect of the initial concentration of methyl mercaptan on E_y and R_v of its reaction with air

Reactor dimensions: D = 2.54×10^{-2} m
H = 1.52×10^{-1} m
a = 1.52×10^{-5} m

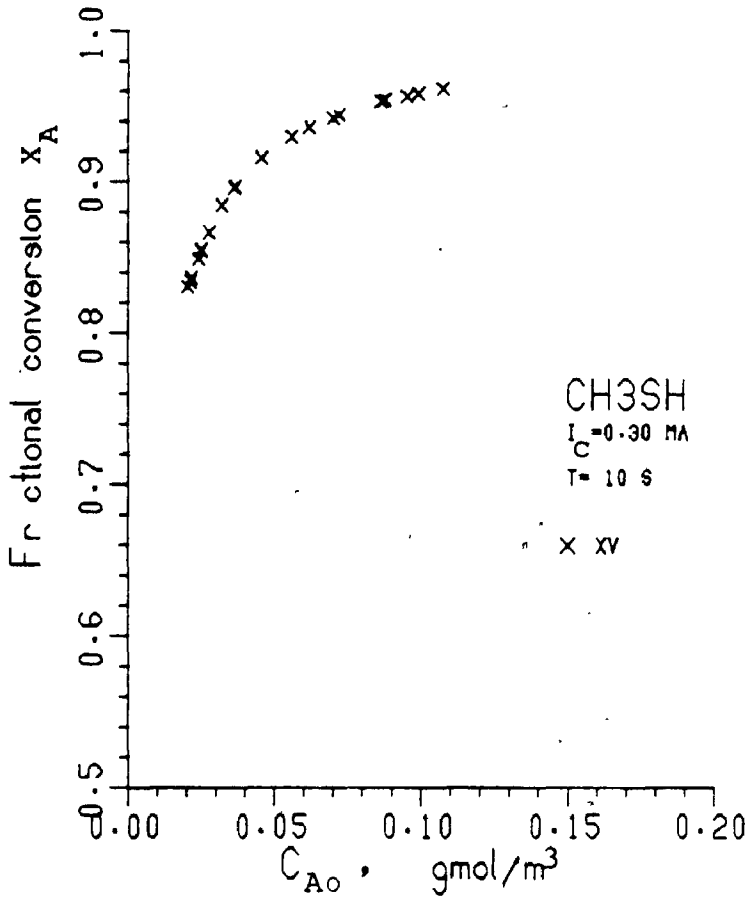

Figure 9.17b: The effect of the initial concentration of methyl mercaptan on its fractional conversion due to reaction with air

Reactor dimensions: D = 2.54×10^{-1} m
H = 1.52×10^{-1} m
a = 1.52×10^{-5} m

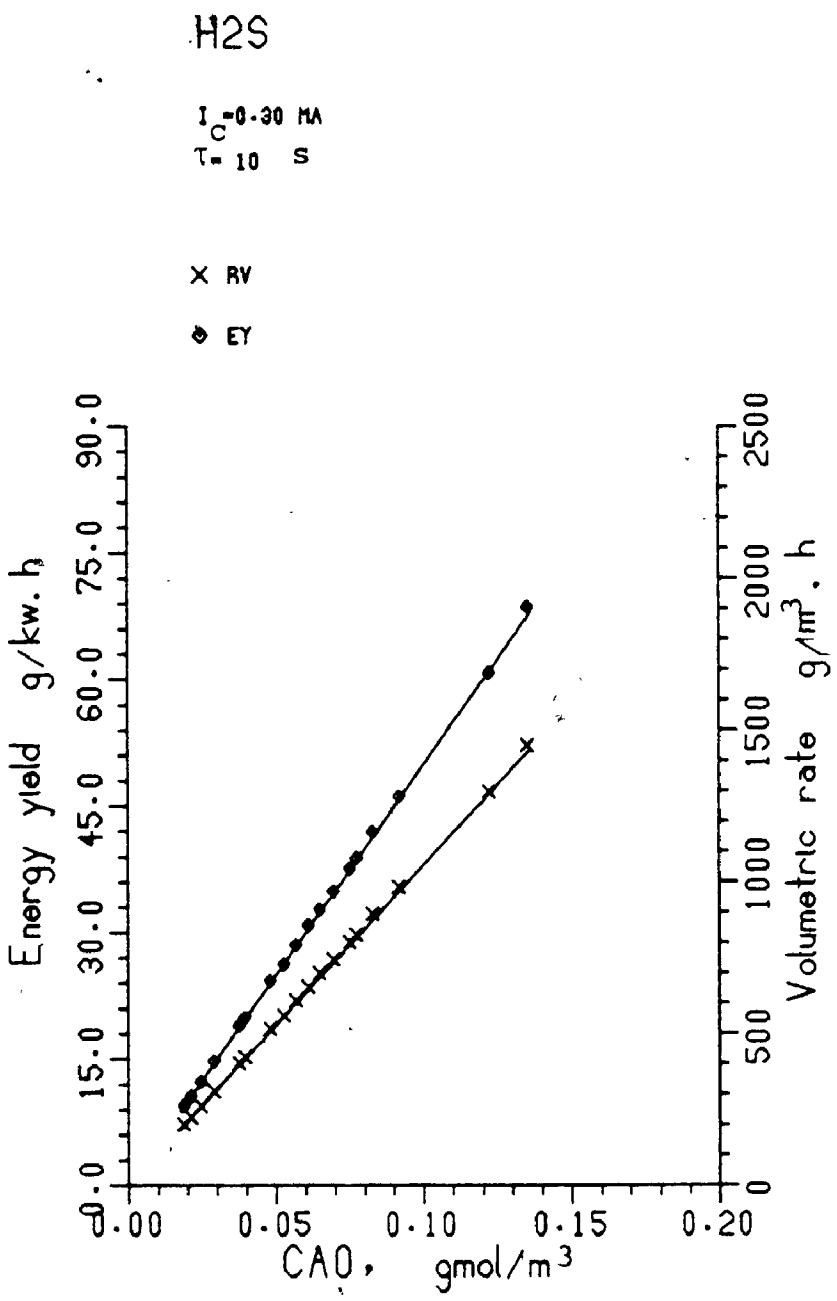

Figure 9.18a: The effect of the initial concentration of hydrogen sulphide on E_y and R_v of its reaction with air

Reactor dimensions: D = 2.54×10^{-2} m
H = 1.52×10^{-1} m
a = 1.52×10^{-5} m

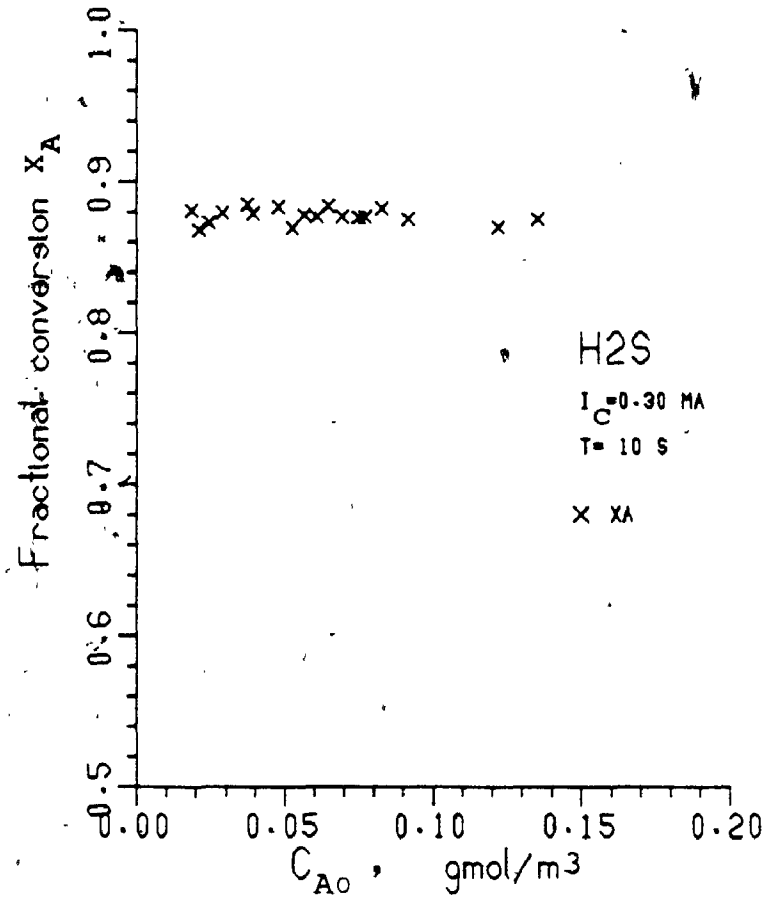

Figure 9.18b: The effect of the initial concentration of hydrogen sulphide on its fractional conversion due to reaction with air

Reactor dimensions: $D = 2.54 \times 10^{-2}$ m
$H = 1.52 \times 10^{-1}$ m
$a = 1.52 \times 10^{-5}$ m

both the energy yield and the volumetric rate of the reactions also increase. In reference to equations (9.1) and (9.2), these results were conventionally expected as far as the relation between both E_y and R_v and C_{Ao} is concerned. In case of methyl mercaptan however, due to the fact that the order of its disappearance in the corona reactor is 1.98, we expect that the increase in C_{Ao} of this compound will, as Figure 9.17b shows, cause its farctional conversion to increase. This later increase would also contribute to the increase of both E_y and R_v of the reaction.

For hydrogen sulphide, the reverse is true since its fractional conversion, due to the order of its reaction in the corona reactor, is not a strong function of its initial concentration in the feed. This is further illustrated in Figure 9.18b.

9.10 THE EFFECT OF INITIAL CONCENTRATION OF WATER IN THE FEED ON THE PROPERTIES OF REACTIONS R1 AND R2

The effect of water on E_y and R_v of reactions R1 and R2 was initiated because of its high contents in the off-gases from kraft mills (see Section 1.2).

In each of the experiments conducted in the present set, a given amount of distilled water was injected into the lecture bottle using a gas-tight syringe (see Section 4.2). The initial concentration of water in the feed to the

reactor was determined in every case by the gas chromatograph as described previously. The range in which this parameter was varied was chosen so that it may be of practical interest. The experimental procedure used was described in Section 4.3.3. Two values of current were used: 0.1 and 0.3 mA. The values of applied voltage at these two values in the range of the water concentration used are summarized in Table 9.4.

Table 9.4 shows that the presence of water in the reaction mixture influences the voltage-current characteristics. This influence is more appreciable at higher values of these tow parameters. For example, an increase of about 27% in the applied voltage is observed at 0.3 mA while it is only about 16% at 0.1 mA. These results are in agreement with previous investigations [58]. Being a polar compound, the presence of water in the reaction mixture may influence the voltage-current characteristics in several ways:

1- Water molecules would reduce the applied voltage by an amount proportional to its dielectric constant [161]. From a molecular point of view, the dielectric constant of a compound is directly related to the dipole moment of the molecules [162]. The presence of the electric field will induce a proportional dipole moment in the water molecules from i) the polarization due to the direct influence of the

TABLE 9.4: THE EFFECT OF THE INITIAL WATER CONCENTRATION ON THE CURRENT-VOLTAGE CHARACTERISTICS*

I_c mA	C_{WO_3} kmol/m	V_s kV	I_c mA	C_{WO_3} kmol/m	V_s kV
0.1	0.014	3.84	0.3	0.009	5.51
	0.065	3.86		0.024	5.66
	0.087	3.88		0.095	5.78
	0.129	3.87		0.109	6.34
	0.179	3.92		0.186	6.60
	0.206	3.92		0.264	5.93
	0.248	3.96		0.296	6.08
	0.382	3.98		0.402	6.12
	0.392	3.98		0.485	6.12
	0.498	4.04		0.505	6.22
	0.504	4.08		0.541	6.20
	0.609	4.09		0.742	6.28
	0.634	4.12		0.846	6.52
	0.816	4.17		0.888	6.49
	0.837	4.18		1.010	6.71
	0.934	4.23		1.022	6.83
	1.061	4.23		1.208	6.77
	1.109	4.28		1.389	6.88
	1.211	4.37		1.440	6.79
	1.293	4.40		1.478	7.02
	1.403	4.41		1.478	7.02

* OTHER EXPERIMENTL CONDITIONS ARE:

Temperature	=423	K
Mean residense time	= 10^{-2}	s
Reactor diameter	= 2.54×10^{-5}	m
Wire diameter	= 3.05×10^{-2}	m
Reactor neight	=15.24x10	m
Average initial concentration of the sulphur reactant	=25.0×10^{-6}	kmol/m^3

electric field and from ii) the partial net alignment by the field of the permanent dipole moment of the water molecules. The total induced polarization forms a field of an opposite sign which simply acts to reduce the apparent field [162].

2- Water molecules possess a higher coefficient of electron attachment than that of air (see Table 3.2). They will, therefore, attract a proportional number of electrons and form negative ions. Since the mobility of the negative ions of water is, as discussed in Section 3.4, about 60% less than that of the molecules of the air constituents, the effect is to reduce the current for a given applied voltage.

3- The tendency of electrons to be attracted to the water molecules will supress the energy of electrons and their number available to react with the oxygen molecules and form their excited species responsible for the oxidation of the sulphur compounds.

4- They can cluster around negative ions:

$$O_2^- + nH_2O + M \rightarrow O_2^-(H_2O)_n + M \qquad (9.10)$$

in which M may be oxygen or nitrogen molecules and n is an integer and does not exceed 3 [163]. Such hydrated ions have lower mobilities and hence, reduce the current attained for a given voltage.

From Figures 9.19a and 9.20a, for a given set of current, temperature, and mean residence time, the fractional conversion of the sulphur reactants and the volumetric rate of the respective reaction seem independent of the initial concentration of water in the feed. Referring to equation (7.11), these results were obtained since the factors upon which the fractional conversion of the sulphur reactants remain constant. This is so provided that the contribution of ions $O_2^-(H_2O)_n$ to the current is negligible within the range of the experimental conditions attempted. Otherwise, the current due to the free electrons and subsquently the fractional conversion of the sulphur reactants would have been reduced. (Note that the total current in the discharge is given by:

$$I_c = I_e + I_- + I_+ \qquad (9.11)$$

where the three terms on the right hand side represent the current due to free electrons, negatively charged spesies, and positively charged species.)

The results moreover show that the fractional conversion of the sulphur reactants are, within the range examined, independent of the total power dissipated in the reactor (given by the product of voltage and current). This may provide an additional proof that the power which should be used to index the extent of the reactions of the sulphur

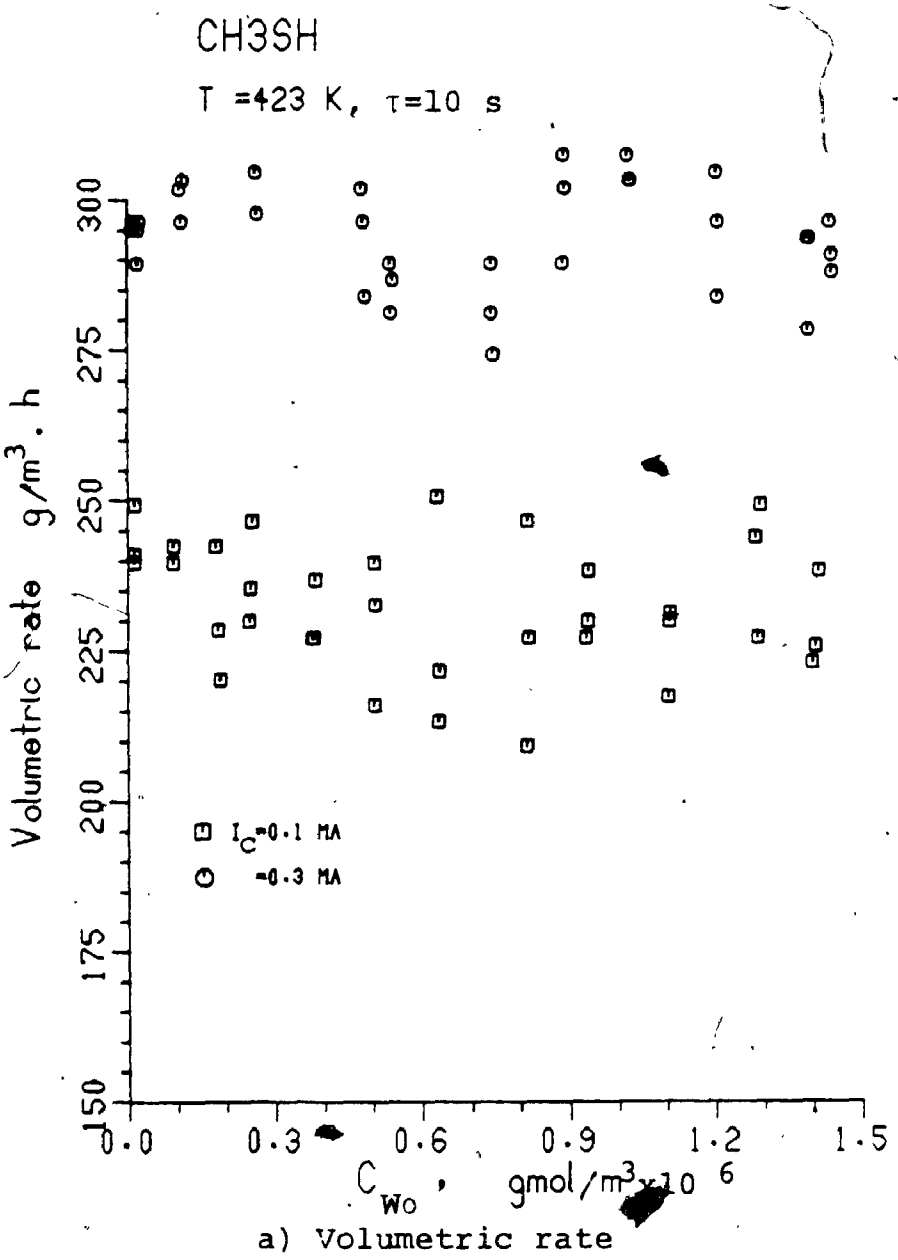

a) Volumetric rate

Figure 9.19: The effect of the initial concentration of water in the feed on E_v and R_v of the reaction of methyl mercaptan with air

Reactor dimensions: D = 2.54×10^{-2} m
H = 1.52×10^{-1} m
a = 1.52×10^{-5} m

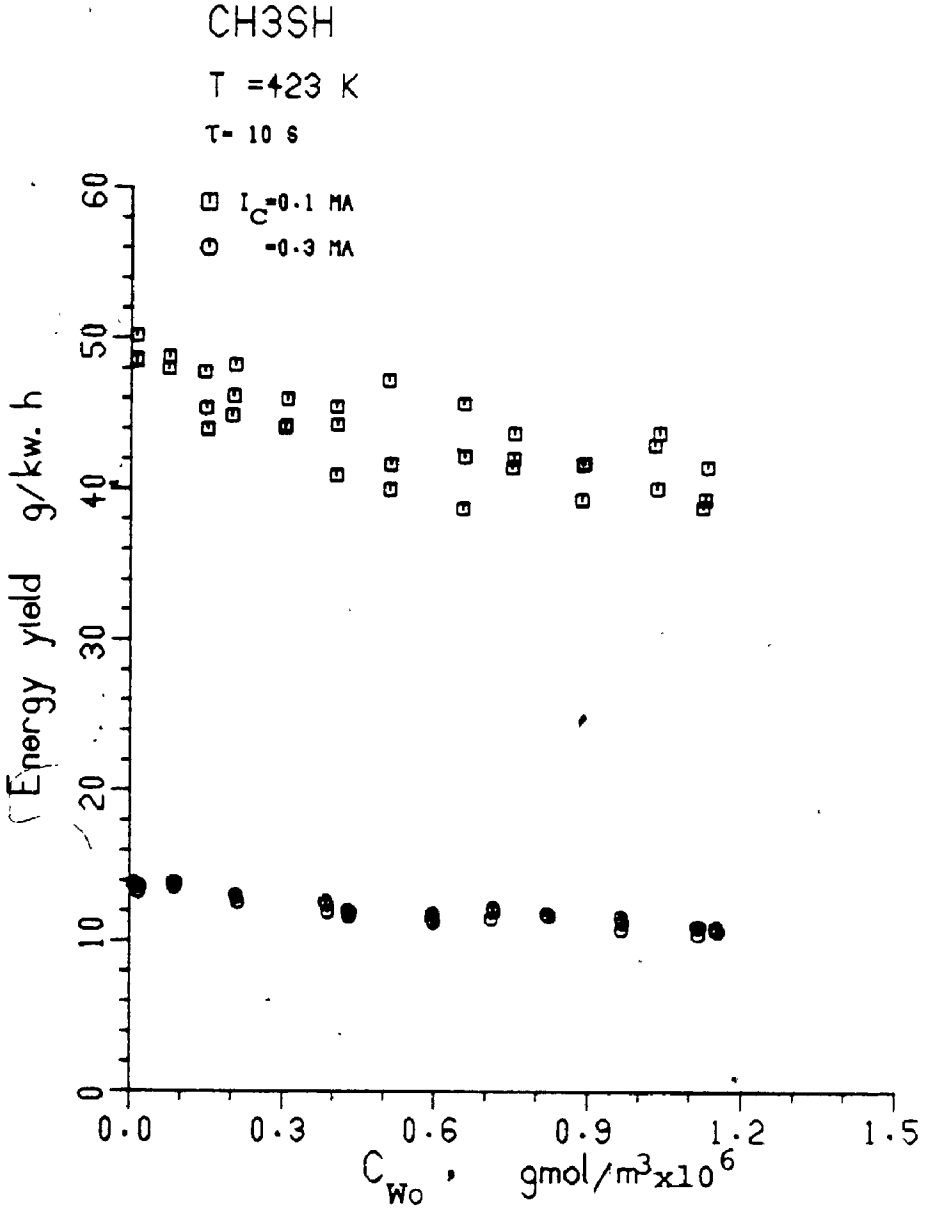

b) Energy yield

Figure 9.19: cont'd

31- Denisova,E.P., S.A.,Barisenkova, and T.Danilova: Study of the Oxidation of Some Sulphur-Containing Organic Compounds in the Presence of Phthalocyanine Complex, Chem Abstr. 93:238,770w (1979), From Katal. Sint. Org. Soedin. Sery, 92-5 (1979).

32- Adamis,V.B., C.deFigueiredo, C.Maria, and F.Nogueire: Catalytic Process for Mercaptan Removal from Light Petroleum Distillates, Chem. Abstr. 92:25,260x (1979). From Bol. Tec. Pertobras, 22(3), 183-9 (1979).

33- Kubicek,D.H.: Conversion of Alkane and/or Cycloalkane Thiol to Disulphide with a Catalyst System Comparised of Cobalt Molybdate and an Alkali or Alkaline Earth Metal Hydroxide, Chem Abstr. 95:149,953g (1981). U.S. 4277, 623 (cl. 568-26, C07C149/10), 07 Jul. 1981, Appl. 67,645, 17 Aug. 1979, 5pp.

34- Rayer,H.B. and F.E.Murray: The Photolytic Oxidation of Methyl Mercaptan, Dimethyl Sulphide,a nd Dimethyl Disulphide, Pulp Paper Mag. Can., 71(7), 75-7 (1970).

35- Thompson,H.W. and N.S.Kelland: The Kinetics of the Oxidation of Hydrogen Sulphide, J. Chem. Soc., 1809 (1931).

36- Semenov,N.N.: Some Problems in Chemical Kinetics and Reactivity, Vol. 1, Pergamon Press, New York (1959).

37- Bradley,J.N. and D.C.Dobson: Oxidation of Hydrogen Sulphide in Shock Waves, J. Chem. Phys., 46(8), 2865-71 (1967).

38- Marsden,D.G.H. : A Mass Spectrometric Study of the Oxidation of Hydrogen Sulphide, Can. J. Chem., 41, 2607 (1963).

39- Panov,G.E. and G.V.Starikova: Transformation of Hydrogen Sulphide in Atmospheric Air, Chem. Abstra. 92:46,646t (1979). From Gazov. Prom-St., 9, 26-7 (1979).

40- Singleton,D.L., R.S.Irwin, W.S.Nip, and R.J.Cvetanovic: Kinetics and Mechanism of the reaction of Oxygen Atoms with Hydrogen Sulphide, J. Phys. Chem., 83(17), 2195-200 (1979).

41- Liuti,G., S.Dondes, and P.Hartech: The Reaction of Hydrogen Sulphide and Atomic Oxygen, J. Am. Chem. Soc., 88, 3212 (1966).

42- Gregor,I.K. and I.K.Martin: The Reaction between Ozonized Oxygen and Hydrogen Sulphide in the Gaseous Phase, Aust. J. Chem., 14, 462 (1961).

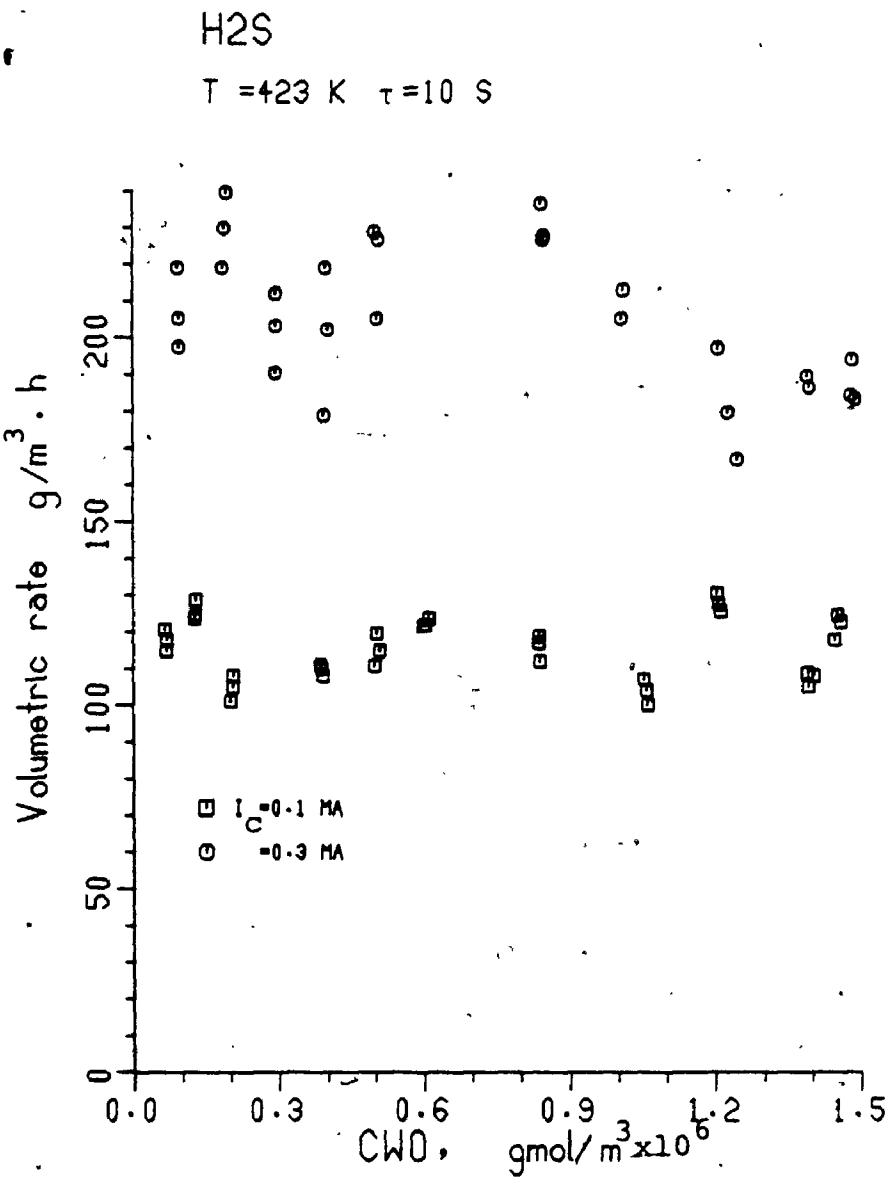

b) Volumetric rate

Figure 9.20: cont'd

compounds is in fact not the total power but rather the power dissipitated in the ionized sheath.

The effect of water concentration on the energy yield of reactions R1 and R2 is illustrated by Figures 9.19b and 9.20b for the two currents tested. As expected, the energy yield of the reaction depends upon the concentration of water where they are inversely related. The effect is more pronounced at higher values of current. By referring to Table 9.4 and equation (9.1), an increase in the water concentration causes the applied voltage to increase for a given current. Since the conversion are unchanged , the energy yield is reduced.

9.11 THE EFFECT OF TEMPERATURE ON E_y AND R_v OF REACTIONS R1 AND R2

The data obtained previously will be used here to study the effect of temperature on the energy yield and the volumetric rate of reactions R1 and R2. As seen, five temperatures 298, 323, 373, 423, and 453 K which may cover the industrial range were examined. The results are plotted in Figures 9.21 and 9.22 for reactions R1 and R2, respectively.

As indicated by these figures, both properties of the reactions are directly proportional to temperature.

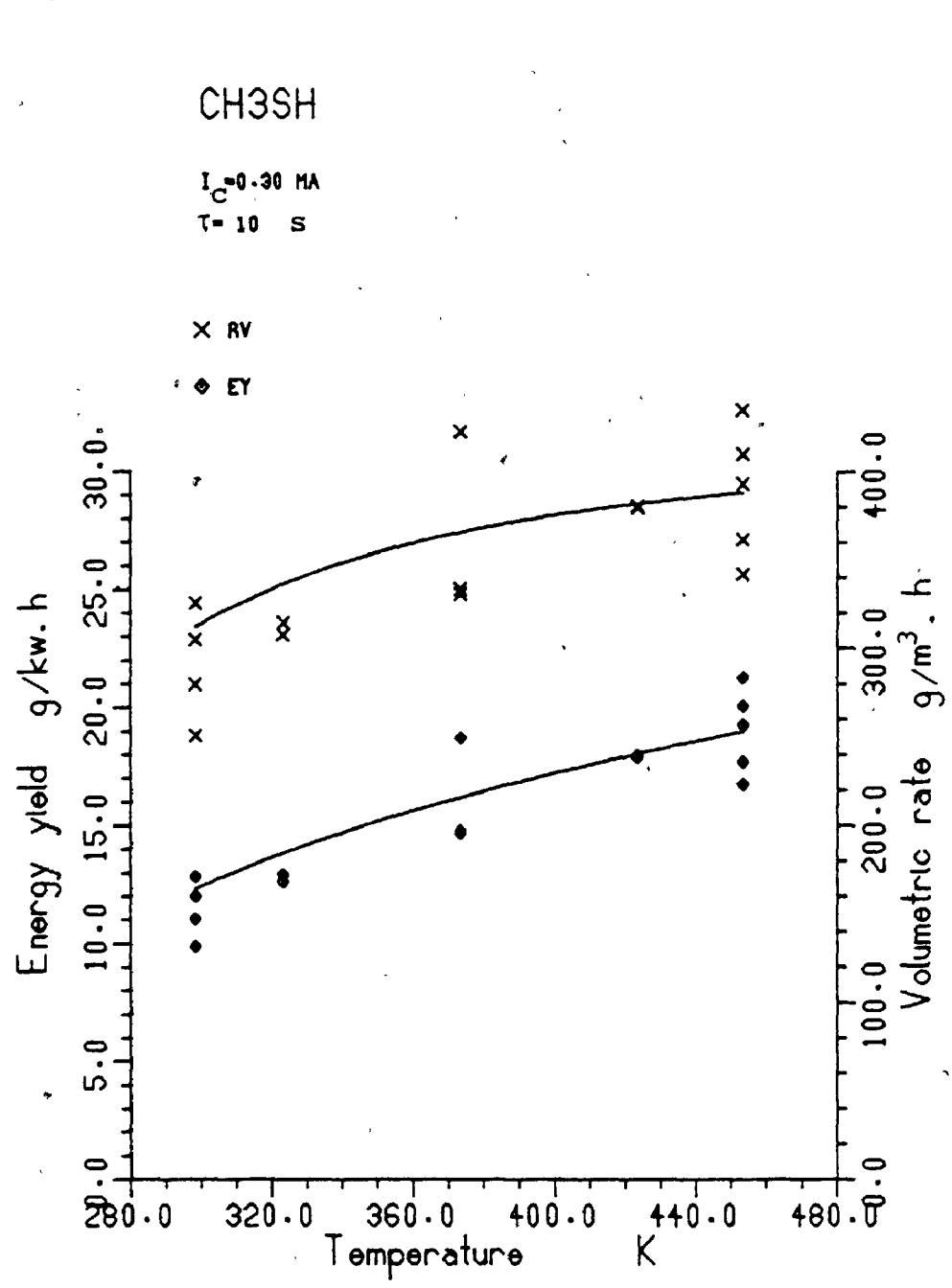

Figure 9.21: Temperature-dependency of E_v and R_v of the reaction between methyl mercaptan and air

Reactor dimensions: D = 2.54×10^{-2} m
H = 1.52×10^{-1} m
a = 1.52×10^{-5} m

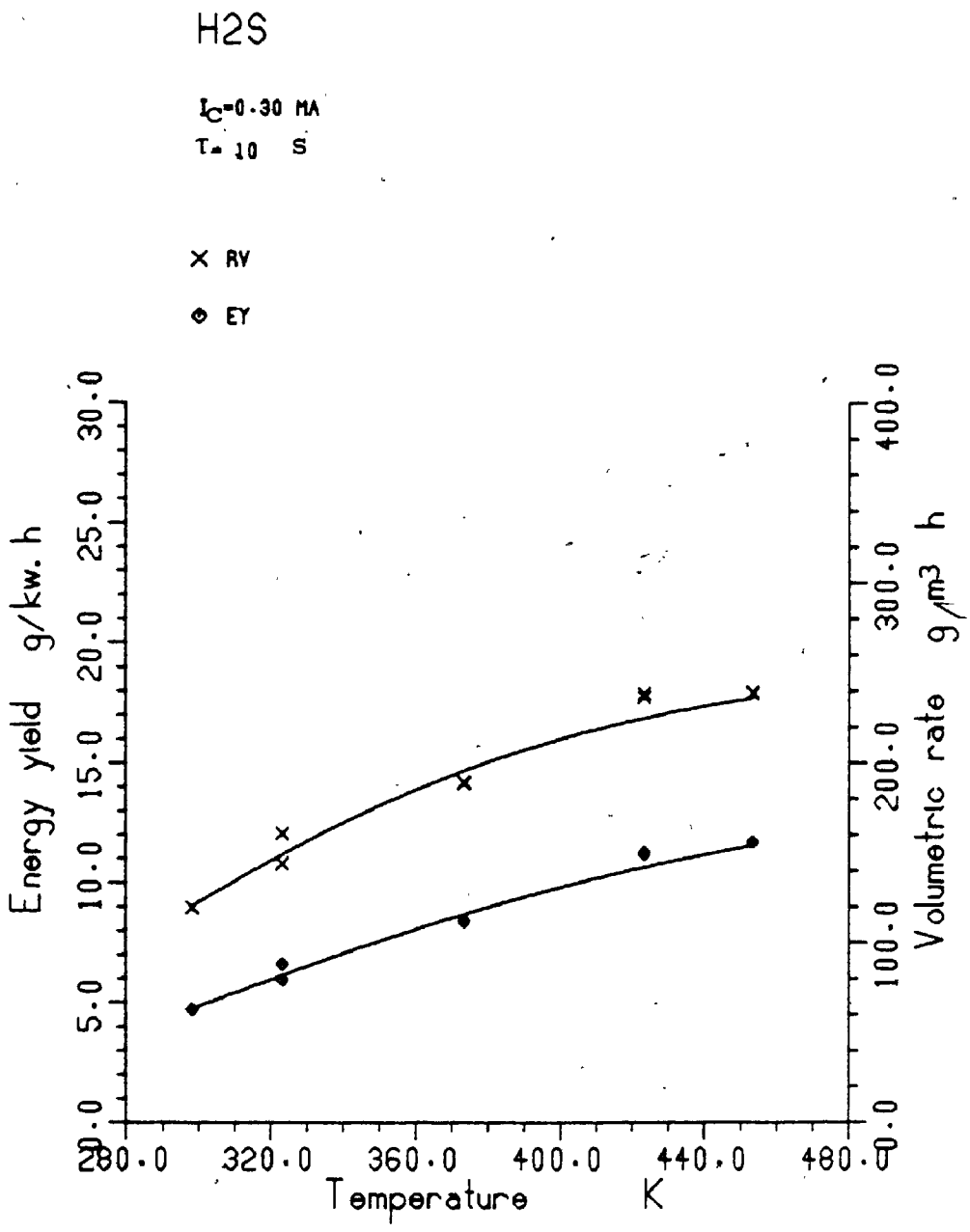

Figure 9.22: Temperature-dependency of E_y and R_V of the reaction between hydrogen sulphide and air

Reactor dimension: D = 2.54×10^{-2} m
H = 1.52×10^{-1} m
a = 1.52×10^{-5} m

In the case of the volumetric rate, the results are cuased by the increase in the fractional conversion of the sulphur compound with the increase in temperature (equations (7.12) and (9.2)).

In addition to the increase in the fractional conversion, the decrease in the applied voltage with the increase in temperature (for a given current) contributes to the increase in the energy yield (equation (9.1)).

CHAPTER 10

CONCLUSIONS AND RECOMMENDATIONS FOR FURTHER STUDY

A novel approach was investigated for the removal of malodorous methyl mercaptan and hydrogen sulphide from air streams. Such an approach would prove beneficial to air pollution abatement in the kraft pulp mills.

The approach will allow the oxidation of methyl mercaptan and hydrogen sulphide to lesser offensible compounds by air in an electrostatic-precipitator-type-reactor. Compared to present methods of controlling the emissions of these compounds, the method investigated here has many advantages:

1- Possible treatment of low concentration pollutants present in large amounts of air.

2- Since there are no solid packings inside the corona reactor the pressure drop of flow is very small (usually negligible compared to scrubbers or filters) and then power requirements for flow is minimal. Also for this reason, any problem associated with solid fouling and mechanical handling is eliminated.

3- Since the reactor will be operated electrically easy and immediate control of the reactor operation iseadily accessible.

4- Energy requirement is available considering the depletion of oil resources in the world.

The oxidation of methyl mercaptan and of hydrogen sulphide by air was studied in a corona reactor of the wire-cylinder arrangement. The results obtained allowed the development of the mechanisms of the reactions as well as the evaluation of their kinetics. Two functions "the energy yield" and "the volumetric rate" of a reaction were introduced and used to present the data obtained. These variables may be of particular interest to industry as they can be used in the evaluation of the operating and fixed costs of the process, respectively. The effect of the physical dimensions of the reactor and the operating conditions on these two variables were studied and discussed.

10.1 CONCLUSIONS

The detailed conclusions and implications of the study done herein were discussed in the respectives sections of the text. However, the most significant conclusions made from the results are as follows:

1- The oxidation of methyl mercaptan by air in the corona reactor was found to form three end products: water, sulphur dioxide, and dimethyl sulphone and two intermediate products: dimethyl disulphide and dimethyl sulphide. By

using higher values of current and/or low values of mean residence time through the reactor, the intermediates products could be converted to the end products.

2- The oxidation of hydrogen sulphide by air in the corona reactor always formed water and sulphur dioxide.

3- The thermal reaction of the sulphur compounds was unimportant within the temperature range attempted.

4- The main contribution found for the corona discharge was to produce some kinds of excited oxygen molecules: the two singlet species $O_2^*(a\,^1\Delta_g)$ and $O_2^*(b\,^1\Sigma_g^+)$ and the triplet species $O_2^*(A\,^3\Sigma_u^+)$. The latter species was found to constitute more than 90% of all the excited and ionized species found in the corona discharge. There were indications of the essential role played by these species in the oxidation of the sulphur compounds.

5- Ozone, which may be formed in corona discharge of air, was proven not take a part in the oxidation processes.

6- The reactions of methyl mercaptan and of hydrogen sulphide with air occured totally in the gas phase. The first reaction moreover was found to proceed in a series of three consecutive reactions, namely:

$$2CH_3SH + \tfrac{1}{2}O_2^* \rightarrow (CH_3)_2S_2 + H_2O$$

$$(CH_3)_2S_2 + O_2^* \rightarrow (CH_3)_2S + SO_2$$

$$(CH_3)_2S + O_2^* \rightarrow (CH_3)_2SO_2$$

The rate of each of these reactions was determined individually in $kmol/m^3.s$:

$$-r_{CH_3SH}=78\times10^{-4}\ e^{-1638/T}\ \left(\frac{\bar{E}\Delta aI_c}{Q}\right)^{1.13}\ C_{CH_3SH}^{1.98}$$

$$-r_{(CH_3)_2S_2}=72\times10^{-6}\ e^{-730/T}\ \left(\frac{\bar{E}\Delta aI_c}{Q}\right)^{0.91}\ C_{(CH_3)_2S_2}^{0.96}$$

$$-r_{(CH_3)_2S}=72\times10^{-7}\ e^{-413/T}\ \left(\frac{\bar{E}\Delta aI_c}{Q}\right)^{1.06}\ C_{(CH_3)_2S}^{1.01}$$

Similarily, the second reaction took place according to:

$$H_2S + 3/2O_2^* \rightarrow H_2O + SO_2$$

and its rate was determined as:

$$-r_{H_2S}=3.35\times10^{-4}\ e^{-1535/T}\ \left(\frac{\bar{E}\Delta aI_c}{Q}\right)^{0.96}\ C_{H_2S}^{0.98}$$

7- The effect of the physical dimensions of the corona reactor and of the operating conditions on the energy yield and volumetric rate of the above reactions were in such a way that if they increase the value of one variable they reduce that of the other. This indicated that there are optimum range of the reactor dimensions and the operating conditions at which the two functions are maximum.

8- The oxidation of methyl mercaptan and of hydrogen sulphide could proceed to completion even at room temperature. Depending upon the operating conditions, mainly corona current, the reactions may take as low as 5 seconds for complete conversion of these compounds.

9- A computer program to evaluate the order of a reaction before previous knowledge of its rate constant was written. It was successfully used to determine the order of the above reactions.

10- The applicability of the Townsend theory to correlate the kinetics of the present chemical reactions. However, this may be extrapolated to conclude any chemical reaction taking place in a corona discharge.

10.2 RECOMMENDATIONS FOR FURTHER STUDY

1- The results reported above admittedly apply only to the experimental set-up and the operating conditions used. Therefore, an obvious follow-up to the present study is to investigate the potential of the corona reactor when using a typical mixture from a kraft mill as feed.

2- Study the effect of scale-up of the reactor on the results. This would prove beneficial to industry since a reliable cost estimation will then be permissible.

3- Design an appropriate experiment by which the existence of the excited species of oxygen and their role in the oxidation processes can be verified. Such an experiment would have to rely on spectroscopic techniques.

REFERENCES

1- Walter, J.E. and H.R. Amberg: "Odor Control In The Kraft Industry", Ch. Eng. Proc., 66(3), (1970).

2- Leonardos,G.,D.Kendall, and N.Bernard: Odour Threshold Determination of 53 Odorant Chemicals, J. Air. Pollution Control Assosc., 19, 91-95 (1969).

3- Sitting, M. : Pulp And Paper Manufacture, Energy Conservation and Pollution, Noyan Data Corporation, New Jersey (1977).

4- Cederlof,R., M.l.,Edfors, L.Friberg, and T.Lindvall: On the Determination of Odour Threshold in Air Pollution Control, J. Air Pollution Control Assosc., 16, 92-4 (1966).

5- Rydholm, S.A. : Pulping Processes, Interscince Publisher, New York (1965).

6- Calkin,J.B., Editor: Modern Pulp and Paper Making, Peinhold Publishing Corporation, 3rd Ed. (1957).

7- Sarkanen, K.V., B.F. Hrutfiord, L.N. Johanson, and H.S. Gardner: Kraft Odor, Tappi, 53(5), 766-83 (1970).

8- Collins,T.T.: Oxidation of Black Liquor, Paper Trade J., 146, 39-48 (1962).

9- Murray,F,E.: Kinetics of Oxidation of Kraft Black Liquor, Tappi 42, 761-7 (1959).

10- De Haas,G.G. and G.A.Hansen: Abatement of Kraft Pulp Mill Odour by Burning, Tappi, 38, 732-8 (1955).

11- Landry,J.E.: Black Liquor Oxidation Practice and Development, Tappi, 46(12), 766-72 (1963).

12- Murray,F.E.: Proceedings of the International Conference on Atmospheric Emissions from Sulphate Pulpings, pp. 184-203, Painter Printing Co., Florida (1959).

13- Silander, R. : Reduction of the Emission of Odorous Compounds in Chemical Pulping, Paperi ja Puu, No 2,1981.

14-White,H.R.: Industrial Electrostatic Precipitation, Addison-Wesley, Mass. (1963).

15-Theodore,L. and A.J.Buonicore: Industrial Air Control Equipment for Particulates, CRC Press, Inc., Ohio (1976).

16- Oglesby jr,S. and G.B.Nichols, Electrostatic Precipitators, Marcel Dekker, Inc., New York (1978).

17- Drossos,A.A.: An Electrochemical Flow Reactor to Control Air from Methyl Mercaptan, M.Eng.Sci. Thesis, The University of Western Ontario, London, Canada,1973.

18- Wiseman,N.: Oxidation In Electric Discharge, Ph.D. Thesis, McGill University, Montreal, Canada (1971).

19- Cullis,C.F. and L.C.Roselaar: The Gaseous Oxidation of Alkline Thiols, Trans. Faraday Soc., 55, 272-79 (1959).

20- Meisoner,M. and H.W.Thompson: The Photolysis of Mercaptans, Trans. Faraday Soc., 34, 1238 (1939).

21- Skerrett,N.P. and H.W.Thompson: The Photolysis of Mercaptans, Trans. Faraday Soc., 37, 81 (1941).

22- Sehon,A.H. and B.DeB. Darment: The Thermal Decomposition of Mercaptans, J.Am.Soc., 76, 4806 (1954).

23-Thompson,C.J., R.A.Meyer, and J.S.Ball: Thermal Decomposition of Sulphur Compounds, J.Am.Soc., 74, 3284-3287 (1952).

24-Harkness,A.C. and F.E.Murray: Gas Phase Oxidation of Methyl Mercaptan, Air Wat. Poll. Int. J., 10, 245-51 (1966).

25-Slagle,I.R., R.E.Graham, and D.Gutman: Direct Indentification of Reactive Routes and Measurements of Rate Constants in the Reactions of Oxygen Atoms with Methanethiol, Ethanethiol, and Dimethyl Sulphide, Int. J. Chem. Kinet., 8, 451-8 (1976).

26- Kirchner,K., R.Vettermann, and H.Indruch: Kinetics of the Reaction with O(3P) Under Consideration of the Influence of Molecular Oxygen, Ber. Bunsenges. Phys. Chem., 82, 1223-30 (1978).

27- Haimsohn,J., J.Bashour, and J.Rabatin: Chem. Abstr. 53:798C (1959).

28- Harkness,A.C., F.E.Murray, and L.Girard: Catalytic Oxidation of Sulphurous Air Pollutants, Atm. Environ., 2, 303-20 (1968).

29- Kokes,R.J., H.Tobin, and P.H.Emmett: New Micro-catalytic Chromatographic Technique for Studying Catalytic Reactions, J. Am. Chem. Soc., 77, 5860-2 (1955).

30- Nametkin,N.S. and V.M.Sobolev: Chem. Abstr. 93:P188,9998 (1979).

31- Denisova,E.P., S.A.,Barisenkova, and T.Danilova: Study of the Oxidation of Some Sulphur-Containing Organic Compounds in the Presence of Phthalocyanine Complex, Chem Abstr. 93:238,770w (1979), From Katal. Sint. Org. Soedin. Sery, 92-5 (1979).

32- Adamis,V.B., C.deFigueiredo, C.Maria, and F.Nogueire: Catalytic Process for Mercaptan Removal from Light Petroleum Distillates, Chem. Abstr. 92:25,260x (1979). From Bol. Tec. Pertobras, 22(3), 183-9 (1979).

33- Kubicek,D.H.: Conversion of Alkane and/or Cycloalkane Thiol to Disulphide with a Catalyst System Comparised of Cobalt Molybdate and an Alkali or Alkaline Earth Metal Hydroxide, Chem Abstr. 95:149,953g (1981). U.S. 4277, 623 (cl. 568-26, C07C149/10), 07 Jul. 1981, Appl. 67,645, 17 Aug. 1979, 5pp.

34- Rayer,H.B. and F.E.Murray: The Photolytic Oxidation of Methyl Mercaptan, Dimethyl Sulphide,a nd Dimethyi Disulphide, Pulp Paper Mag. Can., 71(7), 75-7 (1970).

35- Thompson,H.W. and N.S.Kelland: The Kinetics of the Oxidation of Hydrogen Sulphide, J. Chem. Soc., 1809 (1931).

36- Semenov,N.N.: Some Problems in Chemical Kinetics and Reactivity, Vol. 1, Pergamon Press, New York (1959).

37- Bradley,J.N. and D.C.Dobson: Oxidation of Hydrogen Sulphide in Shock Waves, J. Chem. Phys., 46(8), 2865-71 (1967).

38- Marsden,D.G.H. : A Mass Spectrometric Study of the Oxidation of Hydrogen Sulphide, Can. J. Chem., 41, 2607 (1963).

39- Panov,G.E. and G.V.Starikova: Transformation of Hydrogen Sulphide in Atmospheric Air, Chem. Abstra. 92:46,646t (1979). From Gazov. Prom-St., 9, 26-7 (1979).

40- Singleton,D.L., R.S.Irwin, W.S.Nip, and R.J.Cvetanovic: Kinetics and Mechanism of the reaction of Oxygen Atoms with Hydrogen Sulphide, J. Phys. Chem., 83(17), 2195-200 (1979).

41- Liuti,G., S.Dondes, and P.Hartech: The Reaction of Hydrogen Sulphide and Atomic Oxygen, J. Am. Chem. Soc., 88, 3212 (1966).

42- Gregor,I.K. and I.K.Martin: The Reaction between Ozonized Oxygen and Hydrogen Sulphide in the Gaseous Phase, Aust. J. Chem., 14, 462 (1961).

43- Brewer,A.K. and J.W.Westhaver: Chemical action in the glow discharge. IV The synthesis of ozone, J. Phys. Chem., 34, 1280-93 (1930).

44- Cadle,R.D. and M.Ledford: The Reaction of Ozone with Hydrogen Sulphide, Air&WAt. Pollut. Int. J., 10, 25-30 (1966).

45- Hales,J.M., J.O.Wilks, and J.L.York: The Rate of Reaction between Dilute Hydrogen Sulphide and Ozone in Air, Atm. Environ., 3, 657-67 (1969).

46- Gamson,B.W. and R.H.Elkins: Sulphur from hydrogen sulphide, Chem. Eng. Prog., 49, 203-15 (1953).

47- Swinarski,A. and J. Siedlewski: Influence of pore dimensions on catalytic activity of carbon activated by oxygen for oxidation of hydrogen sulphide, Actes. Congr. Int. Catal. 2nd, 2, 2345 (1961).

48- Steijns,M., F.Derks, A.Verloop, and P.Mars: The Mechanism of the Catalytic Oxidation of Hydrogen Sulphide, J. Catalysis, 42, 87-95(1967).

49- Brodsky,M. and P.Pagny: Oxidation of dilute H2S, Bull. Soc. Chim. Fr., 15, 584 (1948).

50- Cariaso,O.: Oxidation of hydrogen sulphide over porous carbon. Chemical Abstract 80:72468h.

51- Prettre,M. and R.Z.Sion: Catalytic oxidation of hydrogen sulphide in contact with absorbents, Elektrochem. 63, 100, (1959).

52-Sreeramamurthy,R. and P.G.Menon: Oxiadation of hydrogen sulphide on active carbon catalyst, J. Catal., 37, 287-96 (1975).

53- Dudzik,Z. and M.Ziolek: The Specific Catalytic Activity of Faujasites in Hydrogen Sulphide Oxixdation, J. Catal., 51(3), 345 (1978).

54- Thornton,J.D.: Chemical Engineering Aspects of Chemical Synthesis, Adv. Chem. Ser., 80, 372-89 (1969).

55-Willard,H.H., L.L.Merritt,Jr., and J.A.Dean: Instrumental Methods of Analysis, 5th Ed., D. van Nostrand Co., Toronto (1974), Ch. 24.

56- Awad.M.B.: Mechanisms Affecting the Generation of Ozone in Positive, Negative, and A.C. Corona Discharge, M.Eng.Sci. Thesis, The University of Western Ontario, London, Canada (1972).

57- Castle,G.P.S.: Private Communications, Faculty of Engineering Science, The University of western Ontarion, Loandon, Canada.

58- Robinson,M.: Electrostatic Precipitation, from Electrostatics and Its Applications, Ed. D.Moore, John Wiley & Sons, Toronto (1973), Ch. 9.

59- Strauss,W. : Industrial Gas Cleaning, Pergamon Press, New York, pp. 393 (1966).

60- Loeb,L.B.: Electrical Corona: Their Basic Physical Mechanism, University of California Press, Berkeley, U.S. (1964).

61- von Engel,A.: Ionized Gases", The Clarendon Press, Oxford, U.K. (1965).

62- Levitt,L.S. and B.W.Levitt: Inductive Effects on Molecular Ionization Potentials, IV: Hydrogen Sulphide and Mercaptans, J. Org. Chem., 37(2), 322 (1972).

63- Suzuki,M.: "Electrification of Particles in Corona Glow Region in Air and Other Gases", M.A.Sc. Thesis, The University of Western Ontario, London, Canada (1976).

64- Robinson,M.: A history of the electric wind, Am. J. Phys., 30, 366 (1962).

65- Robinson,M.: Movement of Air in the Electric Wind of the Corona Discharge, Trans. Am. Inst. Elect. Engrs., 801, 143-50 (1961).

66- Peek,F.W.: Dielectric Phenomena in High Voltage Engineering, 3rd, Ed., McGraw-Hill Co., New York (1929).

67- Townsend,J.S.: Electricity in Gases, Oxford University Press, New York (1914).

68- Cobine,J.D.: Gaseous Conductors: Theory and Engineering Applications, Dover Publications, Inc., New York (1958).

69- Awad,M.B. and G.S.P.Castle: Ozone Generation in an Electroctrostaic Precipitator with a Heated Corona Wire, J. Air Poll. Assoc., 25(4), 369-74 (1975).

70- Castle,G.S.P.: Electrostatic Precipitation in Electrified Media and Positive Corona Ozone Generation in the Design of High Efficiency Air Cleaners, Ph.D. Thesis, The University of Western Ontario, London, Canada (1969).

71- Lunt,R.: Some Problems of the Kinetics of Discharge

72- Howatson, A.M.:An Introduction of Gas Discahrge, 2nd ed., Pergamon International Library (1976).

73- Dalgarno,A.: Inelastic Collisions at Low Energies, Can. J. Chem., 47, 1723-29 (1969).

74- Kondrate'v,V.N.: Chemical Kinetics of Gas Reactions, Pergamon Press, New York (1964), pp.483.

75- Spedding,P.L.: Chemical Reactions in Non-Disruptive Electric Discharge, The Chem. Eng., Jan/Feb CE17-50 (1969).

76- Reid,C.: Excited States in Chemistry and Biology, Butterworths Sci. Publications, London, U.K. (1957),

77- Wooley,G.L. and R.J.Cvetanovic: Production of Hydrogen Atoms by Photolysis of Hydrogen Sulphide and the Rates of their Addition to Olefin, J. Chem. Phys., 50, 4697 (1969).

78- Yardly, J.T.: Dynamic properties of electronically excited molecules, in Chemical and Biochemical Applications of Lasers, Vol I, Ed. C.B. Moore, Academic Press (1974), Ch. 8.

79- Fite,W.L.: Positive Ion Reactions, Can. J. Chem., 47, 1797-807 (1969).

80- Ferguson,E.E.: Negative Ion-Molecule Reactions, Can. J. Chem., 47, 1815-20 (1969).

81- Field,F.H. and J.L. Franklin: Electron Impact Phenomena, Academic Press, New york (1957).

82- Willard,H.H., L.L.Merritt Jr., and J.A.Dean: Instrumental Methods of Analysis, 5th Ed., D. van Nostrand Co. , Toronto (1974), Ch.6, 8, and 16.

83- The Aldrich Library of NMR Spectra, Aldrich Chemical Co., Inc., Wisconsin (1980).

84- Cymerman,J. and J.Willis: Infra-red Spectra and Chemical Structure of Some Atomic Disulphides, Disulphones, and Thiosulphonates, J. Chem. Soc., 1332 (1951).

85- Bernard,D., J.M.Fabian, and H.P.Koch: Valence Vibration Frequencies and Hydrogen Bond of Sulphoxide and Sulphone Groups, J. Chem. Soc., 2443 (1949).

86-Bodyrev,V.G., L.P.Slesarchuk, E.E.Gatala, T.A.Trafimova, and E.N.Vasenko: Studies in the Field of Thiosulphonic Acids, J. Org. Chem. USSR, 2, 91 (1966).

87- Cross,A.D.: An Introduction to Practical Infra-red Spectroscopy, London, U.K. (1969), pp. 95

88- Scott,D.W. and J.P.McCullough: Characteristic Vibrational Frequencies of Organic Sulphur Compounds, J. Am. Chem. Soc., 80, 3554 (1958).

89- Cross,A.D.: An Introduction to Practical Infra-red Spectroscopy, London, U.K. (1969).

90- ibid, pp.94.

91- Trotter, andThompson: The infra-red spectra of thiols, sulphides, and disulphides, J. Chem. Soc., 48 (1946).

92- Sheppard,N. : The vibrational spectra of some organic sulphur compounds and the characteristic frequencies of C-S linkages, Trans. Faraday Soc., 46, 429 (1950).

93- The Aldrich Library of IR Spectra, Aldrich Chemical Co., Inc., Wisconsin (1980).

94- The Aldrich Catalog Handbook of Organic and Biochemicals, Aldrich Chemical Co., Inc., Wisconsin (1978), pp.537.

95- Adamson,A.W.: A Text Book Of Physical Chemistry, Academic Press, New York (1973).

96- Bellamy,L.J.: The Infra-red Spectra of Organo-Sulphur Compounds, From Organic Sulphur Compounds, Ed. N.Kharasch, Vol. I, Pergamon Press, New York (1961),

97- Wilson,C.L. and D.W.Wilson: Ed. Comprehensive Analytical Chemistry, Classical Analysis, Vol.I, Part A, Elsevier Publishing Co., (1959).

98- Fresenius,C.R.: Manual of Qualitative Chemistry Analysis, John-Wiley & Sons (1904).

99- Kolthoff,I.M. and R.Belcher: Volumetric Analysis, V III, John Wiley&Sons (1957).

100- KimballJ,W. R.L.Kramer, and E.E.Reid: The iodometric estimation of mercaptans, J. Amer. Chem. Soc., 43, 1199-201 (1921).

101- Karchmer,J.H., Ed.: The Analytical Chemistry of Sulphur and its Compounds, Part 1, Wiley-Interscience, New York (1970).

102- Worthing,A.G. and J.Geffner: Treatment of

Experimental Data, John Wiley & Sons, Inc., New York (1943).

103- McNair,H.M. and E.J.Bonelli: Basic Gas Chromatography, Varian Aerograph, Lithographed by Consolidated Printers (1969).

104- Simpson,G.: Gas Chromatography, Kogan Page, N.Y. (1970).

105- Levenspiel,O.: Chemical Reactions Engineering, John-Wiley & Sons (1967).

106- Smith,J.M.: Chemical Engineering Kinetics, McGraw-Hill Book Company, New York (1981), Ch.3.

107- Cullis,C.F. and L.C.Roselaar: The Gaseous Oxidation of Dimethyl Disulphide, Trans. of Faraday Soc., 55, 1562-64 (1959).

108- Reid,E.E.: Organic Chemistry of Bivalent Sulphur, Vol.I, Chemical Publications Co., New York (1958).

109-Tarbell,D.S.: The Mechanism of Oxidation of Thiols to Disulphides, From Organic Sulphur Compounds, Ed. N.Kharasch, Vol.I, Ch. 10, Pergamon Press, Inc. (1961).

110- Oae,S,Ed.: Organic Chemistry of Sulphur, Plenum Press, New York (1977).

111- Foss,O.: Ionic Scission of the Sulphur-Sulphur Bond, from organic Sulphur Compounds, op. cit., Ch. 9.

112- King,J.: Private communications. Faculty of Chemistry, The Univessity of Western Ontario, London, Canada.

113- Schonberg,A. and M.Z.Barakat: Organic sulphur compounds. XXXII. The action of triphenylphoshine od organic sulphide, J. Chem. Soc., &&&,892 (1949).

114- Bernard,D.: Oxidation of Organic Sulphides, Part IX: The Reactions of Ozone with Organic Sulphur Compounds, J. Chem. Soc., &&&,4547-55 (1957).

115- Bernard,D. L.Bateman, and J.I.Cunneen: Oxoidation of Organic Sulphides from Organic Sulphur Compounds, Ed. N.Kharasch, op. cit., Ch. 21.

116- Isenberg,N. and M.Grdinic, Thiosulphonates, Int. J. Sulph. Chem., 8, 307 (1973).

117- Shelton,J.R. and K.E.Davis: Decomposition of Sulphoxides III, Int. J. Sulph. Chem., 8, 217 (1973).

118- Kice,J.L.: Desulphonylation Reactions, from The Chemistry of Organic Sulphur Compounds, Ed. N.Kharasch and C.Y.Meyers, Vol.II, Ch. 5, Pergamon Press, Inc. (1966).

119- Kice,J.C. and F.M.Parham: The thermal decomposition of thiosulphates II, J. Am. Chem. Soc., 82, 6168 (1960).

120- Winstein,S., A.Gagneux, and W.G.Young: Rearrangement of allylic azides, J. Am. Chem. Soc., 82, 5956-7 (1960).

121- Smith,S.G.: Rearrangement of allylic thiobenzoates, J. Am. Chem. Soc., 83, 4285-7 (1961).

122- Strating,J.: The Sulphur Group and Its Effects in Organic Compounds, From Organic Sulphur Compounds, op. cit., p. 146.

123- Coffman,J.A.: Corona chemistry, Scietific American, June (1965) p.91.

124- Byers,D.H. and B.E.Saltzman: Determination of Ozone in Air by Neutral and Alkaline Iodide Procedures, Adv. Chem. Ser., 21, 93-101 (1959).

125- Devins,J.C.: Mechanism of Ozone Formation in the Silent Electric Discharge, J. Electrochem. Soc., 103, 460-6 (1956).

126- Makin,b. and I.I.Incult: Generation of ozone from heated positive corona wires for electrostatic charging, IEEE-IAS Conf. on Electrostatics, Milwaukee, 381-89 (1973).

127- White,H.J. and W.H.Cole: Design and performance characteristics of high velocity, high efficiency air cleaning, 10(3), 237-45 (1960).

128- Benson,S.W. and E.Axworthy,Jr.: Mechanism of the Gas Phase, Thermal Decomposition of Ozone, J. Chem. Phys., 26(6), 1718-26 (1957).

129- Davidson,R.C.: Ozone Formation in Gas Discharge, IEEE-IAS Annual Meeting, Toronto, 152-5 (1978).

130- Benson,S.W. and A.E.Axworthy,Jr.: Implications of Data on the Gas Phase Decomposition of Ozone, Adv. Chem. Ser, 21, 398-404 (1958).

131- Benson,S.W.: Kinetic considerations of efficiency of ozone production in gas discharge, Adv. Chem. Ser., 21, 405-9 (1958).

132- Maggiolo,A. and A.Blair: Ozone Oxidation of Sulphides and Sulphoxides, Ozone Chem. and Tech., Adv. Chem. Ser,

21, 200-1 (1959).

133- Inoue,E. and K.Sugino: Inhibiting Action of Hydrocarbons on Ozone Formation by Silent Electrical Discharge, Adv. Chem. Ser., 21, 313-6 (1959).

134- Schiff,H.I.: Neutral Reactions Involving Oxygen and Nitrogen, Can. J. Chem., 47, 1903- (1969).

135- Bailey,P.S., S.S.Bath, and J.B.Ashton, Initial Attack of Ozone on an Unsaturated System, Adv.Chem.Ser., 21, 143-52 (1959).

136- Schlumbohm,H.: StoBionisierungskoeffizient a, mittlere Elektronenenergien und die Beweglichkeit von Elektroner in Gasen, Z. Physik, 184, 492-505 (1965).

137- Emele'us,K.G., R.Lunt, and C.A.Meek: Ionization, excitation, and chemical reaction in uniform electric field I, Proc. Roy. Soc. A156, 394-&&&(1936).

138- Llewellyn-Jones,F.: The Glow Discharge, Methuen, London, U.K. (1966).

139- Lunt,R. and C.A. Meek: Ionization, excitation, and chemical reaction in uniform electric field II, Proc. Roy. Soc. A157, 146-&&&(1936).

140- Lunt,R.: Some probless of the kinetics of discharge reactions, Adv. Chem. Ser., 80, 452-506 (1969).

141- Peterson,L.R., S.S.Prasad, and A.E.S.Green: Semi Empirical Electron Impact-Cross-Sections for Atmospheric Gases, Can. J. Chem., 47, 1774-77 (1969).

142- Massey,H.S.W.: Negative Ions, Cambridge University Press, London, U.K. (1976).

143- Watson,C.E., V.A.Dulock, R.S.Stolarski, and A.E.S.Green: Electron Impact Cross-Sections for Atmospheric Species. 3: Molecular Oxygen, J. Geophys. Res., 72, 3961-&&&(1967).

144- Noyes,W.A. and P.A.Leighton: The Photochemistry of Gases, Reinhold, New York (1941).

145- Stolarski,R.S., V.A.Dulock, C.E.Watson, and A.E.S.Green: Electron Impact Cross-Sections for Atmospheric Species. 2: Molecular Nitrogen, J. Geophys. Res., 72, 3953-(1967).

146- Luiti,G., S.Dondes, and P.Harteck: The reaction of Hydrogen Sulphide and Oxygen, J. Am. Chem. soc., 88,

3212 (1966).

147- Wayne,R.P.: Laboratory Studies on the Activation and Deactivation of Singlet Oxygen, Ann. N. Y. Acad. Sci., 171 (Art. 1), 199 (1970).

148- Krassovsky,V.I., N.N.Shefov, and V.I.Yarin: Atlas of the Air-Glow Spectrum, Planetary Space Sci., 9, 883 (1962).

149- Ranby,B. and J.E.Rabek, Ed.: Singlet Oxygen: Reactions with Organic Compounds and Polymers, John Wiley Sons, Inc, New York (1978).

150- McDaniel,E.W., V.Cermak, A.Dalgarno, E.E.Feruson, and L.Friedman: Ion-Molecule Reactions, Wiley-Interscience, Inc., New York (1970).

151- Bird,R.B., W.E.Steward, and E.N.Lightfoot: Transport Phenomena, John Wiley Sons, New York (1960).

152- Kronbelb,S. and M.W.P.Stradberg: Use of paramagnetic resonance techniques in the study of atomic oxygen combinations, J. Chem. Phy., 31(5), 1169 (1959).

153- Debigh,K.G.: Velocity and yield in continuous reaction systems, Trans. Faraday Soc., 40, 352-6 (1953).

154- Wen,C.Y. and L.T.Fan: Models for Flow Systems and Chemical Reactions, Marcel Dekker, Inc., New York (1975).

155- Castle,G.S.P., I.I.Inculet, and K.I.Burgess: Ozone generation in positive corona electrostatic precipitatore, IEEE Trans. on Industry and General Applications, IGA-5(4), 489-96 (1969).

156- Burges,K.I.: Ozone generation in Electrostatic precipitators, E.S. 400 Project Report, Faculty of Engineering Science, The University of Western Ontario, London, Canada (1968).

157- Freund,J.E.: Modern Elementary Statistics, 3rd. ed., Prentice-Hall, Inc., New Jersey (1967).

158- Nie,N.H., O.H.Hull, J.G.Jenkins, K.Steinbrenner, and D.A.Bent, Statistical Package for the Social Sciences, 2nd ed., McGraw-Hill Book Co., New York (1975).

159- Thornton,J.D.: Chemical Engineering Aspects of Chemical Synthesis, Adv. Chem. Ser., 80, 372-89 (1969).

160- Thornton,J.D., W.D.Charlton, and P.L.Spedding: Hydrazin Synthesis in a Silent Electrical Discharge, Adv.Chem.Ser., 80, 165-75 (1969).

161-Clifford,A.F.: Inorganic Chemistry Qualitative Analysis, Prentice-Hall, Inc., Englewood Cliffs, New Jersey (1961), pp.13-4.

162- Adamson,A.W.: A Text Book of Physical Chemistry, Academic Press, New York (1973), pp. 91-8.

163- Berger,G. and M.Goldman: Nature of ions and influence of humidity in air, IEEE Power Eng. Soc., Summer Meeting Papers, 65-8 (1974).

164- Sarma,M.P. and W.Janischewekyj: D.C. corona on smooth conductors in air, Proc. IEE, 116(1), 161-6 (1969).

165- Perry,R., C.Chilton, and F.Kirkpatrick: Chemical Engineers' Handbook, 4th ed.,, McGraw-Hill Co., New York (1963).

166- Pierre,D.A.: Optimization Theory with Applications, John Wiley Sons, New York (1969).

167- Maron,F. and C.Prutton: Principles of Physical Chemistry, 4th ed., Macmillan Co., (1965).

168- Schlichting,H.: Boundry-Layer Theory, 7th ed., McGraw-Hill Co., New York (1979).

169- Jenson,V.G. and G.V.Jeffreys: Mathematical Methods in Chemical Engineering, Academic Press (1972).

170- Smith,G.D.: Numerical Solutions of Partial Differential Equations, Oxford University Press, U.K. (1971).

171- Carnahan,B., H.A.Luther, and J.O.Wilkes: Applied Numerical Methods, John Wiley Sons (1969).

172- Cleland,F.A. and R.H.Wilhelm: Diffusion and reaction in viscous-flow tubular reactor, A.I.Ch.E. J., 2(4), 489-95 (1956).

173- Vignes,J.P. and P.J.Trambouze: Diffusion et reaction chimique dans un reacteur tubulaire en regime laminaire, Chem. Eng. Sci., 17, 73-86 (1962).

174- Dean,J.A. Ed.: Lange's Handbook of Chemistry, 7th ed., McGraw-Hill Book Co., New York (1973).

175- Pappas,D.C.: Corona Discharge and Sulphur Removal from Gases, M.E.Sc. Thesis, The University of Western Ontario, London, Canada (1972).

176- Fite,W.L.: Chemical Physics of discharges, Adv. Chem. Ser., 80, 1-17 (1969).

APPENDIX A

Calculation of Mean Residence Time of Gases through Electrostatic Precipitator

Basis: 1 s

Maximum flow rate = 120 m^3/s

Length of precipitator = 6m

Then

Height of precipitator = 3m

Total cross section area (A)=

$= Q/v = 120/1.2 = 100.0 m^2$

If width of a duct (assumed) t = 0.25 m

Then, Number of ducts (N) = W/t

= 33.3/0.25 = 133

and, flow rate per duct (q) = Q/N

= 120/133 = 0.90 m^3/s

Therefore, the velocity (v) = q/Hxt

= 0.90/(3x0.25) = 1.2 m/s

and the contact time (t) = L/v

= 6/1.2 = 5 s

A check on these numbers was done by calculating the

collecting area required. This is illustrated as follows:

The calculated collecting area

$$= 2 \times H \times L \times Q/1000$$

$$= 575\ m^2/1000m^3$$

which is within the practical range (14,1[illegible].

APPENDIX B

B1: Preparation of Mixture of the Sulphur Compounds and Nitrogen

A sulphur compound in the present appendix will be one of the following compounds: methyl mercaptan, hydrogen sulphide, dimethyl sulphide, and dimethyl disulphide.

A mixture of the sulphur compound and nitrogen was prepared by withdrawing a sample of the sulphur compound from the respective bottle using a Hamilton gas-tight syringe. The sample was then injected in the mixture bottle which was then pressurized with nitrogen gas.

In order to prevent contamination of the methyl mercaptan or hydrogen sulphide mixtures and nitrogen, each mixture was prepared as follows (refer to Figure B.1):

1- The exit of the lecture bottle containing the sulphur compound was first sealed by a rubber septum S1 and a Swag-Lok.

2- The needle tip of the syringe was inserted through about half the thickness of another rubber septum S2.

3-By tight-pressing the surfaces of the two septa against one another, the needle was pushed all the way through the septa into the exit tubing of the bottle.

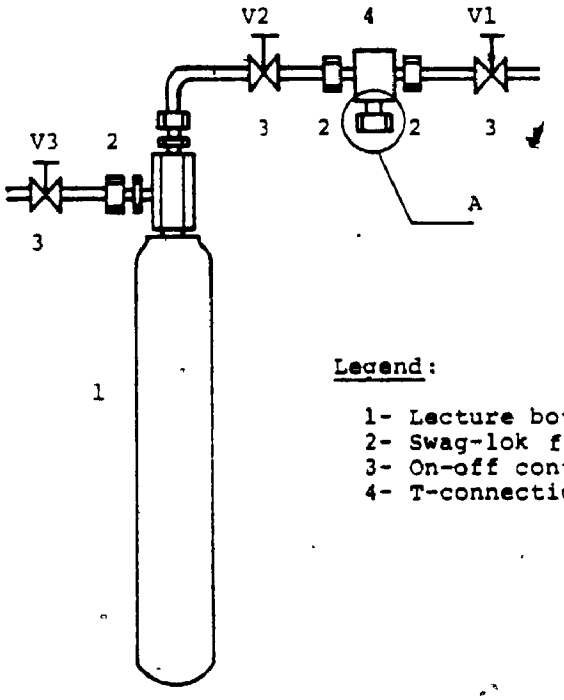

Legend:

1- Lecture bottle.
2- Swag-lok fittings.
3- On-off control valves.
4- T-connection.

Section A:

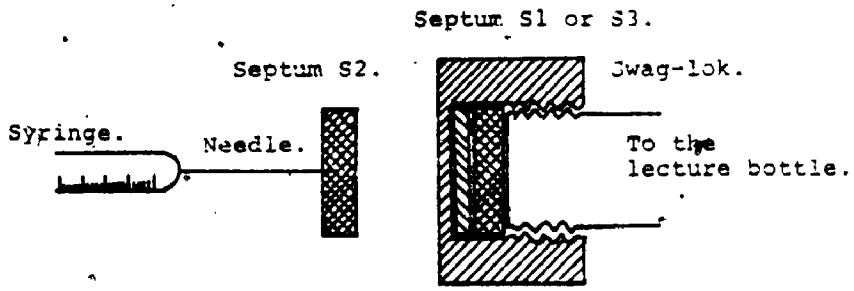

Figure B.1: Schematic diagram showing the mixture bottle and the injection arrangement.

4- The lecture bottle valve was turned on.

5- By removing the plunger completely from the syringe, the syringe could be flushed by the gaseous sulphur compound flowing under the inside pressure of the bottle.

6- By returning the plunger to the syringe and holding it in place by finger-force, a sample of the sulphur compound could be trapped inside the syringe.

7- Still forcing the septa surfaces' tight together, the needle was pulled back to its original position (i.e., half-way the thickness of septum S2).

8- In the mean time, the mixture bottle was flushed with nitrogen gas under atmospheric pressure.

9- Between valves V1 and V2, a T-connection was installed and sealed by means of a rubber septum S3 and a Swag-Lok. The syringe was placed in such position that the surfaces of septa S1 and S3 were touching. By tight-pressing the two septa together, the sample was injected into the mixture lecture bottle.

10- Turn on valve V1 and then valve V2 so that nitrogen gas was allowed (under pressure) into the mixture bottle.

By adjusting the amount of the sulphur compound trapped inside the syringe and the pressure of the nitrogen gas cylinder, a mixture within the desired range of compostion was prepared. However, the accurate composition was determined by the chromatographic analysis.

B2: Specifications of and Calibration Curves for the Rotameters used in the Experimental Apparatus

B2.1 Rotameters for Feed Mixtures:

In reference to Section 4.2 in the text, two precision rotameters (R1 and R2) were used to monitor the flow rate of the sulphur compound/nitrogen mixture and the air, respectively. It should be mentioned that for higher flow rates of gases through the reactor (higher than 14×10^{-6} m^3/s) rotameter R2 was replaced by or connected in pararell with another precision rotameter R3 having higher flow rates capacity. The specifications of rotameters R1, R2, and R3 are given in Table B.1 below.

Rotameters R1 and R2 were calibrated in the laboratory at the prevailing conditions of temperature and pressure with a standard soap-bubble flowmeter provided with the gas chromatograph instrument. Rotameter R3 was on the other hand calibrated by a precision wet-test meter, provided by GCA/Precision Scietific, Chicago, USA).

The calibration curves obtained were then standarized at 298 K and 101 kPa using the ideal gas equation:

$$Q_s = \frac{298\ Q_m\ P_m}{101\ T_m}$$

where subscript s refers to the standard conditions 298 K and 101 kPa while subscript m refers to the quantities measured at the time of calibration. The calibration curves are given in Figures B.2, B.3a, and B.3b.

B2.2 Rotameters Required for the Operation of the Flame Ionization Detector:

Two rotameters (R4 and R5) were required to monitor air and hydrogen to the flame ionization detector of the gas chromatograph. They were supplied by Fisher and Porter Co. of canada Limited and their specifications are also listed in Table B2.1. The rotameters were calibrated also with the soap-bubble flowmeter and standarized at 298 K and 101 kPa as discussed above. The results obtained are shown in Figure B.5.

On the other hand, flow rate of helium to the operating and the reference colums of the gas chromatograph were determined at their exit with the soap-bubble flowmeter at a given inlet presssure (usually 65 psig). The rotameters provided with the chromatograph were consulted only for relative readings. During experiments where temperature programming conditions were in effect, these flow rates were found to drop. This was due to in the rise in pneumatic resistance in the colums brought about by the increase in helium viscosity with temperature. Nevertheless, no adjustment was made to correct for this drop.

CH3SH

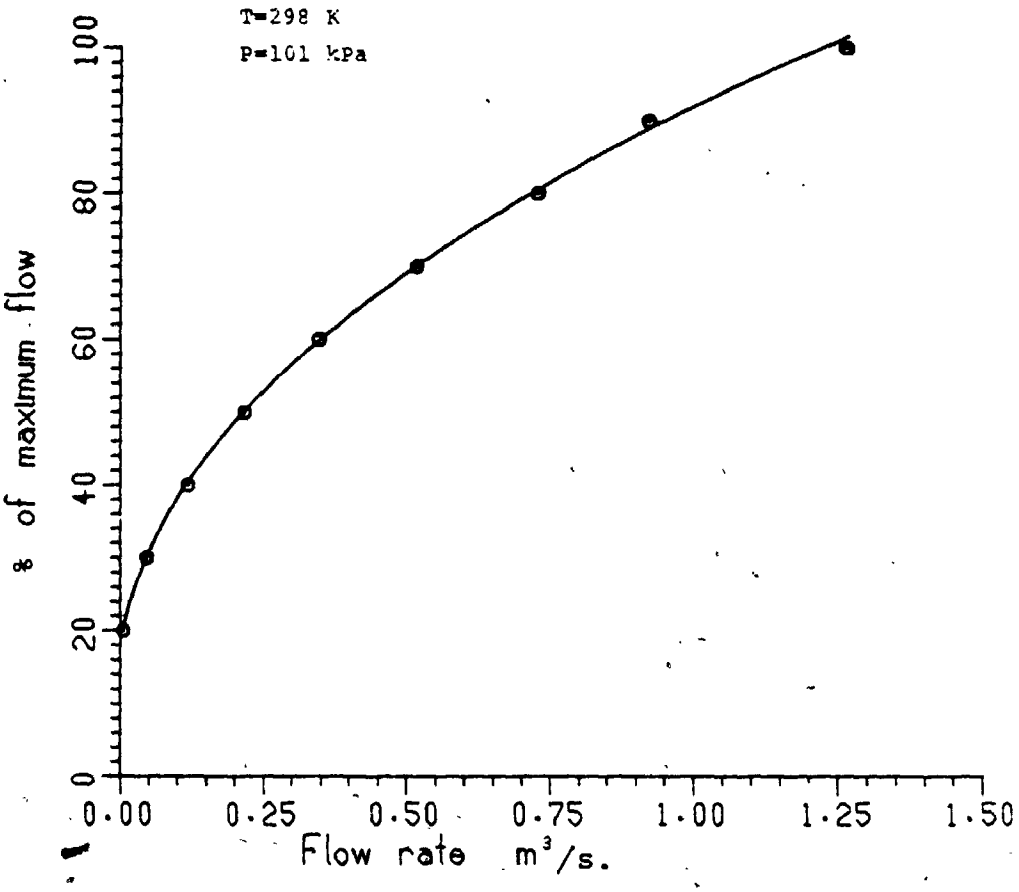

Figure B.2: Calibration curve of rotameter R1 to monitor the flow rate of the sulphur compound/nitrogen mixtures to the reactor.

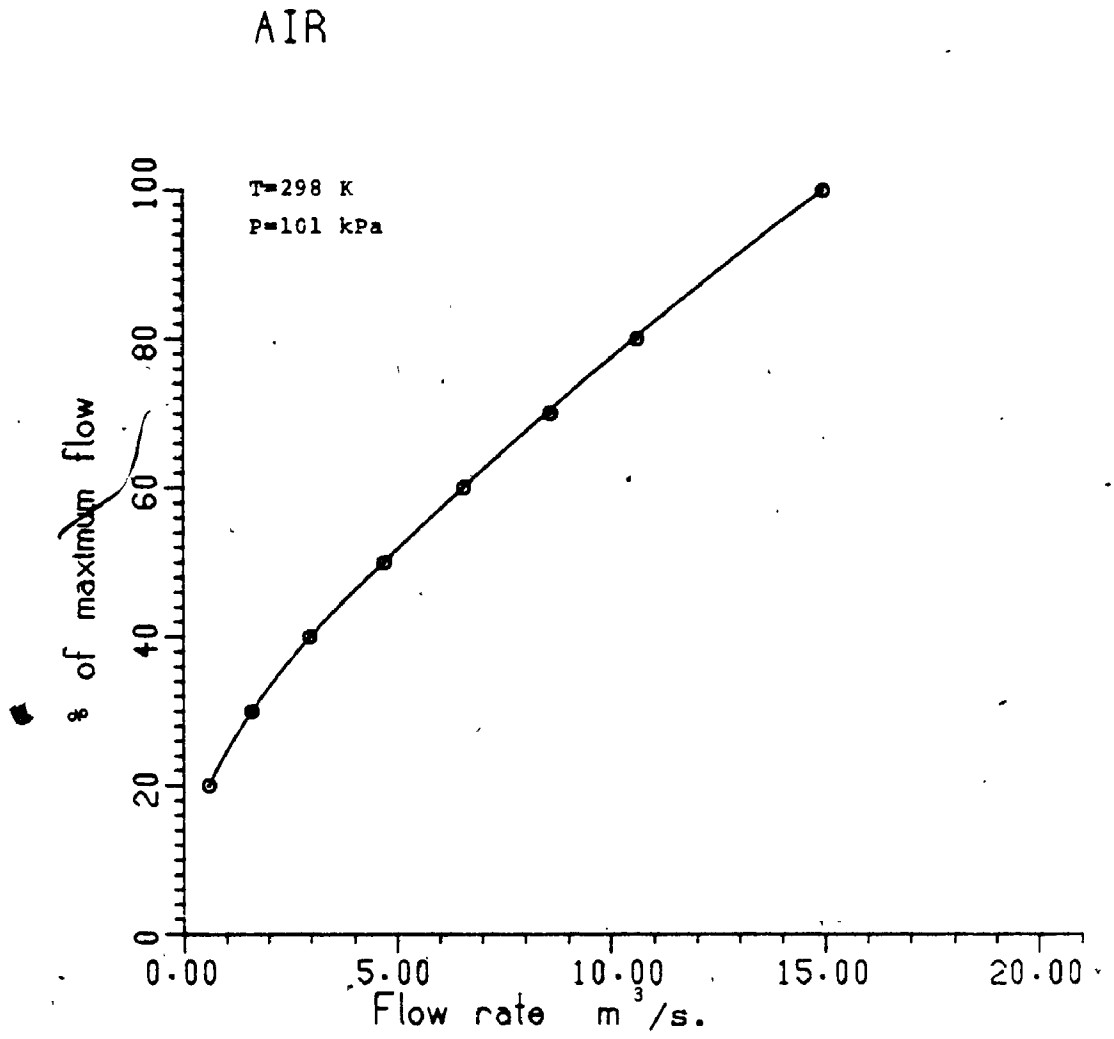

Figure B.3a: Calibration curve of rotameter R2 to monitor low flow rates of air to the reactor.

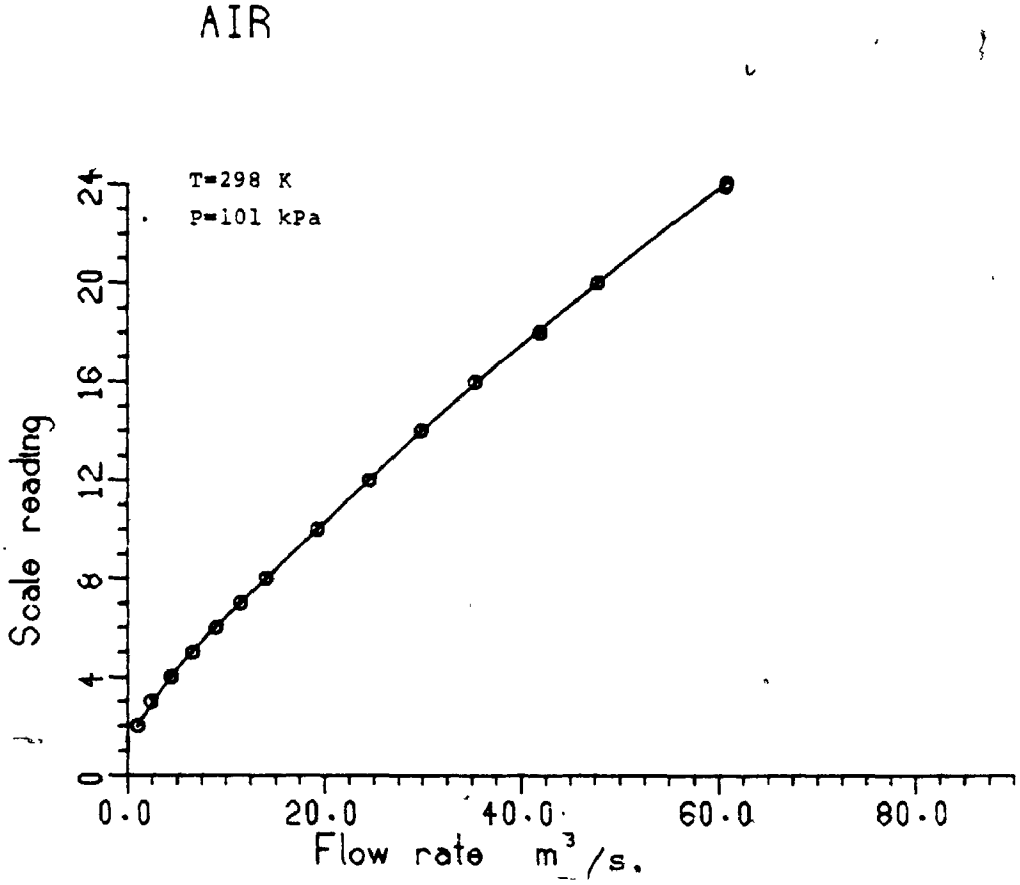

Figure B.3b: Calibration curve of rotameter R3 to monitor high flow rates of air to the reactor.

FID

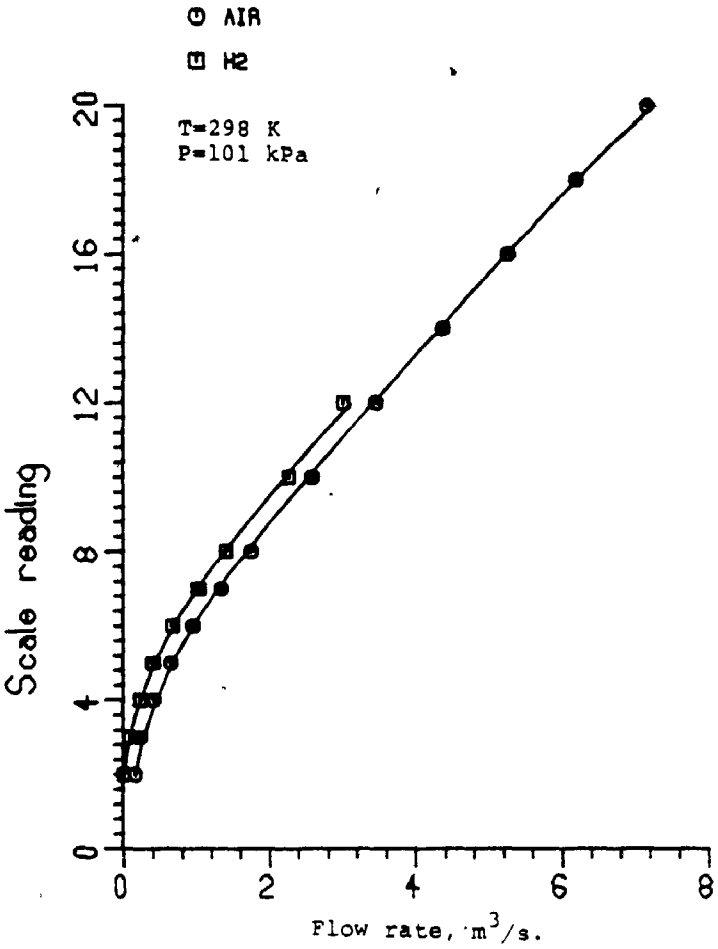

Figure B.5: Calibration curves of the rotameters monitoring the flow rate of air and hydrogen to the flame ionization detector.

TABLE B.1: SPECIFICATIONS OF THE ROTAMETERS EMPLOYED IN THE EXPERIMENTAL APPARATUS.

Rotameter	Tube	Float	Maximum flow rate at 298K and 101 kPa ($m^3 x 10^6/s$)	Accuracy at maximum flow rate.
R1	FP-1/16-10-G-5*	Sapphire	1.25	±1%
R2	FP-1/8-08P3/37*	Stainless steel	14.95	±2%
R3	FP-1/8-25-G-5*	"	61.00	±3%
R4	FP-1/16-10-G-5*	"	2.30	±1%
R5	FP-1/16-20-G-5*	"	7.1	±2%

* Tri-flat meters supplied by Fisher and Porter Co. of Canada Limited.

B3: The Minimum Average Drift Velocity of the Charged Particles

The average drift velocity v' (m/s) of charged particles moving in an electrical field of strength having an average value of E' (V/m) may be determined from the relation [68]:

$$v' = b' E' \qquad (B.1)$$

where b' is the average value of the particles mobility.

A value for E' may be obtained from [70]:

$$E' = \frac{E_c + E_g}{2} \qquad (B.2)$$

where E_c and E_g are the electrical field strength (V/m) at the wire surface and the ground electrode, respectively.

Referring to Section 4.3 in the text, E_c was found in the order of 25×10^6 V/m. Assuming a zero value for E_g (E_g is usually higher than zero), a minimum value of 12.5×10^6 V/m was obtained for E'.

Taking b' equal to 1.96×10^{-4} $m^2/V.s$ (see the text), a minimum average value for v' is 2,450 m/s.

B4: Estimation of the Average Mobility b' of the Charged Particles

Referring to Flow Diagram B.6, the procedure of estimation bo', that is the average mobility of the charge particles at 273 K and 101 kPa, may be summarized as follows:

1- Assume a value b' (where $i=1,2,....I$) for b'. Substitute this value into equation (3.6):

$$\Phi = \left(\frac{R}{E_c\, a}\right)^2 \left(\frac{I_c}{2\,\pi\, H\, \varepsilon\, b'}\right)^2 \qquad (3.6)$$

By substituting every single value observed of other parameters of equation (3.5) such as I_{c_j} (where $j=1,2, \ldots ,J$) in the equation, generate a set of Φ_{ij} values.

2- Substitute Φ_{ij} values into equation (3.5):

$$\frac{V_s - V_c}{V_c} \ln(R/a) = (1+\Phi)^{\frac{1}{2}} - 1 - \ln\frac{1+(1+\Phi)^{\frac{1}{2}}}{2} \qquad (3.5)$$

and obtain another set $V'_{s_{ij}}$ for the estimated voltage.

3- From every individual value of set $V'_{s_{ij}}$, subtract the corresponding value of the observed applied voltage V_{s_j}:

$$\Delta V_{s_{ij}} = V'_{s_{ij}} - V_{s_j} \qquad (B.3)$$

4- Square the $\Delta V_{s_{ij}}$ values and add them up so that a set DV_i is formed:

$$DV_i = \sum_{j=1}^{J} (\Delta V_{s_{ij}})^2 \qquad (B.4)$$

Note that each value of DV_i is correspondent to the value $b_o' i$.

5- Repeat steps 1 to 4 for several values of b_o'.

6- Minimize DV_i against b_o'. The value b_o' which produces the minimum DV_i is the representative value of the mobility b_o' of the charged particles [165].

According to the calculations (performed using computer) Figure B.7 was constructed and a value of $(1.96 \pm 0.03) \times 10^{-4}$ m/V.s was obtained for b_o'.

Using the above average mobility, the deviation between the experimental values V'_{s_k} and those predicted V_{s_k} was evaluated from:

$$\Delta V = \sum_{k=1}^{K} \frac{V'_{s_k} - V_{s_k}}{V_{s_k}} \times 100\% \qquad (B.5)$$

and it was found equal to ±8%.

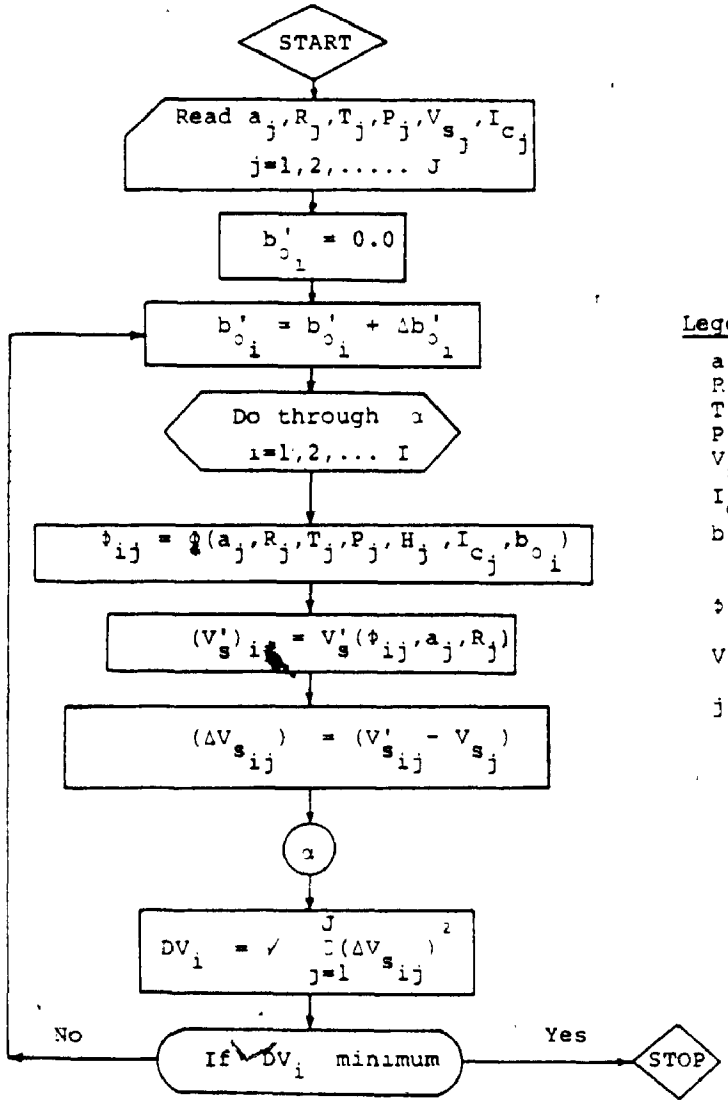

Legend:

a = corona wire radius (m).
R = reactor radius (m).
T = reactor temperature (K).
P = atmospheric pressure (Pa).
V_s = applied voltage (V).
I_c = current (A).
b'_o = average mobility of charged species at 273 K and 101 kPa.
ϕ = function calculated from equation (3.6).
V'_s = voltage calculated from equation (3.5).
j and i are counters.

Figure B.6: Flow diagram for evaluating the average mobility of the charged particles in the corona reactor at 273 K and 101 kPa.

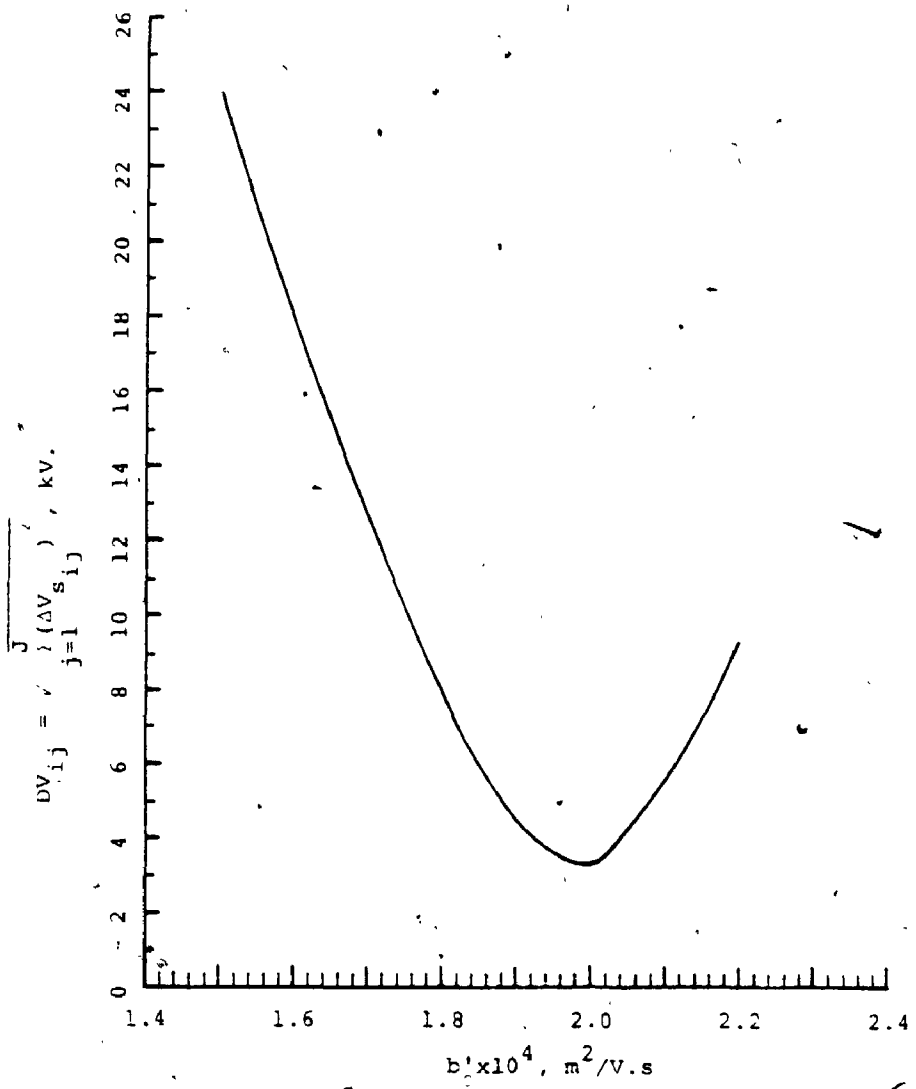

Figure B.7: The mobility b' as a function of the square root of the difference between the voltage estimated from equation (3.5) and that observed.

B5: Control of Axial Temperature Profile in the Reactor

Heating the reactor to a certain temperature was provided by placing the reactor in a Marshall cylindrical furnace (see sub-section 4.2.3).

The furnace (Figure B.8) was provided with a shunt panel on which "shunt posts" were placed. By attaching shunt wires of correct values between the posts, any desired uniformity of temperature along the furnace length could be attained. The procedure followed to accomplish this task may be summarized as follows:

1- Make an iron-constantan thermocouple by welding the junction with an oxy-acetylene Torch and borax as a flux. The thermocouple was calibrated against room temperature 298 K, boiling water 373 K, and boiling aniline 457 K. Then, shield the thermocouple with a glass tubing open from both ends.

2- Assemble the reactor and place it in the furnace tube. Then, close both ends of the furnace as tightly as possible using heat - resistant wool. This prevented a thermal draft up through the bore of which would upset good temperature control within the furnace.

3- Heat the furnace to the test temperature and allow

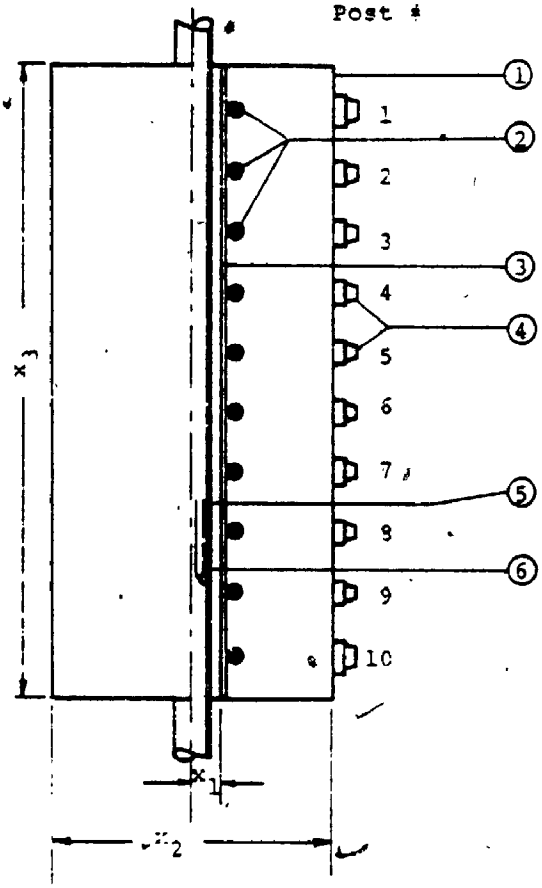

Legend:

1- Outer shell.
2- Heating elements.
3- Inner furnace tube.
4- Shunt posts.
5- Reactor tube.
6- Thermocouple.

x_1= 63.5 mm.
x_2=254 mm.
x_3=406 mm.

Figure B.8: Schematic diagram of the furnace.

sufficient time to reach thermal equilibrium. The temperatures of interest attempted were 325, 373, 423, and 453 K.

4- Pass a stream of air in the same manner as in actual experiments. Two flow rates were tried: 2×10^{-6} and 32×10^{-6} m3/s which represented the minimum and maximum of the range of interest.

5- Position the thermal junction of the thermocouple inside the reactor at given points along its length and take the temperature readings making sure that steady state thermal conditions were obtained. A curve representing the axial temperature profile can be quickly sketched. This curve shows at a glance where shunts must be done. The results summarized in Table B.2 show the positions and resistances of the shunt wires used.

The axial temperature profiles of the reactor at the temperatures attempted are shown in Figure B.9. As indicated from the above figure, excellent isothermal conditions along the reactor length were achievable.

TABLE B2: POSITION AND RESISTANCE OF SHUNT WIRES USED TO OBTAIN ISOTHERMAL CONDITIONS AT THE TEMPERATURES OF INTEREST

Between taps	Shunt resistance (ohm)	
	323 and 373 K	423 and 453 K
1 - 2	9.2	9.1
2 - 3	7.1	7.0
3 - 4	5.3	5.3
4 - 5	4.8	4.4
5 - 6	3.8	3.6
6 - 7	4.5	4.2
7 - 8	5.1	4.9
8 - 9	6.8	6.8
9 - 10	9.6	9.6

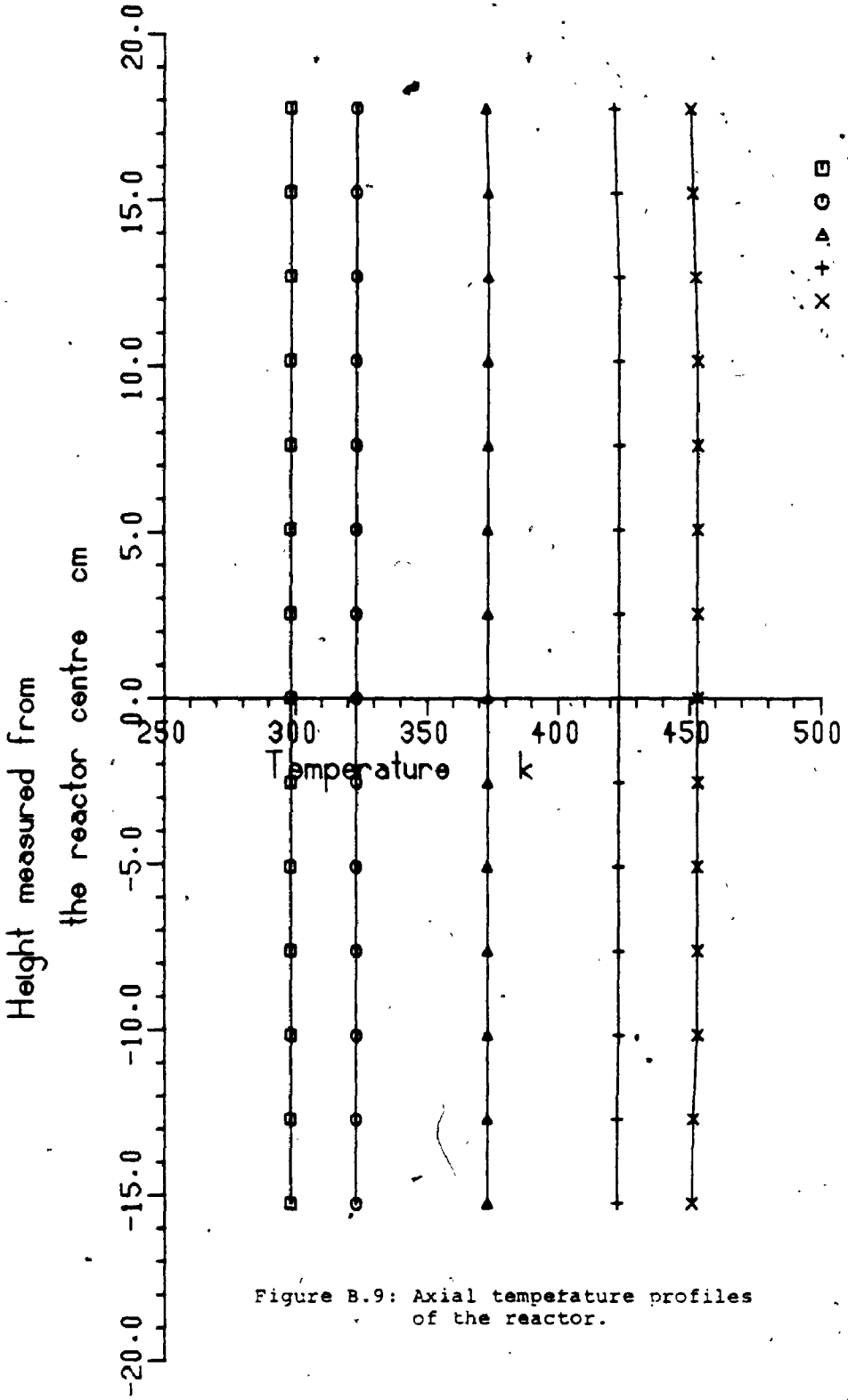

Figure B.9: Axial temperature profiles of the reactor.

B6: Description of the Sampling Valve

The basic function of the sampling valve used was to reproducibly introduce a portion of the continuously flowing gas stream into the carrier gas helium and eventually into the gas chromatograph.

The operation of the 8-port rotary sample valve used can be described by referring to Figure B.10.

In position (1), the sampling gas is continuously purged through the sample line waste i.e., from port 1, to port 2, to port 3, passes through the sample loop and finally vents into the atmosphere at port 4. Helium enters at port 5 and exits at port 8 into the gas chromatograph flow system.

Position (2) is the injection position of the sampling valve. In this position, the flow of sample is cut off the sample loop. Helium entering port 5 sweeps the trapped sample from the sample loop and out at port 8. The path 1-7-6-4 is used for sample purge into the atmosphere.

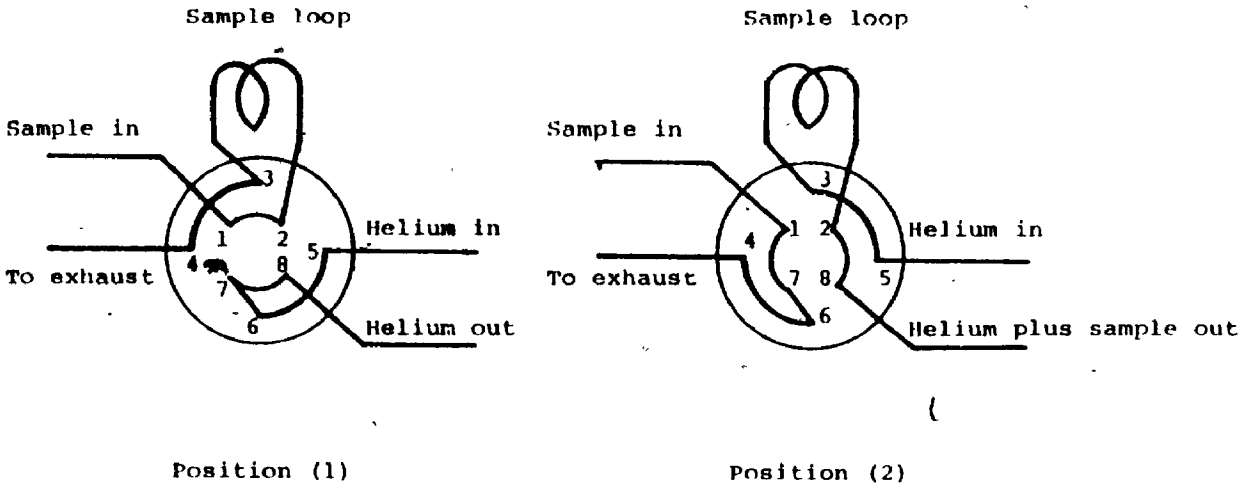

Figure B.10: Schematic diagram of the 8-port rotary sample valve.

B7: Preconditioning of the Columns

As stated in the text, all newly prepared columns were preconditioned before using to avoid contamination of the detectors and column bleeding as well.

The Preconditioning of the columns was performed in accordance with the procedure provided by the manufacturer. This may be summarized as follows:

i- Install columns. Do not attach end of columns to fitting at rear of oven.

ii- Connect helium lines and adjust its flow rates.

iii- Turn detector and injector temperatures to minimum settings and the power off the thermal conductivity and the electrometer.

iv- Set oven temperature at about 620 K and set temperature program mode selector to isothermal.

v- Bake columns for at least 12 hours with helium flowing as set in step ii above.

B8: Maximum Pressure Drop in the Sample Loop

The sample loop was a stainless steel tube having a length (L) of about 0.16 m and an inside diameter (d_i) of 3.184×10^{-3} m. The cross-section area As of the loop is then:

$$A_s = \pi (d_i)^2 / 4 \qquad (B.7)$$

To estimate the maximum pressure drop ΔP (Pa) in the sample loop, consider the following:

i- Air is the flowing gas. This assumption was justified as discussed in the text. Therefore, the properties of air were used in the calculations:

Density of air $\rho = 1.1843$ kg/m^3 (at 298 K).
Kinematic viscosity $\upsilon = 15.4 \times 10^{-6}$ m^2/s (at 298 K).

ii- Maximum flow rate Qm was 25.74×10^{-6} m3/s which corresponds to mean residence time of 3 s.

Accordingly:
Maximum velocity $v_m = Q_m/A_s = 3.25$ m/s (B.8)
and the corresponding Reynold's number is
$Re = d_i v_m / \upsilon = 670$ (B.9)

From Moody diagram [151], the friction factror f is 0.024. Then,, the pressure loss dP due to friction is [151]:

$$P = \frac{4\ f\ L\ \rho\ v^2}{2\ d_i} \qquad (B.6)$$

Since the pressure of the surroundings was in the order of 97.8 kPa the effect of the above pressure drop is negligible. Thereupon, the flow of gases through the sample valve was considered to be under atmospheric pressure.

B9: Brief Description of Nuclear Magnetic Resonance, Infre-red, and Mass Spectroscopies

Spectrosmetric methods of analysis make use of the discrete energy levels of molecules and the emission or absorption of radiation which usually accompanies changes by a molecule from one energy level to another.

Nuclear magnetic resonance (NMR), infra-red (IR), and mass spectroscpy (MS) techniques were used in the present study for product- identification. Therefore, a brief on each is given in the following sections.

B9.1 Nuclear Magnetic Resonance Spectroscopy:

NMR spectroscopy measures the relative energies of the nuclear spin transition states of a molecule in a magnetic field. At the magnetic fields commonly available, the frequency of the radiation used is in the radio frequency range of the spectrum, generally less than 200 Hz. This method may be applied to the study of any atom having a nuclear spin. Most applications at present have been concerned with the 1H, 19F, and 31P nuclei. The first was exclusively used in this study.

The frequencies involved with such transitions are

specific to molecules and the number of peaks exhibited is equivalent to the number of the different environments in which the hydrogen proton is present. The position of these frequencies can be defined in terms of "chemical shift δ" given as:

$$\delta = \frac{H_s - H_r}{H_r} \times 100 \qquad \text{(B.10)}$$

In this equation, H_s is the magnetic field strength at which a maximum appearance for a given proton while H_r is the field strength for some reference. Tri-methyl silane (TMS) was the reference used in the present investigation.

B9.2 Infra-red Spectroscopy:

Atoms or atomic groups in molecules are in a continuous vibrational motion with respect to one another. Upon interaction with IR radiation, molecules absorb portions of the incident radiation at particular wavelengths.

the multiplicity of vibrations occuring simultanuously produces a highly complex absorption spectrum, which is uniquely characteristic of the functional groups comprising the molecules, such as -CHO and C=C groups, and of the overall configuration of the atoms as well. The IR spectrum involves the twisting, bending, rotational, and vibrational motions of atoms in a molecule.

An important feature of IR spectroscopy is that the vibration caused by radiation must entail a change in the electrical dipole moment of the functional groups. The characteristic absorption bands of a functional group undergo a little change from one compound to another. Thus, by examining the IR spectrum of an unkown compound, one can tell with a fair degree of certainty which functional groups are present.

B9.3 Mass Spectroscopy:

A mass spectrometer produces charged particles consisting of the parent ion and the ionic fragments of the original molecule, and sorts these ions according to their mass-to-charge ratio.

The mass spectrum is a record of the numbers of different kinds of ions-the relative numbers of each are characteristic for every compound including isomers. The spectrum of a compound contains the masses of the ionic fragments and the relative abundance of these ions plus the parent ion. A detailed interpretation of the spectrum frequently makes it possible to place functional groups into certain areas of the molecule and to see how they are connected to one another.

The molecular weight can be determined to ten thousandths of a mass unit on more sophisticated spectrometers.

4- The following parameters were fixed according to the manufacturer's instruction at the values:

The detectors temperature = 415 K
The current to TC detector = 0.15 A
The helium inlet pressure = 505 kPa
The air flow rate to FID = 100 ml/min
The hydrogen flow rate to FID = 25 ml/min

5- By trial and error, adjust: i) the helium flow rates to the operating and reference columns and ii) the heating rate of the gas chromatograph oven so that the best resolution of the mixture constituents is attained.

The results obtained are summarized in Table B.6 and Figures B.12 and B.13.

TABLE B.6: RETENTION TIME DATA *

Compound	Temperature (K)	Time (s)
Air	363	102
Water	363	252
Hydrogen sulphide	363	555
Sulphur dioxide	363	613
Methyl mercaptan	423	1313
Dimethyl sulphide	423	1814
Dimethyl disulphide	453	2339

* Helium flow rate to operating column = 34 ml/min.
* Helium flow rate to reference column = 41 ml/min.

B11a: The Accuracy of the Method by which the Gas Chromatograph was Calibrated for Air

As discussed in the text, the gas chromatograph was calibrated for air by injecting known amounts of air into the instrument and record the area of the corresponding peaks. The amount of air in each sample was determined using the ideal-gas equation at the atmospheric temperature and pressure. The volumes required by this equation were given by the readings of the syringe. The results obtained are summarized in Table B.3.

The accuracy of the above procedure was further verified. This was done by using the results obtained to determine the volume of an auxiliary loop. The volume of this loop was also determined following another method and the results of the two methods were compared.

The auxiliary loop illustrated schematically in Figure B.11 was a square loop abcd having 3.18 mm i.d. and made from glass. Valves V1 and V2 are two-way stopcock-valves made from Teflon and sealed with O-rings.

In one position (Position A), a gas can flow along path eabcdf. Position B could be obtaied by turning valves V1

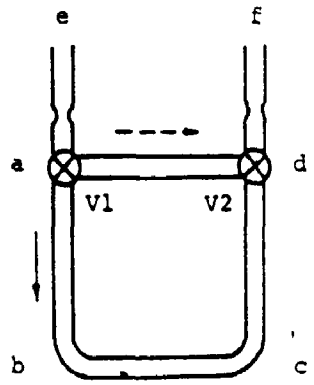

---- Position (A) Position (B)

Figure B.11: Schematic diagram of the auxiliary loop.

and V2 90 degrees. In this position the gas flow is only in path "eadf".

Method 1:

1- Attach the auxiliary loop to the rear of the 8-port rotary valve.

2- Trap a sample of air in the loop and introduce it by the usual manner into the gas chromatograph. Record the peak area (in digitized form) of the sample.

3- Repeat the above two steps several times and average the results.

4- Use this average in conjunction with Figure 4.14 to obtain the correspding average kmoles of the air samples.

5- Then, substitute this value along with the prevailing temperature and pressure into the ideal gas equation to evaluate the average volume of the loop.

The results obtained are listed in Table B.4a.

Method 2:

1- Fill the loop with mercury. Empty the mercury in a pre-weighed beaker. Then, weigh and determine the difference in weight. Repeat this step several times and average the results.

2- Divide the difference by the mercury density at the present temperature so that an average value for the loop volume is obtained.

The results obtained are summarized in Table B.4b.

TABLE B.3: CALIBRATION OF THE GAS CHROMATOGRAPH FOR AIR

Volume $m^3 \times 10^3$	Amount $kmol \times 10^3$	No of digits
0.1	4.01	274503, 273180, 273909
0.2	8.02	482887, 481913, 482688
0.3	12.04	694328, 692055, 692773
0.5	20.06	1113703,1110053,1108814
0.8	32.10	1790717,1709313,1765516
1.0	40.12	2209307,2118086,2166473
1.25	50.15	2708813,2655039,2667408
1.5	60.18	3318731,3199083,3254376

TABLE B.4a: VOLUME OF THE AUXILLIARY LOOP (Method 1)

No. of digits:	2182200, 2179875, 2191123, 2188017, 2169908, 2181815, 2179098, 2180446, 2181668, 2181452
Average=	2181560 ± 5573

The corresponding mass = 41.71×10^{-3} kmol (from Figure 4.14)

The corresponding volume
$= (1.0086 \pm 0.004) \times 10^{-4}$ m^3 (from equation (4.1))

TABLE B.4b: VOLUME OF THE AUXILIARY LOOP (Method 2)

Weight of loop filled with mercury in grams	63.4963, 63.4972, 63.4967, 63.4934, 63.4959, 63.4934, 63.4954, 63.9444, 63.4957,63.4956

Average wieght of mercury = 13.6506 ± 0.0016 gm

Density of mercury at 298 K = 13.5339×10^3 kg/m^3.

Average volume of loop =
$= W/R = (1.0086 \pm 0.002) \times 10^{-3}$ m^3

B11b: Standardization of the Sample Loop

The volume of the sample loop was determined as followed:

1- Attach the sample loop to the sampling valve by means of Swag-lok.

2- Pass a stream of nitrogen through the loop while the sampling valve in Position (1) (see Appendix B6).

3- By switching the valve to Position (2), a sample of nitrogen is trapped. This sample is immediately swept by the flowing helium to the gas chromatograph for analysis.

4- Repeat the above steps and average the results.

5- From the integrator output and Calibration curve 4.14, the amount of nitrogen sample can be evaluated.

6- By using the ideal gas equation, the volume of the sample loop can be determined. The results obtained are listed in Table B.5 below. The average volume of the sample loop was equal to $(1.248 \pm 0.0026) \times 10^{-6}$ m^3.

TABLE B.5: STANDARIZATION OF THE SAMPLE LOOP

No. of digits	2689033	2677911	2683566	2682948
	2681048	2687413	2686128	2681003
	2675473	2687808		

Average No. of digits = 2683233±4459

Average no. of moles from Figure 4.14
= $(50.110 \pm 0.106) \times 10^{-9}$ kmol

Average volume of the loop from equation (4.1)*
= $(1.248 \pm 0.0026) \times 10^{-6}$ m^3

* Atmospheric pressure = 99.26 kPa.

B12a: Retention Time Data

B12a.1 Introduction:

For a given set of column conditions (e.g., temperature and carrier gas flow rate), the retention time of a compound is the length of time spent by this compound in the column. The retention time is constant and will be the same whether the compound is pure or in a mixture. On a chromatogram, the retention time is the distance on the time axis from the point of sample injection to the peak of the eluted compound.

The resolution, on the other hand, is the degree of sparation between two consecutive constituents of the mixture as they emerge from a column.

B12a.2 Procedure:

The retention time data of the compounds in concern were obtained as follows:

1- Prepare a mixture of nitrogen, methyl mercaptan, hydrogen sulphide, water, dimethyl sulphide, dimethyl disulphide, and sulphur dioxide as described in Appendix B1 above.

2- Assemble the apparatus as in actual experiments.

3- Fix the injectors temperature at 420 K so that the mixture components remained in the vapour phase.

4- The following parameters were fixed according to the manufacturer's instruction at the values:

The detectors temperature = 415 K
The current to TC detector = 0.15 A
The helium inlet pressure = 505 kPa
The air flow rate to FID = 100 ml/min
The hydrogen flow rate to FID = 25 ml/min

5- By trial and error, adjust: i) the helium flow rates to the operating and reference columns and ii) the heating rate of the gas chromatograph oven so that the best resolution of the mixture constituents is attained.

The results obtained are summarized in Table B.6 and Figures B.12 and B.13.

TABLE B.6: RETENTION TIME DATA *

Compound	Temperature (K)	Time (s)
Air	363	102
Water	363	252
Hydrogen sulphide	363	555
Sulphur dioxide	363	613
Methyl mercaptan	423	1313
Dimethyl sulphide	423	1814
Dimethyl disulphide	453	2339

* Helium flow rate to operating column = 34 ml/min.
* Helium flow rate to reference column = 41 ml/min.

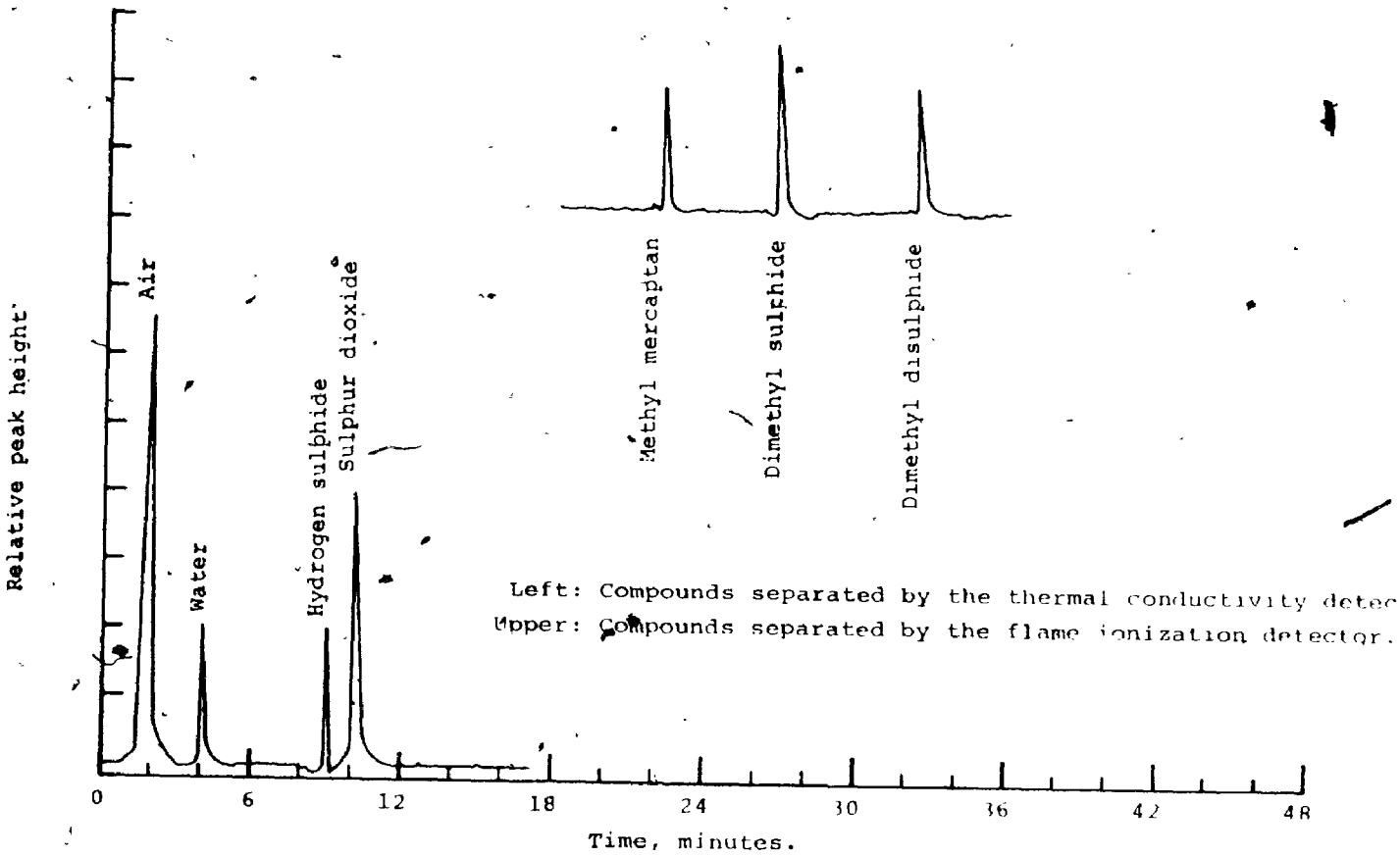

Left: Compounds separated by the thermal conductivity detector.
Upper: Compounds separated by the flame ionization detector.

Figure B.12: A chromatogram showing the resolution of the various compounds by the gas chromatograph.

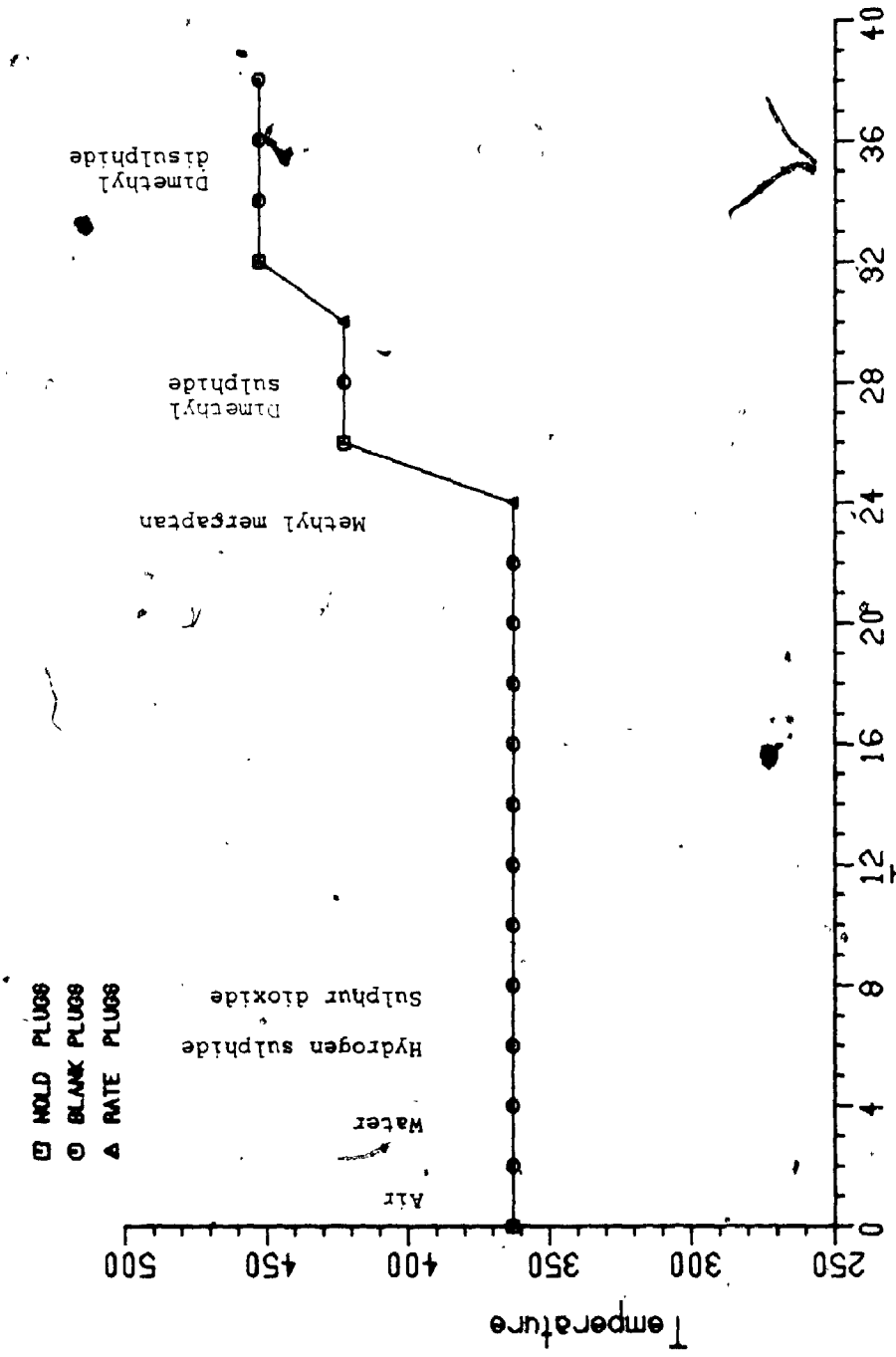

Figure B.13: Temperature programming of the columns oven of the gas chromatograph.

B12b: Sensitivity of the Thermal Conductivity and the Flame Ionization Detectors

Sensitivity S_i of a detector i (in kmol of compound j per cubic metre of carrier gas) to respond to the compound may be given by [103]:

$$S_i = \frac{s_i}{MW_j} \Big/ \frac{T\ q}{298} \qquad \text{kmol/m}^3 \qquad \text{(B.11)}$$

where s_i = the sensitivity of the detector in kg/s,

MW_j = the molecular weight (kg/kmol) of compound j,

T = the temperature (K) of the detector, and

q = the flow rate of the carrier gas m^3/s at 298 K.

According to reference [103], the sensitivity s_i of the thermal conductivity and the flame ionization detectors is in the order of $6x10^{-13}$ and $2x10^{-16}$ kg/s, respectively. Bearing in mind that the former detector was used to monitor the concentration of air, hydrogen sulphide, water, and sulphur dioxide while the latter was used to monitor that of methyl mercaptan, dimethyl sulphide, and dimethyl disulphide, Table B.7 which shows the sensitivity of both detectors for the respective compounds could be constructed.

TABLE B.7 : SENSITIVITY OF THE DETECTORS USED

Detector	Compound	M_i^*	S_i (kg/m^3)
TC	air	28.82	1×10^{-6}
	water	18.02	2×10^{-6}
	Hydrogen sulphide	34.08	1×10^{-6}
	Sulphur dioxide	64.06	0.4×10^{-6}
FID	Methyl mercaptan	48.11	6×10^{-13}
	Dimethyl sulphide	62.13	4×10^{-13}
	Dimethyl disulphide	94.20	3×10^{-13}

* Ref. (174)

B12C: Calibration Of The Gas Chromatograph for the Compunds In Concern

The calibration of the gas chromatograph for the various compounds in concern was, as indicated in the text (Section 4.5), done using the absolute method. This method consists of injecting an amount of the compound into the gas chromatograph for analysis. The peak area obtained is representive to the amount injected. A value for this amount was determined using a procedure based on the respective compound as will be discussed below.

B12.1 Methyl Mercaptan:

The calibration of the gas chromatograph for methyl mercaptan may be summarized as follows:

1- Prepare a concentrated mixture of methyl mercaptan (about 6×10^{-3} kmol/m^3) with nitrogen as described above in Appendix B1.

2- Assemble the sampling and absorption train as shown schematically in Figure B.14.

3- Add 150 ml of cadium sulphate (10 g/l) and then 50 ml of sodium hydroxide (4 g/l) to each impinger.

4- A regulated stream with a flow rate of q (m^3/s) monitored by rotameter R1 was allowed into the sampling system where several samples (normally 3 samples) were introduced to the gas chromatograph for analysis. The peak

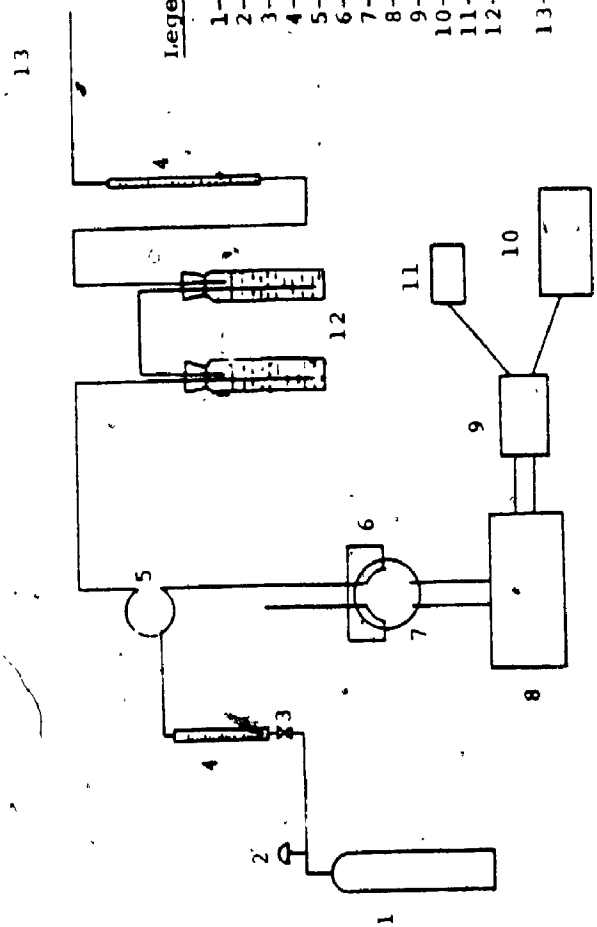

Figure B.14: Sampling and absorption trains used to calibrate the gas chromatograph for methyl mercaptan.

area A' (in digitized form) corresponding to the amount of methyl mercaptan m' (kmol) in every sample was reported.

4- Start the flow of the gas stream through the absorption train by manipulating the control valves and record the initial time. Methyl mercaptan present in the gas stream will then be scrubbed by the cadium sulphate solution.

The flow rate q was monitored, in this case, after emerging from the second impinger to avoid correction for any pressure drop experienced by the gas stream while passing through the scrubbing solution.

5- Record the temperature T_1 of the gas stream and also the temperature T and the pressure P of the surroundings.

6- After sufficient sample has been passed, stop the flow of gas through the impinger by shutting the control valves and record the final time.

7- The amount n' (kmol) of methyl mercaptan scrubbed by the cadium solution during the time period t (second) is related to the quantity m' by:

$$n' = \frac{m'}{v_s} q \frac{P-P_v}{P} t \quad \text{kmol} \qquad (B.12)$$

where v_s (m^3) is the volunme of the sample loop and P_v (Pa) is the vapour pressure of water at T_1.

8- The amount n' was then determined iodometrically as will be discussed later.

9- Pressurize the lecture bottle containing the remainder

5 5

OF / DE

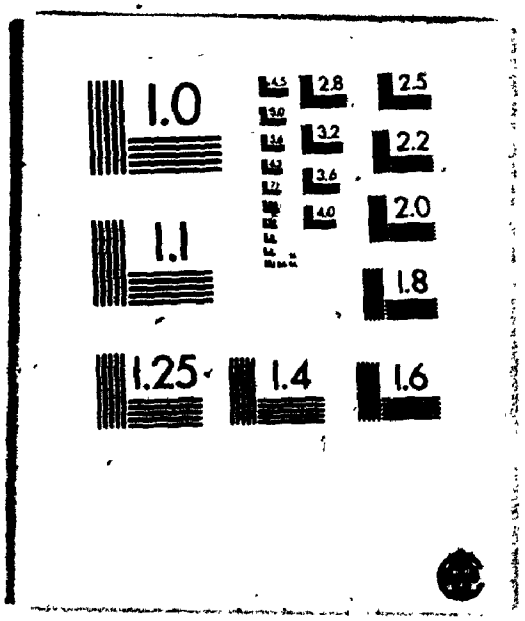

of methyl mercaptan mixture with more nitrogen so that the concentration of the former is reduced. Then, follow Steps 2 to 8 above and obtain a new set of m' and A' values.

10- Plot the data and the best line obtained by linear regression is the calibration curve required.

Titration of Methyl Mercaptan:

The procedure followed to determined the amount n' of methyl mercaptan scrubbed from the gas stream was based on the ASTM D2385-66 [1976] which is applicable over the concentration range from 0 to 0.5×10^{-7} kmol/m3.

Reagents and Materials:

Hydrochloric acid:

Concentrated hydrochloric acid (sp.gr. 1.19) was used.

Iodine Standard solution (0.1N):

Weigh 12.6905 g of resumlimed iodine into a 250 ml beaker. Add 22 g of potassium iodide (KI) and 100 ml of water. Stir until solution is complete, dilute to 1 litre, mix thoroughly, and store in a dark -coloured glass-stoppered bottle.

Iodine standard Solution (0.01N):

Prepare 0.01N iodine solution by exact dilution of 0.1N iodine solution.

Sodium thiosulphate, standard solution 0.1N:

Dissolve 24.8174g of $Na_2S_2O_3.5H_2O$ in 1 litre of freshly boiled and cooled water in a sterile glass bottle.

Both the iodine (0.1N) and the thiosulphate solutions prepared above were standarized with one another. This was done as follows: pipette 25 ml iodine solution into a flask, add 40 ml of water and 5 ml of the concentrated hydrochloric acid. Titrate the iodine solution with the thiosulphate solution until the former fades to a pale yellow. Add 5 ml of the starch solution whereas a blue colour is developed and continue titrating to the disappearance of the blue colour of iodine. The concentration of sodium thiosulphate was found to be within 0.2% in both cases.

Sodium Thiosulphate Standard Solution (0.005N):

Prepare 0.005N sodium thiosulphate solution by exact dilution of 0.1N sodium thiosulphate solution.

Starch Solution:

Make a paste of 0.5 g of soluble starch with a little cold water. Slowly add to 250 ml of boiling water. Cool and transfer to a glass-stoppered bottle.

The titration method proceeded as follows:

i- Place the solution present in the impinger bottle in a flask provided with a magnetic stirrer and rinse the impinger with water and add the latter to the flask. Add 50 ml of the concentrated HCl and mix thoroughly but gently. Again, add to the solution formed an exess amount of the standard iodine solution and mix thoroughly, the solution must show the yellow iodine colour. Record the total volume

V_1 (ml) of iodine solution added. Some of the iodine present will react with methyl mercaptan:

$$2CH_3SH + I_2 \rightarrow (CH_3)_2S_2 + 2HI \qquad (B.13)$$

ii- Titrate the remaining I_2 with the standard solution of $Na_2S_2O_3$ adding the starch solution as Described above. The concentration of iodine and sodium thiosulphate solutions used will depend on the mercaptan concentration in the gas stream. Record burret reading which gives volume of the thiosulphate added. The reaction between iodine and thiosulphate occurs as:

$$2Na_2S_2O_3 + I_2 \rightarrow Na_2S_4O_6 + 2NaI \qquad (B.14)$$

iii- The total amount of methyl mercaptan scrubbed is given by:

$$n' = 0.001(V_1N_1 - V_2N_2) \quad \text{gmol} \qquad (B.15)$$

The results obtained from titration are summarized in Table B.8 while the relation between the number of moles m' and the peak area (expressed in digits) is illustrated in Figure B.15.

B12.2 Hydrogen Sulphide:

The procedure followed to calibrate the gas chromatograph for hydrogen sulphide was similar to that described above. The only differences are i) no sodium hydroxide was added to the cadium sulphate solution, ii) the concentrated hydrochloric acid was added after adding the iodine solution, and iii) the amount n' was given by:

$$n' = 0.001 \frac{V_1N_1 - V_2N_2}{2} \quad \text{gmol} \qquad (B.16)$$

since the reaction in this case proceeds according to:

$$H_2S + I_2 \rightarrow S + 2HI \qquad (B.17)$$

The titration results are given in Table B.9 and the calibration curve is shown in Figure B.16.

B12.3 Sulphur Dioxide:

The gas chromatograph was calibrated for sulphur dioxide following the above procedure except that the scrubbing solution was hydrogen peroxide solution (2%) which had a pH value of about 5 [101]. Morover, the acidic solution formed by reaction:

$$H_2O_2 + SO_2 \rightarrow H_2SO_4 + \tfrac{1}{2}O_2 \qquad (B.18)$$

TABLE B.8: CALIBRATION FOR METHYL MERCAPTAN

	V2 ml	P kPa	t $s \times 10^{3}$	VT $m^3 \times 10^6$	n' kmol$\times 10^{12}$	No. of digits
N1=0.01N	17.9	98.89	9	1452	9.024	1408, 1404, 1402
V1=10 ml	17.1	"	"	"	12.462	1789, 1799, 1795
N2=0.005N	16.7	"	"	"	14.524	1799, 1801, 1803
$q=10 \times 10^{-6}$	16.6	"	"	"	14.611	2099, 2111, 2105
	15.5	98.91	"	"	19.337	2857, 2862, 2866
m^3/s	14.8	"	"	"	22.346	3321, 3316, 3328
	13.6	"	"	"	27.502	4074, 4066, 4082
	12.3	"	"	"	33.089	4905, 4913, 4901
	11.1	99.01	"	"	34.668	5654, 5650, 5658
	9.4	"	"	"	45.551	6725, 6733, 6720
	7.6	"	"	"	53.286	7999, 7987, 7987
N1=0.1N	19.2	98.89	10.8	1743	5.729	8566, 8503, 8513
V1=20 ml	18.9	"	"	"	7.878	11274, 11301, 11259
N2=0.1N	18.7	"	"	"	9.316	13679, 13775, 13729
$q=10 \times 10^{-6}$	18.1	"	"	"	13.607	20152, 20183, 20141
	17.3	99.01	"	"	19.337	28446, 28523, 28501
m^3/s	16.1	"	"	"	27.932	41290, 41170, 41161
	15.4	"	"	"	32.945	50072, 50111, 50208
	14.8	"	"	"	37.243	55001, 54791, 54880
	13.2	98.82	"	"	48.702	71769, 71699, 71909
	12.9	"	"	"	50.850	71161, 71005, 70878
	12.4	98.88	"	"	54.431	79999, 80305, 80209
	11.1	"	"	"	63.742	94101, 93913, 93878
	10.5	"	"	"	68.039	100403, 100118, 100217

$$kmol = 6.823 \times 10^{-15} \text{ (digits)} - 5.076 \times 10^{-13}$$

Correlation coefficient = 0.999

TABLE B.9: CALIBRATION FOR HYDROGEN SULPHIDE

	V2 ml	P kPa	t $s \times 10^{3}$	VT $m^3 \times 10^6$		No. of digits
N1=0.1N	17.9	99.00	9	1452	0.450	218, 215, 216
V1=10 ml	15.8	"	"	"	0.902	434, 436, 432
N2=0.005N	13.4	"	"	"	1.418	680, 683, 679
$q=10 \times 10^{-6}$	10.3	99.05	"	"	2.084	999, 995, 1000
m^3/s	6.6	"	"	"	2.879	1380, 1386, 1376
	5.0	"	"	"	3.223	1546, 1539, 1562
N1=0.01N	21.8	98.99	9	1452	3.911	1891, 1878, 1874
V1=20 ml	18.5	"	"	"	4.619	2215, 2224, 2209
N2=0.005N	16.7	"	"	"	5.006	2399, 2406, 2386
$q=10 \times 10^{-6}$	12.8	"	"	"	5.844	2806, 2812, 2789
m^3/s						
N1=0.1N	18.9	98.83	10.8	1734	3.938	1944, 1929, 1939
V1=20 ml	18.8	"	"	"	4.296	2041, 2052, 2049
N2=0.1N	17.2	"	"	"	10.024	4813, 4801, 4793
$q=10 \times 10^{-6}$	16.7	"	"	"	11.814	5660, 5643, 5648
m^3/s	12.6	"	"	"	26.492	12700, 12661, 12661
	11.3	"	"	"	31.146	13893, 13003, 13981
	10.1	98.88	"	"	35.442	16887, 17045, 16955
	7.7	"	"	"	44.034	21151, 21044, 21003
	6.1	"	"	"	49.763	23793, 23680, 23841
	4.5	99.09	"	"	55.491	26521, 26607, 26446
	2.2	"	"	"	63.723	30577, 30421, 30456
	1.4	"	"	"	66.589	31878, 31792, 31821

$$kmol = 2.094 \times 10^{-14} \text{ (digits)} + 7.594 \times 10^{-13}$$

Correlation coefficient = 0.999

was titrated by 0.002N sodium hydroxide solution. The end of the reaction was detected by phenolphthaline indicator.

The above method is applicable to a concentartion less than $5x10^{-4}$ gmol/m^3 in air [101].

The amount of sulphur oxide scrubbed is given by:

$$n' = 0.001V_1N_1 \qquad \text{gmol} \qquad (B.19)$$

The results of the titration are presented in Table B.10 and the calibration curve is illustrated in Figure B.17.

B12.4 Dimethyl Sulphide:

Dimethyl sulphide was supplied by Eastman Kodak Company (New York, U.S.) with a specified purity of 98 wt% as tested by GCL. The density of dimethyl sulphide was determined at the lab conditions by weighing 15 ml of the compound using a precision balance and it was found equal to 845.8 kg/m^3.

The calibration of the gas chromatograph for dimethyl sulphide proceeded as follows:

1- Measure halh-ml of the sulphide (i.e., $422.9x10^{-6}$ kg) using a 0.5-ml Hamilton tight-gas syringe and place in a 100-ml volumetric flask. Then, fill the flask with ethanol (more than 99.9% purity) and mix thoroughly.

2- Transfer 1 ml of the above solution into another 100-ml volumetric flask. Fill the flask also with ethanol and mix thoroughly to form a reference solution and store in a dark-coloured glass stoppered bottle. The concentration of dimethyl sulphide in this solution is equal to 66.71 $kmol/m^3$.

3- Several samples of different volumes were drawn from the reference solution using Hamilton gas-tight syringes. The samples were separately injected into the operating column of the gas chromatograph for analysis. record the peak area (in digitized form) corresponding to the sulphide. For a sample of volume v' (m^3), the peak area A' recorded for the sulphur compound is equivalent to an amount m' of the compound where m' is:

$$m' = 66.71 \times 10^{-5} \, v' \qquad \text{kmol} \qquad \text{(B.20)}$$

4- Plot m' versus A' for all samples. The best curve fitted by linear regression to the data is then the required calibration curve.

The results are given in Table B.11 and Figure B.18.

B12.5 Dimethyl Disulphide:

Dimethyl disulphide was obtained also from Eastman Kodak Company with a purity more than 99.99 wt%. The density of this compound determined as described for dimethyl

sulphide was found equal to 1045.8 kg/m^3.

The procedure to calibrate the gas chromatogarph for dimethyl disulphide was similar to the one described above except that the amount m' of this compound in a sample of volume v' (m^3) was given by:

$$m' = 55.51 \times 10^{-5} \; v' \qquad \text{kmol} \qquad \text{(B.21)}$$

The results obtained are presented in Table B.12 and Figure B.19.

A12.6 Water:

The experimental method employed to calibrate the gas chromatograph for water was similar to that given above for methyl mercapatan except that (refer to Figure B.14):

1- Water and nitrogen mixtures were prepared by dividing a nitrogen stream from the pressurized cylinder into two streams q_1 and q_2. Stream q_1 was allowed to bubble in distilled water placed in an impinger (not shown in the figure). Then, stream q_1 was combined again with stream q_2 by means of a T-connection made from glass (not shown in the figure). By manipulating streams q_1 and q_2 by means of precision rotameters, the concentration of water in the feed could be varied.

2- The two impingers were removed. Instead, a U-tube

TABLE B.10: CALIBRATION FOR SULPHUR DIOXIDE

	V2 ml	P kPa	t 10^{-3} s	Q m^3 x10^{6}	n' kmol x10^{11}	No. of digits
N1=0.005N	8.0	98.69	9	1452	0.666	248, 243, 244
V1=40 ml	11.2	"	"	"	0.931	585, 580, 591
q=10x10^{-6} m^3/s	16.9	"	"	"	1.406	924, 939, 907
	22.8	"	"	"	1.897	1269,1251,1244
	25.9	"	"	"	2.154	1441,1426,1221
	34.5	"	"	"	2.870	1813,1784,1792
	39.0	"	"	"	3.244	2062,2043,2031
	41.4	98.84	7.2	"	4.308	2796,2781,2766
	47.1	"	"	"	4.897	3189,3156,3157

kmol = 1.463 x 10^{-14} (digits) + 2.060 x 10^{-13}

Correlation coefficient = 0.997

TABLE B.11: CALIBRATION OF THE GAS CHROMATOGRAPH FOR DIMETHYL SULPHIDE

V ml	n' kmol x10^{11}	No. of digits
5	0.3335	135, 130, 133
10	0.6671	275, 266, 271
15	1.0006	409, 396, 392
20	1.3341	545, 533, 528
30	2.0012	791, 805, 813
40	2.6682	1027,1061,1077
50	3.3353	1344,1328,1320
60	4.0023	1613,1600,1581
70	4.6694	1865,1881,1855
80	5.3364	2100,2202,2132
90	6.0035	2411,2380,2409
100	6.6706	2592,2703,2695

kmol = 2.492 x 10^{-14} (digits) + 1.918 x 10^{-13}

Correlation coefficient = 0.999

TABLE B.12: CALIBRATION OF THE GAS CHROMATOGRAPH FOR DIMETHYL DISULPHIDE

V ml	n' kmol x10^{11}	No. of digits
5	0.3335	135, 130, 133
5	0.2755	165, 159, 172
10	0.5510	351, 348, 346
20	1.1102	686, 699, 700
30	1.6653	1051,1042,1060
40	2.2204	1385,1404,1392
50	2.7755	1752,1764,1716
60	3.3306	2106,2089,2003,2079
70	3.8857	2369,2420,2435,2459
80	4.4408	2797,2775,2801
90	4.9959	3153,3148,3163
100	5.5100	3467,3471,3459

kmol = 1.575 x 10^{-14} (digits) + 3.505 x 10^{-13}

Correlation coefficient = 0.999

made from glass and containing anhydrous magnesium sulphate was added to the absorption train. When a moisturized nitrogen stream passed through the U-tube for a period of time t, water was absorbed by the sulphate and its weight was increased. This increase in weight Δw was equal to the amount of water absorbed in time t. Using equation, considering saturation conditions:

$$q = (q_1+q_2)t + \frac{(\Delta w/MW)\ R\ T}{P} \qquad m^3 \qquad (B.22)$$

gives the total volume of water and nitrogen mixture passed through the U-tube, where q is the flow rate of the combined stream as measured by the rotameter placed after the U-tube. R, T, MW, and P in the above equation are the gas conatant, temperature of the gas stream, molecular weight of water, and the atmospheric pressure. Then, using equation:

$$C_w = \Delta w/q \qquad kmol/m^3 \qquad (B.23)$$

gives the concentarion of water vapour in the feed.

Several samples (usually three) of each of the above mixtures were quantititavely analysed on the gas chromatograph and the results were averaged. In each case, the average peak area (in digitized form) obtained corresponded to an amount of water:

$$m' = C_w v_s \qquad \text{kmol} \qquad (B.24)$$

where C_w is obtained the above equation and v_s is the volume of the sample loop.

The results obtained are summarized in Table B.13 and plotted in Figure B.20.

TABLE B.13: CALIBRATION OF THE GAS CHROMATOGRAPH FOR WATER

t °C	Q m^3/s	P kPa	dW gm	n kmolx10^{12}	Digits		
5.40	50.00	99.17	0.1021	2.42	61	64	66
5.40	41.67	99.33	0.1054	3.24	72	78	74
3.60	33.33	99.71	0.1362	7.86	175	192	163
2.88	25.00	99.75	0.1077	10.36	244	261	269
3.60	23.33	98.98	0.1362	11.23	358	369	357
3.60	20.00	99.05	0.1362	13.10	413	426	393
2.88	16.67	99.19	0.1090	15.72	477	502	462
2.88	13.33	99.15	0.1363	24.57	598	601	578
2.88	10.00	99.70	0.1090	26.19	781	801	751
2.52	6.67	99.63	0.0953	39.28	1145	1179	1123
2.52	4.67	99.45	0.0953	56.10	1639	1601	1659
2.16	3.50	99.42	0.0817	74.77	2157	2118	2195
2.52	25.00	99.46	0.9534	104.61	3008	3091	2913
2.16	18.33	99.42	0.8168	142.49	4073	4112	4052
2.16	15.00	99.58	0.8177	174.24	4976	5042	4921
1.80	10.00	99.25	0.6829	261.46	7442	7368	7417
1.44	8.33	99.71	0.5450	312.67	8923	9011	8821
1.08	7.50	99.63	0.4084	346.91	11463	11258	11655
1.08	5.83	99.52	0.4084	445.05	12726	12881	12579
1.08	5.00	99.52	0.4088	518.99	14854	14513	15180
0.72	4.17	99.78	0.2724	621.24	17813	17523	18081
0.72	3.33	99.79	0.2722	773.68	22241	22563	21939
0.72	2.50	99.82	0.2725	1027.32	29653	29342	29946
0.36	1.67	99.83	0.1362	1524.45	44458	44033	44895

kmol = 3.442×10^{-14} (Digits) + 3.677×10^{-13}

Correlation coefficient = 0.998

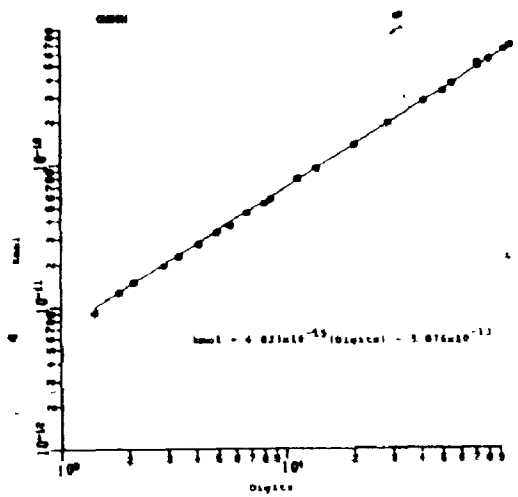

Figure 8.15: Calibration curve of the gas chromatograph for methyl mercaptan

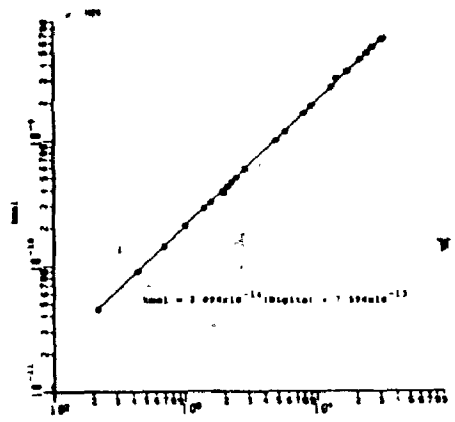

Figure 8.16: Calibration curve of the gas chromatograph for hydrogen sulphide

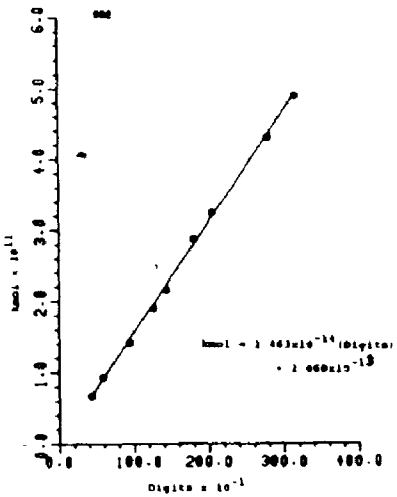

Figure 8.17: Calibration curve of the gas chromatograph for sulphur dioxide

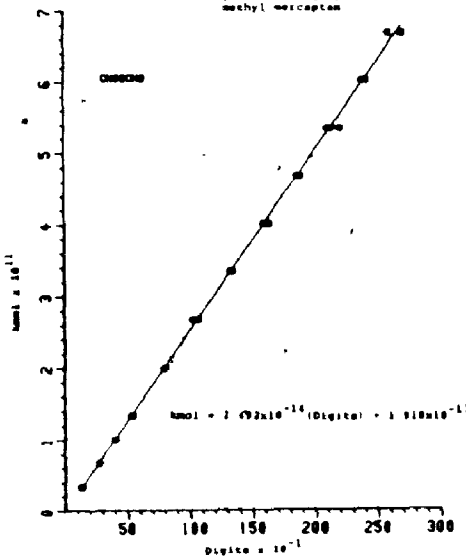

Figure 8.18: Calibration curve of the gas chromatograph for dimethyl sulphide

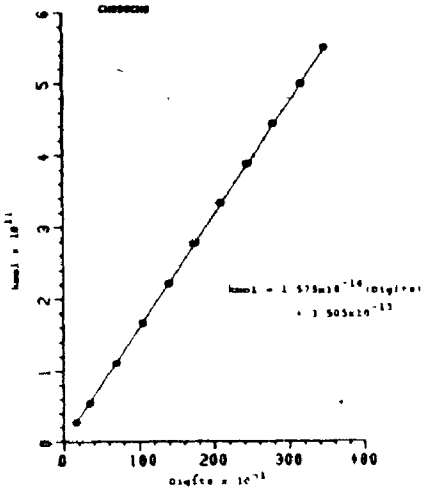

Figure 8.19: Calibration curve of the gas chromatograph for dimethyl disulphide

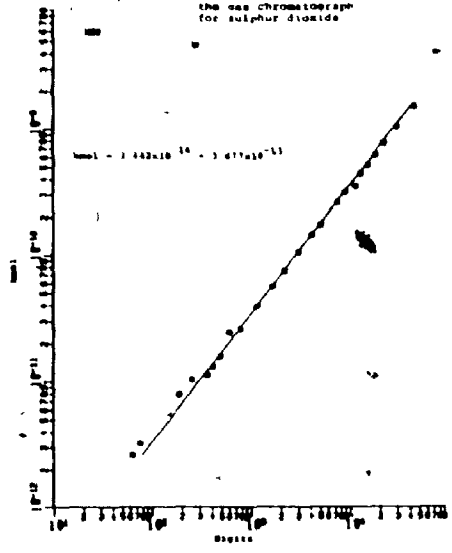

Figure 8.20: Calibration curve of the gas chromatograph for water

$$n_{O_3} = N_1 V_1 / 2 \qquad \text{kmol} \qquad \text{(C1.4)}$$

9- Calculate the concentration C' of ozone, required from:

$$C_{O_3} = \frac{n_{O_3}}{q' t} \qquad \text{kmol/m}^3 \qquad \text{(C1.5)}$$

Note that P_v in equation (C1.2) is the vapour pressure of water at T_1.

The results obtained are summarized in Table C.1.

unaltered. Then, repeat Steps 4 and 5.

7- Pressurize the lecture bottle with more nitrogen so that the methyl mercaptan mixture becomes diluted. Then, determine the composition as in above.

8- Repeat Steps 4, 5, and 6.

9- Repeat Step 7 so as to obtain a more diluted mixture of methyl mercaptan. Then, repeat steps 4,5, and 6.

10- Set the temperature of the reactor at 373 K (see Section 4.2.3).

11- Prepare another concentrated mixture of methyl mercaptan in nitrogen. Then, repeat the above steps and record in each case the respective voltage-current measurements.

12- Raise the reactor temperature to 453 K. Then, repeat the above steps collectively..

As indicated earlier, the results obtained were already summarized in the text, Table 4.1. More results are given in Appendix E.

B14: ENERGY BALANCE AROUND THE CORONA REACTOR

The thermal energy balance around the corona reactor may be given by:

$$\bar{c}_p \, \bar{\rho} \, Q \, \Delta T = I_c \, V_s \qquad (B.25)$$

where $\bar{c}_p$ and $\bar{\rho}$ are the average specific heat and density of the gaseous stream passing through the reactor.. Due to the extremely dilute mixture of the sulphur compounds, values for these two parameters may be taken as equal those of air. That is 0.24 cal/g.K and 1.18×10^{-3} g/ml, respectively. ΔT is the temperature difference between the product and reactant streams.

For typical values of I_c and V_s of 0.3 mA and 7 kV, respectively, ΔT was found equal to about 230 K. However, this rise in the reactor temperature was not sensed by the thermocouple soldered to the outer surface of the stainless steel gauze (see Section 4.3).

This discrepancy between the predicted and measured values of ΔT may be explained as follows:

1- The energy supplied in the reactor is mainly used to accelerate electrons to a level where upon interacting they could excit and ionize the neutral molecules of gases. According to Fite [176], one can think of the electrons in

the discharge as having a temperature in the Maxwellian sense which is much higher than the neutral gas molecules, i.e., typically 30000 K vs 300 K. In this case, it should be referred to Section 6.3.3.3 for discussion on the energy gained by electrons in the discharge.

2- Finally it is believed that, considering the ways described above of energy dissipation in a corona discharge, if there was any significant temperature difference to occur this difference could only be confined to a region very close to the surface of the corona wire. Such a possibility should be subjected to further experiments where the temperature in this region to be measured. For an example, a pyrometer may be used.

APPENDIX C

C1: DETERMINATION OF OZONE CONCENTRATIONS IN THE EXIT AIR STREAM FROM THE OZONIZER

The concentration of ozone in the air stream emerging from the ozonizer was obtained first by absorbing the ozone in an acidic solution of potassium iodide. Then, the iodine librated due to this process was determined using the iodimetry analytical method. The procedure proceeded as follows:

1- Use the experimental arrangement shown in Figure 4.1

2- Place the acidic solution (pH3) of potassium iodide (about 1%) in two impingers connected in series to form an absorption trai. Attach one of the calibrated rotameters (see Appendix B) to the exit of the second impinger.

3- For a given set of ozonizer conditions of temperature T_R, current I_c, and voltage polarity, allow a regulated stream of air to pass through the ozonizer.

4- At time t=0, attach the ozonizer to the exit of the first impinger by a tygon tube so that the ozonized air to be scrubbed by the potassium solution:

$$O_3 + 2I^- + 2H^+ \rightarrow O_2 + H_2O + I_2 \qquad (C1.1)$$

Monitor the flow rate q of gases by the rotameter present and record their temperature T_1. Record also the temperature T and pressure P of the surroundings. Note that the flow rate q' of the gas stream entering the absorption train is:

$$q' = q \; / \; \left(\frac{P}{P - P_v}\right) \qquad (C1.2)$$

Also, the flow rate Q_R of gases through the ozonizer is given by equation (4.1):

$$Q_R = q' \times \frac{T_R}{T} \qquad (4.1)$$

5- After sufficient sample has been scrubbed disconnect the ozonizer from the absortion train. Record the final time t.

6- Titrate the iodine liberated in reaction (C1.1) with a standard solution of sodium thiosulphate (0.005N):

$$I_2 + Na_2S_2O_3 \rightarrow 2I^- + Na_2S_4O_6 \qquad (C1.3)$$

and record volume V_1 aquired. The end point of reaction (C1.3) is indicated by starch solution. Preparation of the reagents and the analytical procedure were discussed previously in Appendix B12C.

7- Since reaction (C1.1) is quantititaive, the amount of ozone absorbed by the KI solution is obtained from:

$$n_{O_3} = N_1 V_1 / 2 \qquad \text{kmol} \qquad \text{(C1.4)}$$

8- Calculate the concentration C' of ozone, required from:

$$C_{O_3} = \frac{n_{O_3}}{q' t} \qquad \text{kmol/m}^3 \qquad \text{(C1.5)}$$

Note that P_v in equation (C1.2) is the vapour pressure of water at T_1.

The results obtained are summarized in Table C.1.

TABLE C.1: CONCENTRATION OF OZONE GENERATED UNDER DIFFERENT OZONIZER CONDITIONS

T_R K	t s	P kPa	q ml/min	q_R	t s	V_1 ml	c_{O_3} kmolx10^7
			Negative corona				
298	5	98.77	957.2	926.6	60	17.7	7.96
	5	98.77	957.2	926.6	60	25.5	11.47
	5	98.77	957.2	926.6	60	24.1	10.85
	10	99.59	478.5	463.3	60	23.4	21.04
	10	99.59	478.5	463.3	60	23.0	20.68
	10	99.59	478.5	463.3	60	20.7	18.62
	10	99.59	478.5	463.3	60	22.3	20.06
	20	99.05	239.3	231.7	60	23.7	42.62
	20	99.05	239.3	231.7	60	22.9	41.18
	20	99.05	239.3	231.7	60	24.3	43.70
	20	99.05	239.3	231.7	60	24.9	44.79
	35	98.95	136.8	132.4	60	22.6	71.12
	35	98.95	136.8	132.4	60	22.1	69.55
	35	98.95	136.8	132.4	60	22.9	72.07
373	5	98.10	764.9	926.6	60	15.6	8.78
	5	98.10	764.9	926.6	60	13.8	7.77
	5	98.10	764.9	926.6	60	14.9	8.39
	10	99.21	382.3	463.3	60	13.3	14.97
	10	99.21	382.3	463.3	60	12.5	15.09
	10	99.21	382.3	463.3	60	13.4	15.08
	20	98.58	191.2	231.7	60	15.7	35.34
	20	98.58	191.2	231.7	60	15.9	35.79
	20	98.58	191.2	231.7	60	15.5	34.89
	35	98.65	109.3	132.4	60	14.7	57.89
	35	98.65	109.3	132.4	60	14.3	56.32
	35	98.65	109.3	132.4	60	15.2	59.86
	35	98.65	109.3	132.4	60	15.0	59.07
453	5	99.22	629.6	926.6	60	8.1	5.54
	5	99.22	629.6	926.6	60	6.9	4.72
	5	99.22	629.6	926.6	60	7.8	5.33
	10	99.25	314.8	463.3	60	9.7	13.26
	10	99.25	314.8	463.3	60	10.0	13.67
	10	99.25	314.8	463.3	60	10.5	14.35
	20	98.33	157.5	231.7	60	7.7	21.05
	20	98.33	157.5	231.7	60	8.1	22.15
	20	98.33	157.5	231.7	60	7.4	20.23
	35	98.41	90.0	132.4	60	8.9	42.58
	35	98.41	90.0	132.4	60	8.6	41.14
	35	98.41	90.0	132.4	60	9.0	43.05
	35	98.41	90.0	132.4	60	9.1	43.53
			Positive corona				
298	5	98.50	957.3	926.6	60	16.4	3.69
	5	98.50	957.3	926.6	60	9.1	4.09
	10	99.05	478.6	463.3	120	9.5	4.27
	10	99.05	478.6	463.3	120	10.9	4.90
	20	99.09	239.3	231.7	120	12.3	11.06
	20	99.09	239.3	231.7	120	11.8	10.61
	20	99.09	239.3	231.7	120	13.4	12.05
	35	98.78	136.8	132.4	120	12.1	19.04
	35	98.78	136.8	132.4	120	11.8	18.57
	35	98.78	136.8	132.4	120	12.4	19.57
373	5	98.90	764.7	926.6	120	7.3	2.05
	5	98.90	764.7	926.6	120	9.5	2.67
	5	98.90	764.7	926.6	120	8.7	2.45
	10	99.22	382.3	463.3	120	7.6	4.28
	10	99.22	382.3	463.3	120	6.5	3.66
	10	99.22	382.3	463.3	120	6.6	3.71
	20	98.62	191.2	231.7	120	7.6	8.55
	20	98.62	191.2	231.7	120	7.3	8.22
	20	98.62	191.2	231.7	120	7.8	8.78
	35	98.33	109.3	132.4	120	7.7	15.16
	35	98.33	109.3	132.4	120	7.8	15.34
	35	98.33	109.3	132.4	120	7.4	14.57
453	5	98.34	629.8	926.6	180	6.3	1.44
	5	98.34	629.8	926.6	180	4.5	1.03
	10	98.45	314.9	463.3	180	7.6	3.46
	10	98.45	314.9	463.3	180	3.6	1.62
	10	98.45	314.9	463.3	180	5.4	2.46
	10	98.45	314.9	463.3	180	5.8	2.64
	20	98.65	157.5	231.7	180	8.5	7.75
	20	98.65	157.5	231.7	180	7.9	7.20
	35	99.02	90.0	132.4	180	6.7	10.68
	35	99.02	90.0	132.4	180	6.3	10.05
	35	99.02	90.0	132.4	180	6.2	9.89

C2: Semi-Empirical Electron Impact Cross Sections for the Excited and Ionized Species of Oxygen and Nitrogen

The present section is intended to present semi-empirical equations describing the cross sections of the excited and ionized species of oxygen and nitrogen. These information are extracted from the work done by Peterson et.al., [141].

All excitation cross sections may be expressed in the form:

$$\sigma_j(E) = \frac{q_o f_o c_o}{W_j^2} \left(\frac{W_j}{E}\right)^{\Omega} \Sigma_s a_s \left(\frac{W_j}{E}\right)^{\Gamma_s} \qquad \text{(C2.1)}$$

with the restrictions $(a_s, \Gamma_1) = (1,0)$ and $\Sigma_s a_s = 0$. The constant q_o in equation (C2.1) is 6.514×10^{-14} $eV^2 m^2$ and other parameters present are found in reference (141).

Similarily, all ionization cross sections are expressed as:

$$\frac{d\sigma_i(E)}{dW} = \frac{q_o A_o}{W^2} \left(\frac{I_i}{W}\right)^p \left(\frac{W}{E}\right)^{\Omega} \Sigma_s a_s \left(\frac{W}{E}\right)^{\Gamma_s} \qquad (C2.2)$$

$$\sigma_i(E) = \int_{I_i}^{(E+I_i)/2} \frac{d\sigma_i}{dW}\, dW \qquad (C2.3)$$

where W is continuous and I_i is the ionization threshold. The parameter p is 1.1 and 1.2 for oxygen and nitrogen, respectively. q_o in equqation C2.2 is the same as in equation C2.1 while other parameters are found in reference (141).

APPENDIX D

D1:THE ENTRANCE LENGTH OF THE CORONA REACTOR

When a gas stream is introduced into a duct, it takes a length y from the duct entrance before the gas flow is fully developed. This length known as the entrance length may be obtained for a laminar flow in a tubular duct by [168]:

$$\frac{y\ \nu}{R^2\bar{v}} = 0.115 \qquad \text{(D1.1)}$$

where ν is the kinematic viscosity (m^2/s) of the gas at the prevailing conditions of temperature and pressure, R is the reactor radius (m), and $\bar{v}$ is the average velocity (m/s) of the gas stream in the duct and given by:

$$\bar{v} = \frac{H}{\tau} \qquad \text{(D1.2)}$$

H and τ are the length of the duct and the mean residence time of the flow through it.

For the extreme conditions of temperature T and the mean residence time τ, by substituting into equations (D1.1) and (D1.2) with the appropriate values of ν, Table D .1 could be constructed. Note that ν is equal to:

$$\nu = \frac{\text{viscosity } \mu}{\text{density } \rho} \qquad \text{(D1.3)}$$

TABLE D .1 THE REACTOR ENTERANCE LENGTH AT DIFFERENT OPERATING CONDITIONS

T	ρ	μ	ν	τ	$\bar{v}$	y
K	kg/m^3	kg/m.s	m^2/s	s	m/s	m
	$x10^2$	$x10^6$	$x10^4$		$x10^2$	$x10^2$
298	118.4	18.56	0.16	3	5.08	5.89
				35	0.44	0.52
543	77.87	25.0	0.32	3	5.08	2.94
				35	0.44	0.26

D2: THE IMPORTANCE OF THE LONGITUDINAL DIFFUSION IN THE MASS BALANCE EQUATION OF THE SULPHUR COMPOUNDS IN THE REACTOR

As indicated in Section 7.2.2 of the text, the longitudinal diffusion in the corona reactor can be neglected if criterion (7.8) was met:

$$\bar{v}_z \frac{\partial C_A}{\partial z} >> D_A \frac{\partial^2 C_A}{\partial z^2} \qquad (7.8)$$

in which D_A is the diffusion coefeicient of component A and $\partial C_A/\partial z$ is its axial concentration gradient in the reactor.

Values of the diffusion coefficients of the several sulphur compounds in concern were not available at the time of the present study. They had therefore to be estimated from the following relation which predicts diffusion coefficients with ±5% error [166]:

$$D_A = \frac{BT^{3/2} \sqrt{(1/M_1) + (1/M_2)}}{Pr_{12}^2 I_d} \qquad (D2.1)$$

where: D_A=gas diffusivity, cm^2/s.

$B=(10.7-2.46\sqrt{1/M_1 + 1/M_2})\times 10^{-4}$,

T=absolute temperature, K,

M_1, M_2=molecular wieght of components 1 and 2,

P=absolute pressure, atm,

r_{12}=collision diameter, ^{o}A,

$= (r_o)_1 + (r_o)_2/2$

$r_o = 1.18 V_o^{1/3}$ (see Table 14.44, ref. [166]),

V_o=molar volume of liquid at normal boling point, (see Tables 14.42 and 14.43, ref. [166]),

I_d=collision integral for diffusion, function kT/ε_{12} (see Table 14.45, ref. [166]),

k=Boltzmann constant=1.38×10^{-6} erg/K,

ε_{12}=energy of molecular interaction, erg.

$\varepsilon_{12}/k = \sqrt{(\varepsilon_1/k)(\varepsilon_2/k)}$ (see Table 14.46, ref [166]).

For non existing data, V_o may be estimated by summing the atomic volumes given in Table 14.42 [166]. Similarily, when ε/k is not known, the following eqauation may be used:

$$\varepsilon/k = 1.15\ T_b$$

where T_b is the normal boiling point BP (K).

Then, by carrying out the appropriate calculations, Table D.2 was established.

The axial concentration gradient for each of the four sulphur compounds was obtained at $\bar{v}_z$=15.2 mm/s, I_d=0.3 mA, and T=423 K by carrying the experiments in the usual manner using four values of the reactor height: 76.2, 152.4,

TABLE D·2 DIFFUSION COEFFICIENTS OF THE SULPHUR COMPOUNDS AT 298 AND 453 K IN AIR

	CH_3SH	H_2S	$(CH_3)_2S_2$	$(CH_3)_2S$	Air
Vo	55.2	32.9	103.0	77.2	29.9
ro	4.5	3.8	5.5	5.0	3.6*
r12	4.1	3.6*	4.6	4.3	3.6*
T_b(K)*	279		310	390	
M_i**	48.11	34.08	94.1	62.3	28.9
ε/k	320.7	301.1	448.5	356.8	97*
ε_{12}/k	176.4	170.9	208.6	186.0	97*
I_d*(298K)	0.57	0.62	0.62	0.58	0.5
D_A(298K)	0.13	0.18	0.09	0.11	
I_d(423K)	0.51	0.50	0.54	0.51	
D_A(423K)	0.24	0.33	0.17	0.21	
I_d(453K)	0.50	0.49	0.52	0.51	
D_A(453K)	0.27	0.39	0.19	0.24	

* Ref. [166].
** Ref. [174].

228.6, and 304.8 mm. The inlet and exit concentrations of the reactants were monitored using the gas chromatograph. The results are shown in Figures D.1a and D.1b.

The exit concentration-reactor height data in each case was fitted by the linear regression routine available in SPSS package [158]. Then, the respective concentration gradient and its second derivative could be evaluated by substituting with z equal to 152.4 mm as an example. (Others values of z can be used as well.)

Using the above results collectively, the respective left and right hand sides of inequality (7.8) were evaluated. The results summarized in Table D.3 indicate the availability of the inequality and thereupon, they indicate the verification of neglecting the longitudinal diffusion in the corona reactor.

However, as check to the above results, one should consider the dispersion coefficient $\bar{D}$ rather than the diffusion coefficient D_A. Estimation of $\bar{D}$ may be obtained using the following equality:

$$\bar{v}_z \frac{\partial C_A}{\partial z} = \bar{D} \frac{\partial^2 C_A}{\partial z^2} \qquad \text{(D2.2)}$$

In the case of methyl mercaptan, for example, $\bar{D}$ was equal to 9.44 cm /s. This value is about 39 times higher

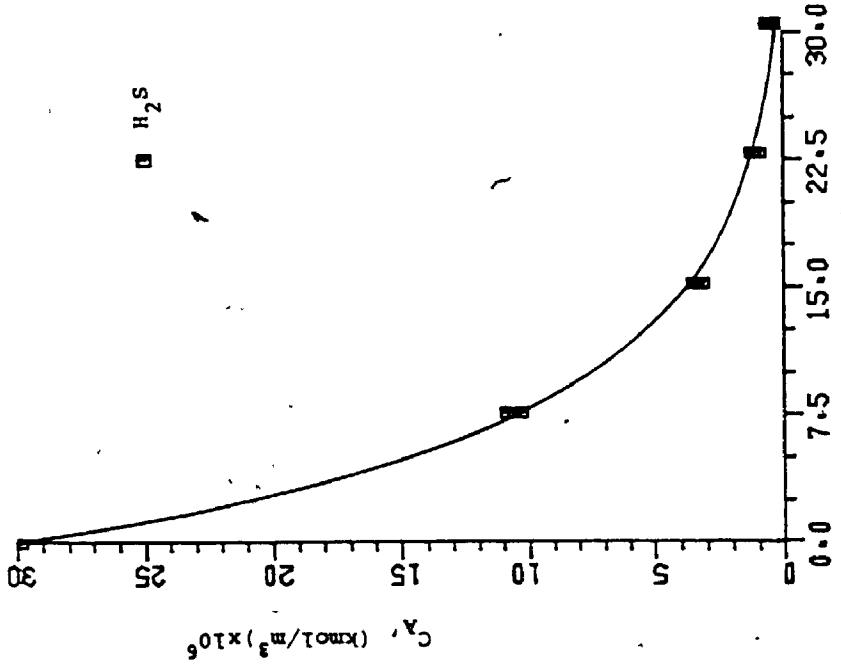

Figure D.1: continued

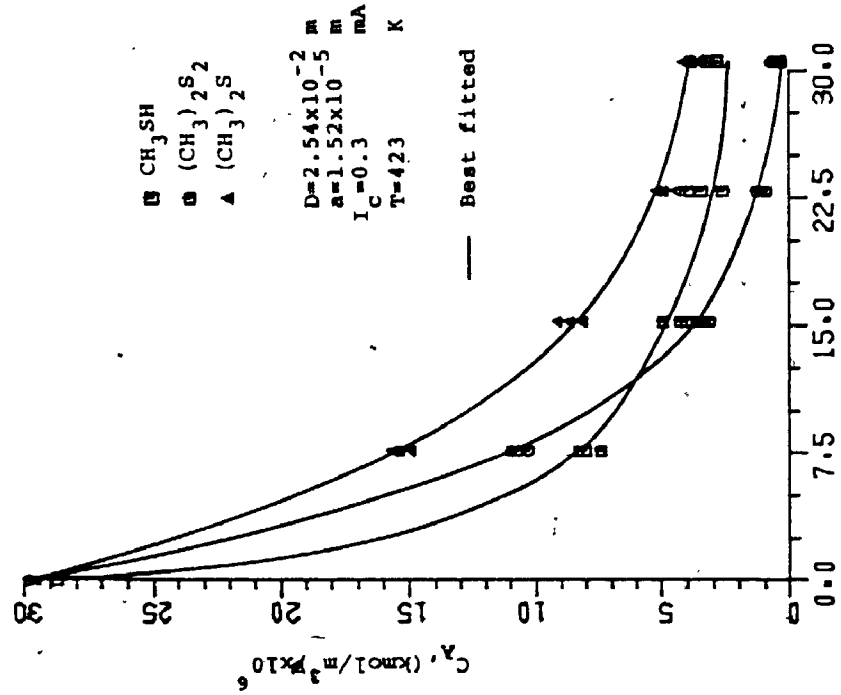

Figure D.1: Concentration-height curves for the sulphur compounds due to reaction with air.

TABLE D.3
COMPARSION BETWEEN $v_z \partial C_A/\partial z$ AND $D_A \partial^2 C_A/\partial z^2$
DURING THE REATIONS OF THE SULPHUR COMPOUNDS
WITH AIR*

Property	CH_3SH	$(CH_3)_2S_2$	$(CH_3)_2S$	H_2S
$\partial C_A/\partial z$	-0.23	-0.15	-0.06	-0.94
$\bar{v}_z \partial C_A/\partial z$*	-2.36	-1.41	-0.61	-1.43
D_A**	0.24	0.17	0.21	0.33
$D_A \partial^2 C_A/\partial z^2$	-0.06	-0.03	-0.01	-0.05
Ratio	2.5	2.1	1.6	3.5

* $\bar{v}_z$=0.0152 m

**From Table D.2.

than D_A. Therefore, even though we consider the values of the diffusion coefficient listed in Table D.2 were lesser by an order of 10 the inequality relation (7.8) could still be applicable.

D3: THE IMPORTANCE OF THE RADIAL DIFFUSION IN THE MASS BALNACE FOR THE SULPHUR COMPPOUNDS IN THE REACTOR

In reference to Section 7.2, the mass balance equation for species i in a differential cylinderical volume shown, assuming negligible longitudinal diffusion, is:

$$-\bar{v}_z \frac{\partial C_A}{\partial z} + D_A \left(\frac{1}{r} \frac{\partial C_A}{\partial r} + \frac{\partial^2 C_A}{\partial r^2}\right) = (-r_A) \qquad (7.2b)$$

The reaction term $(-r_A)$ was shown to be:

$$-r_A = k\, C_A^n \qquad (7.6a)$$

in which k is a constant function of the system opearting conditions and n is the reaction order.

Solution of eqaution (7.2) with the appropriate boundary conditions:

$$\frac{\partial C_A}{\partial r} = 0 \text{ for } r>0 \text{ and } z=0$$
$$\frac{\partial C_A}{\partial r} = 0 \text{ for } r=0 \text{ and } z>0 \qquad (D3.1)$$

can only be obtained by numerical methods [170]. Using

these methods, it is normally to express equation (7.2) and its boundary conditions in dimensionless forms:

$$-(1 - r^{*2})\frac{\partial C_A^*}{\partial \lambda} + \left(\frac{\partial^2 C_A^*}{\partial r^{*2}} + \frac{1}{r^*}\frac{\partial C_A^*}{\partial r^*}\right) = C_A^{*n} \qquad \text{(D3.2)}$$

where: $r^* = r/R$, $\quad C_A^* = C_A/C_{Ao}$, (D3.3)

$\lambda = kC_{Ao}^{n-1}z/2\bar{v}_z$, and $\alpha = D_A/(C_{Ao}^{n-1}kR^2)$

Similarily, equations (D3.1) become:

$$\frac{\partial C_A^*}{\partial r^*} = 0 \text{ for } r^* > 0 \text{ and } \lambda = 0$$

$$\frac{\partial C_A^*}{\partial r^*} = 0 \text{ for } r^* = 0 \text{ and } \lambda > 0 \qquad \text{(D3.4)}$$

An average value of the concentration of species i at any height z may be evaluated by integration:

$$\bar{C}_A = \frac{\int_0^R 2\pi r v(r) C_A(r) dr}{\int_0^R 2\pi r v(r) dr} \qquad \text{(D3.5)}$$

where values for $C_A(r)$, the radial concentration, are available from the numerical solution.

From the present experimental work, values of the outlet concentration C_A at the respective operating conditions were known. In order to evaluate the reaction order n, these data had to be used in conjunction with the

above equations. To do so, the following trial and error scheme:

1- Assume a value n_i for the reaction order and a value k_i for its rate constant.

2- Find values for λ_i and α_i.

3- Carry out the numerical solution for equation (D3.2) using the boundaries conditions (D3.4). Normally, the implicit method of the finite difference is used since it gives stable and fast-convergent solution [170,171].

4- Obtain a value for $\bar{C}_A$ for λ_i and α_i.

5- Repeat the above steps so as to construct a set of curves similar to those shown in Figure D.2.

6- Experimental results would now be applied to one particulr curve. If this does not produce consistancy of λ_i and α_i one would conclude this was not the correct combination of n_i and k_i. Progress to another curve. Presumably, the set of plot finally giving consistant results would be the one corresponds to the correct order and rate constant of the reaction.

Numerical solutions for the above eqautions are available in the literature for first and second order reactions [172,173]. By stipulating that the recation of methyl mercaptan with air in the corona discharge is second order while other reactions involving the other three sulphur compounds, namely, dimethyl disulphide, dimethyl

sulphide, and hydrogen sulphide are of the first order type it was able to use the results reported in the above references. Errors introduced in the results due to the use of this method can only be evaluated by solution of equation (D3.2) with the conditions (D3.4), precisely the task to be avoided. However, it is obvious that using this procedure would introduce but negligible errors in the results.

Now, by using the values reported in the text for the rate constants of all reactions in concern at the experimental conditions employed (see Table D.4), values for λ_i and α_i can be evaluated from equations (D3.3). For a typical value of C_{Ao} of 25×10^{-6} kmol/m^3 for all the reactant sulphur compounds in concern, columns 1 and 2 of Table D.4 were constructed.

Using the values of λ_i and α_i tabulated above in conjunction with Figures 3 and 2 in references [172] and [173], respectively the exit concentration of each compound was evaluated sometimes by interplotation. These values are listed in columns 3 and 4 of Table D.4. In the same table, the experimental values of these concentrations are also given (column 5). Furthermore, column 6 of the table gives the difference between the respective concentrations. The fact that these differences are negligible indicates the correct combination of the order and the rate constant for each reaction in concern.

TABLE D.4

COMPARISON BETWEEN EXPERIMENTAL DATA OF THE EXIT CONCENTRATION OF THE SULPHUR COMPOUNDS DUE REACTION WITH AIR AND THOSE ESTIMATED FROM REFERNCES [172] AND [173]:

Compound	λ_i	α_i	$C^*_{A_{est}}$	$C_{A_{est}}$	$C_{A_{exp}}$	Diff %
CH_3SH	3.27	0.23	0.14	3.5	3.7	6.7
$(CH_3)_2S_2$	1.13	0.91	0.14	3.5	3.3	7.7
$(CH_3)_2S$	0.67	0.79	0.31	7.8	8.0	2.5
H_2S	1.21	0.54	0.12	3.0	3.2	6.3

Experimental conditions:

$\bar{v}_z = 1.52 \times 10^{-2}$	m/s
$D = 2.54 \times 10^{-2}$	m
$a = 1.52 \times 10^{-5}$	m
$C_{A_0} = 25 \times 10^{-6}$	kmol/m^3
$T = 423$	K
$I_C = 0.3$	mA
$\tau = 10$	s

From references [172] and [173], at the values listed for λ_i and α_i in each case, it is obvious that the estimated curves (see Figure D.2) obtained based on the above results can be approximated by those which may be obtained for α is ∞. This condition yield fractional conversions equivalent to plug flow, exactly the approach used in the present study to analysis the data obtained. In this case, as discussed earlier, the radial diffusion in considered absent and the concentration profile is flat.

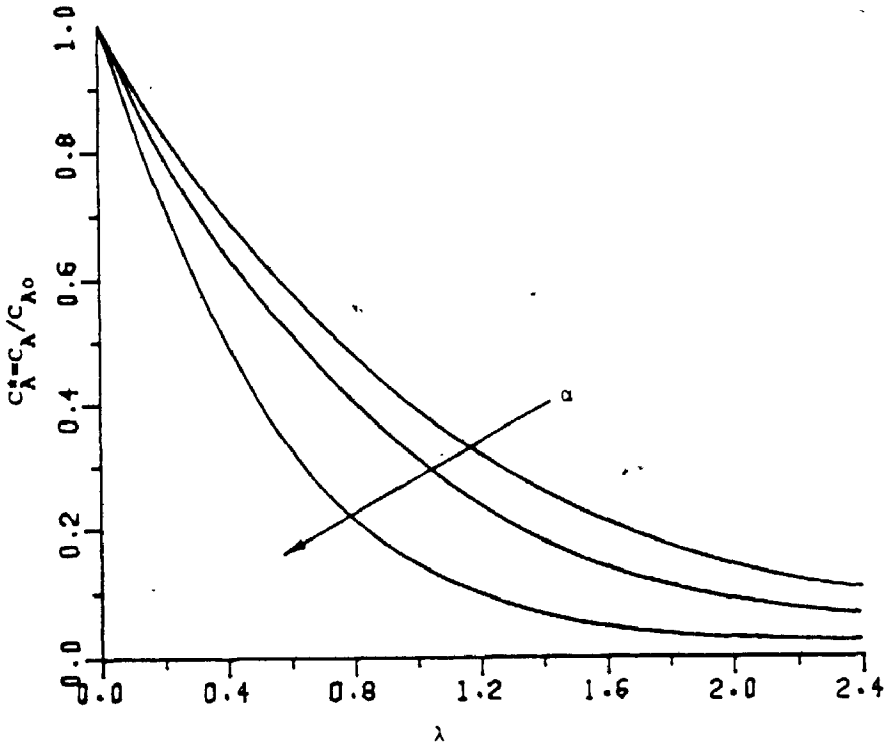

Figure D.2: Theoretical curves of C_A^* vs. λ with α as a parameter (172,173).

TABLE E1.a

DATA FOR THE REACTION OF METHYL MERCAPTAN WITH AIR IN THE CORONA REACTOR
(Without considering dimeth/l sulphone)

D_R	D_w	H	T	P	I_c	V_s	-	Digits				
			K	kPa	mA	kV	s	CH_3SH in	CH_3SH out	$(CH_3)_2S_2$ out	$(CH_3)_2S$ out	H_2O out	SO_2 out
mx10^2	mx10^5	mx10											
2.54	3.05	15.24	298	99.35	0.10	4.65	5	4367	3898	59	0	37	64
2.54	3.05	15.24	298	99.43	0.10	4.65	5	4485	3986	68	0	27	60
2.54	3.05	15.24	298	98.95	0.10	4.68	10	4353	2872	163	41	148	130
2.54	3.05	15.24	298	99.11	0.10	4.65	10	4367	2887	167	57	168	129
2.54	3.05	15.24	298	99.15	0.10	4.66	15	4441	1993	142	88	248	381
2.54	3.05	15.24	298	99.55	0.10	4.69	15	4485	2008	149	79	238	401
2.54	3.05	15.24	298	99.01	0.10	4.65	25	4191	982	9	27	309	703
2.54	3.05	15.24	298	99.46	0.10	4.64	25	4462	988	11	17	299	683
2.54	3.05	15.24	298	98.99	0.10	4.68	35	4235	567	6	4	349	826
2.54	3.05	15.24	298	99.52	0.10	4.66	35	4338	571	4	4	369	959
2.54	3.05	15.24	298	99.51	0.30	6.71	3	4602	4016	87	0	47	57
2.54	3.05	15.24	298	99.38	0.30	6.66	3	4016	3561	59	0	27	60
2.54	3.05	15.24	298	99.48	0.30	6.64	5	5056	3429	211	48	148	97
2.54	3.05	15.24	298	99.43	0.30	6.63	5	4426	3136	186	29	118	85
2.54	3.05	15.24	298	99.48	0.30	6.71	5	5071	3444	218	46	158	115
2.54	3.05	15.24	298	99.52	0.30	6.69	10	5129	1685	156	107	329	598
2.54	3.05	15.24	298	99.55	0.30	6.71	10	4235	1583	116	75	268	463
2.54	3.05	15.24	298	98.93	0.30	6.69	10	4880	1656	133	93	319	572
2.54	3.05	15.24	298	99.21	0.30	6.65	10	4587	1627	118	86	278	518
2.54	3.05	15.24	298	99.30	0.30	6.68	15	5217	908	15	30	409	940
2.54	3.05	15.24	298	99.33	0.30	6.65	15	5217	898	18	19	429	960
2.54	3.05	15.24	298	99.42	0.30	6.64	25	4367	879	9	27	349	776
2.54	3.05	15.24	298	99.46	0.30	6.64	25	5086	381	22	7	449	1063
2.54	3.05	15.24	298	99.43	0.30	6.63	25	5071	375	13	4	429	1065
2.54	3.05	15.24	298	99.52	0.30	6.67	25	4235	388	4	5	359	867
2.54	3.05	15.24	298	99.45	0.30	6.67	35	5129	234	22	7	469	1108
2.54	3.05	15.24	298	99.35	0.30	6.69	35	5100	239	12	5	479	1119
2.54	3.05	15.24	298	99.39	0.30	6.63	35	4485	228	5	1	409	976
2.54	3.05	15.24	298	99.71	0.60	8.33	5	4470	2359	198	54	189	266
2.54	3.05	15.24	298	99.64	0.60	8.31	5	4455	2344	194	75	208	244
2.54	3.05	15.24	298	99.59	0.60	8.36	10	4206	938	14	16	309	686
2.54	3.05	15.24	298	99.38	0.60	8.30	10	4455	945	16	25	329	746
2.54	3.05	15.24	298	99.51	0.60	8.35	15	4529	483	4	4	399	940
2.54	3.05	15.24	298	99.38	0.60	8.30	15	4294	476	11	2	369	867
2.54	3.05	15.24	298	99.35	0.60	8.36	25	4338	220	13	3	390	930
2.54	3.05	15.24	298	99.46	0.60	8.34	25	4177	226	0	1	369	916
2.54	3.05	15.24	298	99.46	0.60	8.37	35	4294	146	12	7	399	935
2.54	3.05	15.24	298	99.33	0.60	8.32	35	4646	151	3	2	419	1005
2.54	3.05	15.24	298	99.43	1.20	11.11	5	5027	1597	144	100	319	476
2.54	3.05	15.24	298	99.41	1.20	11.16	5	5012	2198	160	92	449	577
2.54	3.05	15.24	298	99.34	1.20	11.08	10	5056	527	5	4	429	1038
2.54	3.05	15.24	298	99.25	1.20	11.12	10	5086	520	3	4	419	1045
2.54	3.05	15.24	298	99.15	1.20	11.12	15	5027	278	1	5	469	1092
2.54	3.05	15.24	298	99.22	1.20	11.09	15	4998	283	3	7	449	1085
2.54	3.05	15.24	298	99.13	1.20	11.20	20	4968	190	5	0	419	1099
2.54	3.05	15.24	298	99.30	1.20	11.10	20	4954	196	1	4	429	1099
2.54	3.05	15.24	323	99.10	0.10	4.49	5	4485	3840	106	7	47	58
2.54	3.05	15.24	323	99.13	0.10	4.54	5	4265	3679	104	1	500	52
2.54	3.05	15.24	323	99.19	0.10	4.52	10	4543	2623	231	78	168	183
2.54	3.05	15.24	323	99.35	0.10	4.51	10	4617	2697	213	88	2047	189
2.54	3.05	15.24	323	99.25	0.10	4.48	15	4499	1671	151	107	228	467
2.84	3.05	15.24	323	99.42	0.10	4.50	15	4558	1685	149	106	289	445
2.54	3.05	15.24	323	99.13	0.10	4.50	25	4631	777	9	35	379	831
2.54	3.05	15.24	323	99.19	0.10	4.51	25	4514	782	3	31	3726	825
2.54	3.05	15.24	323	99.35	0.10	4.51	35	4763	454	4	4	4309	990
2.54	3.05	15.24	323	99.38	0.10	4.52	35	4763	449	5	3	429	990
2.54	3.05	15.24	323	99.48	0.30	6.15	5	4367	2799	199	48	148	115
2.54	3.05	15.24	323	99.43	0.30	6.12	5	4499	2843	212	52	158	122
2.54	3.05	15.24	323	99.37	0.30	6.09	10	4631	1304	117	100	322	607
2.54	3.05	15.24	323	99.25	0.30	6.16	10	4558	1311	114	96	317	593
2.54	3.05	15.24	323	99.10	0.30	6.12	15	4499	689	4	25	368	846
2.54	3.05	15.24	323	99.29	0.30	6.11	15	4631	681	3	23	379	874
2.54	3.05	15.24	323	99.35	0.30	6.18	25	4910	293	3	4	449	1058
2.54	3.05	15.24	323	99.19	0.30	6.18	25	4866	301	0	6	439	1045
2.54	3.05	15.24	323	99.13	0.30	6.14	35	4910	190	5	7	459	1075
2.54	3.05	15.24	323	99.51	0.30	6.15	35	4954	186	6	4	459	1092
2.54	3.05	15.24	323	99.51	0.60	8.23	5	4807	2125	237	104	268	341
2.54	3.05	15.24	323	99.66	0.60	8.21	5	4939	2140	250	111	279	361
2.54	3.05	15.24	323	99.56	0.60	8.21	10	4792	770	15	35	399	887
2.54	3.05	15.24	323	99.60	0.60	8.18	10	4778	777	17	36	379	880
2.54	3.05	15.24	323	99.50	0.60	8.22	15	4719	396	6	4	429	996
2.54	3.05	15.24	323	99.39	0.60	8.25	15	4704	387	2	4	419	988
2.54	3.05	15.24	323	99.35	0.60	8.29	25	4778	190	3	4	449	1058
2.54	3.05	15.24	323	99.29	0.60	8.22	25	4939	203	4	7	469	1092
2.54	3.05	15.24	323	99.35	0.60	8.23	35	4778	132	0	5	459	1072
2.54	3.05	15.24	323	99.18	0.60	8.22	35	4924	124	4	7	479	1106
2.54	3.05	15.24	323	99.66	1.20	11.06	3	4573	2242	243	75	238	210
2.54	3.05	15.24	323	99.51	1.20	11.08	3	4704	2272	256	80	228	225
2.54	3.05	15.24	323	99.84	1.20	11.06	5	4792	1158	142	104	329	635
2.54	3.05	15.24	323	99.52	1.20	11.07	5	4924	1172	148	107	359	654
2.54	3.05	15.24	323	99.42	1.20	11.06	10	4998	381	3	4	449	1051
2.54	3.05	15.24	323	99.35	1.20	11.02	10	5071	392	2	4	459	1065
2.54	3.05	15.24	323	99.31	1.20	11.10	15	4807	205	0	4	439	1051
2.54	3.05	15.24	323	99.15	1.20	11.04	15	4895	198	1	7	459	1072
2.54	3.05	15.24	323	99 25	1.20	11.02	25	4939	117	3	7	469	1126
2.54	3.05	15.24	323	99 51	1.20	11.02	25	4866	124	3	7	469	1092
2.54	3.05	15.24	323	99.52	1.20	11.06	35	5247	88	4	5	510	1188
2.54	3.05	15.24	323	99.27	1.20	11.06	35	5086	93	0	5	490	1147
2.54	3.05	15.24	373	98.91	0.10	4.17	5	4631	3635	161	12	128	51
2.54	3.05	15.24	373	98.99	0.10	4.15	5	4602	3605	165	15	98	55
2.54	3.05	15.24	373	99.09	0.10	4.14	10	4807	2154	269	107	258	299
2.54	3.05	15.24	373	99.33	0.10	4.17	10	4792	2143	259	111	268	299
2.54	3.05	15.24	373	99.22	0.10	4 18	15	4748	1246	148	140	349	620
2.54	3.05	15.24	373	99.50	0.10	4 17	15	4778	1260	145	143	349	627
2.54	3.05	15.24	373	99.35	0.10	4 20	25	4602	542	3	34	399	914
2.54	3.05	15.24	373	99.21	0.10	4.18	25	4617	550	1	31	390	914
2.54	3.05	15.24	373	99.39	0.10	4.20	35	4807	322	3	4	449	1030
2.54	3.05	15.24	373	99.34	0 10	4.20	35	4822	314	3	4	453	1038
2.54	3.05	15.24	373	99 59	0.30	5.94	5	5452	2623	358	207	289	252
2.54	3.05	15 24	373	99 55	0.30	5 90	5	5467	2648	363	208	278	248
2.54	3.05	15.24	373	99.42	0.30	5.96	10	5467	996	123	144	439	874

2.54	3.05	15.24	373	99.39	0.30	5.93	10	4485	952	89	114	359	689
2.54	3.05	15.24	373	99.37	0.30	5.58	10	4455	947	91	111	349	682
2.54	3.05	15.24	373	99.02	0.30	5.93	15	5525	498	3	35	510	1140
2.54	3.05	15.24	373	99.01	0.30	5.95	15	5481	489	1	31	479	1127
2.54	3.05	15.24	373	98.99	0.30	5.96	25	5511	220	2	6	530	1214
2.54	3.05	15.24	373	99.35	0.30	5.98	25	5481	229	0	6	520	1208
2.54	3.05	15.24	373	98.97	0.30	5.88	35	5628	146	0	4	557	1271
2.54	3.05	15.24	373	99.06	0.30	5.91	35	5672	139	5	6	530	1270
2.54	3.05	15.24	373	98.91	0.60	7.37	3	4895	2858	294	60	198	128
2.54	3.05	15.24	373	98.95	0.60	7.40	3	4910	2863	301	62	218	133
2.54	3.05	15.24	373	99.11	0.60	7.38	5	5056	1616	269	152	329	477
2.54	3.05	15.24	373	99.15	0.60	7.37	5	5042	1612	269	148	349	473
2.54	3.05	15.24	373	99.19	0.60	7.39	8	4734	762	60	92	369	819
2.54	3.05	15.24	373	99.26	0.60	7.39	8	5027	777	66	100	399	880
2.54	3.05	15.24	373	99.39	0.60	7.41	10	5232	542	9	44	469	1051
2.54	3.05	15.24	373	99.35	0.60	7.36	10	4602	527	3	35	399	908
2.54	3.05	15.24	373	99.45	0.60	7.42	15	4968	282	3	4	459	1079
2.54	3.05	15.24	373	99.33	0.60	7.39	15	4880	278	1	4	449	1058
2.54	3.05	15.24	373	99.51	0.60	7.42	25	4954	154	3	7	479	1112
2.54	3.05	15.24	373	99.37	0.60	7.40	25	5088	146	0	7	500	1140
2.54	3.05	15.24	373	99.35	0.60	7.38	25	4770	102	1	7	459	1072
2.54	3.05	15.24	373	98.99	1.20	10.25	3	6126	2066	428	164	469	449
2.54	3.05	15.24	373	98.98	1.20	10.27	3	6317	2081	447	172	419	464
2.54	3.05	15.24	373	99.07	1.20	10.20	5	5686	913	161	153	469	900
2.54	3.05	15.24	373	99.19	1.20	10.24	5	5701	923	155	148	479	908
2.54	3.05	15.24	373	99.41	1.20	10.30	10	5804	293	2	4	560	1270
2.54	3.05	15.24	373	98.90	1.20	10.24	10	5848	301	1	4	540	1277
2.54	3.05	15.24	373	99.35	1.20	10.22	15	5511	161	3	7	510	1229
2.54	3.05	15.24	373	98.94	1.20	10.26	15	5525	156	4	5	530	1235
2.54	3.05	15.24	373	99.02	1.20	10.31	20	6551	117	1	6	640	1482
2.54	3.05	15.24	373	99.07	1.20	10.26	20	6126	121	2	4	590	1387
2.54	3.05	15.24	373	99.26	1.20	10.28	25	5598	102	2	6	530	1263
2.54	3.05	15.24	373	99.19	1.20	10.18	25	5760	109	2	7	540	1304
2.54	3.05	15.24	423	98.95	0.05	3.15	5	3869	3371	79	0	47	97
2.54	3.05	15.24	423	99.03	0.05	3.14	5	3884	3385	79	0	47	93
2.54	3.05	15.24	423	99.22	0.05	3.14	10	4206	2477	231	56	168	122
2.54	3.05	15.24	423	99.17	0.05	3.13	10	3869	2359	199	48	148	101
2.54	3.05	15.24	423	99.14	0.05	3.13	15	3972	1568	193	115	228	313
2.54	3.05	15.24	423	99.25	0.05	3.11	15	3986	1583	193	115	248	320
2.54	3.05	15.24	423	99.37	0.05	3.16	25	3928	754	35	104	339	640
2.54	3.05	15.24	423	99.21	0.05	3.10	25	3913	747	41	100	309	654
2.54	3.05	15.24	423	99.18	0.05	3.10	35	3942	425	2	36	309	791
2.54	3.05	15.24	423	99.02	0.05	3.09	35	4001	439	3	31	349	806
2.54	3.05	15.24	423	98.90	0.10	3.84	3	4485	3972	79	4	67	60
2.54	3.05	15.24	423	98.99	0.10	3.82	3	4807	4235	98	4	47	54
2.54	3.05	15.24	423	99.11	0.10	3.79	5	4895	3473	231	23	128	54
2.54	3.05	15.24	423	99.18	0.10	3.87	5	4763	3415	224	23	138	53
2.54	3.05	15.24	423	99.01	0.10	3.80	10	4910	1788	294	144	309	375
2.54	3.05	15.24	423	99.23	0.10	3.83	10	4866	1778	288	138	299	383
2.54	3.05	15.24	423	99.33	0.10	3.86	15	4807	982	136	160	379	709
2.54	3.05	15.24	423	99.42	0.10	3.86	15	4573	967	123	152	339	669
2.54	3.05	15.24	423	98.87	0.10	3.85	25	4954	434	6	40	449	1030
2.54	3.05	15.24	423	99.43	0.10	3.86	25	4851	425	3	40	429	1003
2.54	3.05	15.24	423	99.39	0.10	3.84	35	5071	251	2	4	469	1106
2.54	3.05	15.24	423	99.31	0.10	3.87	35	5012	249	1	4	449	1092
2.54	3.05	15.24	423	98.91	0.30	5.51	3	4016	2828	174	15	108	54
2.54	3.05	15.24	423	98.97	0.30	5.51	3	3781	2711	155	15	98	56
2.54	3.05	15.24	423	99.06	0.30	5.50	3	3400	2506	123	12	77	54
2.54	3.05	15.24	423	99.02	0.30	5.51	3	4265	2946	198	19	118	54
2.54	3.05	15.24	423	98.98	0.30	5.51	3	4338	2975	205	19	138	53
2.54	3.05	15.24	423	98.93	0.30	5.49	5	3825	1773	224	75	189	183
2.54	3.05	15.24	423	99.35	0.30	5.48	5	3854	1768	231	80	193	179
2.54	3.05	15.24	423	99.02	0.30	5.52	5	3605	1729	205	67	168	162
2.54	3.05	15.24	423	98.89	0.30	5.52	5	4045	1817	250	84	208	197
2.54	3.05	15.24	423	99.13	0.30	5.49	5	3972	1803	237	80	198	190
2.54	3.05	15.24	423	99.17	0.30	5.50	10	3722	669	60	100	289	601
2.54	3.05	15.24	423	99.14	0.30	5.53	10	3459	659	53	88	258	546
2.54	3.05	15.24	423	99.52	0.30	5.48	10	3810	678	60	96	304	620
2.54	3.05	15.24	423	99.14	0.30	5.49	10	3752	674	63	100	299	607
2.54	3.05	15.24	423	99.26	0.30	5.50	10	3864	666	66	104	329	635
2.54	3.05	15.24	423	99.07	0.30	5.51	10	4133	683	72	111	339	682
2.54	3.05	15.24	423	99.59	0.30	5.47	15	4177	354	1	23	359	859
2.54	3.05	15.24	423	99.26	0.30	5.53	15	3722	352	3	19	329	757
2.54	3.05	15.24	423	99.33	0.30	5.48	15	3840	345	0	19	349	785
2.54	3.05	15.24	423	99.35	0.30	5.49	15	3854	353	2	22	339	789
2.54	3.05	15.24	423	99.62	0.30	5.50	15	3752	361	3	16	309	764
2.54	3.05	15.24	423	98.94	0.30	5.47	20	3605	239	0	4	329	771
2.54	3.05	15.24	423	98.91	0.30	5.47	20	4074	229	3	4	365	880
2.54	3.05	15.24	423	99.10	0.30	5.51	20	3972	235	6	4	359	853
2.54	3.05	15.24	423	99.42	0.30	5.49	20	3752	238	4	4	339	806
2.54	3.05	15.24	423	99.07	0.30	5.48	20	3825	234	3	4	349	919
2.54	3.05	15.24	423	99.06	0.30	5.50	30	3898	149	0	5	369	859
2.54	3.05	15.24	423	98.91	0.30	5.49	30	3708	143	5	4	349	812
2.54	3.05	15.24	423	99.35	0.30	5.45	30	3972	146	4	6	369	874
2.54	3.05	15.24	423	98.99	0.30	5.48	35	4367	120	3	7	419	976
2.54	3.05	15.24	423	99.09	0.30	5.49	35	4323	117	5	7	409	962
2.54	3.05	15.24	423	99.15	0.30	5.50	35	4602	114	3	7	449	1030
2.54	3.05	15.24	423	98.98	0.60	7.14	5	5203	1175	281	180	379	580
2.54	3.05	15.24	423	99.07	0.60	7.13	5	5232	1169	279	184	399	584
2.54	3.05	15.24	423	99.23	0.60	7.15	10	5320	366	3	48	500	1206
2.54	3.05	15.24	423	99.26	0.60	7.20	10	4910	370	3	44	436	1010
2.54	3.05	15.24	423	99.21	0.60	7.16	10	4748	361	2	46	419	976
2.54	3.05	15.24	423	99.74	0.60	7.18	10	4265	364	3	35	379	867
2.54	3.05	15.24	423	99.68	0.60	7.18	15	5364	205	2	4	500	1182
2.54	3.05	15.24	423	99.66	0.60	7.20	15	5379	213	3	4	510	1188
2.54	3.05	15.24	423	99.79	0.60	7.20	20	5437	146	3	7	520	1216
2.54	3.05	15.24	423	99.51	0.60	7.16	20	5423	150	3	7	525	1208
2.54	3.05	15.24	423	99.35	1.20	9.43	3	4895	1480	327	144	326	402
2.54	3.05	15.24	423	99.07	1.20	9.45	3	4910	1493	327	151	339	395
2.54	3.05	15.24	423	99.13	1.20	9.48	5	5056	666	110	144	409	959
2.54	3.05	15.24	423	99.38	1.20	9.49	5	5042	659	113	140	399	853
2.54	3.05	15.24	423	99.27	1.20	9.50	8	4734	308	5	15	429	1003
2.54	3.05	15.24	423	98.89	1.20	9.51	8	5027	311	3	19	459	1072
2.54	3.05	15.24	423	99.41	1.20	9.48	10	5232	220	3	4	479	1147
2.54	3.05	15.24	423	99.55	1.20	9.49	10	4602	215	6	4	399	1003
2.54	3.05	15.24	423	99.42	1.20	9.50	15	4968	132	3	6	459	1113
2.54	3.05	15.24	423	99.10	1.20	9.47	15	4880	131	2	5	436	1092
2.54	3.05	15.24	453	99.63	0.05	3.00	5	5555	4357	183	14	108	56
2.54	3.05	15.24	453	99.13	0.05	3.05	5	5555	4338	201	8	2	55
2.54	3.05	15.24	453	98.98	0.05	3.02	10	5452	2506	384	100	17	210
2.54	3.05	15.24	453	99.09	0.05	2.99	10	5467	2520	377	104	27	217
2.54	3.05	15.24	453	99.15	0.05	3.03	15	5481	1465	319	196	363	532
2.54	3.05	15.24	453	99.37	0.05	3.00	15	5496	1469	318	200	369	538
2.54	3.05	15.24	453	99.22	0.05	2.99	25	5349	645	56	155	449	976
2.54	3.05	15.24	453	99.19	0.05	3.02	25	5379	630	64	160	459	980
2.54	3.05	15.24	453	99.26	0.05	3.00	35	5496	359	9	56	510	1161
2.54	3.05	15.24	453	99.21	0.05	2.97	35	5511	366	7	52	520	1167
2.54	3.05	15.24	453	99.43	0.10	3.64	3	5862	4836	174	0	77	56
2.54	3.05	15.24	453	99.07	0.10	3.63	3	5467	4573	148	0	67	54

2.54	3.05	15.24	453	99.19	0.10	3.63	5	5701	3561	346	38	198	85
2.54	3.05	15.24	453	99.22	0.10	3.85	5	5686	3547	339	40	208	81
2.54	3.05	15.24	453	99.29	0.10	3.64	10	5672	1612	371	192	419	498
2.54	3.05	15.24	453	99.46	0.10	3.62	10	5437	1583	346	184	369	470
2.54	3.05	15.24	453	99.48	0.10	3.63	15	5686	854	172	222	469	908
2.54	3.05	15.24	453	99.35	0.10	3.63	15	5686	835	161	212	459	901
2.54	3.05	15.24	453	99.39	0.10	3.64	25	5789	352	6	52	540	1235
2.54	3.05	15.24	453	99.47	0.10	3.67	25	5745	343	9	52	530	1222
2.54	3.05	15.24	453	99.59	0.10	3.64	35	5848	220	3	4	570	1298
2.54	3.05	15.24	453	99.64	0.10	3.65	35	5774	226	6	4	540	1277
2.54	3.05	15.24	453	99.63	0.30	5.30	3	6111	3547	417	52	248	101
2.54	3.05	15.24	453	99.83	0.30	5.31	3	6536	3679	472	60	278	115
2.54	3.05	15.24	453	99.71	0.30	5.31	5	6038	1964	479	172	399	402
2.54	3.05	15.24	453	99.79	0.30	5.30	5	6126	1978	482	176	409	409
2.54	3.05	15.24	453	99.72	0.30	5.32	10	5247	645	91	155	459	935
2.54	3.05	15.24	453	99.66	0.30	5.32	10	4968	630	85	148	419	880
2.54	3.05	15.24	453	99.82	0.30	5.29	10	4792	632	79	140	409	840
2.54	3.05	15.24	453	99.63	0.30	5.32	10	4455	627	72	128	359	771
2.54	3.05	15.24	453	99.52	0.30	5.30	10	4250	638	66	124	339	730
2.54	3.05	15.24	453	99.39	0.30	5.28	15	6082	337	6	44	560	1311
2.54	3.05	15.24	453	99.19	0.30	5.29	15	6053	344	4	46	550	1304
2.54	3.05	15.24	453	99.06	0.30	5.27	25	6111	156	5	4	580	1378
2.54	3.05	15.24	453	98.95	0.30	5.29	25	6097	161	6	7	570	1366
2.54	3.05	15.24	453	98.91	0.60	6.91	3	6273	2345	529	132	359	278
2.54	3.05	15.24	453	98.98	0.60	6.88	3	5994	2301	491	124	329	265
2.54	3.05	15.24	453	98.86	0.60	6.93	5	6522	1084	371	256	510	906
2.54	3.05	15.24	453	98.83	0.60	6.94	5	6390	1073	365	252	520	791
2.54	3.05	15.24	453	98.91	0.60	6.93	8	6419	489	66	192	590	1263
2.54	3.05	15.24	453	99.25	0.60	6.89	8	6126	483	60	144	550	1201
2.54	3.05	15.24	453	99.02	0.60	6.90	10	6258	337	3	93	580	1338
2.54	3.05	15.24	453	99.13	0.60	6.96	10	6038	332	2	60	570	1284
2.54	3.05	15.24	453	99.19	0.60	6.97	15	5921	189	3	4	560	1318
2.54	3.05	15.24	453	99.29	0.60	6.99	15	6463	190	6	4	620	1448
2.54	3.05	15.24	453	99.35	0.90	7.97	3	6287	1640	510	197	429	456
2.54	3.05	15.24	453	99.46	0.90	7.98	3	6287	1627	510	188	459	449
2.54	3.05	15.24	453	99.35	0.90	8.01	5	6346	703	224	232	530	1003
2.54	3.05	15.24	453	99.38	0.90	8.00	5	6354	712	231	242	550	1015
2.54	3.05	15.24	453	99.51	0.90	8.04	8	6536	322	3	71	600	1393
2.54	3.05	15.24	453	99.52	0.90	8.04	8	6478	313	3	71	580	1379
2.54	3.05	15.24	453	99.64	0.90	7.99	10	6390	240	2	12	590	1414
2.54	3.05	15.24	453	99.72	0.90	7.96	10	6361	234	10	15	610	1406
2.54	3.05	15.24	453	99.66	0.90	8.04	15	6361	127	5	7	621	1434
2.54	3.05	15.24	453	99.35	0.90	7.97	15	6361	132	6	4	616	1450
2.54	3.05	15.24	423	99.51	0.10	3.87	10	3503	1465	174	88	198	231
2.54	3.05	15.24	423	99.46	0.10	3.86	10	5129	1803	313	155	339	402
2.54	3.05	15.24	423	99.42	0.10	3.89	10	5437	1964	339	168	339	436
2.54	3.05	15.24	423	99.48	0.10	3.85	10	5965	1803	390	192	399	498
2.54	3.05	15.24	423	99.13	0.10	3.89	10	6859	1978	472	232	459	593
2.54	3.05	15.24	423	99.06	0.10	3.88	10	8779	2169	657	316	650	819
2.54	3.05	15.24	423	99.35	0.10	3.86	10	10069	2096	777	377	781	976
2.54	3.05	15.24	423	98.99	0.10	3.84	10	10376	2184	809	392	811	1011
2.54	3.05	15.24	423	99.03	0.10	3.88	10	13161	2286	1082	521	1062	1345
2.54	3.05	15.24	423	99.11	0.10	3.86	10	6654	1964	453	220	469	573
2.54	3.05	15.24	423	98.89	0.10	3.86	10	15345	2345	1297	625	1294	1605
2.54	3.05	15.24	423	98.91	0.10	3.89	10	12853	2272	1050	509	1032	1304
2.54	3.05	15.24	423	98.93	0.10	3.86	10	15814	2359	1342	650	1334	1666
2.54	3.05	15.24	423	98.99	0.10	3.89	10	13176	2286	1082	525	1072	1345
2.54	3.05	15.24	423	99.01	0.10	3.86	10	17411	2389	1501	726	1495	1858
2.54	3.05	15.24	423	99.10	0.10	3.90	10	18276	2401	1589	766	1555	1968
2.54	3.05	15.24	423	99.17	0.10	3.89	10	16092	2359	1368	661	1364	1700
2.54	3.05	15.24	423	99.22	0.10	3.89	10	9629	2154	733	356	731	922
2.54	3.05	15.24	423	99.19	0.10	3.84	10	8310	2081	611	296	600	764
2.54	3.05	15.24	423	99.15	0.10	3.86	10	15198	2345	1278	621	1263	1592
2.54	3.05	15.24	423	99.39	0.10	3.90	10	15195	2342	1291	628	1253	1598
2.54	3.05	15.24	423	99.35	0.30	5.47	10	3796	703	60	100	299	614
2.54	3.05	15.24	423	99.33	0.30	5.46	10	4016	718	66	107	329	662
2.54	3.05	15.24	423	99.09	0.30	5.48	10	4441	733	79	124	379	743
2.54	3.05	15.24	423	99.07	0.30	5.47	10	3957	718	66	107	349	648
2.54	3.05	15.24	423	99.07	0.30	5.49	10	4602	733	85	128	359	771
2.54	3.05	15.24	423	99.02	0.30	5.46	10	4617	741	85	128	369	778
2.54	3.05	15.24	423	98.98	0.30	5.46	10	5129	747	98	148	409	880
2.54	3.05	15.24	423	99.05	0.30	5.47	10	5906	740	117	172	510	1038
2.54	3.05	15.24	423	98.90	0.30	5.47	10	6698	766	142	200	570	1195
2.54	3.05	15.24	423	98.91	0.30	5.45	10	6756	759	149	204	580	1208
2.54	3.05	15.24	423	98.94	0.30	5.44	10	8456	777	186	264	771	1550
2.54	3.05	15.24	423	99.09	0.30	5.46	10	11417	791	269	369	1032	2152
2.54	3.05	15.24	423	99.42	0.30	5.47	10	13249	806	313	429	1233	2528
2.54	3.05	15.24	423	99.47	0.30	5.45	10	16092	813	390	529	1525	3109
2.54	3.05	15.24	423	99.41	0.30	5.46	10	17499	821	428	581	1665	3389
2.54	3.05	15.24	423	99.50	0.30	5.47	10	18247	831	447	606	1736	3546
2.54	3.05	15.24	423	99.51	0.30	5.48	10	12868	806	300	417	1193	2452
2.54	3.05	15.24	423	99.54	0.30	5.44	10	10303	791	231	325	942	1926
2.54	3.05	15.24	423	99.59	0.30	5.46	10	15829	806	384	521	1484	3054
2.54	3.05	15.24	423	99.35	0.30	5.47	10	19742	821	491	658	1856	3847
2.54	3.05	15.24	423	99.59	0.60	7.18	10	4367	381	3	35	399	894
2.54	3.05	15.24	423	99.55	0.60	7.17	10	6727	410	3	53	610	1427
2.54	3.05	15.24	423	99.64	0.60	7.16	10	5628	415	3	52	500	1182
2.54	3.05	15.24	423	99.66	0.60	7.17	10	6067	405	3	56	540	1277
2.54	3.05	15.24	423	99.66	0.60	7.17	10	8178	411	9	80	761	1763
2.54	3.05	15.24	423	99.48	0.60	7.16	10	8999	401	15	92	851	1947
2.54	3.05	15.24	423	99.35	0.60	7.14	10	11388	405	22	120	1093	2494
2.54	3.05	15.24	423	99.27	0.60	7.18	10	11842	422	28	124	1123	2596
2.54	3.05	15.24	423	99.37	0.60	7.17	10	14260	400	34	152	1354	3149
2.54	3.05	15.24	423	99.26	0.60	7.15	10	9878	407	15	100	942	2145
2.54	3.05	15.24	423	99.22	0.60	7.16	10	15550	410	41	168	1495	3443
2.54	3.05	15.24	423	99.33	0.60	7.17	10	12560	414	28	132	1213	2760
2.54	3.05	15.24	423	99.25	0.60	7.17	10	16547	428	47	180	1584	3669
2.54	3.05	15.24	423	99.18	0.60	7.15	10	12590	410	28	132	1223	2767
2.54	3.05	15.24	423	99.23	0.60	7.16	10	19024	425	60	208	1836	4237
2.54	3.05	15.24	423	99.17	0.60	7.17	10	21808	431	72	241	2118	4873
2.54	3.05	15.24	423	99.02	0.60	7.18	10	20328	420	66	224	1976	4531
2.54	3.05	15.24	423	98.98	0.60	7.20	10	9438	410	15	96	871	2049
2.54	3.05	15.24	423	99.46	0.60	7.18	10	8750	420	15	88	821	1892
2.54	3.05	15.24	423	98.97	0.60	7.16	10	15389	401	41	168	1495	3403
2.54	3.05	15.24	423	99.35	0.60	7.17	10	21061	425	66	228	2057	4702
2.54	2.54	15.24	423	98.93	0.30	5.33	10	3928	510	69	107	309	635
2.54	2.54	15.24	423	98.98	0.30	5.34	10	3766	518	56	100	299	601
2.54	2.54	15.24	423	98.89	0.30	5.36	10	3649	513	50	96	289	580
2.54	2.54	15.24	423	98.86	0.30	5.34	10	4045	527	72	111	319	654
2.54	2.54	15.24	423	98.86	0.30	5.31	10	4177	532	74	115	339	682
2.54	2.54	15.24	423	98.91	0.30	5.32	10	3972	513	66	107	319	641
2.54	2.54	15.24	423	98.98	0.30	5.31	10	3722	510	59	100	289	593
2.54	2.54	15.24	423	98.91	0.30	5.31	10	3752	519	60	100	299	601
2.54	2.54	15.24	423	98.99	0.30	5.30	10	4294	524	79	120	349	709
2.54	2.54	15.24	423	99.01	0.30	5.35	10	4235	527	72	115	339	696
2.54	2.97	15.24	423	99 35	0 30	5.35	10	3986	571	66	107	309	648
2.54	2 97	15.24	423	99 39	0 30	5 36	10	3796	560	60	100	319	614
2.54	2.97	15.24	423	99.42	0.30	5.33	10	3576	557	53	92	278	573

2.54	2.97	15.24	423	99.42	0.30	5.33	10	3576	557	53	92	278	573
2.54	2.97	15.24	423	99.51	0.30	5.34	10	3972	572	66	107	309	648
2.54	2.97	15.24	423	99.46	0.30	5.34	10	4221	575	72	115	349	696
2.54	2.97	15.24	423	99.46	0.30	5.35	10	3840	571	60	104	309	620
2.54	2.97	15.24	423	99.52	0.30	5.33	10	3752	498	60	100	309	607
2.54	2.97	15.24	423	98.93	0.30	5.35	10	3825	527	66	104	299	614
2.54	2.97	15.24	423	98.89	0.30	5.36	10	3986	542	66	104	309	648
2.54	2.97	15.24	423	98.87	0.30	5.35	10	4265	571	72	115	349	703
2.54	3.56	15.24	423	98.85	0.30	5.48	10	4045	689	66	107	339	669
2.54	3.56	15.24	423	98.90	0.30	5.49	10	3722	676	63	96	299	601
2.54	3.56	15.24	423	98.98	0.30	5.47	10	3854	667	56	100	289	627
2.54	3.56	15.24	423	98.91	0.30	5.49	10	3796	674	60	103	278	620
2.54	3.56	15.24	423	98.87	0.30	5.48	10	4074	689	66	107	309	675
2.54	3.56	15.24	423	98.97	0.30	5.47	10	3561	674	53	92	268	573
2.54	3.56	15.24	423	99.02	0.30	5.48	10	4162	689	66	111	339	689
2.54	3.56	15.24	423	99.07	0.30	5.48	10	3972	689	66	104	319	654
2.54	3.56	15.24	423	99.11	0.30	5.48	10	3429	659	47	88	258	546
2.54	3.56	15.24	423	99.30	0.30	5.48	10	3898	674	60	104	309	641
2.54	3.05	7.62	423	99.35	0.30	7.09	10	4485	356	3	40	409	914
2.54	3.05	7.62	423	99.35	0.30	7.11	10	4016	347	9	34	339	812
2.54	3.05	7.62	423	99.35	0.30	7.10	10	4001	352	9	31	359	806
2.54	3.05	7.62	423	99.35	0.30	7.11	10	3796	349	3	29	329	764
2.54	3.05	7.62	423	99.35	0.30	7.08	10	4074	360	3	35	369	825
2.54	3.05	7.62	423	99.35	0.30	7.09	10	3810	348	6	25	349	764
2.54	3.05	7.62	423	99.35	0.30	7.10	10	4133	352	3	35	339	840
2.54	3.05	7.62	423	99.35	0.30	7.08	10	3942	352	9	31	349	791
2.54	3.05	7.62	423	99.35	0.30	7.11	10	3708	337	4	31	319	743
2.54	3.05	7.62	423	99.35	0.30	7.07	10	3898	352	3	31	349	785
2.54	3.05	22.86	423	98.95	0.30	4.77	10	4367	879	148	148	339	580
2.54	3.05	22.86	423	99.02	0.30	4.75	10	4074	869	136	132	309	532
2.54	3.05	22.86	423	98.95	0.30	4.76	10	3869	865	123	124	258	498
2.54	3.05	22.86	423	99.15	0.30	4.74	10	3664	850	117	115	248	464
2.54	3.05	22.86	423	99.07	0.30	4.75	10	4309	879	148	144	309	573
2.54	3.05	22.86	423	99.25	0.30	4.78	10	3942	865	129	128	278	511
2.54	3.05	22.86	423	98.85	0.30	4.75	10	4148	859	142	136	309	546
2.54	3.05	22.86	423	98.91	0.30	4.82	10	3679	850	117	115	238	464
2.54	3.05	22.86	423	99.13	0.30	4.75	10	4235	879	142	140	339	559
2.54	3.05	22.86	423	99.29	0.30	4.74	10	4045	865	136	132	299	525
2.54	3.05	30.48	423	99.43	0.30	4.25	10	3825	1128	161	120	248	388
2.54	3.05	30.48	423	99.26	0.30	4.23	10	4133	1143	186	136	278	436
2.54	3.05	30.48	423	99.35	0.30	4.24	10	3869	1137	167	124	248	395
2.54	3.05	30.48	423	99.41	0.30	4.23	10	3825	1128	167	120	238	388
2.54	3.05	30.48	423	99.35	0.30	4.25	10	4235	1158	193	140	289	449
2.54	3.05	30.48	423	99.35	0.30	4.24	10	3679	1114	155	115	238	368
2.54	3.05	30.48	423	99.46	0.30	4.23	10	4441	1172	205	148	289	477
2.54	3.05	30.48	423	99.60	0.30	4.24	10	3810	1128	161	120	238	388
2.54	3.05	30.48	423	99.27	0.30	4.23	10	4294	1187	193	144	299	457
2.54	3.05	30.48	423	99.38	0.30	4.25	10	4133	1143	186	136	258	436
2.54	3.04	7.62	423	98.93	0.30	7.12	5	4500	1246	231	148	314	478
2.54	3.04	7.62	423	98.93	0.30	7.15	5	4383	1290	219	144	303	464
2.54	3.04	7.62	423	98.93	0.30	7.14	5	4236	1159	212	136	291	443
2.54	3.04	15.20	423	99.68	0.30	5.52	10	4207	792	73	116	335	696
2.54	3.04	15.20	423	99.68	0.30	5.47	10	4134	690	66	112	329	683
2.54	3.04	15.20	423	99.68	0.30	5.44	10	3958	660	59	104	311	648
2.54	3.04	22.80	423	99.63	0.30	4.71	15	4383	572	15	72	369	847
2.54	3.04	22.90	423	99.63	0.30	4.69	15	4500	455	20	76	381	867
2.54	3.04	22.90	423	99.63	0.30	4.74	15	4266	646	15	68	361	819
2.54	3.04	30.50	423	98.94	0.30	4.30	20	4295	484	3	36	372	874
2.54	3.04	30.50	423	98.94	0.30	4.26	20	4383	543	0	40	381	895
2.54	3.04	30.50	423	98.94	0.30	4.27	20	4163	631	6	36	358	840
5.08	3.05	15.24	423	98.94	0.30	9.68	10	4265	1803	250	92	218	217
5.08	3.05	15.24	423	98.93	0.30	9.66	10	3869	1729	212	80	189	190
5.08	3.05	15.24	423	98.91	0.30	9.68	10	3972	1759	224	84	208	197
5.08	3.05	15.24	423	98.87	0.30	9.67	10	4148	1788	237	88	218	210
5.08	3.05	15.24	423	98.99	0.30	9.66	15	3942	1026	148	128	278	449
5.08	3.05	15.24	423	99.35	0.30	9.66	15	4294	1040	157	144	299	504
5.08	3.05	15.24	423	99.42	0.30	9.68	15	4485	1055	174	155	309	538
5.08	3.05	15.24	423	99.51	0.30	9.69	15	3825	1011	136	124	268	436
5.08	3.05	15.24	423	99.52	0.30	9.69	20	4206	659	60	115	339	703
5.08	3.05	15.24	423	99.60	0.30	9.68	20	3429	645	41	88	248	546
5.08	3.05	15.24	423	99.13	0.30	9.70	20	3986	659	53	107	309	654
5.08	3.05	15.24	423	99.22	0.30	9.69	20	3854	659	53	104	289	627
5.08	3.05	15.24	423	99.35	0.30	9.68	25	4338	471	3	67	359	840
5.08	3.05	15.24	423	99.39	0.30	9.70	25	3752	454	3	56	309	709
5.08	3.05	15.24	423	99.02	0.30	9.67	25	4279	467	3	63	379	825
5.08	3.05	15.24	423	98.97	0.30	9.71	25	4426	465	9	67	369	859
5.08	3.05	15.24	423	99.39	0.30	9.69	35	4235	278	3	4	390	901
5.08	3.05	15.24	423	99.35	0.30	9.70	35	4617	280	5	3	419	990
5.08	3.05	15.24	423	98.93	0.30	9.72	35	4016	275	6	6	369	846
5.08	3.05	15.24	423	98.89	0.30	9.70	35	3708	277	5	5	349	778
5.08	3.05	15.24	423	98.87	1.20	18.22	10	3869	674	66	104	329	627
5.08	3.05	15.24	423	98.85	1.20	18.23	10	3913	645	70	101	289	635
5.08	3.05	15.24	423	98.99	1.20	18.21	10	3957	703	60	107	339	648
5.08	3.05	15.24	423	99.03	1.20	18.21	10	4148	659	75	111	349	682
5.08	3.05	15.24	423	99.01	1.20	18.20	10	4191	703	72	115	339	689
5.08	3.05	15.24	423	99.26	1.20	18.21	10	4074	630	66	116	347	669

TABLE E1.8

THE CONCENTRATION DISTRIBUTION OF THE PRODUCTS OF THE REACTION BETWEEN METHYL MERCAPTAN AND AIR IN THE CORONA REACTOR*

t	r	Digits						Weight
hr	m	CH_3SH in	CH_3SH out	$(CH_3)_2S_2$ out	$(CH_3)_2S$ out	H_2O out	SO_2 out	$(CH_3)_2SO_2$ out gm
	T=298 K		Ic=0.10	mA				
3	5	4823	4063	70	3	5	1	0.0002
3	5	4852	4183	75	1	3	2	
3	5	5042	4148	72	2	5	0	
3	10	5174	3134	240	69	20	181	0.0067
3	10	5072	3173	220	59	19	175	
3	10	5130	3057	418	69	20	176	
3	15	5028	1956	168	94	29	455	0.0159
3	15	4984	2038	164	94	30	468	
3	15	4954	1880	161	95	29	441	
3	25	5218	1000	53	72	40	923	0.0303
3	25	5277	958	58	73	41	912	
3	25	5233	1003	58	72	40	925	
3	35	5277	594	4	4	44	1089	0.0273
3	35	5218	583	2	3	45	1091	
3	35	5292	544	3	3	44	1087	
	T=298 K		Ic=0.30	mA				
3	3	5218	4395	173	36	12	36	0.0003
3	3	5277	4470	182	39	12	41	
3	5	5511	3924	220	39	17	136	0.0043
3	5	5555	3966	212	41	18	141	
3	10	5218	2698	185	126	35	657	0.0358
3	10	5174	2573	189	130	35	647	
3	15	5028	1461	44	20	40	942	0.0498
3	15	5072	1623	47	22	40	967	
3	25	5365	656	5	2	48	1125	0.0405
3	25	5321	546	5	4	47	1126	
3	35	5160	176	3	1	47	1107	0.0292
3	35	5101	74	2	0	47	1094	
	T=298 K		Ic=1.20	mA				
3	3	5805	2997	347	113	29	365	0.0383
3	3	5849	2846	355	117	30	360	
3	5	5951	1896	233	129	43	751	0.0882
3	5	6010	2033	257	142	44	735	
3	10	5775	530	0	6	51	1189	0.1060
3	10	5658	465	2	5	49	1165	
3	15	5863	306	3	0	54	1294	0.0774
3	15	5746	244	5	4	53	1236	
3	25	5761	131	3	1	54	1295	0.0462
3	25	5834	74	1	6	55	1319	
3	35	6024	74	6	1	56	1366	0.0350
3	35	6098	86	2	7	57	1390	
	T=373 K		Ic=0.10	mA				
3	5	5922	4401	255	29	12	36	0.0006
3	5	5849	4463	249	26	12	41	
3	10	5467	2177	347	121	32	365	0.0071
3	10	5365	2402	344	121	31	353	
3	15	6083	1456	198	194	44	795	0.0262
3	15	6200	1606	203	198	44	808	
3	25	5614	462	1	46	47	1147	0.0366
3	25	5526	510	0	46	47	1126	
3	35	5321	389	5	2	48	1141	0.0294
3	35	5365	286	3	2	49	1147	
	T=373 K		Ic=0.30	mA				
3	3	6259	3909	1639	246	21	101	0.0019
3	3	6186	3741	1566	276	23	71	
3	5	7168	2982	526	144	41	373	0.0137
3	5	7080	3086	517	139	40	366	
3	10	6904	1167	192	213	57	1082	0.0657
3	10	6831	1020	192	210	56	1073	
3	15	6684	471	5	75	59	1425	0.0758
3	15	6787	544	7	75	60	1428	
3	25	7270	218	4	4	67	1594	0.0591
3	25	7168	287	5	0	66	1575	
3	35	6845	74	2	1	64	1503	0.0398
3	35	6801	74	7	8	63	1495	

	T=373	K	Ic=1.20	mA				
3	3	7124	1836	493	221	51	609	0.0493
3	3	7080	1685	492	221	51	603	
3	5	6743	1008	204	197	58	1039	0.1225
3	5	6669	865	200	196	57	1025	
3	8	7549	672	0	56	68	1561	0.1599
3	8	7519	6105	1	58	68	1573	
3	10	7065	298	10	2	65	1494	0.1401
3	10	6992	281	3	0	64	1487	
3	15	6347	137	6	0	58	1355	0.0849
3	15	6405	125	8	2	59	1361	
3	25	7461	103	9	3	69	1664	0.0601
3	25	7402	118	5	4	68	1648	
3	35	6479	87	10	6	60	1440	0.0369
3	35	6552	80	3	1	60	1453	

	T=423	K	Ic=0.05	mA				
3	5	4442	3786	120	3	6	1	0.0001
3	5	4339	3614	118	2	6	2	
3	10	4544	2354	272	66	18	157	0.0014
3	10	4603	2429	275	67	19	164	
3	15	4163	1423	230	136	27	368	0.0074
3	15	4192	1309	231	136	26	374	
3	25	4295	623	41	119	35	745	0.0178
3	25	4266	661	42	118	35	731	
3	35	4617	301	4	37	40	968	0.0219
3	35	4661	395	6	15	40	982	

	T=423	K	Ic=0.10	mA				
3	5	4339	3059	196	14	12	50	0.0008
3	5	4295	2986	193	14	12	48	
3	10	4119	1530	250	132	23	303	0.0080
3	10	4163	1464	254	133	24	306	
3	15	4485	780	133	148	34	684	0.0226
3	15	4544	879	136	149	35	688	
3	25	4735	400	9	35	40	983	0.0312
3	25	4559	343	4	33	39	942	
3	35	4075	154	11	3	36	866	0.0229
3	35	4119	236	8	0	37	877	

	T=423	K	Ic=0.30	mA				
3	3	4412	3072	182	20	11	36	0.0013
3	3	4485	3114	199	20	11	36	
3	5	4280	2013	254	86	20	205	0.0084
3	5	4295	2041	253	85	20	204	
3	10	4647	843	78	118	35	733	0.0489
3	10	4735	820	81	125	35	749	
3	10	3342	560	46	88	26	565	0.0350
3	10	3269	546	47	84	25	537	
3	15	4911	389	13	0	42	1018	0.0552
3	15	4940	365	4	1	43	1026	
3	25	4691	207	1	0	42	997	0.0369
3	25	4559	202	3	6	40	973	
3	35	4119	115	1	0	37	885	0.0232
3	35	4207	120	3	0	38	910	

	T=453	K	Ic=0.05	mA				
3	5	5438	3936	211	11	11	18	0.0003
3	5	5350	4031	207	11	11	13	
3	5	5321	3957	207	11	11	20	
3	10	5321	2068	383	134	29	279	0.0045
3	10	5380	2249	389	136	29	292	
3	10	5438	2327	391	137	29	281	
3	15	5746	1322	355	204	44	607	0.0144
3	15	5702	1256	354	203	43	613	
3	15	5658	1247	348	200	43	513	
3	25	5951	603	51	168	52	1128	0.0304
3	25	5907	541	48	167	52	1131	
3	25	5863	537	51	164	52	1133	
3	35	5585	294	0	41	50	1178	0.0295
3	35	5526	238	0	41	50	1175	
3	35	5541	293	3	41	50	1156	

	T=453	K	Ic=0.10	mA				
3	3	6083	4400	266	27	14	46	0.0001
3	3	5907	4391	258	26	13	45	
3	5	5702	3169	415	59	24	100	0.0015
3	5	5555	2979	403	57	23	96	
3	10	5878	1525	400	219	40	612	0.0174
3	10	6112	1596	419	229	42	638	
3	15	6303	516	189	225	52	1038	0.0369
3	15	5980	535	174	212	50	986	
3	25	6537	352	2	66	61	1353	0.0476
3	25	6479	337	4	65	60	1342	
3	35	6230	185	1	5	58	1391	0.0359
3	35	6552	210	0	4	61	1466	

*Reactor dimensions: $D=2.54\times10^{-2}$, $H=1.52\times10^{-1}$, and $a=1.52\times10^{-5}$ m

TABLE E1.c
THE EFFECT OF THE INITIAL CONCENTRATION OF WATER ON THE REACTION OF METHYL MERCAPTAN WITH AIR*

P	I_c	V_s	Digits						
kPa	mA	kV	CH_3SH in	H_2O in	CH_3SH out	$(CH_3)_2S_2$ out	$(CH_3)_2S$ out	H_2O out	SO_2 out
98.99	0.10	3.83	3943	367	1393	212	92	576	273
98.99	0.10	3.84	3958	396	1320	216	116	614	277
98.99	0.10	3.82	3899	352	1364	206	108	587	266
98.99	0.10	3.86	4002	2633	1466	219	96	2856	279
98.99	0.10	3.84	3987	2691	1422	212	116	2900	275
98.99	0.10	3.88	3943	2516	221	209	100	2746	273
99.33	0.10	3.89	3811	5306	1393	200	108	5794	259
99.33	0.10	3.92	3841	5189	1276	204	100	5425	266
99.33	0.10	3.87	3782	5422	1452	200	84	5648	259
98.85	0.10	3.94	3973	7281	1481	212	104	7490	293
98.85	0.10	3.95	4002	7397	1393	219	112	7624	279
98.85	0.10	3.96	3943	7194	1510	207	86	7432	269
99.10	0.10	3.97	3577	11000	1173	180	88	11186	238
99.10	0.10	3.98	3504	10942	1100	174	96	11148	225
99.10	0.10	3.98	3533	11087	1027	179	84	11276	232
99.25	0.10	4.06	4002	14690	1540	218	108	14916	279
99.25	0.10	4.07	3973	14602	1437	212	96	14844	284
99.25	0.10	4.08	3973	14632	1686	210	100	14847	271
99.07	0.10	4.11	4324	18467	1979	244	128	18702	314
99.07	0.10	4.10	4485	18321	1833	257	120	18609	327
99.07	0.10	4.12	4383	18408	2126	250	116	18664	320
99.38	0.10	4.16	3943	23754	1540	212	112	23949	271
99.38	0.10	4.17	3899	23667	1686	206	104	23885	273
99.38	0.10	4.17	4016	23696	1408	222	103	23908	279
99.26	0.10	4.22	3826	27211	1393	200	92	27418	259
99.26	0.10	4.21	3855	27270	1334	193	100	27505	266
99.26	0.10	4.23	3870	27124	1466	208	98	27360	272
98.86	0.10	4.26	3723	32121	1290	180	96	32307	252
98.86	0.10	4.27	3650	32063	1349	187	92	32240	245
98.86	0.10	4.28	3665	32209	1217	168	90	32403	241
99.46	0.10	4.38	3973	37235	1393	225	104	37426	279
99.46	0.10	4.40	3929	37554	1290	212	107	37752	273
99.46	0.10	4.38	3870	37380	1466	193	100	37627	266
99.03	0.10	4.43	3782	40808	1393	180	96	40991	259
99.03	0.10	4.44	3811	40663	1452	200	104	40855	263
99.03	0.10	4.43	3811	40983	1290	208	100	41177	254
99.18	0.30	5.51	3943	250	807	79	101	561	642
99.18	0.30	5.51	3973	221	851	60	108	535	648
99.18	0.30	5.53	3899	279	777	73	106	608	635
99.30	0.30	5.61	3797	686	660	47	100	971	614
99.30	0.30	5.59	3855	599	733	60	105	913	628
99.30	0.30	5.62	3753	570	690	73	96	884	607
98.98	0.30	5.59	4002	3098	807	53	113	3391	655
98.98	0.30	5.63	4016	3156	880	66	108	3467	659
98.98	0.30	5.63	3958	3243	748	79	112	3557	648
99.07	0.30	6.06	4398	7572	1173	92	120	7903	731
99.07	0.30	6.08	4383	7659	1232	73	117	8005	728
99.07	0.30	6.07	4354	7485	1100	66	125	7862	724
99.42	0.30	6.13	4236	13992	1100	60	116	14309	703
99.42	0.30	6.14	4222	13905	1027	53	114	14231	698
99.42	0.30	6.12	4192	14080	1188	79	112	14402	696
99.39	0.30	6.20	3841	15707	807	60	100	16029	621
99.39	0.30	6.20	3855	15590	880	47	104	15916	628
99.39	0.30	6.18	3811	15532	748	66	104	15858	626
99.26	0.30	6.28	3753	21575	690	79	96	21848	607
99.26	0.30	6.26	3650	21633	748	60	103	21906	587
99.26	0.30	6.28	3709	21546	733	47	96	21828	601
98.82	0.30	6.48	4016	25933	821	66	108	26221	655
98.82	0.30	6.49	3958	25788	895	92	113	26096	648
98.82	0.30	6.47	3973	25875	719	47	104	26221	653
98.85	0.30	6.64	4134	29739	924	53	112	30035	683
99.60	0.30	6.66	4178	29826	968	73	115	30195	690
99.60	0.30	6.67	4104	29681	851	53	107	29977	676
99.60	0.30	6.77	4236	35085	1100	66	121	35419	703
99.55	0.30	6.75	4222	34969	997	79	116	35308	713
99.55	0.30	6.78	4192	35027	1188	60	111	35375	696
99.55	0.30	6.86	4060	40518	953	79	108	40869	669
99.70	0.30	6.88	3973	40343	865	60	102	40695	648
99.70	0.30	6.87	4016	40431	1071	47	110	40724	662
99.43	0.30	6.98	3811	41767	733	79	103	42063	621
99.43	0.30	6.97	3841	41825	792	41	98	42116	616
99.43	0.30	6.98	3826	41709	690	73	100	41996	624

Experimental conditions:

D = 2.54x10 m^{-2}
H = 1.52x10 m^{-4}
a = 1.52x10 m^{-5}
t = 10 s
T = 423 K

TABLE E2.4

DATA FOR THE REACTION OF DIMETHYL DISULPHIDE WITH AIR IN THE CORONA REACTOR
(Without considering dimethyl sulphone)

D_R	D_w	E	T	P	I_c	V_s		Digits			
			K	kPa	mA	kV					
10^{-2} m	10^{-5} m	10 m						$(CH_3)_2S_2$ in	$(CH_3)_2S_2$ out	$(CH_3)_2S$ out	SO_2 out
2.54	3.05	1.52	298	99.84	0.10	4.64	5	1730	1533	116	252
2.54	3.05	1.52	298	99.87	0.10	4.64	10	1653	1038	309	724
2.54	3.05	1.52	298	99.96	0.10	4.66	15	1868	682	345	1414
2.54	3.05	1.52	298	99.68	0.10	4.65	20	1857	307	184	1749
2.54	3.05	1.52	298	99.88	0.10	4.61	25	1876	104	96	1940
2.54	3.05	1.52	298	99.98	0.10	4.62	35	1749	3	8	1886
2.54	3.05	1.52	298	99.82	0.30	6.66	5	1850	1330	285	642
2.54	3.05	1.52	298	99.75	0.30	6.65	5	1952	1400	293	655
2.54	3.05	1.52	298	99.67	0.30	6.63	8	2085	917	305	1359
2.54	3.05	1.52	298	99.82	0.30	6.67	8	1971	866	353	1318
2.54	3.05	1.52	298	99.84	0.30	6.65	10	1888	530	281	1592
2.54	3.05	1.52	298	99.88	0.30	6.65	10	1952	549	269	1592
2.54	3.05	1.52	298	99.74	0.30	6.66	15	1914	104	84	1954
2.54	3.05	1.52	298	99.71	0.30	6.67	15	1971	117	88	2043
2.54	3.05	1.52	298	99.58	0.30	6.65	25	2073	5	2	2214
2.54	3.05	1.52	298	99.62	0.30	6.65	25	1933	4	3	2009
2.54	3.05	1.52	298	99.52	0.30	6.64	35	2130	2	4	2159
2.54	3.05	1.52	298	99.68	0.30	6.66	35	2206	5	6	2316
2.54	3.05	1.52	298	99.66	0.50	7.71	5	1793	1082	125	874
2.54	3.05	1.52	298	99.59	0.50	7.75	5	1711	1006	309	954
2.54	3.05	1.52	298	99.52	0.50	7.74	8	1895	511	253	1605
2.54	3.05	1.52	298	99.58	0.50	7.74	8	1939	523	261	1619
2.54	3.05	1.52	298	99.54	0.50	7.73	10	1876	238	148	1134
2.54	3.05	1.52	298	99.51	0.50	7.74	10	1895	244	160	1865
2.54	3.05	1.52	298	99.47	0.50	7.75	15	2060	3	12	2173
2.54	3.05	1.52	298	99.56	0.50	7.75	15	1914	3	4	2036
2.54	3.05	1.52	298	99.62	0.50	7.72	20	2092	7	3	2186
2.54	3.05	1.52	298	99.75	0.50	7.73	20	2015	2	4	2145
2.54	3.05	1.52	298	99.66	0.80	9.42	3	1927	1419	273	621
2.54	3.05	1.52	298	99.59	0.80	9.39	3	1952	1438	257	628
2.54	3.05	1.52	298	99.62	0.80	9.45	5	1787	784	317	1188
2.54	3.05	1.52	298	99.45	0.80	9.44	5	1736	758	309	1154
2.54	3.05	1.52	298	99.52	0.80	9.42	8	1844	225	128	1824
2.54	3.05	1.52	298	99.58	0.80	9.41	8	2073	257	160	2050
2.54	3.05	1.52	298	99.55	0.80	9.40	10	1952	166	40	2022
2.54	3.05	1.52	298	99.64	0.80	9.39	10	2092	173	44	2234
2.54	3.05	1.52	373	99.79	0.05	3.34	5	149	136	0	0
2.54	3.05	1.52	373	99.59	0.05	3.35	10	1469	1076	245	484
2.54	3.05	1.52	373	99.45	0.05	3.35	15	1660	841	373	983
2.54	3.05	1.52	373	99.52	0.05	3.35	20	1685	511	317	1366
2.54	3.05	1.52	373	99.58	0.05	3.33	25	1666	282	293	1585
2.54	3.05	1.52	373	99.74	0.05	3.34	35	1666	3	76	1769
2.54	3.05	1.52	373	99.79	0.10	4.17	3	2015	1901	96	136
2.54	3.05	1.52	373	99.72	0.10	4.16	3	2073	1958	76	177
2.54	3.05	1.52	373	99.68	0.10	4.18	5	1952	1673	188	348
2.54	3.05	1.52	373	99.67	0.10	4.20	5	1965	1685	197	320
2.54	3.05	1.52	373	99.84	0.10	4.21	8	2092	1425	357	819
2.54	3.05	1.52	373	99.74	0.10	4.22	8	1990	1355	349	778
2.54	3.05	1.52	373	99.82	0.10	4.18	10	1977	1095	397	1024
2.54	3.05	1.52	373	99.71	0.10	4.18	10	2092	1165	417	1127
2.54	3.05	1.52	373	99.66	0.10	4.18	15	2034	555	417	1728
2.54	3.05	1.52	373	99.70	0.10	4.21	15	2009	549	357	1653
2.54	3.05	1.52	373	99.74	0.10	4.17	20	2060	200	225	2063
2.54	3.05	1.52	373	99.76	0.10	4.22	20	2066	206	213	2043
2.54	3.05	1.52	373	99.66	0.10	4.23	25	2269	47	120	2405
2.54	3.05	1.52	373	99.64	0.10	4.17	25	2257	47	108	2398
2.54	3.05	1.52	373	99.63	0.30	5.90	5	1787	1171	345	744
2.54	3.05	1.52	373	99.52	0.30	5.87	5	1863	1222	329	913
2.54	3.05	1.52	373	99.62	0.30	5.89	8	1895	663	405	1414
2.54	3.05	1.52	373	99.58	0.30	5.87	8	1888	657	381	1462
2.54	3.05	1.52	373	99.55	0.30	5.91	10	2060	403	301	1920
2.54	3.05	1.52	373	99.60	0.30	5.94	10	1920	371	329	1804
2.54	3.05	1.52	373	99.64	0.30	5.90	15	2104	41	56	2241
2.54	3.05	1.52	373	99.64	0.30	5.88	15	2022	34	84	2152
2.54	3.05	1.52	373	99.60	0.30	5.86	25	2136	4	3	2309
2.54	3.05	1.52	373	99.66	0.30	5.96	25	2161	7	0	2316
2.54	3.05	1.52	373	99.64	0.30	5.88	35	2047	0	2	2159
2.54	3.05	1.52	373	99.68	0.30	5.91	35	2117	4	1	2303
2.54	3.05	1.52	373	99.64	0.50	6.96	3	2015	1565	301	539
2.54	3.05	1.52	373	99.54	0.50	6.99	3	2073	1609	257	594
2.54	3.05	1.52	373	99.52	0.50	6.94	5	1952	993	385	1120
2.54	3.05	1.52	373	99.52	0.50	6.94	5	1965	1000	405	1168
2.54	3.05	1.52	373	99.51	0.50	6.95	8	2092	384	297	1940
2.54	3.05	1.52	373	99.47	0.50	6.97	8	1990	365	309	1824
2.54	3.05	1.52	373	99.54	0.50	6.93	10	1977	130	140	2241
2.54	3.05	1.52	373	99.56	0.50	6.96	10	2092	142	136	2152
2.54	3.05	1.52	373	99.60	0.50	6.96	15	2034	3	4	2200
2.54	3.05	1.52	373	99.58	0.50	6.97	15	2009	0	4	2173
2.54	3.05	1.52	373	99.55	0.50	6.95	20	2066	3	1	2241
2.54	3.05	1.52	373	99.60	0.50	6.92	20	2073	0	0	2200
2.54	3.05	1.52	373	99.64	0.50	6.98	25	2276	5	2	2453
2.54	3.05	1.52	373	99.66	0.50	6.96	25	2257	4	1	2371
2.54	3.05	1.52	423	99.74	0.10	3.89	3	1927	1806	108	177
2.54	3.05	1.52	423	99.70	0.10	3.89	3	2028	1901	72	177
2.54	3.05	1.52	423	99.67	0.10	3.85	5	2073	1749	201	389
2.54	3.05	1.52	423	99.75	0.10	3.83	5	1920	1622	184	389
2.54	3.05	1.52	423	99.72	0.10	3.90	8	2073	1361	441	1011
2.54	3.05	1.52	423	99.70	0.10	3.88	8	2028	1336	397	933
2.54	3.05	1.52	423	99.82	0.10	3.87	10	2149	1133	493	1236
2.54	3.05	1.52	423	99.67	0.10	3.86	10	2142	1133	465	1209
2.54	3.05	1.52	423	99.70	0.10	3.84	15	2200	536	433	1927
2.54	3.05	1.52	423	99.72	0.10	3.88	15	2073	504	441	1817
2.54	3.05	1.52	423	99.76	0.10	3.86	25	2092	28	112	2180
2.54	3.05	1.52	423	99.71	0.10	3.90	35	2136	3	8	2145
2.54	3.05	1.52	423	99.64	0.30	5.50	3	2066	1736	229	457
2.54	3.05	1.52	423	99.63	0.30	5.49	3	2073	1742	229	396
2.54	3.05	1.52	423	99.60	0.30	5.47	5	2136	1342	401	1004
2.54	3.05	1.52	423	99.66	0.30	5.49	5	2130	1342	441	983
2.54	3.05	1.52	423	99.56	0.30	5.47	8	1996	625	433	1599
2.54	3.05	1.52	423	99.55	0.30	5.52	8	2123	669	461	1681

2.54	3.05	1.52	423	99.52	0.30	5.53	15	2098	22	92	2262
2.54	3.05	1.52	423	99.55	0.30	5.49	15	2060	22	84	2200
2.54	3.05	1.52	423	99.62	0.30	5.47	20	2111	0	4	2282
2.54	3.05	1.52	423	99.62	0.30	5.46	25	2149	6	1	2296
2.54	3.05	1.52	423	99.60	0.30	5.45	30	2015	2	4	2173
2.54	3.05	1.52	423	99.62	0.30	5.48	35	2206	1	0	2405
2.54	3.05	1.52	423	99.70	0.50	6.57	3	1774	1336	249	532
2.54	3.05	1.52	423	99.66	0.50	6.58	3	1933	1457	277	580
2.54	3.05	1.52	423	99.60	0.50	6.55	5	2009	949	445	1298
2.54	3.05	1.52	423	99.64	0.50	6.54	5	2111	993	473	1298
2.54	3.05	1.52	423	99.72	0.50	6.58	8	1876	276	293	1797
2.54	3.05	1.52	423	99.63	0.50	6.57	8	2282	339	329	2234
2.54	3.05	1.52	423	99.59	0.50	6.56	10	2301	111	188	2364
2.54	3.05	1.52	423	99.60	0.50	6.56	10	2257	104	184	2350
2.54	3.05	1.52	423	99.70	0.50	6.53	15	2339	0	16	2508
2.54	3.05	1.52	423	99.46	0.50	6.54	15	2238	4	4	2398
2.54	3.05	1.52	423	99.48	0.50	6.58	20	2276	2	0	2405
2.54	3.05	1.52	423	99.52	0.50	6.57	20	2225	5	1	2357
2.54	3.05	1.52	423	99.56	0.60	7.05	5	2263	942	489	1619
2.54	3.05	1.52	423	99.60	0.60	7.02	5	2307	961	510	1612
2.54	3.05	1.52	423	99.58	0.60	7.03	8	2092	219	249	2084
2.54	3.05	1.52	423	99.58	0.60	7.00	8	2028	212	225	2009
2.54	3.05	1.52	423	99.56	0.60	7.05	10	2327	60	128	2439
2.54	3.05	1.52	423	99.60	0.60	7.02	10	2327	60	116	2426
2.54	3.05	1.52	423	99.60	0.60	7.01	15	2263	0	2	2467
2.54	3.05	1.52	423	99.62	0.60	7.02	15	2244	5	0	2439
2.54	3.05	1.52	423	99.66	0.60	7.02	20	2282	9	2	2419
2.54	3.05	1.52	453	99.56	0.05	3.01	5	1679	1527	96	197
2.54	3.05	1.52	453	99.60	0.05	3.03	5	1876	1704	104	218
2.54	3.05	1.52	453	99.60	0.05	2.98	10	1984	1387	341	751
2.54	3.05	1.52	453	99.55	0.05	3.04	10	2009	1400	365	724
2.54	3.05	1.52	453	99.58	0.05	3.05	15	2047	930	485	1312
2.54	3.05	1.52	453	99.62	0.05	3.03	15	2111	961	518	1414
2.54	3.05	1.52	453	99.58	0.05	2.99	25	2041	231	317	1995
2.54	3.05	1.52	453	99.56	0.05	2.97	25	2041	231	349	1981
2.54	3.05	1.52	453	99.54	0.05	3.00	35	2073	15	96	2186
2.54	3.05	1.52	453	99.58	0.05	2.99	35	2085	15	108	2234
2.54	3.05	1.52	453	99.52	0.10	3.62	3	2282	2136	108	177
2.54	3.05	1.52	453	99.51	0.10	3.64	3	2225	2079	112	170
2.54	3.05	1.52	453	99.51	0.10	3.63	5	2104	1761	213	423
2.54	3.05	1.52	453	99.51	0.10	3.62	5	2174	1819	233	450
2.54	3.05	1.52	453	99.52	0.10	3.62	8	2238	1438	453	977
2.54	3.05	1.52	453	99.60	0.10	3.61	8	2206	1419	421	929
2.54	3.05	1.52	453	99.46	0.10	3.63	10	2149	1088	518	1270
2.54	3.05	1.52	453	99.47	0.10	3.60	10	2206	1114	510	1346
2.54	3.05	1.52	453	99.47	0.10	3.62	15	2206	485	461	1961
2.54	3.05	1.52	453	99.51	0.10	3.63	15	2155	473	477	1954
2.54	3.05	1.52	453	99.50	0.10	3.61	25	1977	9	92	2063
2.54	3.05	1.52	453	99.52	0.10	3.62	25	2142	15	124	2296
2.54	3.05	1.52	453	99.52	0.10	3.62	35	2161	4	0	2296
2.54	3.05	1.52	453	99.54	0.10	3.63	35	2092	1	0	2282
2.54	3.05	1.52	453	99.55	0.30	5.24	3	2085	1742	245	430
2.54	3.05	1.52	453	99.52	0.30	5.23	3	2155	1800	213	443
2.54	3.05	1.52	453	99.56	0.30	5.23	5	2212	1368	457	1038
2.54	3.05	1.52	453	99.62	0.30	5.22	5	2123	1311	445	997
2.54	3.05	1.52	453	99.56	0.30	5.23	8	2155	644	461	1804
2.54	3.05	1.52	453	99.58	0.30	5.25	8	2092	625	437	1749
2.54	3.05	1.52	453	99.58	0.30	5.20	10	2282	352	397	2214
2.54	3.05	1.52	453	99.59	0.30	5.22	10	2060	314	321	1988
2.54	3.05	1.52	453	99.58	0.30	5.23	15	2149	15	64	2282
2.54	3.05	1.52	453	99.62	0.30	5.25	15	2155	15	96	2309
2.54	3.05	1.52	453	99.54	0.30	5.21	25	2104	6	2	2248
2.54	3.05	1.52	453	99.59	0.30	5.23	25	2288	0	2	2432
2.54	3.05	1.52	453	99.52	0.30	5.21	35	2047	0	2	2180
2.54	3.05	1.52	453	99.55	0.30	5.26	35	2174	2	5	2371
2.54	3.05	1.52	453	99.62	0.50	6.49	3	2282	1711	377	696
2.54	3.05	1.52	453	99.66	0.50	6.49	3	2225	1666	329	696
2.54	3.05	1.52	453	99.71	0.50	6.45	5	2022	930	441	1277
2.54	3.05	1.52	453	99.64	0.50	6.46	5	2212	1019	522	1455
2.54	3.05	1.52	453	99.66	0.50	6.52	8	2307	327	353	2248
2.54	3.05	1.52	453	99.62	0.50	6.50	8	2238	314	317	2200
2.54	3.05	1.52	453	99.58	0.50	6.48	10	2155	92	176	2227
2.54	3.05	1.52	453	99.62	0.50	6.45	10	2117	92	144	2234
2.54	3.05	1.52	453	99.60	0.50	6.47	15	2295	4	16	2453
2.54	3.05	1.52	453	99.54	0.50	6.46	15	2358	0	8	2576
2.54	3.05	1.52	423	99.52	0.10	3.82	10	2149	1127	465	1270
2.54	3.05	1.52	423	99.51	0.10	3.85	10	2142	1120	497	1216
2.54	3.05	1.52	423	99.52	0.10	3.80	10	4003	2149	1196	2303
2.54	3.05	1.52	423	99.55	0.10	3.81	10	4028	2168	919	2316
2.54	3.05	1.52	423	99.48	0.10	3.78	10	6269	3361	1424	3608
2.54	3.05	1.52	423	99.50	0.10	3.83	10	4853	2593	1075	2795
2.54	3.05	1.52	423	99.47	0.10	3.84	10	5215	2790	1172	3027
2.54	3.05	1.52	423	99.52	0.10	3.82	10	6358	3412	1400	3663
2.54	3.05	1.52	423	99.51	0.10	3.81	10	7000	3761	1561	4005
2.54	3.05	1.52	423	99.47	0.10	3.80	10	6733	3615	1485	3865
2.54	3.05	1.52	423	99.52	0.10	3.83	10	7615	4098	1721	4415
2.54	3.05	1.52	423	99.54	0.10	3.84	10	8555	4612	1898	4927
2.54	3.05	1.52	423	99.56	0.10	3.84	10	9082	4904	2062	5228
2.54	3.05	1.52	423	99.51	0.10	3.82	10	8447	4555	1926	4893
2.54	3.05	1.52	423	99.50	0.10	3.83	10	9038	4879	2010	5180
2.54	3.05	1.52	423	99.48	0.30	5.51	10	2212	358	373	2091
2.54	3.05	1.52	423	99.52	0.30	5.48	10	1939	307	321	1865
2.54	3.05	1.52	423	99.54	0.30	5.53	10	1673	263	281	1585
2.54	3.05	1.52	423	99.51	0.30	5.54	10	2942	485	473	2808
2.54	3.05	1.52	423	99.46	0.30	5.55	10	4028	682	658	3800
2.54	3.05	1.52	423	99.47	0.30	5.51	10	4663	796	778	4435
2.54	3.05	1.52	423	99.52	0.30	5.53	10	5927	1031	979	5625
2.54	3.05	1.52	423	99.54	0.30	5.53	10	5425	936	891	5119
2.54	3.05	1.52	423	99.54	0.30	5.56	10	7634	1349	1252	7238
2.54	3.05	1.52	423	99.56	0.30	5.52	10	6301	1101	987	5946
2.54	3.05	1.52	423	99.54	0.30	5.51	10	9107	1628	1477	8591
2.54	3.05	1.52	423	99.55	0.30	5.51	10	10688	1927	1713	10054
2.54	3.05	1.52	423	99.52	0.30	5.49	10	9742	1749	1597	9220
2.54	3.05	1.52	423	99.51	0.30	5.50	10	7482	1323	1232	7087
2.54	3.05	1.52	423	99.55	0.30	5.53	10	3520	587	578	3355
2.54	3.05	1.52	423	99.52	0.50	6.59	10	1647	73	132	1728
2.54	3.05	1.52	423	99.56	0.50	6.57	10	1857	85	156	1961
2.54	3.05	1.52	423	99.56	0.50	6.58	10	2333	117	188	2432
2.54	3.05	1.52	423	99.54	0.50	6.59	10	4320	244	349	4510
2.54	3.05	1.52	423	99.60	0.50	6.61	10	5907	346	477	5932
2.54	3.05	1.52	423	99.60	0.50	6.60	10	5590	327	425	5789
2.54	3.05	1.52	423	99.66	0.50	6.59	10	6365	377	477	6588
2.54	3.05	1.52	423	99.64	0.50	6.60	10	6561	390	526	6821
2.54	3.05	1.52	423	99.70	0.50	6.62	10	4904	282	405	5126
2.54	3.05	1.52	423	99.66	0.50	6.56	10	8657	536	698	9015
2.54	3.05	1.52	423	99.62	0.50	6.58	10	10574	669	843	11014

2.54	3.05	1.52	423	99.64	0.50	6.62	10	4022	225	309	4182
2.54	3.05	0.76	423	98.93	0.30	7.12	5	1952	676	429	1359
2.54	3.05	0.76	423	98.93	0.30	7.13	5	1825	631	401	1270
2.54	3.05	0.76	423	98.93	0.30	7.14	5	1895	657	417	1318
2.54	3.05	1.52	423	99.68	0.30	5.49	10	1800	206	289	1701
2.54	3.05	1.52	423	99.68	0.30	5.49	10	1761	187	281	1667
2.54	3.05	1.52	423	99.68	0.30	5.46	10	1736	174	277	1646
2.54	3.05	2.29	423	99.63	0.30	4.72	15	1857	60	172	1920
2.54	3.05	2.29	423	99.63	0.30	4.76	15	1825	47	168	1866
2.54	3.05	2.29	423	99.63	0.30	4.75	15	1806	34	168	1865
2.54	3.05	3.05	423	98.94	0.30	4.29	20	1996	9	100	2125
2.54	3.05	3.05	423	98.94	0.30	4.33	20	1958	3	100	2084
2.54	3.05	3.05	423	98.94	0.30	4.31	20	2009	22	104	2139

TABLE E2.b

THE CONCENTRATION DISTRIBUTION OF THE PRODUCTS OF THE REACTION BETWEEN DIMETHYL DISULPHIDE AND AIR IN THE CORONA REACTOR*

t		Digits				Weight, gm
hr	s	$(CH_3)_2S_2$ in	$(CH_3)_2S_2$ out	$(CH_3)_2S$ out	SO_2 out	$(CH_3)_2SO_2$ out
3	5	1812	1062	349	760	0.0240
3	5	1838	1077	358	783	
3	5	1844	1080	373	763	
3	10	1857	1088	282	1734	0.1064
3	10	1888	1107	279	1777	
3	10	1914	1122	281	1776	
3	10	2098	1231	311	1974	0.1201
3	10	2079	1219	315	1950	
3	10	2117	1242	318	1970	
3	15	2104	1234	62	2257	0.1242
3	15	1952	1144	60	2092	
3	15	1971	1156	64	2104	
3	20	1939	1137	13	2079	0.0935
3	20	1888	1107	16	2004	
3	20	1939	1137	19	2081	
3	25	1869	1096	3	2008	0.0723
3	25	1958	1148	3	2110	
3	25	1990	1167	1	2139	

* Reactor dimensions: D = 2.54×10^{-2} m, H=1.52×10^{-1} m, and a = 1.52×10^{-5} m.

and operating conditions: T = 423 K and I_- = 0.3 mA.

TABLE E3.A

DATA FOR THE REACTION OF DIMETHYL SULPHIDE WITH AIR IN THE CORONA REACTOR
(Without considering dimethyl sulphone)

D_R	D_v	E	T	P	I_c	V_s		Digi	
			K	kPa	mA	kV	s		
m$\times 10^2$	m$\times 10^5$	m$\times 10$						$(CH_3)_2S$ in	$(CH_3)_2S$ out
2.54	3.05	15.24	298	99.66	0.10	4.67	5	1140	1023
2.54	3.05	15.24	298	99.59	0.10	4.64	10	1208	782
2.54	3.05	15.24	298	99.60	0.10	4.67	15	1236	429
2.54	3.05	15.24	298	99.60	0.10	4.66	20	1192	172
2.54	3.05	15.24	298	99.62	0.10	4.64	25	1196	52
2.54	3.05	15.24	298	99.54	0.10	4.63	35	1184	3
2.54	3.05	15.24	298	99.52	0.30	6.66	3	1095	967
2.54	3.05	15.24	298	99.52	0.30	6.65	5	1216	851
2.54	3.05	15.24	298	99.55	0.30	6.68	10	1244	277
2.54	3.05	15.24	298	99.58	0.30	6.62	15	1091	28
2.54	3.05	15.24	298	99.52	0.30	6.62	20	1156	3
2.54	3.05	15.24	298	99.51	0.50	7.74	3	1136	919
2.54	3.05	15.24	298	99.51	0.50	7.71	5	1188	642
2.54	3.05	15.24	298	99.58	0.50	7.72	10	1300	96
2.54	3.05	15.24	298	99.56	0.50	7.72	15	1204	3
2.54	3.05	15.24	298	99.60	0.80	9.40	3	1192	847
2.54	3.05	15.24	298	99.66	0.80	9.39	5	1148	429
2.54	3.05	15.24	298	99.71	0.80	9.43	8	1180	84
2.54	3.05	15.24	298	99.68	0.80	9.43	10	1067	12
2.54	3.05	15.24	373	99.64	0.05	3.31	5	1276	1212
2.54	3.05	15.24	373	99.60	0.05	3.32	10	1192	959
2.54	3.05	15.24	373	99.67	0.05	3.33	15	1156	698
2.54	3.05	15.24	373	99.62	0.05	3.32	20	1200	481
2.54	3.05	15.24	373	99.54	0.05	3.30	25	1168	273
2.54	3.05	15.24	373	99.52	0.05	3.34	35	1136	56
2.54	3.05	15.24	373	99.52	0.10	4.21	5	1196	1071
2.54	3.05	15.24	373	99.48	0.10	4.22	10	1035	654
2.54	3.05	15.24	373	99.48	0.10	4.20	15	1067	369
2.54	3.05	15.24	373	99.46	0.10	4.21	25	1099	48
2.54	3.05	15.24	373	99.51	0.10	4.21	35	1148	3
2.54	3.05	15.24	373	99.54	0.30	5.88	3	1188	1051
2.54	3.05	15.24	373	99.55	0.30	5.90	5	1240	875
2.54	3.05	15.24	373	99.50	0.30	5.88	10	1196	277
2.54	3.05	15.24	373	99.47	0.30	5.89	15	1216	36
2.54	3.05	15.24	373	99.42	0.30	5.86	20	1216	3
2.54	3.05	15.24	373	99.43	0.50	6.90	3	1244	1003
2.54	3.05	15.24	373	99.45	0.50	6.94	5	1276	686
2.54	3.05	15.24	373	99.45	0.50	6.92	8	1320	253
2.54	3.05	15.24	373	99.46	0.50	6.91	10	1320	96
2.54	3.05	15.24	373	99.39	0.50	6.92	15	1364	3
2.54	3.05	15.24	423	99.47	0.05	3.13	5	1067	1015
2.54	3.05	15.24	423	99.45	0.05	3.11	10	1083	879
2.54	3.05	15.24	423	99.52	0.05	3.17	15	1119	449
2.54	3.05	15.24	423	99.41	0.05	3.12	20	1127	469
2.54	3.05	15.24	423	99.39	0.05	3.13	25	1168	289
2.54	3.05	15.24	423	99.43	0.05	3.15	35	1220	72
2.54	3.05	15.24	423	99.43	0.10	3.89	3	1055	1015
2.54	3.05	15.24	423	99.42	0.10	3.90	3	1051	1011
2.54	3.05	15.24	423	99.42	0.10	3.86	5	1216	1087
2.54	3.05	15.24	423	99.35	0.10	3.87	5	1196	1071
2.54	3.05	15.24	423	99.38	0.10	3.86	10	1292	814
2.54	3.05	15.24	423	99.39	0.10	3.91	10	1264	798
2.54	3.05	15.24	423	99.35	0.10	3.90	15	1316	453
2.54	3.05	15.24	423	99.42	0.10	3.88	15	1304	449
2.54	3.05	15.24	423	99.41	0.10	3.87	25	1316	60
2.54	3.05	15.24	423	99.45	0.10	3.88	25	1360	60
2.54	3.05	15.24	423	99.43	0.10	3.87	35	1320	3
2.54	3.05	15.24	423	99.52	0.10	3.89	35	1304	3
2.54	3.05	15.24	423	99.48	0.30	5.50	3	1059	939
2.54	3.05	15.24	423	99.48	0.30	5.51	3	1051	935
2.54	3.05	15.24	423	99.45	0.30	5.51	5	1059	754
2.54	3.05	15.24	423	99.43	0.30	5.49	5	1158	831
2.54	3.05	15.24	423	99.41	0.30	5.53	10	1071	257
2.54	3.05	15.24	423	99.41	0.30	5.52	10	1035	249
2.54	3.05	15.24	423	99.43	0.30	5.52	15	1071	36
2.54	3.05	15.24	423	99.39	0.30	5.48	15	1192	40
2.54	3.05	15.24	423	99.39	0.60	7.02	3	1316	1011
2.54	3.05	15.24	423	99.41	0.60	7.01	3	1180	907
2.54	3.05	15.24	423	99.42	0.60	7.05	5	1200	562
2.54	3.05	15.24	423	99.42	0.60	7.03	5	1316	618
2.54	3.05	15.24	423	99.39	0.60	7.04	8	1304	176
2.54	3.05	15.24	423	99.35	0.60	7.03	8	1320	180
2.54	3.05	15.24	423	99.38	0.60	7.00	10	1288	52
2.54	3.05	15.24	423	99.47	0.60	7.01	10	1316	52
2.54	3.05	15.24	453	99.45	0.05	3.00	3	1284	1260
2.54	3.05	15.24	453	99.42	0.05	3.02	5	1340	1276
2.54	3.05	15.24	453	99.39	0.05	2.99	8	1368	1200
2.54	3.05	15.24	453	99.45	0.05	3.01	10	1396	1131
2.54	3.05	15.24	453	99.52	0.05	2.99	15	1328	814
2.54	3.05	15.24	453	99.47	0.05	3.03	20	1292	534
2.54	3.05	15.24	453	99.48	0.05	3.01	25	1404	345
2.54	3.05	15.24	453	99.39	0.05	3.03	35	1332	76
2.54	3.05	15.24	453	99.48	0.10	3.60	5	1404	1268
2.54	3.05	15.24	453	99.54	0.10	3.61	10	1340	879
2.54	3.05	15.24	453	99.55	0.10	3.59	15	1400	530
2.54	3.05	15.24	453	99.54	0.10	3.61	20	1376	237
2.54	3.05	15.24	453	99.52	0.10	3.62	25	1396	84
2.54	3.05	15.24	453	99.51	0.10	3.60	35	1340	0
2.54	3.05	15.24	453	99.52	0.30	5.20	3	1449	1284
2.54	3.05	15.24	453	99.46	0.30	5.21	3	1408	1248
2.54	3.05	15.24	453	99.47	0.30	5.20	5	1328	943

2.54	3.05	15.24	453	99.31	0.30	5.23	10	1404	337
2.54	3.05	15.24	453	99.45	0.30	5.22	15	1449	52
2.54	3.05	15.24	453	99.46	0.50	6.49	3	1408	1148
2.54	3.05	15.24	453	99.46	0.50	6.49	3	1449	1180
2.54	3.05	15.24	453	99.48	0.50	6.51	5	1408	790
2.54	3.05	15.24	453	99.52	0.50	6.47	5	1376	770
2.54	3.05	15.24	453	99.54	0.50	6.48	8	1368	301
2.54	3.05	15.24	453	99.50	0.50	6.49	8	1453	321
2.54	3.05	15.24	453	99.56	0.50	6.47	10	1432	132
2.54	3.05	15.24	453	99.55	0.50	6.50	10	1436	132
2.54	3.05	15.24	453	99.52	0.50	6.48	15	1312	0
2.54	3.05	15.24	453	99.45	0.50	6.46	15	1340	0
2.54	3.05	15.24	423	99.51	0.10	3.83	10	943	606
2.54	3.05	15.24	423	99.54	0.10	3.81	10	1047	674
2.54	3.05	15.24	423	99.56	0.10	3.84	10	1292	831
2.54	3.05	15.24	423	99.58	0.10	3.80	10	1264	810
2.54	3.05	15.24	423	99.60	0.10	3.78	10	2151	1376
2.54	3.05	15.24	423	99.59	0.10	3.79	10	2797	1786
2.54	3.05	15.24	423	99.64	0.10	3.82	10	3459	2207
2.54	3.05	15.24	423	99.63	0.10	3.78	10	3074	1962
2.54	3.05	15.24	423	99.59	0.10	3.82	10	3760	2396
2.54	3.05	15.24	423	99.52	0.10	3.81	10	4029	2564
2.54	3.05	15.24	423	99.56	0.10	3.80	10	6027	3824
2.54	3.05	15.24	423	99.58	0.10	3.82	10	4542	2889
2.54	3.05	15.24	423	99.54	0.10	3.83	10	3535	2255
2.54	3.05	15.24	423	99.51	0.30	5.54	10	1071	269
2.54	3.05	15.24	423	99.47	0.30	5.52	10	1035	261
2.54	3.05	15.24	423	99.42	0.30	5.53	10	2536	622
2.54	3.05	15.24	423	99.45	0.30	5.52	10	2271	562
2.54	3.05	15.24	423	99.46	0.30	5.51	10	3102	758
2.54	3.05	15.24	423	99.41	0.30	5.51	10	3571	871
2.54	3.05	15.24	423	99.41	0.30	5.53	10	3431	839
2.54	3.05	15.24	423	99.43	0.30	5.50	10	4221	1023
2.54	3.05	15.24	423	99.39	0.30	5.53	10	3872	943
2.54	3.05	15.24	423	99.35	0.30	5.51	10	4542	1099
2.54	3.05	15.24	423	99.46	0.30	5.53	10	1782	441
2.54	3.05	15.24	423	99.47	0.30	5.54	10	5562	1336
2.54	3.05	15.24	423	99.45	0.30	5.53	10	6445	1545
2.54	3.05	15.24	423	99.51	0.30	5.52	10	4831	1168
2.54	3.05	15.24	423	99.50	0.30	5.54	10	3467	847
2.54	3.05	15.24	423	99.56	0.60	7.05	10	1288	72
2.54	3.05	15.24	423	99.46	0.60	7.05	10	1316	72
2.54	3.05	15.24	423	99.47	0.60	7.04	10	1047	60
2.54	3.05	15.24	423	99.42	0.60	7.01	10	1709	96
2.54	3.05	15.24	423	99.39	0.60	7.03	10	2552	144
2.54	3.05	15.24	423	99.38	0.60	7.00	10	3740	205
2.54	3.05	15.24	423	99.35	0.60	7.06	10	2211	124
2.54	3.05	15.24	423	99.31	0.60	7.03	10	3098	172
2.54	3.05	15.24	423	99.31	0.60	7.06	10	3864	213
2.54	3.05	15.24	423	99.29	0.60	6.99	10	4542	249
2.54	3.05	15.24	423	99.34	0.60	7.00	10	3535	197
2.54	3.05	15.24	423	99.35	0.60	7.03	10	6553	349
2.54	3.05	15.24	423	99.39	0.60	7.04	10	6188	333
2.54	3.05	15.24	423	99.41	0.60	7.03	10	5361	289
2.54	3.05	15.24	423	99.38	0.60	7.04	10	6950	369
2.54	3.05	0.76	423	98.93	0.30	7.13	5	1107	618
2.54	3.05	0.76	423	98.93	0.30	7.15	5	1121	610
2.54	3.05	0.76	423	98.93	0.30	7.12	5	1103	590
2.54	3.05	1.52	423	99.68	0.30	5.43	10	1071	357
2.54	3.05	1.52	423	99.68	0.30	5.42	10	1067	337
2.54	3.05	1.52	423	99.68	0.30	5.47	10	1076	317
2.54	3.05	2.29	423	99.63	0.30	4.77	15	1188	168
2.54	3.05	2.29	423	99.63	0.30	4.75	15	1180	197
2.54	3.05	2.29	423	99.63	0.30	4.72	15	1176	188
2.54	3.05	3.05	423	98.94	0.30	4.33	20	1324	144
2.54	3.05	3.05	423	98.94	0.30	4.31	20	1340	156
2.54	3.05	3.05	423	98.94	0.30	4.29	20	1348	132

TABLE E3.b

THE CONCENTRATION DISTRIBUTION OF THE PRODUCTS OF THE REACTION OF DIMETHYL SULPHIDE AND AIR IN THE CORONA REACTOR*

t hr	τ s	Digits $(CH_3)_2S$ in	Digits $(CH_3)_2S$ out	Weight gm $(CH_3)_2SO_2$ out
3	5	1111	785	0.0636
3	5	1091	770	
3	5	1131	799	
3	10	1280	904	0.1277
3	10	1296	915	
3	10	1240	875	
3	10	1172	827	0.1171
3	10	1216	858	
3	10	1127	796	
3	15	1320	932	0.1246
3	15	1340	946	
3	15	1312	927	
3	20	1364	964	0.1031
3	20	1392	983	
3	20	1332	941	
3	25	1268	895	0.0770
3	25	1292	912	
3	25	1308	924	

* Reactor dimensions: D = 2.54×10^{-2} m, H=1.52×10^{-1} m, and s = 1.52×10^{-3} m.

and operating conditions: T = 423 K and I_c = 0.3 mA.

TABLE E4

DATA OF THE REACTION OF HYDROGEN SULFIDE WITH AIR IN THE CORONA REACTOR

D_R	D_V	R	T	P	I_c	V_s	τ	Digits			
								in	out	out	out
$m \times 10^2$	$m \times 10^5$	$m \times 10$	K	kPa	mA	kV	s	H_2S	H_2S	H_2O	SO_2
2.54	3.05	1.52	298	98.94	0.05	3.78	3	1224	1210	1	2
2.54	3.05	1.52	298	99.09	0.05	3.77	3	1277	1262	4	13
2.54	3.05	1.52	298	99.02	0.05	3.76	5	1224	1186	3	13
2.54	3.05	1.52	298	98.97	0.05	3.78	5	1043	1009	12	20
2.54	3.05	1.52	298	98.93	0.05	3.78	10	1224	1086	53	156
2.54	3.05	1.52	298	99.21	0.05	3.77	10	1224	1086	59	163
2.54	3.05	1.52	298	99.33	0.05	3.78	15	1171	904	137	355
2.54	3.05	1.52	298	99.35	0.05	3.76	15	1143	880	137	320
2.54	3.05	1.52	298	99.46	0.05	3.79	20	1133	723	218	546
2.54	3.05	1.52	298	99.60	0.05	3.78	20	1138	727	224	546
2.54	3.05	1.52	298	99.45	0.05	3.80	25	1219	613	343	806
2.54	3.05	1.52	298	99.41	0.05	3.78	25	1195	598	340	792
2.54	3.05	1.52	298	99.33	0.05	3.77	35	1143	298	480	1168
2.54	3.05	1.52	298	99.13	0.05	3.78	35	1181	312	521	1209
2.54	3.05	1.52	298	99.35	0.10	4.65	3	1086	1062	3	13
2.54	3.05	1.52	298	99.42	0.10	4.64	3	1119	1095	1	20
2.54	3.05	1.52	298	99.19	0.10	4.66	5	1157	1086	338	74
2.54	3.05	1.52	298	99.03	0.10	4.65	5	1124	1057	21	74
2.54	3.05	1.52	298	99.03	0.10	4.65	10	1138	904	125	286
2.54	3.05	1.52	298	98.89	0.10	4.64	10	1162	923	128	293
2.54	3.05	1.52	298	99.51	0.10	4.62	15	1148	594	268	655
2.54	3.05	1.52	298	99.60	0.10	4.64	15	1219	742	308	642
2.54	3.05	1.52	298	99.75	0.10	4.63	25	1095	278	480	1154
2.54	3.05	1.52	298	99.75	0.10	4.65	25	1167	302	512	1236
2.54	3.05	1.52	298	99.66	0.10	4.66	35	1143	68	631	1503
2.54	3.05	1.52	298	99.82	0.10	4.64	35	1148	68	637	1496
2.54	3.05	1.52	298	99.50	0.30	6.68	3	1176	1095	38	81
2.54	3.05	1.52	298	99.46	0.30	6.69	3	1148	1066	35	95
2.54	3.05	1.52	298	99.26	0.30	6.70	5	1095	909	93	245
2.54	3.05	1.52	298	99.06	0.30	6.68	5	1157	961	102	259
2.54	3.05	1.52	298	99.03	0.30	6.66	10	1148	565	338	744
2.54	3.05	1.52	298	99.33	0.30	6.68	10	1152	570	332	806
2.54	3.05	1.52	298	99.03	0.30	6.67	15	1210	255	515	1277
2.54	3.05	1.52	298	98.99	0.30	6.69	15	1191	250	544	1264
2.54	3.05	1.52	298	98.95	0.30	6.69	20	1138	54	637	1503
2.54	3.05	1.52	298	98.87	0.30	6.70	20	1162	59	651	1564
2.54	3.05	1.52	298	98.86	0.30	6.68	25	1124	12	666	1551
2.54	3.05	1.52	298	98.94	0.30	6.65	25	1148	12	683	1592
2.54	3.05	1.52	298	99.29	0.90	10.24	3	1081	980	85	225
2.54	3.05	1.52	298	99.35	0.90	10.25	5	1114	646	247	607
2.54	3.05	1.52	298	98.90	0.90	10.26	8	1176	302	503	1223
2.54	3.05	1.52	298	98.94	0.90	10.24	10	1143	130	512	1216
2.54	3.05	1.52	298	98.87	0.90	10.24	15	1219	17	718	1687
2.54	3.05	1.52	298	98.87	1.20	11.11	3	1162	890	125	320
2.54	3.05	1.52	298	98.85	1.20	11.13	5	1238	608	364	792
2.54	3.05	1.52	298	98.91	1.20	11.10	8	1200	197	570	1380
2.54	3.05	1.52	298	98.94	1.20	11.09	10	1257	64	707	1633
2.54	3.05	1.52	298	98.93	1.60	13.02	3	1243	871	227	560
2.54	3.05	1.52	298	98.90	1.60	13.03	3	1248	875	195	532
2.54	3.05	1.52	298	98.86	1.60	12.99	5	1272	493	439	1086
2.54	3.05	1.52	298	99.02	1.60	13.04	8	1200	97	640	1551
2.54	3.05	1.52	323	99.13	0.05	3.69	3	1176	1157	1	6
2.54	3.05	1.52	323	98.99	0.05	3.66	5	1210	1162	9	47
2.54	3.05	1.52	323	98.97	0.05	3.70	10	1238	1052	79	177
2.54	3.05	1.52	323	98.93	0.05	3.69	10	1171	995	108	225
2.54	3.05	1.52	323	98.98	0.05	3.67	15	1152	804	195	450
2.54	3.05	1.52	323	99.11	0.05	3.68	20	1272	675	338	792
2.54	3.05	1.52	323	99.19	0.05	3.67	25	1243	460	445	949
2.54	3.05	1.52	323	99.22	0.05	3.69	35	1291	173	631	1564
2.54	3.05	1.52	323	98.29	0.10	4.49	3	1176	1143	3	26
2.54	3.05	1.52	323	98.22	0.10	4.48	5	1152	1362	35	136
2.54	3.05	1.52	323	98.18	0.10	4.48	10	1219	880	181	464
2.54	3.05	1.52	323	98.06	0.10	4.52	10	1234	890	201	450
2.54	3.05	1.52	323	98.02	0.10	4.51	15	1181	570	332	813
2.54	3.05	1.52	323	98.20	0.10	4.49	25	1248	154	631	1571
2.54	3.05	1.52	323	98.02	0.10	4.48	35	1277	7	721	1769
2.54	3.05	1.52	323	98.40	0.30	6.15	3	1238	1133	24	88
2.54	3.05	1.52	323	98.51	0.30	6.14	5	1181	933	120	320
2.54	3.05	1.52	323	98.62	0.30	6.09	10	1291	508	419	1072
2.54	3.05	1.52	323	98.41	0.30	6.15	10	1152	450	393	983
2.54	3.05	1.52	323	98.36	0.30	6.18	15	1234	135	564	1476
2.54	3.05	1.52	323	98.49	0.30	6.17	25	1152	31	701	1646
2.54	3.05	1.52	323	98.40	0.30	6.16	35	1305	36	770	1851
2.54	3.05	1.52	323	98.99	0.50	7.72	3	1281	1114	62	197
2.54	3.05	1.52	323	99.07	0.50	7.71	3	1200	1043	56	184
2.54	3.05	1.52	323	99.15	0.50	7.71	5	1191	809	195	389
2.54	3.05	1.52	323	99.29	0.50	7.72	10	1219	255	358	1250
2.54	3.05	1.52	323	99.35	0.50	7.70	10	1324	283	596	1441
2.54	3.05	1.52	323	99.26	0.50	7.73	15	1320	75	727	1817
2.54	3.05	1.52	323	99.22	0.50	7.70	25	1272	36	791	1769
2.54	3.05	1.52	323	99.42	0.90	9.76	3	1181	918	137	286
2.54	3.05	1.52	323	99.51	0.90	9.77	3	1224	952	125	334
2.54	3.05	1.52	323	99.46	0.90	9.75	5	1234	618	332	819
2.54	3.05	1.52	323	99.42	0.90	9.78	5	1305	656	343	881
2.54	3.05	1.52	323	99.37	0.90	9.76	8	1272	207	619	1414
2.54	3.05	1.52	323	99.29	0.90	9.77	8	1334	221	644	1476
2.54	3.05	1.52	323	99.26	0.90	9.73	10	1257	59	692	1701
2.54	3.05	1.52	323	99.34	0.90	9.73	10	1234	54	666	1551
2.54	3.05	1.52	373	98.90	0.05	3.37	3	1234	1205	-	26
2.54	3.05	1.52	373	98.94	0.05	3.36	5	1076	1004	18	47
2.54	3.05	1.52	373	98.87	0.05	3.37	10	1138	875	120	314
2.54	3.05	1.52	373	98.83	0.05	3.38	15	1234	689	294	744
2.54	3.05	1.52	373	98.91	0.05	3.36	25	1195	231	535	1298

2.54	3.05	1.52	373	98.99	0.05	3.37	35	1248	25	704	1619
2.54	3.05	1.52	373	99.02	0.10	4.18	3	1219	1162	7	40
2.54	3.05	1.52	373	99.03	0.10	4.20	5	1267	1114	56	170
2.54	3.05	1.52	373	98.98	0.10	4.18	8	1181	856	137	389
2.54	3.05	1.52	373	98.93	0.10	4.16	10	1234	746	256	519
2.54	3.05	1.52	373	98.86	0.10	4.17	10	1176	708	216	587
2.54	3.05	1.52	373	99.06	0.10	4.20	15	1286	412	439	1079
2.54	3.05	1.52	373	99.13	0.10	4.20	25	1229	30	689	1619
2.54	3.05	1.52	373	99.15	0.10	4.16	35	1200	31	724	1667
2.54	3.05	1.52	373	99.22	0.30	5.91	3	1200	1047	56	163
2.54	3.05	1.52	373	99.26	0.30	5.99	5	1234	852	186	478
2.54	3.05	1.52	373	99.30	0.30	5.95	8	1291	503	422	1038
2.54	3.05	1.52	373	99.35	0.30	5.96	10	1181	259	518	1264
2.54	3.05	1.52	373	99.46	0.30	5.99	10	1176	259	503	1229
2.54	3.05	1.52	373	99.30	0.30	5.97	15	1028	6	576	1414
2.54	3.05	1.52	373	99.37	0.30	5.98	25	1133	36	707	1592
2.54	3.05	1.52	373	99.33	0.50	6.98	3	1238	985	120	320
2.54	3.05	1.52	373	99.25	0.50	6.99	5	1248	665	306	758
2.54	3.05	1.52	373	99.10	0.50	6.67	8	1200	231	518	1380
2.54	3.05	1.52	373	99.02	0.50	7.00	10	1320	87	695	1681
2.54	3.05	1.52	373	98.94	0.50	6.99	10	1181	73	616	1544
2.54	3.05	1.52	373	98.87	0.50	7.00	15	1305	31	785	1886
2.54	3.05	1.52	373	98.91	0.50	6.99	20	1148	36	689	1674
2.54	3.05	1.52	373	98.95	0.50	7.00	25	1343	36	794	1906
2.54	3.05	1.52	373	98.94	0.90	9.11	3	1286	852	210	553
2.54	3.05	1.52	373	98.98	0.90	9.10	5	1234	388	396	1086
2.54	3.05	1.52	373	99.09	0.90	9.12	8	1200	40	657	1619
2.54	3.05	1.52	373	98.99	0.90	9.09	10	1148	21	683	1592
2.54	3.05	1.52	373	99.27	0.90	9.12	10	1305	8	770	1804
2.54	3.05	1.52	423	98.99	0.05	3.14	3	1243	1200	5	40
2.54	3.05	1.52	423	98.93	0.05	3.15	5	1148	1043	35	102
2.54	3.05	1.52	423	98.89	0.05	3.15	10	1320	904	195	423
2.54	3.05	1.52	423	98.95	0.05	3.14	10	1191	813	172	457
2.54	3.05	1.52	423	99.07	0.05	3.14	15	1152	489	332	724
2.54	3.05	1.52	423	99.13	0.05	3.16	25	1277	102	660	1530
2.54	3.05	1.52	423	99.19	0.05	3.16	35	1315	10	770	1845
2.54	3.05	1.52	423	98.99	0.10	3.85	3	1248	1167	27	67
2.54	3.05	1.52	423	99.06	0.10	3.83	5	1181	980	76	218
2.54	3.05	1.52	423	99.07	0.10	3.85	10	1320	632	369	867
2.54	3.05	1.52	423	99.14	0.10	3.82	10	1277	608	332	854
2.54	3.05	1.52	423	99.18	0.10	3.86	15	1320	240	602	1476
2.54	3.05	1.52	423	99.26	0.10	3.83	25	1181	21	695	1681
2.54	3.05	1.52	423	99.35	0.10	3.86	35	1248	36	727	1790
2.54	3.05	1.52	423	98.94	0.30	5.49	3	1277	1043	82	225
2.54	3.05	1.52	423	98.98	0.30	5.50	5	1248	718	282	703
2.54	3.05	1.52	423	98.97	0.30	5.47	8	1224	288	523	1182
2.54	3.05	1.52	423	98.93	0.30	5.49	10	1286	126	666	1633
2.54	3.05	1.52	423	98.91	0.30	5.48	10	1272	121	634	1612
2.54	3.05	1.52	423	98.87	0.30	5.49	15	1181	26	712	1660
2.54	3.05	1.52	423	98.85	0.30	5.46	20	1334	36	820	1879
2.54	3.05	1.52	423	99.01	0.30	5.48	25	1382	36	829	2022
2.54	3.05	1.52	423	99.03	0.50	6.58	3	1277	914	169	361
2.54	3.05	1.52	423	98.98	0.50	6.59	5	1234	489	410	1045
2.54	3.05	1.52	423	99.25	0.50	6.58	8	1291	102	689	1585
2.54	3.05	1.52	423	99.33	0.50	6.58	10	1391	6	826	1879
2.54	3.05	1.52	423	99.35	0.50	6.57	10	1334	6	770	1872
2.54	3.05	1.52	423	99.59	0.50	6.57	15	1320	36	805	1920
2.54	3.05	1.52	423	99.51	0.90	8.55	3	1305	727	332	833
2.54	3.05	1.52	423	99.52	0.90	8.53	3	1286	718	320	690
2.54	3.05	1.52	423	99.59	0.90	8.54	5	1234	235	573	1270
2.54	3.05	1.52	423	99.56	0.90	8.56	5	1339	255	622	1523
2.54	3.05	1.52	423	99.35	0.90	8.55	8	1363	7	782	1817
2.54	3.05	1.52	423	99.27	0.90	8.53	10	1425	31	829	2043
2.54	3.05	1.52	453	98.94	0.05	3.01	3	1291	1238	12	40
2.54	3.05	1.52	453	98.99	0.05	3.03	5	1382	1234	59	136
2.54	3.05	1.52	453	98.86	0.05	3.01	10	1191	756	245	594
2.54	3.05	1.52	453	99.07	0.05	3.00	10	1229	780	213	594
2.54	3.05	1.52	453	99.03	0.05	3.01	15	1076	384	390	956
2.54	3.05	1.52	453	98.93	0.05	3.03	15	1305	474	486	1120
2.54	3.05	1.52	453	98.89	0.05	3.01	25	1367	59	770	1865
2.54	3.05	1.52	453	98.85	0.05	3.04	35	1272	31	762	1804
2.54	3.05	1.52	453	99.01	0.10	3.63	3	1176	1081	41	81
2.54	3.05	1.52	453	99.23	0.10	3.64	5	1219	971	117	320
2.54	3.05	1.52	453	99.27	0.10	3.66	8	1200	675	300	744
2.54	3.05	1.52	453	99.31	0.10	3.65	10	1305	536	451	1093
2.54	3.05	1.52	453	99.35	0.10	3.65	10	1129	460	381	936
2.54	3.05	1.52	453	99.60	0.10	3.62	15	1272	159	654	1564
2.54	3.05	1.52	453	99.52	0.10	3.63	25	1353	31	811	1954
2.54	3.05	1.52	453	99.59	0.10	3.63	35	1339	36	826	1906
2.54	3.05	1.52	453	99.22	0.30	5.30	3	1377	1100	146	375
2.54	3.05	1.52	453	99.26	0.30	5.29	5	1320	708	355	819
2.54	3.05	1.52	453	99.29	0.30	5.29	8	1334	264	605	1496
2.54	3.05	1.52	453	99.35	0.30	5.30	10	1248	83	689	1612
2.54	3.05	1.52	453	99.42	0.30	5.28	10	1243	83	683	1551
2.54	3.05	1.52	453	99.17	0.50	6.54	3	1377	933	236	614
2.54	3.05	1.52	453	99.13	0.50	6.53	3	1339	904	245	628
2.54	3.05	1.52	453	99.07	0.50	6.56	5	1420	479	532	1325
2.54	3.05	1.52	453	98.99	0.50	6.54	5	1477	503	564	1366
2.54	3.05	1.52	453	98.94	0.50	6.52	8	1391	68	791	1817
2.54	3.05	1.52	453	98.85	0.50	6.56	8	1525	78	855	1961
2.54	3.05	1.52	453	98.86	0.50	6.55	10	1439	12	831	1995
2.54	3.05	1.52	423	98.91	0.05	3.13	10	1162	818	181	471
2.54	3.05	1.52	423	98.93	0.05	3.15	10	1052	703	189	505
2.54	3.05	1.52	423	98.86	0.05	3.14	10	1597	1100	274	690
2.54	3.05	1.52	423	98.78	0.05	3.16	10	2122	1458	387	995
2.54	3.05	1.52	423	98.79	0.05	3.13	10	2604	1792	468	1141
2.54	3.05	1.52	423	98.86	0.05	3.15	10	2819	1959	515	1175
2.54	3.05	1.52	423	98.90	0.05	3.15	10	2967	2045	535	1209
2.54	3.05	1.52	423	98.93	0.05	3.16	10	3650	2504	680	1633
2.54	3.05	1.52	423	98.99	0.05	3.16	10	3335	2303	596	1448
2.54	3.05	1.52	423	98.97	0.05	3.15	10	4658	3220	829	2050
2.54	3.05	1.52	423	98.90	0.05	3.15	10	3937	2724	738	1687
2.54	3.05	1.52	423	98.77	0.05	3.13	10	4849	3378	963	1975
2.54	3.05	1.52	423	98.63	0.05	3.12	10	7279	5064	1299	3143
2.54	3.05	1.52	423	98.73	0.05	3.17	10	5613	3898	1003	2262
2.54	3.05	1.52	423	98.71	0.05	3.14	10	9192	5689	1468	3567

2.54	3.05	1.52	423	98.94	0.10	3.86	10	1028	455	311	785
2.54	3.05	1.52	423	98.91	0.10	3.84	10	1210	570	364	981
2.54	3.05	1.52	423	98.98	0.10	3.83	10	1692	809	506	1120
2.54	3.05	1.52	423	98.87	0.10	3.86	10	2155	1057	554	1496
2.54	3.05	1.52	423	98.81	0.10	3.84	10	2977	1410	913	2207
2.54	3.05	1.52	423	98.77	0.10	3.83	10	2623	1253	741	1790
2.54	3.05	1.52	423	98.94	0.10	3.85	10	3712	1783	1135	2624
2.54	3.05	1.52	423	99.03	0.10	3.86	10	3010	1458	921	2098
2.54	3.05	1.52	423	99.03	0.10	3.86	10	4433	2184	1311	3143
2.54	3.05	1.52	423	99.13	0.10	3.83	10	4175	2036	1261	2911
2.54	3.05	1.52	423	99.17	0.10	3.85	10	5044	2470	1503	3471
2.54	3.05	1.52	423	99.11	0.10	3.86	10	5388	2628	1569	3793
2.54	3.05	1.52	423	99.06	0.10	3.86	10	7160	3526	2142	5153
2.54	3.05	1.52	423	99.06	0.10	3.87	10	5197	2547	1526	3738
2.54	3.05	1.52	423	99.01	0.10	3.88	10	6573	3244	1988	4517
2.54	3.05	1.52	423	98.99	0.10	3.85	10	1530	727	486	1120
2.54	3.05	1.52	423	98.98	0.10	3.83	10	4968	2432	1494	3629
2.54	3.05	1.52	423	99.01	0.30	5.49	10	1081	97	564	1264
2.54	3.05	1.52	423	99.03	0.30	5.51	10	1425	150	747	1804
2.54	3.05	1.52	423	99.13	0.30	5.50	10	1697	173	863	2125
2.54	3.05	1.52	423	99.18	0.30	5.46	10	2193	221	1139	2754
2.54	3.05	1.52	423	99.22	0.30	5.45	10	1224	130	590	1462
2.54	3.05	1.52	423	99.18	0.30	5.48	10	2318	250	1232	2938
2.54	3.05	1.52	423	99.22	0.30	5.48	10	2819	298	1462	3526
2.54	3.05	1.52	423	99.14	0.30	5.53	10	3101	374	1578	3629
2.54	3.05	1.52	423	99.06	0.30	5.52	10	3349	379	1735	3991
2.54	3.05	1.52	423	99.07	0.30	5.52	10	4104	474	2171	5078
2.54	3.05	1.52	423	98.97	0.30	5.53	10	3817	412	1991	4791
2.54	3.05	1.52	423	98.93	0.30	5.52	10	4428	517	2322	5529
2.54	3.05	1.52	423	98.90	0.30	5.53	10	4901	566	2569	6124
2.54	3.05	1.52	423	98.85	0.30	5.53	10	5436	646	2862	6828
2.54	3.05	1.52	423	98.78	0.30	5.54	10	7236	909	3766	8830
2.54	3.05	1.52	423	98.85	0.30	5.49	10	4562	536	2397	5679
2.54	3.05	1.52	423	98.86	0.30	5.50	10	3597	412	1874	4346
2.54	3.05	1.52	423	98.93	0.30	5.46	10	9024	971	4062	9528
2.54	3.05	1.52	423	98.94	0.50	6.62	10	1515	11	872	2022
2.54	3.05	1.52	423	98.99	0.50	6.57	10	1544	30	860	2091
2.54	3.05	1.52	423	99.03	0.50	6.57	10	1353	6	794	1906
2.54	3.05	1.52	423	98.97	0.50	6.58	10	2088	21	1218	2808
2.54	3.05	1.52	423	98.93	0.50	6.60	10	1234	21	721	1693
2.54	3.05	1.52	423	98.99	0.50	6.56	10	2394	40	1357	5337
2.54	3.05	1.52	423	98.93	0.50	6.56	10	2876	64	1642	3888
2.54	3.05	1.52	423	98.89	0.50	6.57	10	3129	73	1796	4244
2.54	3.05	1.52	423	98.87	0.50	6.57	10	4185	111	2409	5652
2.54	3.05	1.52	423	98.89	0.50	6.59	10	3278	59	1924	4346
2.54	3.05	1.52	423	98.98	0.50	6.58	10	3984	78	2299	5454
2.54	3.05	1.52	423	99.01	0.50	6.57	10	4682	116	2679	6383
2.54	3.05	1.52	423	99.02	0.50	6.56	10	5388	126	3193	7388
2.54	3.05	1.52	423	99.02	0.50	6.60	10	4858	121	2737	6499
2.54	3.05	1.52	423	98.97	0.50	6.62	10	7375	207	4283	10191
2.54	3.05	1.52	423	98.78	0.50	6.60	10	4763	126	2708	6520
2.54	3.05	1.52	423	98.73	0.50	6.59	10	3898	73	2267	5276
2.54	3.05	1.52	423	98.81	0.50	6.59	10	8110	231	4649	11004
2.54	2.54	1.52	423	98.89	0.30	5.32	10	1286	126	660	1619
2.54	2.54	1.52	423	98.91	0.30	5.31	10	1272	121	631	1462
2.54	2.54	1.52	423	98.94	0.30	5.33	10	1234	107	634	1476
2.54	2.54	1.52	423	98.98	0.30	5.34	10	1176	126	579	1421
2.54	2.54	1.52	423	99.06	0.30	5.31	10	1100	97	564	1394
2.54	2.79	1.52	423	98.97	0.30	5.36	10	1286	126	666	1503
2.54	2.79	1.52	423	98.97	0.30	5.37	10	1272	121	654	1592
2.54	2.79	1.52	423	98.90	0.30	5.36	10	1171	87	593	1339
2.54	2.79	1.52	423	98.93	0.30	5.36	10	1286	116	645	1546
2.54	2.79	1.52	423	98.85	0.30	5.37	10	1320	126	616	1380
2.54	3.05	1.52	423	99.07	0.30	5.47	10	1286	126	637	1435
2.54	3.05	1.52	423	99.06	0.30	5.48	10	1272	121	622	1510
2.54	3.05	1.52	423	98.98	0.30	5.46	10	1090	97	553	1216
2.54	3.05	1.52	423	98.97	0.30	5.47	10	1377	126	692	1592
2.54	3.05	1.52	423	98.90	0.30	5.45	10	1320	121	619	1571
2.54	3.56	1.52	423	98.98	0.30	5.49	10	1286	126	645	1578
2.54	3.56	1.52	423	99.09	0.30	5.50	10	1272	121	643	1462
2.54	3.56	1.52	423	99.17	0.30	5.51	10	1076	97	535	1305
2.54	3.56	1.52	423	99.25	0.30	5.49	10	1248	114	616	1510
2.54	3.56	1.52	423	99.35	0.30	5.50	10	1334	111	660	1496
2.54	3.05	0.76	423	99.42	0.30	7.08	10	1229	5	715	1722
2.54	3.05	0.76	423	99.47	0.30	7.09	10	1138	9	695	1701
2.54	3.05	0.76	423	99.52	0.30	7.11	10	1200	4	683	1653
2.54	3.05	0.76	423	99.60	0.30	7.10	10	1234	11	728	1674
2.54	3.05	0.76	423	99.66	0.30	7.10	10	1195	8	695	1667
2.54	3.05	0.76	423	99.71	0.30	7.09	10	1348	12	782	1851
2.54	3.05	1.52	423	99.66	0.30	5.47	10	1195	111	599	1496
2.54	3.05	1.52	423	99.51	0.30	5.46	10	1176	111	587	1318
2.54	3.05	1.52	423	99.35	0.30	5.48	10	1315	126	651	1592
2.54	3.05	1.52	423	99.29	0.30	5.46	10	1243	116	616	1530
2.54	3.05	1.52	423	99.17	0.30	5.44	10	1162	107	587	1353
2.54	3.05	1.52	423	99.21	0.30	5.47	10	1138	107	561	1373
2.54	3.05	2.29	423	99.11	0.30	4.75	10	1272	278	518	1270
2.54	3.05	2.29	423	99.03	0.30	4.76	10	1248	274	532	1284
2.54	3.05	2.29	423	98.97	0.30	4.74	10	1367	302	596	1441
2.54	3.05	2.29	423	98.89	0.30	4.77	10	1095	235	436	1093
2.54	3.05	2.29	423	98.85	0.30	4.76	10	1320	288	587	1373
2.54	3.05	2.29	423	98.91	0.30	4.76	10	1339	293	570	1325
2.54	3.05	3.05	423	98.95	0.30	4.23	10	1176	384	431	970
2.54	3.05	3.05	423	98.90	0.30	4.24	10	1367	450	477	1277
2.54	3.05	3.05	423	99.26	0.30	4.25	10	1339	436	535	1209
2.54	3.05	3.05	423	99.35	0.30	4.24	10	1200	388	454	1120
2.54	3.05	3.05	423	99.46	0.30	4.26	10	1052	336	399	929
2.54	3.05	3.05	423	99.35	0.30	4.24	10	1401	460	553	1257
2.54	3.05	0.76	423	98.93	0.30	7.12	5	1386	675	439	1052
2.54	3.05	0.76	423	98.93	0.30	7.12	5	1353	656	416	1011
2.54	3.05	0.76	423	98.93	0.30	7.12	5	1343	622	413	990
2.54	3.05	1.52	423	99.68	0.30	5.47	10	1363	274	534	1517
2.54	3.05	1.52	423	99.68	0.30	5.47	10	1386	274	543	1578
2.54	3.05	1.52	423	99.68	0.30	5.47	10	1339	307	643	1496
2.54	3.05	2.29	423	99.63	0.30	4.74	15	1382	145	733	1756
2.54	3.05	2.29	423	99.63	0.30	4.74	15	1363	102	831	2104
2.54	3.05	2.29	423	99.63	0.30	4.74	15	1343	92	712	1708
2.54	3.05	3.05	423	98.94	0.30	4.29	20	1501	40	892	2016
2.54	3.05	3.05	423	98.94	0.30	4.29	20	1520	68	860	2002
2.54	3.05	3.05	423	98.94	0.30	4.29	20	1530	25	907	2180
5.08	3.05	1.52	423	99.17	0.30	9.73	10	1224	398	471	1045
5.08	3.05	1.52	423	99.06	0.30	9.72	10	1090	350	422	915
5.08	3.05	1.52	423	98.98	0.30	9.72	10	1176	379	477	1182
5.08	3.05	1.52	423	98.94	0.30	9.73	10	1219	393	486	1241
5.08	3.05	1.52	423	98.89	0.30	9.73	13	1234	173	593	1428
5.08	3.05	1.52	423	98.91	0.30	9.73	13	1272	178	561	1394
5.08	3.05	1.52	423	98.91	0.30	9.72	13	1124	154	535	1332
5.08	3.05	1.52	423	98.87	0.30	9.74	13	1257	178	631	1476
5.08	3.05	1.52	423	98.94	0.30	9.74	15	1090	64	584	1428
5.08	3.05	1.52	423	98.93	0.30	9.73	15	1305	87	689	1612
5.08	3.05	1.52	423	98.95	0.30	9.72	15	1248	83	654	1599
5.08	3.05	1.52	423	98.83	0.30	9.72	15	1224	78	631	1585
5.08	3.05	1.52	423	98.86	0.30	9.73	20	1277	6	753	1845
5.08	3.05	1.52	423	98.89	0.30	9.73	20	1219	2	712	1749
5.08	3.05	1.52	423	98.95	0.30	9.74	20	1291	8	747	1756
5.08	3.05	1.52	423	98.95	0.30	9.76	20	1152	5	660	1530

TABLE E4.b
THE EFFECT OF THE INITIAL CONCENTRATION OF WATER ON THE REACTION OF HYDROGEN SULPHIDE WITH AIR*

P kPa	I_c mA	V_s kV	Digits				
			H_2S in	H_2O in	H_2S out	H_2O out	SiF_2 out
98.99	0.10	3.83	1219	1935	661	2159	519
98.99	0.10	3.84	1214	1994	641	2139	505
98.99	0.10	3.86	1224	1877	637	2121	553
99.25	0.10	3.87	1305	3[illegible]	699	3926	553
99.25	0.10	3.87	1315	3737	689	4001	587
99.25	0.10	3.87	1305	3650	703	3914	560
99.51	0.10	3.91	1138	5829	646	6020	525
99.51	0.10	3.92	1138	5974	627	6174	484
99.51	0.10	3.90	1157	6003	632	6221	505
98.86	0.10	3.97	1195	11261	661	11491	539
98.86	0.10	3.98	1205	11378	680	11625	512
98.86	0.10	3.98	1181	11174	641	11389	491
99.33	0.10	4.07	1277	14573	694	14806	546
99.33	0.10	4.08	1272	14748	713	14974	539
99.33	0.10	4.04	1262	14457	723	14713	587
99.59	0.10	4.09	1324	17508	732	17775	614
99.59	0.10	4.09	1320	17682	718	17938	573
99.59	0.10	4.11	1315	17363	723	17615	566
99.13	0.10	4.16	1234	24364	689	24608	566
99.13	0.10	4.14	1214	24248	646	24486	553
99.13	0.10	4.17	1200	24306	622	24524	512
99.50	0.10	4.23	1152	30727	646	30936	512
99.50	0.10	4.24	1143	30582	622	30750	505
99.50	0.10	4.23	1133	30814	646	31012	491
99.46	0.10	4.35	1353	35027	732	35274	587
99.46	0.10	4.37	1324	35172	713	35378	614
99.46	0.10	4.37	1334	34960	699	35207	560
98.73	0.10	4.40	1171	40750	646	41000	498
98.73	0.10	4.39	1162	40401	651	40282	519
98.73	0.10	4.38	1167	40343	637	40587	505
99.06	0.10	4.43	1305	42116	699	42392	573
99.06	0.10	4.44	1286	41999	713	42211	553
99.06	0.10	4.42	1291	42348	694	42537	594
99.18	0.30	5.53	1219	2691	154	3231	1195
99.18	0.30	5.52	1210	2749	250	3263	1209
99.18	0.30	5.53	1200	2720	202	3217	1229
99.51	0.30	5.61	1320	5480	202	6026	1339
99.51	0.30	6.60	1315	5393	250	5959	1366
99.51	0.30	5.59	1320	5596	154	6154	1298
99.64	0.30	6.08	1138	8589	107	9109	1141
99.64	0.30	6.07	1143	8559	154	9056	1175
99.64	0.30	6.07	1129	8530	202	9027	1120
99.70	0.30	6.12	1234	11668	250	12194	1216
99.70	0.30	6.14	1219	11523	154	12020	1195
99.70	0.30	6.11	1214	11407	345	11953	1236
99.58	0.30	6.22	1305	14661	202	15239	1353
99.58	0.30	6.24	1296	14573	298	15096	1298
99.58	0.30	6.24	1315	14457	202	15006	1298
99.26	0.30	6.51	1353	24480	250	25105	1353
99.26	0.30	6.52	1358	24568	250	25152	1339
99.26	0.30	6.53	1353	24451	202	25041	1332
99.30	0.30	6.69	1200	29187	202	29675	1188
99.30	0.30	6.71	1191	29332	154	29867	1223
99.30	0.30	6.73	1181	36281	250	36411	1175
99.14	0.30	6.81	1205	36131	393	36627	1223
99.14	0.30	6.82	1219	35550	345	36099	1264
99.14	0.30	6.83	1210	34969	250	35465	1216
99.03	0.30	6.94	1124	40314	202	40791	1141
99.03	0.30	6.93	3044	40518	59	41851	3055
99.03	0.30	5.50	1109	40431	202	40948	1072
98.93	0.30	7.03	1191	43161	298	43652	1161
98.93	0.30	7.02	1195	42929	298	43469	1182
98.93	0.30	7.06	1195	42987	250	43487	1236

Experimental conditions:

D = 2.54×10^{-4} m^2
B = 1.52×10^{-1} m^{-1}
a = 1.52×10^{-5} m^{-1}
q10 B
T = 423 K

END

0 7 0 9 8 4

FIN